



HAL
open science

A polytopal approach to Apollonian packings and discrete knotted structures

Iván Rasskin

► **To cite this version:**

Iván Rasskin. A polytopal approach to Apollonian packings and discrete knotted structures. *Combinatorics [math.CO]*. Université de Montpellier, 2021. English. NNT: . tel-03480927v1

HAL Id: tel-03480927

<https://hal.science/tel-03480927v1>

Submitted on 15 Dec 2021 (v1), last revised 20 Dec 2021 (v2)

HAL is a multi-disciplinary open access archive for the deposit and dissemination of scientific research documents, whether they are published or not. The documents may come from teaching and research institutions in France or abroad, or from public or private research centers.

L'archive ouverte pluridisciplinaire **HAL**, est destinée au dépôt et à la diffusion de documents scientifiques de niveau recherche, publiés ou non, émanant des établissements d'enseignement et de recherche français ou étrangers, des laboratoires publics ou privés.

**THÈSE POUR OBTENIR LE GRADE DE DOCTEUR
DE L'UNIVERSITE DE MONTPELLIER**

En Mathématiques et Modélisation

École doctorale : Information, Structures, Systèmes

Unité de recherche : Institut Montpellierain Alexander Grothendieck

**A polytopal approach to Apollonian packings
and discrete knotted structures**

Présentée par Iván Rasskin

Le 10/12/2021

Sous la direction de Jorge Luis Ramírez Alfonsín

Devant le jury composé de

Jorge L. Ramírez Alfonsín	Professeur, Univ. de Montpellier	Directeur
Katherine E. Stange	Assistant Professor, Univ. of Colorado, Boulder	Rapporteuse
Hao Chen	Priv.-Doz. Dr. rer. nat. habil., Georg-August-Univ. Göttingen	Rapporteur
Shalom Eliahou	Professeur, Univ. du Littoral Côte d'Opale	Président du jury
Éric Colin de Verdière	Directeur de Recherche, Lab. d'Informatique Gaspard Monge	Examineur



**UNIVERSITÉ
DE MONTPELLIER**

A mi hermano.

Un pas
entre le blanc et le noir
entre la terre de là haut et celle de là
bas
juste un pas...
l'ombre furtive
des angles morts

*Marcel Camill', Francophonie ou de part et
d'autre des miroirs*

Remerciements

En premier lieu, je voudrais remercier mon directeur de thèse, Jorge Ramírez, pour m'avoir donné l'opportunité de travailler avec lui sur des sujets passionnants, toujours avec patience, bienveillance et enthousiasme, tout en me transmettant un regard esthétique des mathématiques. En effet, les mots que j'ai les plus entendu de lui lorsqu'une relation surprenante apparaissait sur son tableau n'étaient pas "*C'est intéressant...*" mais "*¡Qué bonito!*".

Ma reconnaissance va également aux membres du jury de ma thèse, Katherine Stange, Hao Chen, Shalom Eliahou et Éric Colin de Verdière pour leurs relectures approfondies du manuscrit et la pertinence de leurs conseils.

Un grand merci à ma tante Debbie, pour sa correction méticuleuse du texte et à mon oncle Diego, le premier à m'avoir introduit aux problèmes des *sphere packings*.

Je remercie ma famille mexicaine de Puebla et l'équipe de mathématiciens de Querétaro qui m'ont si bien accueilli pendant mon séjour en 2019, spécialement Luis Montejano avec lequel c'était un vrai plaisir de travailler.

Je remercie chaleureusement les (post)doctorant(e)s de l'IMAG, en particulier mes co-bureaux Maud Joubaud, Abel Lacabanne, Jérémy Nusa, The-Cang Nguyen, Francesco Bonaldi et mathématicien le jour, grimpeur et boulanger la nuit, Raphaël Paegelow. Merci aux collègues avec qu'on a partagé des bons moments ensemble pendant ces 4 ans, Néstor Fernández Vargas, Pelle Steffens, Robert Rapadamnaba, Abdourahim Ibrahim Youssouf, Emmanuel Gnandi, Thiziri Moulla, Mario Veruete, Nicolás León et Berardo Ruffini. Je tiens à remercier aussi l'équipe administrative de l'IMAG, Sophie Cazanave, Carmela Madonia, Éric Hougounenq, Baptiste Chapisat, Nathalie Collain et Brigitte Labric qui ont su toujours me dépanner avec beaucoup de patience et de bonne humeur.

Je dois remercier mes amis de Montpellier, les Romains, Marina, Benoit, Anaëlle, Adèle, Christian et Laura, y a mis amigos de Montpellier, Goiz, Laura, Vio, Abel, Patri, Pelu, Adro et David, por cambiarme la silla y la pantalla por raclettes y randonnées. Sin olvidar a Manu y Vivien, musicantes y viajeros incansables, que siguen pedaleando sin perder el compás, y a mi camarada Iván González Tobar por haberme inspirado para hacer una tesis y por las incontables guitarreadas en Deux Ponts.

Agradezco también a mis abuelos Abel y Susana por esperarme siempre con una tertulia de sobremesa, a mi familia cacereña Irina, José, Adrián y Nahuel, que de tesis saben un rato, a Juan, Enri y Cancamusa, por acogerme y cuidarme en plena redacción, a mis padres, que nunca han dejado de apoyarme, guiarme y llenarme los días de música, y a mi hermano Pablo, siempre pendiente de empujarme cuando flojeo para que llegue a la meta.

Las últimas palabras de agradecimiento van para ti, Bea, mi compañera de la randonnée de la vida, por tus risas cariñosas, las tardes de biblioteca y la inmensa ayuda y amor que me has dado durante estos años, sin los cuales esta tesis no habría sido posible.

Contents

Abstract	v
Résumé	vii
Résumé étendu	ix
Introduction	1
1 General background	5
1.1 The space of oriented hyperspheres	5
1.1.1 The spherical model	6
1.1.2 The hyperbolic model	8
1.1.3 The Lorentzian model	8
1.1.4 The Möbius group	11
1.1.5 Coordinate systems	12
1.1.6 Packings	14
1.1.7 Möbius uniqueness of d -ball packable graphs	16
1.2 Preliminaries on knot theory	17
1.2.1 Diagrams of knots and links	17
1.2.2 Tangles	19
1.2.3 Rational tangles	21
1.2.4 Braids	23
1.2.5 Polygonal representations	24
2 An upper bound on the ball number	27
2.1 Introduction	27
2.2 From links to circle packable graphs	28
2.3 Square-pyramidal disk arrangements	29
2.4 The crossing sphere arrangement	33
2.5 The proof of the upper bound	36
2.6 An algorithm for knotted necklaces	40

3	Polytopal ball packings	43
3.1	Introduction	43
3.2	The projective model of the space of oriented hyperspheres.	45
3.3	Polytopes	46
3.4	The ball-arrangement projection.	49
3.4.1	Centered Ball Packing projections of regular polytopes	50
3.5	Duality of polytopal d -ball packings	51
3.6	Möbius uniqueness of edge-scribable polytopes	52
3.6.1	The Möbius spectra	57
3.6.2	Non edge-scribable 4-polytopes.	58
3.7	Apollonian groups and packings	60
3.7.1	The Platonic Apollonian Groups	62
4	The Polytopal Descartes' Theorem	69
4.1	Introduction	69
4.2	The Polytopal Descartes' Theorem	71
4.3	Integrality of the Platonic Apollonian packings	80
4.3.1	Octahedral Apollonian packings	82
4.3.2	Cubical Apollonian packings	84
4.3.3	Icosahedral Apollonian packings	85
4.3.4	Dodecahedral Apollonian packings	86
5	Apollonian sections of the orthoplicial Apollonian packing	87
5.1	Introduction	87
5.2	The orthoplicial sphere packing	88
5.2.1	Orthoplicial trinities	90
5.2.2	Apollonian groups of the orthoplicial sphere packing	91
5.3	Apollonian sections	94
5.3.1	Construction of orthoplicial Apollonian packings containing a given integral section	99
6	Orthoplicial Apollonian packings and rational links	105
6.1	Introduction	105
6.2	Orthoplicial necklace representations	106

6.3	Algebraic links in the cubical Apollonian section	108
6.3.1	Orthocubical shifts	110
6.3.2	An upper bound on the ball number of rational links	113
6.4	A geometric interpretation of continued fractions	117
Conclusions: current and future work		123
7.1	Möbius uniqueness	123
7.2	Integral packings	124
7.3	Diophantine equations	126
7.4	Necklace representations and the ball number	127
7.5	Further knotted constructions	129
7.6	Software <code>Polytopack</code>	130
A Appendices		139
A.1	Regular polytopes data	139
A.2	CBP projections of the Platonic solids	140
A.3	CBP projections of the regular 4-polytopes	140
Bibliography		143

Abstract

In the last decades, Apollonian packings have drawn increasing attention due to their applications in number theory, geometric group theory, hyperbolic geometry, fractal structures and discrete geometry. In this thesis, we study a class of sphere packings where the combinatorics is carried by an edge-scribed polytope. Through this connection, Apollonian packings can be generalized in different geometric settings and in higher dimensions. The polytopal structure also allows us to obtain a generalization of the Descartes' Theorem for the sphere packings which are based on the regular polytopes in every dimension. We use the polytopal generalization of the Descartes' Theorem to find integrality conditions of the Apollonian packings based on the Platonic solids. Then, we introduce the notion of Apollonian section, and we use it to show that the set of curvatures of any integral tetrahedral, octahedral or cubical Apollonian packing is contained in the set of curvatures of an integral orthoplicial Apollonian packing.

The polytopal approach that we propose also allows us to extend the applications of Apollonian packings into a novel direction in the area of topology. In this thesis, we introduce two methods of construction of necklace representations of knots and links. The first method follows directly from the Koebe-Andreev-Thurston Circle Packing Theorem and gives a linear upper bound on the minimum number of spheres needed to construct a necklace representation in terms of the crossing number. In the second method, we use the fractal structure of orthoplicial Apollonian packings to construct necklace representations of rational links with interesting arithmetical properties.

Résumé

Les empilements apolloniens ont attiré l'attention des mathématiciens en raison de leurs applications en théorie des nombres, théorie géométrique des groupes, géométrie hyperbolique, structures fractales et géométrie discrète. Dans cette thèse, nous introduisons une classe d'empilements de sphères où la combinatoire est donnée par un polytope inscrit aux arêtes. À travers cette connexion, nous généralisons les empilements apolloniens dans d'autres contextes géométriques et en dimensions supérieures. Cette structure polytopale permet également d'obtenir une généralisation du théorème de Descartes pour les empilements de sphères provenant des polytopes réguliers dans toutes les dimensions. Nous utilisons ce résultat pour caractériser l'intégralité des empilements apolloniens provenant des solides platoniciens. Puis, nous introduisons la notion de section apollonienne, et nous l'utilisons pour montrer que l'ensemble des courbures de tout empilement apollonien intégral tétraédrique, octaédrique ou cubique est contenu dans l'ensemble des courbures d'un empilement apollonien orthoplicial intégral.

L'approche polytopale que nous proposons nous permet également d'étendre les applications des empilements apolloniens dans une nouvelle direction dans le domaine de la topologie. Dans cette thèse, nous introduisons deux méthodes de construction de représentations en colliers de nœuds et d'entrelacs. La première méthode découle directement du théorème d'empilements de cercles de Koebe-Andreev-Thurston, et donne une borne supérieure linéaire sur le nombre minimal de sphères nécessaires pour construire une représentation en collier en termes du nombre minimal de croisements. Dans la seconde méthode, nous utilisons la structure fractale des empilements apolloniens orthopliciaux pour construire des représentations en collier des entrelacs rationnels avec des propriétés arithmétiques intéressantes.

Résumé étendu

Les empilements de sphères sont des objets qui apparaissent très souvent, non seulement en mathématiques, mais aussi en divers champs scientifiques comme la chimie pour les structures cristallines, la physique pour la modélisation des milieux granulaires ou l'informatique pour les codes correcteurs. Parmi la variété infinie des configurations possibles, les *empilements apolloniens* ont attiré l'attention des mathématiciens en raison de leurs applications en théorie des nombres, théorie géométrique de groupes, géométrie hyperbolique, structures fractales ou géométrie discrète. Dans cette thèse, nous utilisons la combinatoire des polytopes pour généraliser les empilements apolloniens et les appliquer dans la construction polygonale des nœuds et entrelacs dans l'espace.

En premier lieu, nous introduisons les différents modèles géométriques qui sont utilisés pour étudier les empilements de sphères. Nous rappelons la bijection qui existe entre l'ensemble des boules euclidiennes en dimension d et l'ensemble des vecteurs unitaires dans l'espace lorentzien en dimension $d + 2$. Cette bijection fait de l'algèbre linéaire, appliquée aux espaces lorentziens, un outil très adapté pour étudier les empilements de sphères.

Nous continuons avec les notions basiques de la théorie des nœuds, en faisant un point sur les entrelacs rationnels introduits par Conway, et finissons cette section en décrivant les invariants géométriques qui sont liés aux représentations polygonales des nœuds. La *longueur en sphères* est l'un de ces invariants, défini comme le nombre minimal de sphères dans un collier ayant la forme d'un nœud ou entrelacs donné. Dans le chapitre 2, en utilisant la géométrie lorentzienne et le théorème de Koebe-Andreev-Thurston sur les empilements de cercles, nous prouvons une borne linéaire de la longueur en sphères en fonction du nombre minimal de croisements d'un nœud. La méthode utilisée dans la preuve inspire un premier algorithme de construction des représentations de nœuds en collier à partir d'un diagramme de nœuds planaire. Ce type de représentations a été récemment utilisée pour l'étude du volume hyperbolique de 3-variété hyperbolique.

Dans le chapitre 3, nous faisons le lien entre les empilements et les polytopes. Pour cela, nous voyons d'abord les définitions classiques associées aux polytopes et le modèle projectif de l'espace de boules. Dans ce modèle, une boule d -dimensionnelle correspond à un point dans l'espace euclidien de dimension $d + 1$ ayant une norme strictement plus grande que 1. De manière analogue, un empilement de boules d -dimensionnelles correspond à un polytope de dimension $d + 1$ vérifiant certaines propriétés géométriques. Les empilements issus de cette correspondance seront appelés *polytopaux*. Nous étudions ensuite l'unicité sous transformations de Möbius et la dualité des empilements polytopaux. Cette dernière permet de bien généraliser les empilements apolloniens dans d'autres combinatoires et en dimensions plus grandes.

L'application des empilements apolloniens dans la théorie des nombres vient du fait qu'il existe une infinité d'empilements apolloniens *intégraux* dont les courbures de tous les cercles contenus dans l'empilement sont des entiers. C'est le théorème de Descartes sur les courbures d'un empilement de 4 cercles deux-à-deux tangents qui permet de créer le lien, car il donne les conditions nécessaires pour qu'un empilement apollonien soit intégral. Dans le chapitre 4, nous utilisons la géométrie lorentzienne pour donner une généralisation du théorème de Descartes pour les empilements polytopaux réguliers. Nous appliquerons ce résultat pour caractériser l'intégralité des empilements apolloniens polytopaux, lorsque le polytope correspondant est l'un des solides de Platon.

Le chapitre 5 est dédié à l'étude d'une famille d'empilements polytopaux réguliers en dimension 3: les *empilements orthopliciaux*. Ceux-ci sont des empilements ayant la combinatoire de l'orthoplex, l'analogue de l'octaèdre en dimension 4. La version apollonienne pour les empilements orthopliciaux a été introduite par Dias et Nakamura en 2014, comme une généralisation des empilements apolloniens trois dimensionnelles ayant une structure algébrique plus riche. Cela leur a permis de résoudre des problèmes arithmétiques, dans les cas des empilements apolloniens orthopliciaux, qui restent toujours ouverts pour les empilements apolloniens classiques en dimension 2. Avec les outils développés dans les chapitres précédents,

nous montrons l'unicité de Möbius des empilements orthopliciaux et nous calculons les groupes apolloniens associés. Puis, nous introduisons la notion de *section apollonienne* qui généralise, d'une manière algébrique, l'action d'intersecter un empilement avec un hyperplan. Les sections apolloniennes nous permettent de montrer que les ensembles des entiers qui se trouvent dans les empilements apolloniens intégraux venant d'un tétraèdre, un octaèdre ou un cube sont toujours contenus dans l'ensemble des entiers d'un empilement apollonien intégral ayant la combinatoire de l'orthoplex.

Dans le chapitre 6, nous regardons les questions évoquées au chapitre 2 sur les représentations en collier et la longueur en sphères des nœuds, dans les empilements apolloniens orthopliciaux. En utilisant les structures obtenues dans le chapitre 5, nous prouvons plusieurs résultats. Tout d'abord, nous montrons que tout entrelacs admet une représentation en collier contenue dans les empilements apolloniens orthopliciaux. Puis, avec une projection déterminée, nous perfectionnons ce résultat en montrant que tous les entrelacs rationnels, et plus généralement les entrelacs algébriques, admettent une représentation en collier dans une section apollonienne cubique d'un empilement apollonien orthoplicial. Ce dernier résultat nous permet d'améliorer la borne supérieure de la longueur en sphères qui a été donnée au chapitre 2, dans les cas des entrelacs rationnels. Enfin, nous montrons deux corollaires arithmétiques du dernier résultat.

Nous finissons ce manuscrit par une discussion sur les résultats obtenus dans cette thèse, le travail qui est en cours et les perspectives sur les possibles applications dans la théorie des nombres et la théorie des nœuds.

Introduction

Sphere packings appear diversely in chemistry, physics, computer science and mathematics. There is a long trajectory on numerical and analytic approaches, but many questions about the algebraic and combinatorial aspects of non-congruent sphere packings remain open to date. Among the great variety of possible configurations, the *Apollonian packings* have drawn increasing attention by mathematicians due to their applications in number theory, geometric group theory, hyperbolic geometry, fractal structures or discrete geometry.

The origin of the term Apollonian packings goes back to a problem apparently raised by Apollonius of Perga around 230 BCE, following the writings of Pappus of Alexandria on Apollonius' works [31]. The problem of Apollonius concerned the number of circles that can be added to be tangent to three given circles. If the three given circles are pairwise tangent, then the answer is two. The packing made by these five circles gives the first step towards an Apollonian packing, which is made by inscribing a new circle at the interstice made by each triplet of circles, and then repeating this process *ad infinitum*. The first record of the whole picture belongs to Leibniz, in a fragment of a letter to Des Bosses in 1706 [70] on his attempts to illustrate the notion of *infinitesimal*.

Beyond mathematics, the space-filling property of the three-dimensional analogue of Apollonian packings has been used in the modelling of granular systems [4], foam structures [86], fluid emulsions [67] and in many other applications [103, 94, 65].

In number theory, research on Apollonian packings has been increasing in the last decades, due to the interesting properties of the integral and algebraic structures behind Apollonian packings revealed in a foundational series of papers by Graham, Lagarias, Mallows, Wilks and Yan [44, 45, 46, 47]. Chen, in his PhD thesis [21], proposed a combinatorial approach to study Apollonian packings by relating them with stacked polytopes. In this thesis, we develop a line of research close to Chen's, by using a polytopal approach to generalize the structure of Apollonian packings in different geometric settings and in higher dimensions.

The approach that we propose allowed us to obtain new results in number theory on Apollonian packings, and also to extend the applications of Apollonian packings into a novel direction in the area of topology. For a given knot K (resp. link), a *necklace representation* is a cyclic chain (resp. chains) of consecutive tangent spheres which are ambient isotopic to K . Necklace representations of knots and links have been recently used for the study of hyperbolic volume of hyperbolic 3-manifolds [41]. In this thesis, we used the fractal structure of polytopal Apollonian packings to construct necklace representations of links and knots with interesting arithmetical properties.

Organization of the manuscript

In Chapter 1, we discuss the classic results and definitions in sphere packings and knots that will be used throughout the rest of the manuscript.

In Chapter 2, we present an upper bound on the minimum number of spheres needed to construct a necklace representation of a given knot or link. We finally describe an algorithm to construct necklace representations, which is based in the constructive proof of the upper bound.

In Chapter 3, we explore the connection between polytopes and sphere packings in any dimension by introducing a class of packings whose combinatorics is based on edge-scribed polytopes. We then study the unicity under Möbius transformations and the duality of these packings. The latter allows us to generalize the Apollonian group and the Apollonian packing within new settings.

In Chapter 4, we generalize the Descartes' theorem for polytopal d -ball packings obtained from a regular polytope. The latter allows us to construct integral Apollonian packings based on the Platonic solids.

In Chapter 5, we review the orthoplicial Apollonian packing, introduced by Dias [33] and Nakamura [79], with the tools developed in the previous chapter. After introducing the notion of *Apollonian section*, we show that the set of curvatures of every integral tetrahedral, octahedral and cubical Apollonian packing is contained in the set of curvatures of an integral orthoplicial Apollonian packing.

Chapter 6 connects the two main objects of this thesis: Apollonian packings and necklace representations. We use the orthoplicial Apollonian packing to produce necklace representations efficiently. The latter reveals interesting geometric and arithmetic properties.

A final section presents general conclusions of our work and includes discussions on some current developments and future perspectives.

The first section of Chapter 1 and the content of Chapter 2 were published in [81]. Chapters 3, 4 and 5 are based on the submitted preprints [82, 84] and Chapter 6 is a part of a preprint in preparation [83].

General background

Contents

1.1	The space of oriented hyperspheres	5
1.1.1	The spherical model	6
1.1.2	The hyperbolic model	8
1.1.3	The Lorentzian model	8
1.1.4	The Möbius group	11
1.1.5	Coordinate systems	12
1.1.6	Packings	14
1.1.7	Möbius uniqueness of d -ball packable graphs	16
1.2	Preliminaries on knot theory	17
1.2.1	Diagrams of knots and links	17
1.2.2	Tangles	19
1.2.3	Rational tangles	21
1.2.4	Braids	23
1.2.5	Polygonal representations	24

In this chapter, we discuss a general background needed throughout the manuscript.

1.1 The space of oriented hyperspheres

In this section, we review the space of d -dimensional oriented hyperspheres (or d -ball) in the Euclidean space through different classic models. The majority of the notations and definitions were adapted from [18, 104, 20].

1.1.1 The spherical model

Let $d \geq 1$ be an integer. We denote \mathbb{R}^d the Euclidean space of dimension d . Let \mathbb{S}^d be the unit d -sphere of \mathbb{R}^{d+1} endowed with the induced metric $\|\cdot\|_{\mathbb{S}}$ from \mathbb{R}^{d+1} . A d -spherical cap α of center $\gamma \in \mathbb{S}^d$ and spherical radius $\rho \in (0, 2\pi)$ is a subset given by

$$\alpha = \{x \in \mathbb{S}^d \mid \|x - \gamma\|_{\mathbb{S}} \leq \rho\} \quad (1.1)$$

which gives a partition of \mathbb{S}^d in three disjoint subsets: the *interior* of α , points of \mathbb{S}^d satisfying (1.1) strictly, the *exterior* of α , points of \mathbb{S}^d not satisfying (1.1) and the *boundary* of α , $\partial\alpha$, points of \mathbb{S}^d satisfying the equality of (1.1). Let $\text{Caps}(\mathbb{S}^d)$ denote the family of d -spherical caps. It is well known that \mathbb{S}^d is homeomorphic to $\widehat{\mathbb{R}}^d$ under the stereographic projection, where $\widehat{\mathbb{R}}^d := \mathbb{R}^d \cup \{\infty\}$ is the one-point compactification of \mathbb{R}^d . We call a d -ball of $\widehat{\mathbb{R}}^d$ the image of a d -spherical cap under the stereographic projection. We denote by $\text{Balls}(\widehat{\mathbb{R}}^d)$ the space of d -balls, isomorphic to $\text{Caps}(\mathbb{S}^d)$ given by the above construction. A d -ball b is called *solid sphere*, *hollow sphere* or *half-space* depending on whether the pole of the stereographic projection lies in either the exterior, the interior or the boundary of the corresponding d -spherical cap α_b . Therefore, we have that a d -ball of $\widehat{\mathbb{R}}^d$ of curvature $\kappa \in \mathbb{R}$ corresponds to one of the following subsets:

- *Solid sphere*: $\{x \in \widehat{\mathbb{R}}^d \mid \|x - c\| \leq 1/\kappa\}$ when $\kappa > 0$.

It is also a standard d -ball of \mathbb{R}^d with center $c \in \mathbb{R}^d$ and radius $\frac{1}{\kappa}$.

- *Hollow sphere*: $\{x \in \widehat{\mathbb{R}}^d \mid \|x - c\| \geq -1/\kappa\}$ when $\kappa < 0$.

It can be regarded as the closure of the complement of a solid sphere.

- *Half-space*: $\{x \in \widehat{\mathbb{R}}^d \mid x \cdot \widehat{n} \leq \delta\}$ when $\kappa = 0$.

By convention, we choose the *normal vector* \widehat{n} pointing towards the interior.

The real number δ represents the *signed distance* from the boundary to the origin (positive if the origin is contained in the interior and negative otherwise).

There is a natural embedding of $\text{Balls}(\widehat{\mathbb{R}}^d) \hookrightarrow \text{Balls}(\widehat{\mathbb{R}}^{d+1})$ where a d -ball b of center c and curvature κ (resp. normal vector \widehat{n} and signed distance δ) is mapped to a $(d+1)$ -ball \widehat{b} of center $(c, 0)$ and curvature κ (resp. normal vector $(\widehat{n}, 0)$ and signed distance δ). We call this embedding the *inflate operation*.

1.1.1.1 The intersection angle

For $d > 1$, let b and b' be two d -balls with intersecting boundaries. We define the *intersection angle* of b and b' , denoted by $\angle(b, b') \in [0, \pi]$, as the angle formed by the vectors \vec{pc} and \vec{pc}' where c and c' are the centers of b and b' and $p \in \partial b \cap \partial b'$ (see Figure 1.1). The intersection angle does not depend on the choice of the point in the intersection.

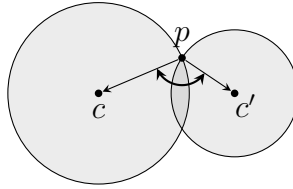


Figure 1.1: The intersection angle of two disks.

Two d -balls b and b' with intersecting boundaries are said to be:

- *Internally tangent* if $\angle(b, b') = 0$.
- *Orthogonal* if $\angle(b, b') = \frac{\pi}{2}$.
- *Externally tangent* if $\angle(b, b') = \pi$.

When the boundaries of b and b' do not intersect the intersection angle $\angle(b, b')$ is not well-defined. In this case we say that b and b' are *disjoint* if they have disjoint interiors and *nested* if one is contained in the other.

Remark 1. *The inflate operation preserves intersection angles.*

We notice that the definition of intersection angle does not apply when $d = 1$, since the boundary of a 1-ball is not simply connected. In this case, we can define the intersection angle of two 1-balls as the intersection angle of the corresponding 2-balls given by the inflate operation.

1.1.2 The hyperbolic model

Let \mathbb{H}^{d+1} be the Poincaré ball model of the hyperbolic space of dimension $d + 1$ embedded in $\widehat{\mathbb{R}}^{d+1}$ as the standard unit $(d + 1)$ -ball. The boundary $\partial\mathbb{H}^{d+1}$ is exactly the unit sphere \mathbb{S}^d . A d -hyperbolic half-space of \mathbb{H}^{d+1} is the intersection $h := \mathbb{H}^{d+1} \cap \widehat{b}_h$ where \widehat{b}_h is a $(d + 1)$ -ball orthogonal to \mathbb{H}^{d+1} . We denote by $\text{Halfs}(\mathbb{H}^{d+1})$ the space of hyperbolic half-spaces of \mathbb{H}^{d+1} . At the boundary of \mathbb{H}^{d+1} , the intersection $\partial\mathbb{H}^{d+1} \cap \widehat{b}_h = \mathbb{S}^d \cap \widehat{b}_h$ is a d -spherical cap α_h which corresponds to a d -ball b_h by the stereographic projection. For any d -ball, the mapping $h \mapsto \alpha_h \mapsto b_h$ can be reversed so we can define the following isomorphisms:

$$\text{Balls}(\widehat{\mathbb{R}}^d) \xrightarrow{\simeq} \text{Caps}(\mathbb{S}^d) \xrightarrow{\simeq} \text{Halfs}(\mathbb{H}^{d+1}) \quad (1.2)$$

The notions of interior, exterior and boundary are easily extended for d -hyperbolic half-spaces. For $d > 1$, two d -balls b and b' have intersecting boundaries if and only if the corresponding d -hyperbolic half-spaces h_b and $h_{b'}$ have intersecting boundaries. Moreover, the intersection angle of b and b' is equal to the *dihedral angle* of h_b and $h_{b'}$ measured at a non-common region.

1.1.3 The Lorentzian model

The Lorentzian space of dimension $d + 2$, denoted by $\mathbb{L}^{d+1,1}$, is a real vector space of dimension $d + 2$ equipped with a bilinear symmetric form $\langle \cdot, \cdot \rangle$ of signature $(d + 1, 1)$. The *Lorentzian product* of two vectors \mathbf{x} and \mathbf{y} of $\mathbb{L}^{d+1,1}$ is the real number $\langle \mathbf{x}, \mathbf{y} \rangle$ and the *Gramian* of a collection of vectors $\mathcal{B} = \{\mathbf{x}_1, \dots, \mathbf{x}_n\}$ of $\mathbb{L}^{d+1,1}$ is the matrix

$$\text{Gram}(\mathcal{B}) := \begin{pmatrix} \langle \mathbf{x}_1, \mathbf{x}_1 \rangle & \cdots & \langle \mathbf{x}_1, \mathbf{x}_n \rangle \\ \vdots & \ddots & \vdots \\ \langle \mathbf{x}_n, \mathbf{x}_1 \rangle & \cdots & \langle \mathbf{x}_n, \mathbf{x}_n \rangle \end{pmatrix}$$

If $\mathcal{B} = \{\mathbf{x}_1, \dots, \mathbf{x}_{d+2}\}$ is a basis of $\mathbb{L}^{d+1,1}$ then $\text{Gram}(\mathcal{B})$ is the matrix of the Lorentzian product in the basis \mathcal{B} . The Lorentzian product of two vectors $\mathbf{x}, \mathbf{y} \in \mathbb{L}^{d+1,1}$ can be computed by

$$\langle \mathbf{x}, \mathbf{y} \rangle = \mathbf{c}_{\mathcal{B}}(\mathbf{x})^T \text{Gram}(\mathcal{B}) \mathbf{c}_{\mathcal{B}}(\mathbf{y}) \quad (1.3)$$

where $c_{\mathcal{B}}(\mathbf{x})$ is the column matrix of the coordinates of \mathbf{x} in the basis \mathcal{B} . By a fundamental theorem of bilinear forms (see [18, Theorem 2.1]), there is always an orthonormal basis $\mathcal{B}_0 = \{e_1, \dots, e_{d+2}\}$ of $\mathbb{L}^{d+1,1}$ such that $\text{Gram}(\mathcal{B}_0) = \text{diag}(1, \dots, 1, -1)$. From now on, we fix an orthonormal basis \mathcal{B}_0 which we shall refer to as the *canonical basis* of $\mathbb{L}^{d+1,1}$. A vector $\mathbf{x} \in \mathbb{L}^{d+1,1}$ is called:

- *Space-like* if $\langle \mathbf{x}, \mathbf{x} \rangle > 0$.
- *Time-like* if $\langle \mathbf{x}, \mathbf{x} \rangle < 0$.
- *Light-like* if $\langle \mathbf{x}, \mathbf{x} \rangle = 0$.
- *Future-directed* (resp. *past-directed*) if $\langle e_{d+2}, \mathbf{x} \rangle > 0$ (resp. < 0).
- *Normalized* if $|\langle \mathbf{x}, \mathbf{x} \rangle| = 1$.

The space of all the normalized space-like (resp. time-like) vectors of $\mathbb{L}^{d+1,1}$ is usually called *de Sitter space* (resp. *anti de Sitter space*). We denote it by $S(\mathbb{L}^{d+1,1})$ (resp. $T(\mathbb{L}^{d+1,1})$). The *anti de Sitter space* can be regarded as the generalization of a two-sheets hyperboloid with two connected components $T^\uparrow(\mathbb{L}^{d+1,1})$ and $T^\downarrow(\mathbb{L}^{d+1,1})$ formed by the future-directed and the past-directed vectors of $T(\mathbb{L}^{d+1,1})$ respectively. The *hyperboloid model* of the $(d+1)$ -hyperbolic space is obtained by taking $T^\uparrow(\mathbb{L}^{d+1,1})$ with the metric induced by the restriction of the Lorentzian product of $\mathbb{L}^{d+1,1}$. The isomorphism which maps the hyperboloid model to the Poincaré ball model can be regarded as the projection $\pi : T^\uparrow(\mathbb{L}^{d+1,1}) \rightarrow \{e_{d+2} = 0\}$ from $-e_{d+2}$ (see Figure 1.2).

A *time-like half-space* is a subset $t_{\mathbf{x}} = \{\mathbf{y} \in \mathbb{L}^{d+1,1} \mid \langle \mathbf{x}, \mathbf{y} \rangle \geq 0\}$ where $\mathbf{x} \in S(\mathbb{L}^{d+1,1})$. The set of time-like half-spaces is in bijection with $S(\mathbb{L}^{d+1,1})$. The image $\pi(t_{\mathbf{x}} \cap T^\uparrow(\mathbb{L}^{d+1,1}))$ is a hyperbolic half-space of \mathbb{H}^{d+1} and every hyperbolic half-space can be obtained in this way. We can then extend the isomorphisms of (1.2) by

$$\text{Balls}(\widehat{\mathbb{R}}^d) \xrightarrow{\cong} \text{Caps}(S^d) \xrightarrow{\cong} \text{Halfs}(\mathbb{H}^{d+1}) \xrightarrow{\cong} S(\mathbb{L}^{d+1,1}) \quad (1.4)$$

The *Lorentzian vector* of a d -ball b , denoted by \mathbf{x}_b , is the normalized space-like vector obtained by the previous isomorphisms.

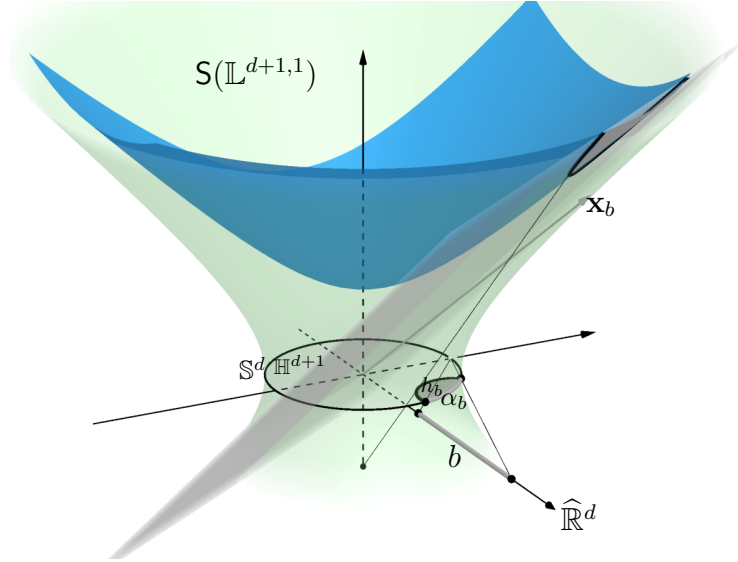


Figure 1.2: Geometric interpretation of the isomorphisms between the different models of the space of d -balls.

The *inversive product* of two d -balls b and b' , denoted by $\langle b, b' \rangle := \langle \mathbf{x}_b, \mathbf{x}_{b'} \rangle$, is the Lorentzian product of their corresponding Lorentzian vectors. Equivalently, we define the Gramian of a collection of d -balls as the Gramian of the collection of the Lorentzian vectors of the d -balls. We denote by $-b$ the d -ball corresponding to the Lorentzian vector $-\mathbf{x}_b$, which is also the d -ball obtained by taking the closure of the complement of b . We notice that $\langle -b, b' \rangle = -\langle b, b' \rangle$. The inversive product is a fundamental tool to encode configurations of d -balls [104]. Indeed,

$$\langle b, b' \rangle = \begin{cases} \cosh d_{\mathbb{H}}(h_b, h_{b'}) & \text{if } b \text{ and } b' \text{ are nested} \\ \cos \angle(b, b') & \text{if } \partial b \text{ and } \partial b' \text{ intersect} \\ -\cosh d_{\mathbb{H}}(h_b, h_{b'}) & \text{if } b \text{ and } b' \text{ are disjoint} \end{cases}$$

where h_b and $h_{b'}$ are the corresponding hyperbolic half-spaces and $d_{\mathbb{H}}(h_b, h_{b'})$ is the hyperbolic distance between ∂h_b and $\partial h_{b'}$. In particular, if the Lorentzian vectors of b and b' are not both past-directed, then

$$\langle b, b' \rangle \begin{cases} < -1 & \text{if } b \text{ and } b' \text{ are disjoint} \\ = -1 & \text{if } b \text{ and } b' \text{ are externally tangent} \\ = 0 & \text{if } b \text{ and } b' \text{ are orthogonal} \\ = 1 & \text{if } b \text{ and } b' \text{ are internally tangent} \\ > 1 & \text{if } b \text{ and } b' \text{ are nested} \end{cases} \quad (1.5)$$

1.1.4 The Möbius group

The Möbius Group $\text{Möb}(\widehat{\mathbb{R}}^d)$ can be defined as the group of the continuous automorphisms of $\widehat{\mathbb{R}}^d$ mapping d -balls to d -balls [101]. An element of the Möbius Group is called a *Möbius transformation*. For every solid or hollow (resp. half-space) d -ball b we define the *inversion on b* , denoted by s_b , as the sphere inversion (resp. Euclidean reflection) on the boundary of b . Alternatively, s_b can be defined as the only Möbius transformation that maps b to $-b$ and fixes a d -ball b' if and only if b' is orthogonal to b [101]. It is well-known that $\text{Möb}(\widehat{\mathbb{R}}^d)$ is generated by the set of inversions. The product $s_b s_{b'}$ of the inversions on two d -balls centered at the origin with non-zero curvatures κ and κ' gives a rescaling of \mathbb{R}^d with scaling factor $(\kappa'/\kappa)^2$. Thus, the group of Euclidean isometries and rescalings of \mathbb{R}^d is a subgroup of $\text{Möb}(\widehat{\mathbb{R}}^d)$.

The Möbius Group defines a group action (on the left) on the space of d -balls. The following group isomorphisms and equivariant group actions can be obtained by using the isomorphisms given in (1.4)

$$\begin{array}{ccccccc} \text{Balls}(\widehat{\mathbb{R}}^d) & \xrightarrow{\cong} & \text{Caps}(\mathbb{S}^d) & \xrightarrow{\cong} & \text{Halfs}(\mathbb{H}^{d+1}) & \xrightarrow{\cong} & \text{S}(\mathbb{L}^{d+1,1}) \\ \uparrow & & \uparrow & & \uparrow & & \uparrow \\ \text{Möb}(\widehat{\mathbb{R}}^d) & \xrightarrow{\cong} & \text{Möb}(\mathbb{S}^d) & \xrightarrow{\cong} & \text{Isom}(\mathbb{H}^{d+1}) & \xrightarrow{\cong} & \text{O}^\uparrow(\mathbb{L}^{d+1,1}) \end{array} \quad (1.6)$$

where $\text{Möb}(\mathbb{S}^d)$ is the Möbius group defined on \mathbb{S}^d acting on the family of d -spherical caps, $\text{Isom}(\mathbb{H}^{d+1})$ is the group of hyperbolic isometries acting on the space of hyperbolic half-spaces and $\text{O}^\uparrow(\mathbb{L}^{d+1,1})$ is the *Orthochronous Lorentz Group* which is the group of linear maps of $\mathbb{L}^{d+1,1}$ preserving the Lorentz product and the time orientation. The latter acts on the space of normalized space-like vectors of $\mathbb{L}^{d+1,1}$. Moreover, for any $b \in \text{Balls}(\widehat{\mathbb{R}}^d)$, the isomorphism $\text{Möb}(\widehat{\mathbb{R}}^d) \rightarrow \text{O}^\uparrow(\mathbb{L}^{d+1,1})$ maps the

inversion s_b to the Lorentzian reflection on the boundary of the time-like half-space $t_{\mathbf{x}_b}$, which corresponds to the linear map

$$\mathbf{y} \mapsto \mathbf{y} - 2\langle \mathbf{y}, \mathbf{x}_b \rangle \mathbf{x}_b \quad (1.7)$$

Since the Orthochronous Lorentz Group preserves the Lorentz product, the Möbius Group preserves the inversive product of d -balls.

1.1.5 Coordinate systems

Based on the previous models, we shall describe two different systems of coordinates for the space of d -balls.

1.1.5.1 Inversive coordinates

In [104], Wilker defined the *inversive coordinates* of a d -ball b as the column-matrix $\mathbf{i}(b)$ given by the Cartesian coordinates of the Lorentzian vector of b with respect to the canonical basis. We shall use these coordinates for most of the computations. The inversive coordinates can be obtained in terms of the curvature κ and center c (normal vector n and signed distance δ for half-spaces) by

$$\mathbf{i}(b) := \mathbf{c}_{\mathcal{B}_0}(\mathbf{x}_b) = \begin{cases} (\kappa c, \frac{1}{2}(\kappa \|c\|^2 - \kappa^{-1} - \kappa), \frac{1}{2}(\kappa \|c\|^2 - \kappa^{-1} + \kappa))^T & \text{if } \kappa \neq 0, \\ (\widehat{n}, \delta, \delta)^T & \text{if } \kappa = 0 \end{cases} \quad (1.8)$$

where $\|\cdot\|$ denotes the Euclidean norm. The curvature of b can be deduced from its inversive coordinates by

$$\kappa(b) = -\langle \mathbf{x}_N, \mathbf{x}_b \rangle \quad (1.9)$$

$$= \mathbf{k}_{d+2} \mathbf{i}(b) \quad (1.10)$$

where $\mathbf{x}_N = e_{d+1} + e_{d+2}$ and e_i denotes the i -th vector of \mathcal{B}_0 and \mathbf{k}_{d+2} is the row-matrix $(0, \dots, 0, -1, 1)$ of length $d + 2$.

Points of $\widehat{\mathbb{R}}^d$ can be seen as d -balls of infinite curvature. By extending continuously the isomorphism between $\text{Balls}(\widehat{\mathbb{R}}^d)$ and $S(\mathbb{L}^{d+1,1})$ we have that points of $\widehat{\mathbb{R}}^d$

correspond to asymptotic directions in the light cone $L(\mathbb{L}^{d+1,1})$ made by all the light-like vectors of $\mathbb{L}^{d+1,1}$. Each direction corresponds to a point in the projective space $\mathbb{P}L(\mathbb{R}^{d+1,1})$. Therefore, we can assign (homogeneous) inversive coordinates to a point $\eta \in \widehat{\mathbb{R}}^d$ by

$$\mathbf{i}(\eta) = \begin{cases} (2\eta, \|\eta\|^2 - 1, \|\eta\|^2 + 1)^T & \text{if } \eta \neq \infty \\ (\mathbf{0}_d, 1, 1) & \text{if } \eta = \infty \end{cases} \quad (1.11)$$

where $\mathbf{0}_d$ is the null vector of length d . Homogeneity means that for every $\lambda \neq 0$, $\lambda\mathbf{i}(\eta)$ are valid inversive coordinates of the same point of $\widehat{\mathbb{R}}^d$ (see [104] for more details).

The following formula to compute the inversive product in inversive coordinates follows from Eq. (1.3)

$$\langle b, b' \rangle = \mathbf{i}(b)^T \mathbf{Q}_{d+2} \mathbf{i}(b') \quad (1.12)$$

where $\mathbf{Q}_{d+2} = \text{diag}(1, \dots, 1, -1)$ is the Gramian of \mathcal{B}_0 . Therefore, the Möbius group is isomorphic to the following group of matrices

$$O_{d+1,1}^\uparrow(\mathbb{R}) = \{\mathbf{M} \in GL_{d+2}(\mathbb{R}) \mid \mathbf{M}^T \mathbf{Q}_{d+2} \mathbf{M} = \mathbf{Q}_{d+2} \quad \text{and} \quad \mathbf{M}_{d+2,d+2} > 0\} \quad (1.13)$$

where the isomorphism is obtained by applying Eq. (1.7), which gives the map

$$s_b \mapsto \mathbf{I}_{d+2} - 2\mathbf{i}(b)\mathbf{i}(b)^T \mathbf{Q}_{d+2} \quad (1.14)$$

where s_b is the inversion on the boundary of $b \in \text{Balls}(\widehat{\mathbb{R}}^d)$ and \mathbf{I}_{d+2} is the identity matrix of size $d+2$.

1.1.5.2 Polyspherical coordinates

These coordinates were introduced by Boyd in [14]. Let $\mathcal{B} = \{\mathbf{x}_1, \dots, \mathbf{x}_{d+2}\}$ be a basis of $\mathbb{L}^{d+1,1}$. The *polyspherical coordinates* of a vector $\mathbf{x} \in \mathbb{L}^{d+1,1}$ with respect to \mathcal{B} , are the column matrix

$$\mathbf{p}_{\mathcal{B}}(\mathbf{y}) = \left(\langle \mathbf{x}_1, \mathbf{y} \rangle \quad \cdots \quad \langle \mathbf{x}_{d+2}, \mathbf{y} \rangle \right)^T \quad (1.15)$$

The polyspherical and Cartesian coordinates with respect to \mathcal{B} are related by

$$\mathbf{c}_{\mathcal{B}}(\mathbf{x}) = \text{Gram}(\mathcal{B})^{-1} \mathbf{p}_{\mathcal{B}}(\mathbf{x}) \quad (1.16)$$

By combining Equations (1.3) and (1.16), we can compute the Lorentzian product in polyspherical coordinates by

$$\langle \mathbf{x}, \mathbf{y} \rangle = \mathbf{p}_{\mathcal{B}}(\mathbf{x})^T \text{Gram}(\mathcal{B})^{-1} \mathbf{p}_{\mathcal{B}}(\mathbf{y}) \quad (1.17)$$

In practice, we shall use Eq. (1.17) to compute the inversive product in a different basis.

Remark 2. *In the literature, the most used system of coordinates is the augmented-curvature-center coordinates introduced by Graham et al. in [45]. This system of coordinates shall not be used in this manuscript.*

1.1.6 Packings

We shall say that an arrangement of d -balls \mathcal{B} is a *d-ball packing* if every two $b_i, b_j \in \mathcal{B}$ are either externally tangent or disjoint. The *tangency graph* of a \mathcal{B} is the simple graph where the vertices represent the d -balls and the edges represent the tangency relations. Reciprocally, a simple graph G is said to be *d-ball packable* if there is a d -ball packing \mathcal{B}_G whose tangency graph is G [21]. If G is d -ball packable then G admits an embedding in $\widehat{\mathbb{R}}^d$ which is obtained by taking the centers of the d -balls of \mathcal{B}_G and the straight segments between the centers of any tangent pair (see Figure 1.3). This embedding is usually called the *carrier* of the d -ball packing. The Möbius Group preserves tangency graphs and maps carriers to carriers [98].

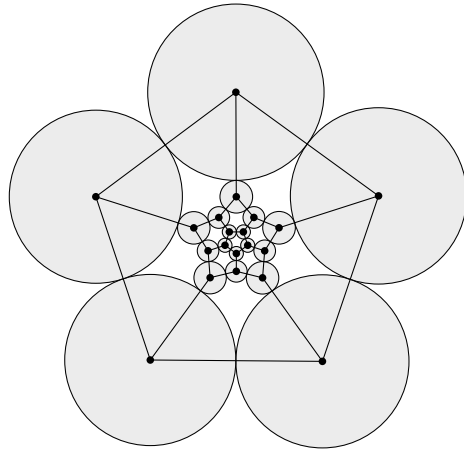


Figure 1.3: A circle packing with its carrier.

In this manuscript, we shall study d -ball packings for $d = 2, 3$. Following the tradition, we shall refer to them as *circle* and *sphere* packings, respectively. Circle packable graphs were fully characterized in 1936 by Koebe [61]. The latter was rediscovered by Thurston by using some results of Andreev on hyperbolic 3-polytopes. The well-known Koebe-Andreev-Thurston Circle Packing Theorem (KAT theorem) is stated below. For a detailed survey on the applications of the KAT theorem we refer the readers to a paper of Bowers [13].

Theorem 1.1.1 (KAT theorem). *A graph G is circle packable if and only if G is simple and planar. Moreover, if G is a triangulation of S^2 , then all the circle packings whose tangency graph is G are equivalent under Möbius transformations.*

The KAT theorem implies that the family of d -ball packable graphs is fully characterized for $d = 1, 2$. Such characterization is still unknown nowadays when $d \geq 3$. Indeed, d -ball packable graphs are closely related to the $(d - 1)$ -ball packable graphs which can be made by $(d - 1)$ -balls of the same size. It has been proved that the recognition of the tangency graphs of circle packings made by equal disks (and more generally disks with a bounded ratio between all the curvatures) is NP-hard (see [15, 50]). However, many properties of sphere packable graphs have been found (see [66, 73, 75, 8, 23]).

A packing \mathcal{B} is said to be *standard* if it contains the half-spaces $b_i = \{x_d \geq 1\}$ and $b_j = \{x_d \leq -1\}$. We denote this property by $[\mathcal{B}]_j^i$. We notice that the tangency

point $b_i \cap b_j$ is at the infinity and the rest of the d -balls of $[\mathcal{B}]_j^i$ must lie inside the region $\{-1 \leq x_d \leq 1\}$. For any d -ball packing \mathcal{B} whose tangency graph contains at least one edge ij , a Möbius transformation $\phi : \mathcal{B} \mapsto [\mathcal{B}]_j^i$ will be called a *standard transformation*. Standard transformations exist for every edge ij of G and they can be obtained as the product of an inversion in a d -ball centered at the tangency point $b_i \cap b_j$, a Euclidean isometry and a rescaling of \mathbb{R}^d (see Fig. 1.4).

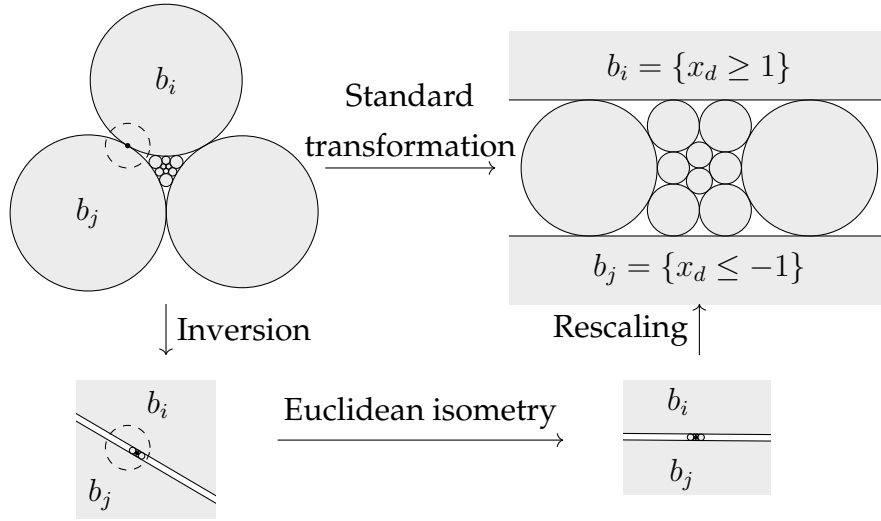


Figure 1.4: Example of a standard transformation.

1.1.7 Möbius uniqueness of d -ball packable graphs

We say that two d -ball packings are *Möbius equivalent* if one can be sent to the other by a Möbius transformation. If such a Möbius transformation is a Euclidean isometry then we say that the two packings are *Euclidean congruent*. A d -ball packable graph G will be *Möbius unique* if all the d -ball packings whose tangency graph is G are Möbius equivalent. A useful result to detect Möbius uniqueness is the following:

Lemma 1.1.1. *Let \mathcal{B}_G and \mathcal{B}'_G be two d -ball packings with same tangency graph G and let ij be an edge of G . Then \mathcal{B}_G and \mathcal{B}'_G are Möbius equivalent if and only if $[\mathcal{B}_G]_j^i$ and $[\mathcal{B}'_G]_j^i$ are Euclidean congruent.*

Proof. Let $\phi : \mathcal{B}_G \mapsto [\mathcal{B}_G]_j^i$ and $\psi : \mathcal{B}'_G \mapsto [\mathcal{B}'_G]_j^i$ be two standard transformations.

(Sufficiency) If there is a Euclidean isometry $\gamma : [\mathcal{B}_G]_j^i \mapsto [\mathcal{B}'_G]_j^i$ then $\psi^{-1} \circ \gamma \circ \phi$ defines a Möbius transformation mapping \mathcal{B}_G to \mathcal{B}'_G .

(Necessity) Let us suppose that there is a Möbius transformation $\mu : \mathcal{B}_G \mapsto \mathcal{B}'_G$. Then $\theta := \psi \circ \mu \circ \phi^{-1}$ is a Möbius transformation mapping $[\mathcal{B}_G]_j^i$ to $[\mathcal{B}'_G]_j^i$ and leaving fixed the half-spaces b_i and b_j . Therefore, θ is generated by inversions on d -balls which are simultaneously orthogonal to b_i and b_j . A d -ball simultaneously orthogonal to two parallel half-spaces must also be a half-space. Therefore, θ can be expressed as a product of Euclidean reflections so θ is a Euclidean isometry. \square

1.2 Preliminaries on knot theory

The main results and notations were adapted from the classic books of Adams [1] and Cromwell [30].

1.2.1 Diagrams of knots and links

A *link* L with n components consists of n disjoint simple closed curves in $\widehat{\mathbb{R}}^3$ (or \mathbb{S}^3). A *knot* K is a link with one component. Two links are said to be *equivalent* if there is an ambient isotopy of $\widehat{\mathbb{R}}^3$ which carries one to the other. A *link diagram* \mathcal{L} is a regular projection of a link L onto a plane in such a way that the projection of each component is smooth and at most two curves intersect at any point. At each crossing point of the link diagram, the curve which goes under the other is specified by deleting a small neighbourhood as in Figure 1.5. The *crossing number* of a L , denoted by $cr(L)$, is the minimum number of crossings among all the diagrams of links which are equivalent to L .

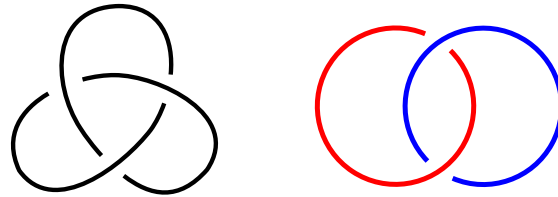


Figure 1.5: (Left) A knot diagram of the *trefoil* (denoted by 3_1 in the Alexander–Briggs notation): the simplest non-trivial knot, (right) a link diagram of the *Hopf link* (denoted by 2_1^2): the simplest non-trivial link.

A link diagram \mathcal{L} is said to be:

- (i) *alternating* if the crossings in the diagram alternate between under and over-passes when one travels along each component.
- (ii) *reduced* if it has no *nugatory crossings* (also called *reducible* or *removable* crossings). Those are, crossings in the diagram such that a closed curve can be drawn meeting the diagram transversely at that crossing, but not meeting the diagram at any other point.

A link L is said to be:

- (i) *alternating* if it admits an alternating diagram.
- (ii) *trivial* if it is equivalent to a link admitting a diagram without crossings. Otherwise, L is said to be *nontrivial*.
- (iii) *splittable* if a plane can be embedded in $\widehat{\mathbb{R}^3}$ such that it separates one or more components of L . Otherwise, L is *nonsplittable*.
- (iv) *amphichiral* if L is equivalent to its *mirror*, i.e. the link obtained from L after applying a reflection. Otherwise, L is *chiral*.

The main result concerning the crossing number of alternating links was conjectured by Tait [99] and proved independently by Kauffman [59], Murasugi [77] and Thistlethwaite [100].

Theorem 1.2.1 (Tait’s conjecture on the crossing number). *Reduced alternating diagrams have the minimum number of crossings.*

1.2.2 Tangles

A n -tangle is a pair (\mathcal{U}, t) where \mathcal{U} is a compact set of \mathbb{R}^3 homeomorphic to a 3-ball and t is a collection $\{\gamma_1, \gamma_2, \dots, \gamma_m\}$ of $1 \leq n \leq m$ disjoint arcs contained in \mathcal{U} satisfying the following conditions:

- (1) For every $1 \leq i \leq m$, γ_i is closed if and only if $i > n$.
- (2) The endpoints of γ_i for every $1 \leq i \leq n$ lie on $\partial\mathcal{U}$ (these are called the *endpoints* of the tangle).

Two n -tangles (\mathcal{U}, t) and (\mathcal{U}', t') are said to be *equivalent* if there is an isotopy of \mathbb{R}^3 carrying \mathcal{U} to \mathcal{U}' , t to t' and the endpoints of (\mathcal{U}, t) to the endpoints of (\mathcal{U}', t') . We shall denote this equivalence relation $t \simeq t'$. Up to equivalence, we may consider that the endpoints of t lie on a same plane H . A *tangle diagram* of (\mathcal{U}, t) is a regular projection of t on H , together with $\mathcal{U} \cap H$ and the crossing information (see Fig. 1.6). The equivalence of tangles corresponds to the equivalence of their tangle diagrams via Reidemeister's moves [30]. In order to simplify the notation, we shall refer to a tangle (\mathcal{U}, t) by t when there is no ambiguity. From now on, we shall focus our attention on 2-tangles and their derived constructions. We shall name the endpoints in a 2-tangle diagram by the cardinal points NE, NW, SE and SW.

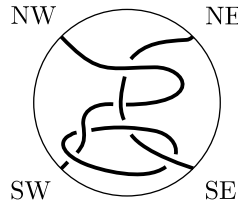


Figure 1.6: A 2-tangle diagram.

The *elementary tangles* t_0 , t_1 and t_∞ are the 2-tangles given in the Figure 1.7.

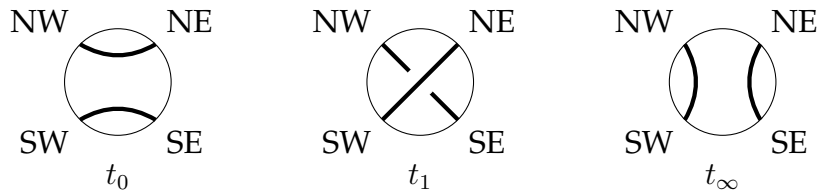


Figure 1.7: The elementary tangles.

Let us now recall some classic operations of 2-tangles. For any 2-tangles t and t' we have the following binary operation

- (i) the *sum* $t + t'$, obtained by connecting the East endpoints of t to the West endpoints of t' ,

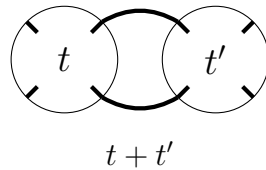


Figure 1.8: Sum of tangles.

and the unary operations:

- (ii) the *mirror* $-t$ is the image of t under the reflection on the plane containing the equator,
 (iii) the *flip* $F(t)$ is the image of t under the reflection on the plane perpendicular to the equator and passing through the endpoints SW and NE,
 (iv) the *positive half-twist* $H^+ : t \mapsto t_1 + t$,
 (v) the *negative half-twist* $H^- : t \mapsto -t_1 + t$.

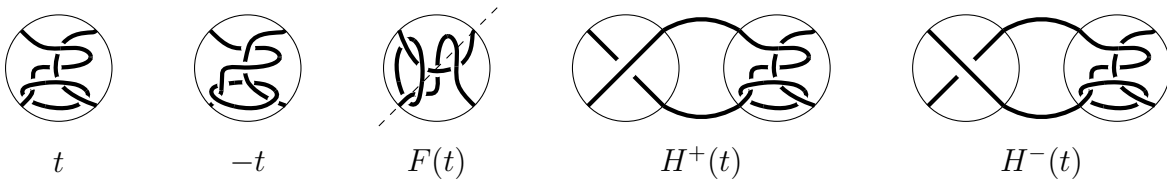


Figure 1.9: Unary operations of tangles.

The *closure* of a 2-tangle (\mathcal{U}, t) is the link formed by joining the endpoints by two disjoint and unlinked paths at the exterior of \mathcal{U} . Up to equivalence, there are two possible closures, the *numerator* $N(t)$, obtained by joining the northern and the

southern endpoints separately, and the *denominator* $D(t)$, obtained by joining the western and the eastern endpoints (Fig. 1.10).

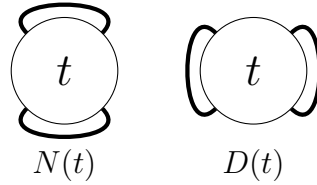


Figure 1.10: The tangle closures.

1.2.3 Rational tangles

Rational tangles were introduced by Conway in his work on enumerating and classifying knots and links [26]. For a given sequence of integers a_1, \dots, a_n all non-zero except maybe a_1 , we denote by $t(a_1, \dots, a_n)$ the *rational tangle* given as follows by Conway's algorithm

$$t(a_1, \dots, a_n) := M(a_1) \circ \dots \circ M(a_n)(t_\infty) \quad \text{where } M(a_i) := \begin{cases} (H^+)^{a_i} F & \text{if } a_i \geq 0 \\ (H^-)^{-a_i} F & \text{if } a_i < 0 \end{cases} \quad (1.18)$$

An example of a rational tangle is illustrated in Fig. 1.11.

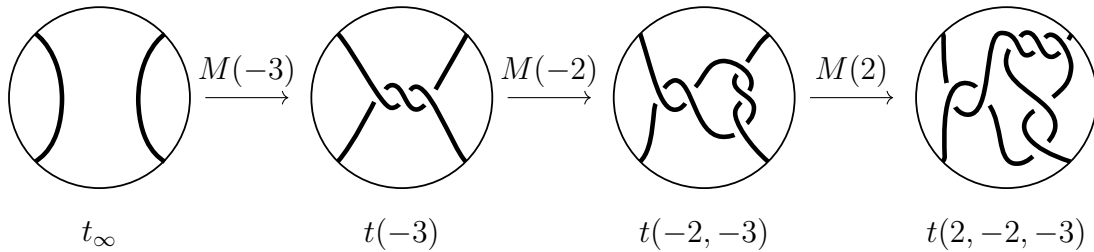


Figure 1.11: The rational tangle $t(2, -2, -3)$ obtained by Conway's algorithm.

The *fraction* of a rational tangle $t(a_1, \dots, a_n)$ is the continued fraction

$$\frac{p}{q} := a_1 + \frac{1}{a_2 + \frac{1}{\ddots + \frac{1}{a_n}}} \quad (1.19)$$

In Conway's famous paper on tangles [26], he gave a full characterization of rational tangles.

Theorem 1.2.2 (Conway). *Two rational tangles $t(a_1, \dots, a_n)$ and $t(b_1, \dots, b_m)$ are equivalent if and only if*

$$a_1 + \frac{1}{a_2 + \frac{1}{\dots + \frac{1}{a_n}}} = b_1 + \frac{1}{b_2 + \frac{1}{\dots + \frac{1}{b_m}}}$$

The origin of the name of *rational tangle* came from the connection established by Conway's theorem, between the family of tangles produced by the Conways' algorithm and the rational numbers. We denote by $t_{p/q}$ the class of the rational tangles with fraction p/q under tangle equivalence. When all a_i have the same sign in $t(a_1, \dots, a_n)$, then the corresponding tangle diagram is alternating. Since there is always a continued fraction expansion of p/q in which all the coefficients have the same sign [30], then $t_{p/q}$ always has an alternating tangle diagram.

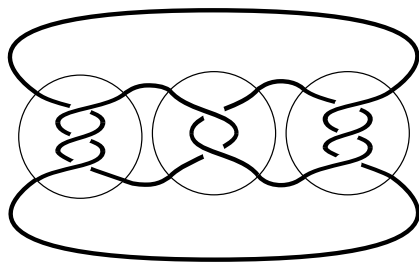
Following Conway's definition, a *rational link* is the closure of a rational tangle. Rational links are also the *2-bridge links*, i.e. links admitting a representation such that the natural height function given by the z-coordinate has only two maxima and two minima as critical points [30]. We shall denote by $C(a_1, \dots, a_n)$ the rational link obtained by the closure of $t(a_1, \dots, a_n)$ (numerator closure if $a_1 \neq 0$ and denominator closure otherwise). By the above discussion, rational links are alternating. Moreover, Theorem 1.2.1 gives

$$a_i > 0, \text{ for every } 1 \leq i \leq n \quad \Rightarrow \quad \text{cr}(C(a_1, \dots, a_n)) = a_1 + \dots + a_n \quad (1.20)$$

Tangles which are obtained by sums and flips of rational tangles are called *algebraic tangles* [1]. Equivalently, links which are obtained by the closure of algebraic tangles are said to be *algebraic* or *arborescent* [42]. A *Pretzel link* (or knot) $P(a_1, \dots, a_n)$ is a particular case of algebraic link defined by

$$P(a_1, \dots, a_n) := N(F(t(a_1)) + \dots + F(t(a_n))) \quad (1.21)$$

We show in Figure 1.12 the Pretzel knot $P(3, -2, 3)$ which corresponds to the knot 8_{19} in the Alexander-Briggs notation [30].

Figure 1.12: The Pretzel knot $P(3, -2, 3)$.

1.2.4 Braids

We consider *oriented* tangles by giving an orientation to the arcs. The endpoints of an oriented tangle (\mathcal{U}, t) shall be called *inputs* or *outputs* according to the orientations. By convention, we shall represent \mathcal{U} by a rectangle in the tangle diagrams, where the orientation will be read from the bottom to the top. An oriented n -tangle (\mathcal{U}, t) is *monotone* if every arc of t never goes back. Thus, a monotone n -tangle does not have closed arcs.

Definition 1.2.1. *A braid of n strands (or n -braid) is a monotone-oriented n -tangle.*

The *closure* of an n -braid is defined by labelling the inputs and the outputs in linear ordering from 1 to n , and then connecting outputs and inputs with the same label by unlinked oriented arcs (Fig. 1.13). One might ask if every link can be represented as the closure of a n -braid. The well-known Alexander's Theorem gives a positive answer [3].

Theorem 1.2.3 (Alexander). *For any link L there is a closed n -braid equivalent to L .*

The minimum number n satisfying the Alexander's Theorem is called the *braid index* of L , and the minimum number of crossings among all the braids representing L is called the *braid length* [102]. We shall represent closed n -braids by diagrams in a square-grid with the crossings lying in the interior of the squares and we shall call these diagrams *square-grid diagrams* (Fig. 1.13). It is easy to see that every closed braid admits a square-grid diagram.

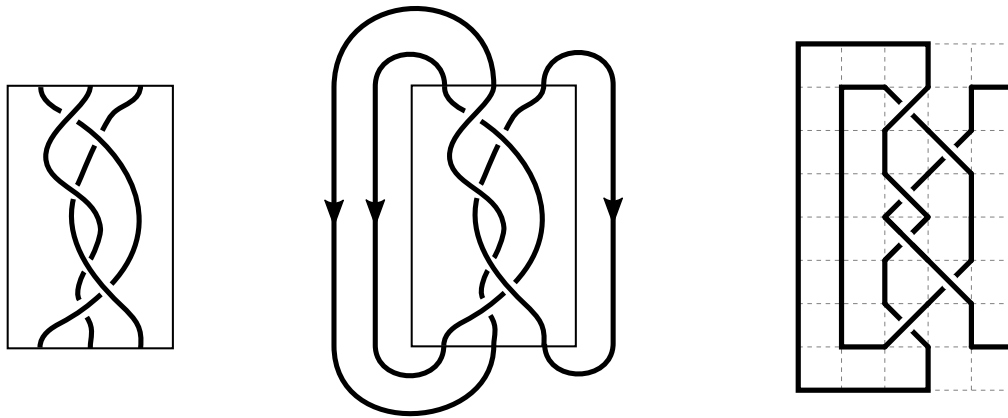


Figure 1.13: A 3-braid (left), its closure (center) and the corresponding square-grid diagram (right).

1.2.5 Polygonal representations

A natural way to better understand knots and links is by representing them as closed polygonal curves in the space. Polygonal representations of links have been of great interest not only in mathematics, but also in chemistry and physics in the study of molecular chains such as DNA and proteins [34, 78]. Moreover, by adding more restrictions to polygonal representations, we can endow more geometric structures to knots. *Lattice representations* are a particular case of polygonal representations where all the vertices have integer coordinates in the space. These representations have been useful to study geometric knot invariants such as the *rope length*, defined as the minimal length needed of a rope with a fixed thickness in order to form a given knot [51]. We define a *necklace representation* of a link as a polygonal representation which is contained in the carrier of a sphere packing. We show in Figure 1.14 an arbitrary polygonal, lattice and necklace representation of the trefoil knot.

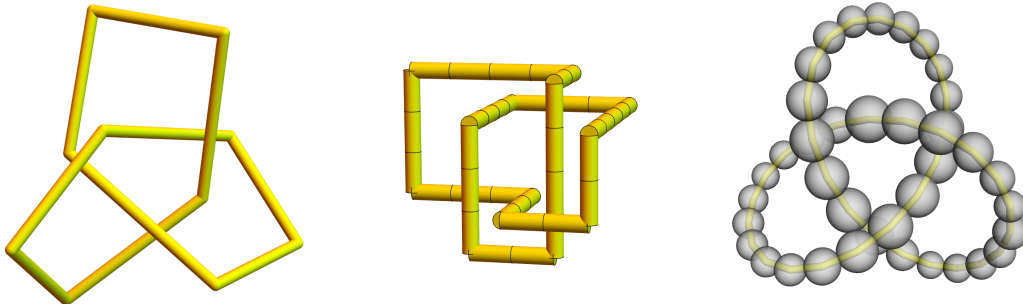


Figure 1.14: A polygonal representation (left), a lattice representation (center) and a necklace representation (right) of the trefoil knot.

Necklace representations of links have been appearing recently in the study of the hyperbolic volume of hyperbolic 3-manifolds [41]. There are also other geometric knot invariants, which are defined for minimal polygonal representations. The *stick number* and the *lattice stick number* of a link L are defined as the minimum number of segments needed to construct a polygonal and lattice representation of L , respectively. In [72], Maehara introduced the *ball number* of a link L , denoted by $\text{ball}(L)$, as the minimum number of spheres needed to construct a necklace representation of L . Little is known about the behavior of the ball number with respect to other geometric invariants. For instance, the stick number of the trefoil knot and the Hopf link is known to be 6 in both cases (see [2] for a nice proof for the trefoil), while their lattice stick number is 12 and 8, respectively [55, 53]. By contrast, Maehara proved that the ball number of the Hopf link is 8, but the ball number of the trefoil is, nowadays, not known. Maehara conjectured that $\text{ball}(3_1) = 12$, and he and Oshiro showed that $9 \leq \text{ball}(3_1) \leq 12$ [75, 72]. As far as we are aware, these are the only known results concerning the ball numbers of links. We show in Fig. 1.15 a minimal polygonal, lattice and necklace representations of the trefoil that are known.

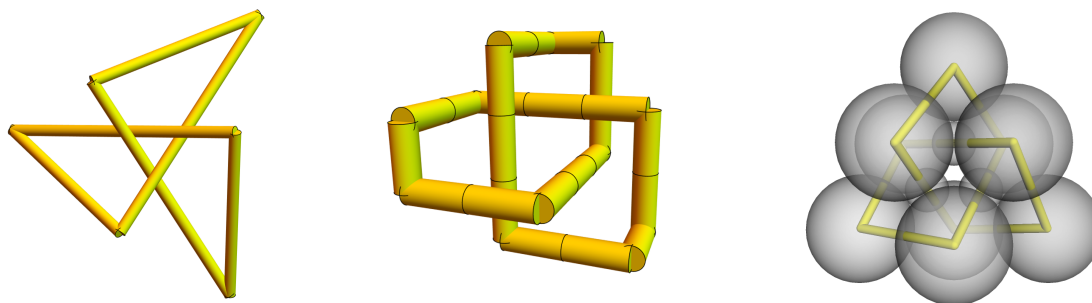


Figure 1.15: From left to right: a minimal polygonal representation with 6 segments, a minimal lattice representation with 12 segments [32] and a conjectured minimal necklace representation with 12 spheres [75] of the trefoil knot.

Linear upper bounds on the stick and the lattice stick number in terms of the crossing number have been found [52, 80, 17, 56]. In Chapters 2 and 6, we shall present different methods of construction of necklace representations. The first gives a linear upper bound on the ball number of nonsplittable and nontrivial links, in terms of the crossing number. The last method will improve this upper bound for rational links with the help of the polytopal sphere packings introduced in Chapter 3.

An upper bound on the ball number

Contents

2.1	Introduction	27
2.2	From links to circle packable graphs	28
2.3	Square-pyramidal disk arrangements	29
2.4	The crossing sphere arrangement	33
2.5	The proof of the upper bound	36
2.6	An algorithm for knotted necklaces	40

2.1 Introduction

In this chapter, we present the following upper bound on the ball number.

Theorem 2.1.1. *For any nontrivial and nonsplittable link L , we have that*

$$\text{ball}(L) \leq 5\text{cr}(L)$$

Let us give a sketch of the proof. We start by considering a minimal crossing diagram of a link L . Then, we construct a simple planar graph with $3\text{cr}(L)$ vertices containing a subgraph admitting a planar embedding isotopically equivalent to a planar projection of L . By applying the KAT theorem, and then the inflate operation, we shall construct a sphere packing whose carrier contains the previous planar projection of L . Finally, for each crossing of the planar projection, we reconstruct the projected crossing by adding two spheres that serve as a "bridge", and in this way,

we obtain a necklace representation of L with $5cr(L)$ spheres.

Given the connection of the ball number with KAT Theorem, a linear bound seems inevitable. The main difficulty in the method described above is to show that two spheres are enough to form the bridges, independently of the chosen link.

2.2 From links to circle packable graphs

Every link diagram \mathcal{L} with at least one crossing leads to a 4-regular planar graph $G_{\mathcal{L}}$ where the vertices are the crossings and the edges are the arcs joining the crossings. This graph is not simple in general (see Fig. 2.1). On the other hand, the *medial graph* of a planar graph G , denoted $med(G)$, is constructed by placing one vertex on each edge of G and joining two vertices if the corresponding edges are consecutive on a face of G . Medial graphs are 4-regular planar graphs but may have loops or multiple edges (see Fig. 2.1 (c)). We define the *simplified medial graph* of G , denoted by $\underline{med}(G)$, the simple planar graph obtained from $med(G)$ by deleting loops and multiple edges. Finally, we define the *patchwork graph* of \mathcal{L} , denoted by $P(\mathcal{L})$, as the simple planar graph given by the simultaneous drawing of $G_{\mathcal{L}} \cup \underline{med}(G_{\mathcal{L}})$. The set of vertices of $P(\mathcal{L})$ can be divided in two sets: V_{\times} , the vertices of $G_{\mathcal{L}}$ (colored in white in Fig. 2.1) and V_m , the vertices of $\underline{med}(G_{\mathcal{L}})$ (colored black in Fig. 2.1). We call the vertices of V_{\times} the *crossing vertices*.

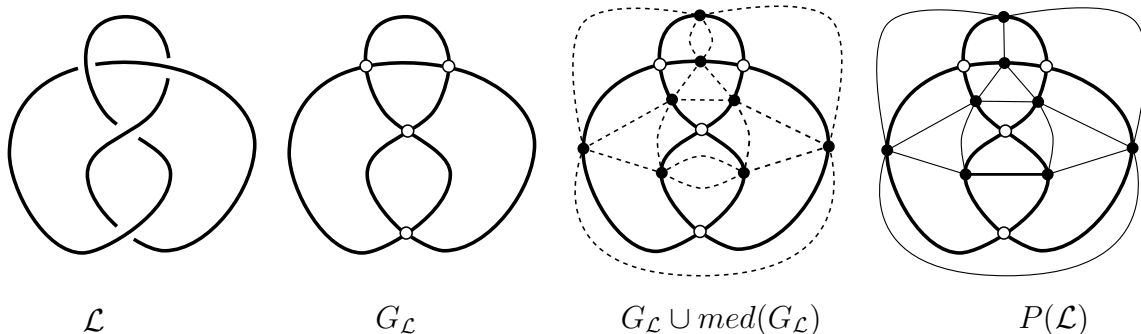


Figure 2.1: From left to right: a diagram of the *Figure-eight knot*, the graph obtained from the diagram, same graph drawn with its medial graph and the patchwork graph of the initial knot diagram.

Let us suppose that $G_{\mathcal{L}}$ is connected and it has no loops. Since $G_{\mathcal{L}}$ is 4-regular, the subgraph of $P(\mathcal{L})$ induced by a crossing vertex and its 4 neighbors is the 1-skeleton of a square-pyramid. We shall call this graph the *square-pyramidal graph*. In the case considered, $P(\mathcal{L})$ can be obtained as the union of n square-pyramidal graphs, where n is the number of crossings of \mathcal{L} . Therefore, we have

$$|V(P(\mathcal{L}))| = |V_{\times}| + |V_m| = n + \frac{1}{2}(4n) = 3n \quad (2.1)$$

2.3 Square-pyramidal disk arrangements

Square-pyramidal graphs are one of the building blocks for constructing the desired necklace representations. From now on, we shall consider square-pyramidal graphs \boxtimes with the labelling on the vertices depicted in Figure 2.2.

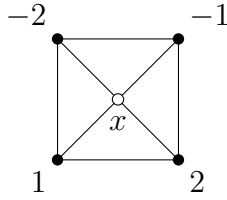


Figure 2.2: The labelling of a square-pyramidal graph \boxtimes .

We say that a circle packing is *square-pyramidal* if its tangency graph is the square-pyramidal graph. As we show below, square-pyramidal graphs are not Möbius unique, that is, there are square-pyramidal circle packings which are not Möbius equivalent. Therefore, all the properties of square-pyramidal circle packings and the added structures must be carefully verified in each equivalence class under Möbius transformations. In the following proposition, we describe the Moduli space \mathcal{M}_{\boxtimes} of all the square-pyramidal circle packings under Möbius transformations.

Proposition 2.3.1. \mathcal{M}_{\boxtimes} is a family of one real parameter.

Proof. Let $[\mathcal{D}_{\boxtimes}]_x^{-1}(\kappa_1) = \{d_x, d_1, d_2, d_{-1}, d_{-2}\}$ be a standard square-pyramidal circle packing where d_2 and d_{-2} are two unit disks tangent to the half-spaces $d_{-1} = \{y \geq 1\}$, $d_x = \{y \leq -1\}$ and d_1 is a disk of curvature $\kappa_1 \in \mathbb{R}$ tangent to d_2, d_{-2} and d_x .

We have that $1 < \kappa_1 < 4$. Indeed, when $\kappa_1 < 1$ (resp. $\kappa_1 > 4$), the disks d_1 and d_{-1} (resp. d_2 and d_{-2}) overlap and, when $\kappa_1 = 1$ (resp. 4), d_1 and d_{-1} (resp. d_2 and d_{-2}) are tangent so the tangency graph would be other than \boxtimes (see Figure 2.3). We notice that the collection of circle packings $\{[\mathcal{D}_{\boxtimes}]_x^{-1}(\kappa_1)\}_{1 < \kappa_1 < 4}$ are Euclidean non-congruent. Therefore, by Lemma 1.1.1, they represent different equivalence classes in \mathcal{M}_{\boxtimes} . Moreover, these are the only possible standard square-pyramidal circle packings under Euclidean isometries. Hence, \mathcal{M}_{\boxtimes} is in bijection to the open interval $(1, 4)$. \square

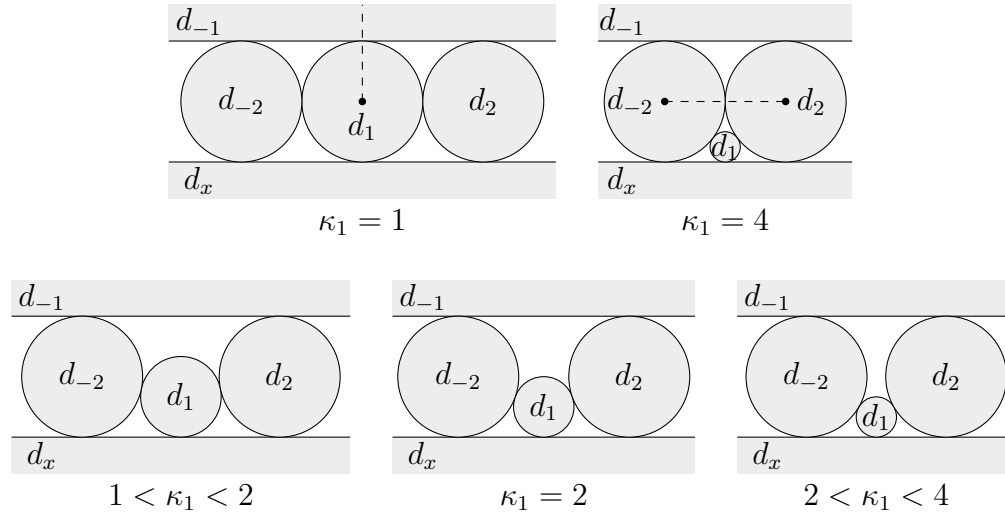


Figure 2.3: Extreme cases with an extra edge (top figures) and the equivalence classes of $\mathcal{M}^2(\boxtimes)$ (bottom figures).

We define, for every $i = 1, 2, -1, -2$, the *standard curvatures* of a square-pyramidal circle packing \mathcal{D}_{\boxtimes} as the real numbers $1 < \kappa_i < 4$ corresponding to the curvature of the disk $d_i \in [\mathcal{D}_{\boxtimes}]_x^{-i}$. The standard curvatures can be used to identify the equivalence class of \mathcal{D}_{\boxtimes} in \mathcal{M}_{\boxtimes} . We define also the *smaller standard curvature*

$$\kappa := \min\{\kappa_1, \kappa_2, \kappa_{-1}, \kappa_{-2}\}$$

We define a *square-pyramidal disk arrangement* as the collection of disks $(\mathcal{D}_{\boxtimes}, d_1^*, d_2^*, d_t)$ formed by

- $\mathcal{D}_{\boxtimes} = \{d_x, d_1, d_2, d_{-1}, d_{-2}\}$: a square-pyramidal circle packing.
- The *mirror disks* d_1^* and d_2^* where d_1^* is the disk orthogonal to d_2, d_{-2}, d_x and $d_1 \subset d_1^*$; d_2^* is the disk orthogonal to d_1, d_{-1}, d_x and $d_2 \subset d_2^*$ (see Figure 2.4).
- The *tangency disk* d_t : the disk whose boundary passes through all the tangency points of d_1, d_2, d_{-1} and d_{-2} , and satisfies $d_x \subset d_t$.

Lemma 2.3.1. *For any square-pyramidal disk arrangement, the mirror disks and the tangency disk are well-defined.*

Proof. We first prove the Lemma for the standard $[\mathcal{D}_{\boxtimes}]_x^{-1}(\kappa_1)$ which appears in the Figure 2.4.

The orthogonality conditions of d_1^* imply that the boundary of d_1^* must be the circle with center $(0, -1)$ which passes through the tangency point $d_x \cap d_2$. The orientation of the interior is determined by the condition $d_1 \subset d_1^*$.

For d_2^* , a disk orthogonal to d_1, d_{-1} and d_x must be a half-space with the y -axis as boundary. As before, the orientation of the interior comes from the condition $d_2 \subset d_2^*$ which gives that d_2^* is the half-space $\{x \geq 0\}$.

For d_t , by symmetry, the only circle passing through the tangency points $d_1 \cap d_2, d_1 \cap d_{-2}$ and $d_{-1} \cap d_2$ must pass through $d_{-1} \cap d_{-2}$. Again, the orientation is determined by the condition $d_x \subset d_t$.

It is clear that the previous arguments work for any standard $[\mathcal{D}_{\boxtimes}]_x^{-1}(\kappa_1)$ with $1 < \kappa_1 < 4$. Since the conditions defining the mirror disks and the tangency disks are preserved under Möbius transformations, the Lemma is also true for the class of $[\mathcal{D}_{\boxtimes}]_x^{-1}(\kappa_1)$ in \mathcal{M}_{\boxtimes} , for any $1 < \kappa_1 < 4$. As is shown in the proof of Proposition 2.3.1, the union of all the classes contains all the square-pyramidal circle packings. \square

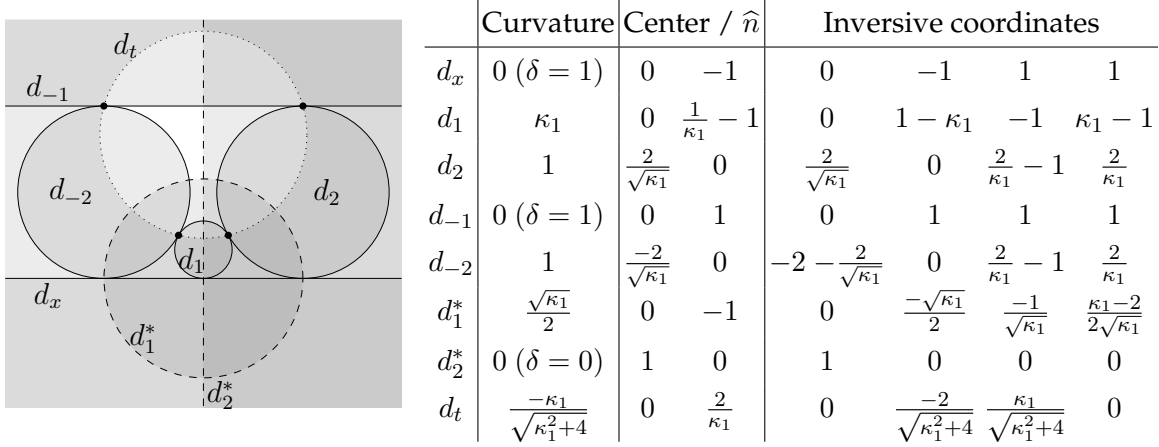


Figure 2.4: (Left) The square-pyramidal disk arrangement containing the standard $[\mathcal{D}_{\boxtimes}]_x^{-1}(\kappa_1)$ with the center of d_1 lying on the y -axis. (Right) Curvature, center and inversive coordinates of the disk in terms of the curvature of d_1 .

Lemma 2.3.2. *The following relations hold for every square-pyramidal disk-arrangement $(\mathcal{D}_{\boxtimes}, d_1^*, d_2^*, d_t)$ and for every $i = 1, 2$:*

- (a) $\langle d_i, d_{-i} \rangle = -1 - 2\kappa_i = -1 - \frac{8}{\kappa_j}$ with $i \neq j$.
- (b) $\kappa_i = \kappa_{-i}$.
- (c) $\kappa_1 \kappa_2 = 4$.
- (d) $-7 < \langle d_i, d_{-i} \rangle < -1$.
- (e) $(1 - \langle d_1, d_{-1} \rangle)(1 - \langle d_2, d_{-2} \rangle) = 16$.
- (f) $\partial d_t \subset d_1 \cup d_2 \cup d_{-1} \cup d_{-2}$.
- (g) d_1^*, d_2^* and d_t are mutually orthogonal.
- (h) $s_{d_i^*}(d_j) = \begin{cases} d_{-j} & \text{if } i = |j| \\ d_j & \text{otherwise} \end{cases}$ for every $j \in \{1, 2, -1, -2, t\}$.

Proof. The relations can be obtained by simple calculations by using the inversive coordinates given in Fig. 2.4. □

The equalities (a), (b) and (c) tell us that a square-pyramidal circle packing has essentially two different standard curvatures κ_1 and κ_2 which are inversely proportional and the smaller standard curvature must verify $1 < \kappa \leq 2$. We define the *closest disjoint pair* of \mathcal{D}_\boxtimes as the disjoint pair $\{d_i, d_{-i}\}$ satisfying that $\kappa = \kappa_i$. The other disjoint pair will be called *the farthest disjoint pair*. In the following we use the indices $\{d_c, d_{-c}\}$ and $\{d_f, d_{-f}\}$ with $\{c, f\} = \{1, 2\}$ and $c \neq f$ to denote the closest and the farthest disjoint pair of \mathcal{D}_\boxtimes . By convention, we define $c = 1$ and $f = 2$ when $\kappa_1 = \kappa_2$.

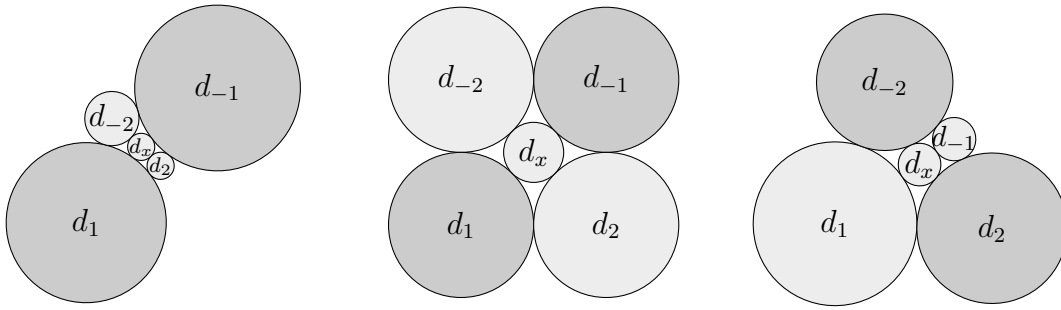


Figure 2.5: The closest disjoint pairs in darker gray in three different cases: (left) $\kappa = \kappa_1 = 1.33$ (center) $\kappa = \kappa_1 = \kappa_2 = 2$ (right) $\kappa = \kappa_2 = 1.6$.

2.4 The crossing sphere arrangement

We define a *square-pyramidal sphere packing* \mathcal{B}_\boxtimes as a sphere packing obtained by inflating a square-pyramidal circle packing. We define equivalently the closest and farthest disjoint pairs as in the planar case. Let $(\mathcal{D}_\boxtimes, d_1^*, d_2^*, d_t)$ be a square-pyramidal disk arrangement. We define, for every $\varepsilon \in \{+, -\}$, the *crossing sphere arrangement* $(\mathcal{B}_\boxtimes, b_1^*, b_2^*, b_t, b_{\varepsilon 3}, b'_{\varepsilon 3})$ as the arrangement of oriented spheres formed by:

- The *square-pyramid sphere packing* \mathcal{B}_\boxtimes obtained by inflating \mathcal{D}_\boxtimes .
- The *mirror spheres* b_1^* and b_2^* : the inflating of the mirror disks d_1^* and d_2^* respectively.
- The *tangency sphere* b_t : the inflating of the tangency disk d_t .
- The *bridge spheres* $b_{\varepsilon 3}$ and $b'_{\varepsilon 3}$ where:

- (i) $b_{\varepsilon 3}$ is the unique sphere externally tangent to b_c, b_f, b_x , internally tangent to b_c^* and contained in the half-space $\{\varepsilon z \geq 0\}$, where $\{b_c, b_{-c}\}$ and $\{b_f, b_{-f}\}$ denotes the closest and the farthest pair of \mathcal{B}_{\boxtimes} .
- (ii) $b'_{\varepsilon 3}$ is the sphere obtained by the inversion of $b_{\varepsilon 3}$ on the mirror-sphere b_c^* .

We also define the *crossing region* \mathcal{X} of a crossing sphere arrangement as

$$\mathcal{X} := \left(\bigcap_{b \in \mathcal{B}_{\boxtimes}} -b \right) \cap b_t.$$

We show in Figure 2.6 three examples of crossing sphere arrangements with their corresponding crossing regions.

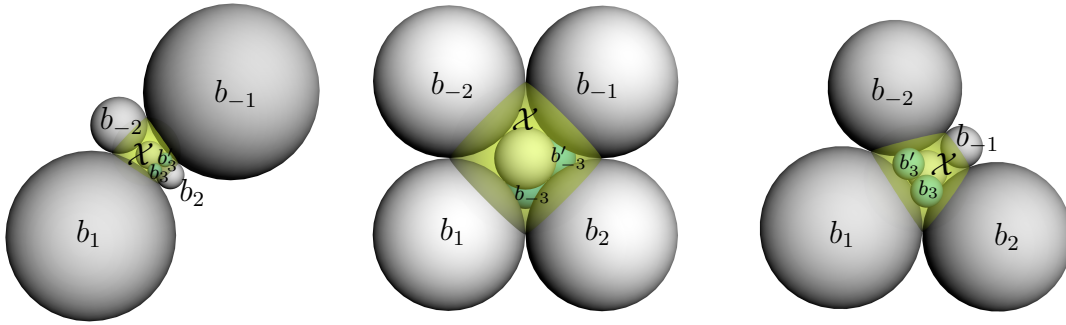


Figure 2.6: The corresponding crossing sphere arrangement of square-pyramidal disk arrangements of Figure 2.5.

Lemma 2.4.1. *Let $(\mathcal{B}_{\boxtimes}, b_1^*, b_2^*, b_t, b_{\varepsilon 3}, b'_{\varepsilon 3})$ be a crossing sphere arrangement. The bridge spheres $b_{\varepsilon 3}$ and $b'_{\varepsilon 3}$ are well-defined for every $\varepsilon \in \{+, -\}$. Moreover, they are externally tangent and both are contained in the crossing region \mathcal{X} .*

Proof. Consider the arrangement of spheres

$$\mathcal{B} = \{b_x, b_c, b_f, b_c^*, b_{\varepsilon z}\}$$

where $\{b_c, b_{-c}\}$ and $\{b_f, b_{-f}\}$ are the closest and the farthest disjoint pair of \mathcal{B}_{\boxtimes} and $b_{\varepsilon z}$ is the half-space $\{\varepsilon z \geq 0\}$. Since the inversive product is preserved by the inflating operation, we can compute the Gramian of \mathcal{B} by using the inversive coordinates given in the Table 2.4 in terms of the smaller standard curvature. For every $1 < \kappa <$

2, we find that $\text{Gram}(\mathcal{B})$ is non-singular and therefore the Lorentzian vectors of \mathcal{B} form a basis of $\mathbb{L}^{4,1}$. Moreover, we have

$$\text{Gram}(\mathcal{B})^{-1} = \frac{1}{2} \begin{pmatrix} \frac{\kappa}{2} & -1 & \frac{\kappa}{2} - 1 & \sqrt{\kappa} & 0 \\ -1 & 0 & -1 & 0 & 0 \\ \frac{\kappa}{2} - 1 & -1 & \frac{\kappa}{2} & \sqrt{\kappa} & 0 \\ \sqrt{\kappa} & 0 & \sqrt{\kappa} & 2 & 0 \\ 0 & 0 & 0 & 0 & 2 \end{pmatrix} \quad (2.2)$$

In order to show that the bridge-spheres are well-defined, we compute the polyspherical coordinates of $b_{\varepsilon 3}$ with respect to \mathcal{B} using the definition of $b_{\varepsilon 3}$ and Eq.(1.5) which gives

$$\mathbf{p}_{\mathcal{B}}(b_{\varepsilon 3}) = \left(-1 \quad -1 \quad -1 \quad 1 \quad \lambda_{z,3} \right)^T \text{ with } \lambda_{z,3} \geq 1 \quad (2.3)$$

By using Eq. (1.17), we can normalize to get $\lambda_{z,3} = \sqrt{3 + 2\sqrt{\kappa} - \kappa} > 1$ for every $1 < \kappa \leq 2$. The latter insures, for every square-pyramidal sphere packing, the existence and the uniqueness of $b_{\varepsilon 3}$, and hence of $b'_{\varepsilon 3} := s_{b_c^*}(b_3)$. Moreover,

$$\begin{aligned} \langle b_{\varepsilon 3}, b'_{\varepsilon 3} \rangle &= \langle b_{\varepsilon 3}, s_{b_c^*}(b_{\varepsilon 3}) \rangle \\ &= \langle b_{\varepsilon 3}, b_{\varepsilon 3} - 2\langle b_{\varepsilon 3}, b_c^* \rangle b_c^* \rangle && \text{by (1.7)} \\ &= 1 - 2\langle b_{\varepsilon 3}, b_c^* \rangle^2 \\ &= -1 \end{aligned}$$

so $b_{\varepsilon 3}$ and $b'_{\varepsilon 3}$ are externally tangent. A sphere b is contained in the crossing region of the crossing sphere arrangement $(\mathcal{B}_{\boxtimes}, b_1^*, b_2^*, b_t, b_{\varepsilon 3}, b'_{\varepsilon 3})$ if and only if

$$\langle b_i, b \rangle \leq -1 \text{ for every } b_i \in \{b_x, b_c, b_f, b_{-c}, b_{-f}\} \text{ and } \langle b_t, b \rangle \geq 1 \quad (2.4)$$

By combining the invariance of the inversive product under inversions and the inflate operation, the intersection angles between the disks of a square-pyramidal disk arrangement and the mirror disks given in Lemma 2.3.2 (h), and the tangency conditions in the definition of $b_{\varepsilon 3}$ we obtain

$$\begin{aligned} \langle b_x, b'_{\varepsilon 3} \rangle &= \langle s_{b_c^*}(b_x), s_{b_c^*}(b'_{\varepsilon 3}) \rangle = \langle b_x, b_{\varepsilon 3} \rangle = -1 \\ \langle b_{-c}, b'_{\varepsilon 3} \rangle &= \langle s_{b_c^*}(b_{-c}), s_{b_c^*}(b'_{\varepsilon 3}) \rangle = \langle b_c, b_{\varepsilon 3} \rangle = -1 \\ \langle b_f, b'_{\varepsilon 3} \rangle &= \langle s_{b_c^*}(b_f), s_{b_c^*}(b'_{\varepsilon 3}) \rangle = \langle b_f, b_{\varepsilon 3} \rangle = -1 \end{aligned}$$

For the rest of inversive products we use Lemma 2.3.2 (h), Eq. (1.17) and the inversive coordinates given in Fig. 2.4.

$$\begin{aligned}
\langle b_c, b'_{\varepsilon 3} \rangle &= \langle s_{b_c^*}(b_c), s_{b_c^*}(b'_{\varepsilon 3}) \rangle \\
&= \langle b_{-c}, b_{\varepsilon 3} \rangle \\
&= \mathbf{p}_{\mathcal{B}}(b_{-c})^T \text{Gram}(\mathcal{B})^{-1} \mathbf{p}_{\mathcal{B}}(b_{\varepsilon 3}) \\
&= \begin{pmatrix} -1 & -2\kappa + 1 & -1 & -\sqrt{\kappa} & 0 \end{pmatrix} \text{Gram}(\mathcal{B})^{-1} \begin{pmatrix} -1 \\ -1 \\ -1 \\ 1 \\ \sqrt{3 + 2\sqrt{\kappa} - \kappa} \end{pmatrix} \\
&= -1 - 2\sqrt{\kappa} < -1 \quad \text{for } 1 < \kappa \leq 2
\end{aligned}$$

By the same procedure, we find that for all $1 < \kappa \leq 2$ we have

$$\begin{aligned}
\langle b_{-f}, b'_{\varepsilon 3} \rangle &= \langle s_{b_c^*}(b_{-f}), s_{b_c^*}(b'_{\varepsilon 3}) \rangle = \langle b_{-f}, b_{\varepsilon 3} \rangle = 3 - \frac{4}{\sqrt{\kappa}} - \frac{8}{\kappa} < -1 \\
\langle b_t, b'_{\varepsilon 3} \rangle &= \langle s_{b_c^*}(b_t), s_{b_c^*}(b'_{\varepsilon 3}) \rangle = \langle b_t, b_{\varepsilon 3} \rangle = \frac{2 + 2\sqrt{\kappa} - \kappa}{\sqrt{4 + \kappa^2}} \geq 1 \quad \square
\end{aligned}$$

We now have all the ingredients to proceed with the proof of the upper bound given in Theorem 2.1.1.

2.5 The proof of the upper bound

Proof of Theorem 2.1.1. Let L be a nonsplittable and nontrivial link, and let \mathcal{L} be a minimal crossing diagram of L . The two conditions on the link L imply that the patchwork graph $P(\mathcal{L}) = (V_{\times} \cup V_m, E)$ has at least two crossing vertices. On the other hand, the minimality of the diagram \mathcal{L} implies that $P(\mathcal{L})$ is a simple planar graph. Therefore, by the KAT theorem, there is a circle packing $\mathcal{D}_{P(\mathcal{L})}$ whose tangency graph is $P(\mathcal{L})$. Let $\mathcal{B}_{P(\mathcal{L})}$ be the inflating of $\mathcal{D}_{P(\mathcal{L})}$. For every crossing vertex $x \in V_{\times}$, $\mathcal{D}_{P(\mathcal{L})}$ admits a square-pyramidal disk arrangement with circle packing $\mathcal{D}_{\boxtimes}(x)$. Therefore, $\mathcal{B}_{P(\mathcal{L})}$ admits a crossing sphere arrangement with square-pyramidal sphere packing

$\mathcal{B}_{\boxtimes}(x)$ and bridge spheres $\{b_{\varepsilon_x 3}, b'_{\varepsilon_x 3}\}$. We notice that

$$\mathcal{D}_{P(\mathcal{L})} = \bigcup_{x \in V_{\times}} \mathcal{D}_{\boxtimes}(x) \quad \text{and} \quad \mathcal{B}_{P(\mathcal{L})} = \bigcup_{x \in V_{\times}} \mathcal{B}_{\boxtimes}(x).$$

We choose ε_x such that the thread of the chain made by the spheres $(b_c, b_{\varepsilon_x 3}, b'_{\varepsilon_x 3}, b_{-c})$ is over/under the thread of the chain (b_f, b_x, b_{-f}) according to the diagram \mathcal{L} . Let $\mathcal{B}_{\wedge(\mathcal{L})}$ be the arrangement of spheres made by the union of all the bridge spheres with the appropriate signs with respect to \mathcal{L} for each crossing vertex, and let $\mathcal{B}_{\mathcal{L}} := \mathcal{B}_{P(\mathcal{L})} \cup \mathcal{B}_{\wedge(\mathcal{L})}$. If $\mathcal{B}_{\mathcal{L}}$ were a packing, then its carrier would contain a polygonal link ambient isotopic to L (by construction). Moreover, the number of spheres $|\mathcal{B}_{\mathcal{L}}| = |\mathcal{B}_{P(\mathcal{L})}| + |\mathcal{B}_{\wedge(\mathcal{L})}| = 3\text{cr}(\mathcal{L}) + 2\text{cr}(\mathcal{L}) = 5\text{cr}(\mathcal{L})$ since \mathcal{L} is a minimal crossing diagram. It remains to show that $\mathcal{B}_{\mathcal{L}}$ is a packing. This is equivalent to showing the following three claims:

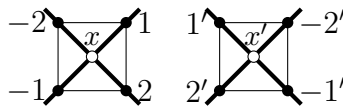
- (1) $\mathcal{B}_{P(\mathcal{L})}$ is a packing.
- (2) Every sphere of $\mathcal{B}_{P(\mathcal{L})}$ is at most tangent to every sphere of $\mathcal{B}_{\wedge(\mathcal{L})}$.
- (3) $\mathcal{B}_{\wedge(\mathcal{L})}$ is a packing.

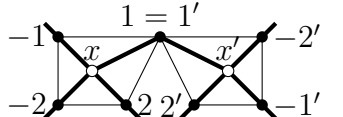
Claim (1)] This is obtained directly by the fact that the inflating operation preserves the inversive product.

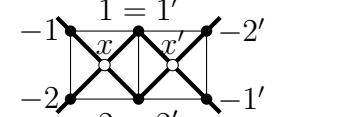
Claim (2)] Let x be a crossing vertex with corresponding square-pyramidal disk arrangement $(\mathcal{D}_{\boxtimes}, d_1^*, d_2^*, d_t)$, crossing sphere arrangement $(\mathcal{B}_{\boxtimes}, b_1^*, b_2^*, b_t, b_{\varepsilon_x 3}, b'_{\varepsilon_x 3})$ and crossing region \mathcal{X} . Since $\mathcal{D}_{P(\mathcal{L})}$ is a packing then, as a consequence of Lemma 2.3.2 (f), any disk $d \in \mathcal{D}_{P(\mathcal{L})} \setminus \mathcal{D}_{\boxtimes}$ must be disjoint to d_t . Therefore, the corresponding sphere $b \in \mathcal{B}_{P(\mathcal{L})} \setminus \mathcal{B}_{\boxtimes}$ must be disjoint to b_t and thus, b is disjoint to \mathcal{X} . Since, by Lemma 2.4.1, $b_{\varepsilon_x 3}, b'_{\varepsilon_x 3} \subset \mathcal{X}$, we have that $b_{\varepsilon_x 3}$ and $b'_{\varepsilon_x 3}$ are disjoint to every sphere of $\mathcal{B}_{P(\mathcal{L})} \setminus \mathcal{B}_{\boxtimes}$. On the other hand, Lemma 2.4.1 ensures that $b_{\varepsilon_x 3}$ and $b'_{\varepsilon_x 3}$ are at most tangent to every sphere of \mathcal{B}_{\boxtimes} .

Claim (3)] We first notice that, by Lemma 2.4.1, the bridge spheres of a crossing sphere arrangement are externally tangent. It remains to show that the bridge spheres of different crossing sphere arrangements do not overlap. Let x and x' be two

different crossing vertices of $P(\mathcal{L})$ and let $\mathcal{D}_{\boxtimes} = \{d_x, d_1, d_2, d_{-1}, d_{-2}\}$ and $\mathcal{D}'_{\boxtimes} = \{d_{x'}, d_{1'}, d_{2'}, d_{-1'}, d_{-2'}\}$ be the corresponding square-pyramidal circle packings in $\mathcal{D}_{P(\mathcal{L})}$. Let n be the number of disks in common of \mathcal{D}_{\boxtimes} and \mathcal{D}'_{\boxtimes} and let \mathcal{X} and \mathcal{X}' be the corresponding crossing regions. Now we show that in each of the five cases ($n = 0, 1, 2, 3, 4$), \mathcal{X} and \mathcal{X}' have disjoint interiors. We may relabel \mathcal{D}'_{\boxtimes} in order to work with the labelling of the graphs shown on the left.

($n = 0$)  Since $\mathcal{D}_{P(\mathcal{L})}$ is a packing then, by Lemma 2.3.2 (f), the boundaries of d_t and $d_{t'}$ do not intersect. Therefore, b_t and $b_{t'}$ are disjoint. Hence, $\mathcal{X} \cap \mathcal{X}' = \emptyset$.

($n = 1$)  The (possibly empty) region $d_t \cap d_{t'}$ must be contained in d_1 so $b_t \cap b_{t'}$ is contained in b_1 . As a consequence, $\text{int}(\mathcal{X}) \cap \text{int}(\mathcal{X}') = \emptyset$.

($n = 2$)  We can apply a standard transformation to get a standard circle packing $[\mathcal{D}_{\boxtimes} \cup \mathcal{D}'_{\boxtimes}]_2^1$ where the disks d_1, d_2, d_t and $d_{t'}$ become half-spaces as in Fig. 2.7.

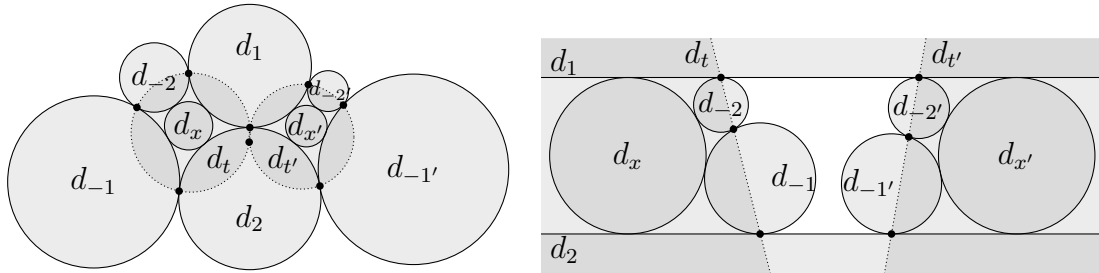
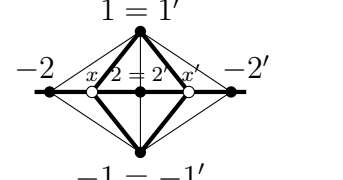


Figure 2.7: (Left) $\mathcal{D}_{\boxtimes} \cup \mathcal{D}'_{\boxtimes}$ in the case $n = 2$ together with their tangency disks; (right) $[\mathcal{D}_{\boxtimes} \cup \mathcal{D}'_{\boxtimes}]_2^1$.

The lines ∂d_t and $\partial d_{t'}$ in $[\mathcal{D}_{\boxtimes} \cup \mathcal{D}'_{\boxtimes}]_2^1$ either intersect in a point lying in $d_1 \cup d_2$ or they are parallel implying, in both cases, that the region $d_t \cap d_{t'}$ is contained in $d_1 \cup d_2$. Therefore, $b_t \cap b_{t'}$ is contained in $b_1 \cup b_2$ and thus $\text{int}(\mathcal{X}) \cap \text{int}(\mathcal{X}') = \emptyset$.

($n = 3$)  The boundaries of d_t and $d_{t'}$ intersect at the tangency points $d_1 \cap d_2$ and $d_{-1} \cap d_2$ (Fig. 2.8). Therefore $d_t \cap d_{t'} \subset d_2$ which implies that $b_t \cap b_{t'} \subset b_2$ and hence $\text{int}(\mathcal{X}) \cap \text{int}(\mathcal{X}') = \emptyset$.

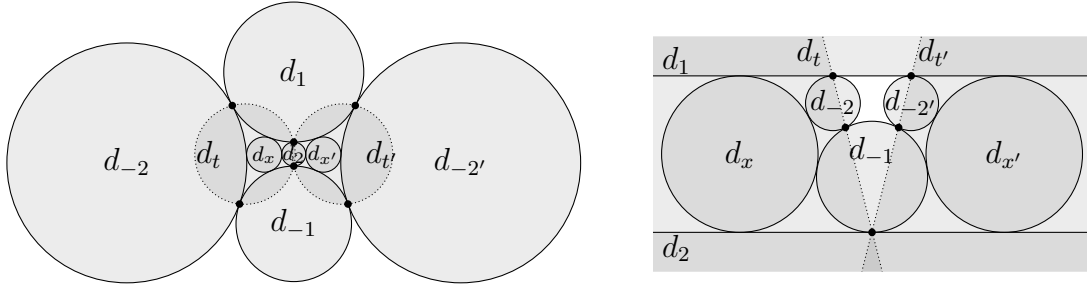
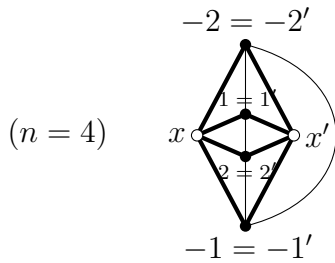


Figure 2.8: (Left) $\mathcal{D}_{\boxtimes} \cup \mathcal{D}'_{\boxtimes}$ for $n = 3$ and the tangency disks (right) $[\mathcal{D}_{\boxtimes} \cup \mathcal{D}'_{\boxtimes}]_2^1$.



In this case, the tangency graph of $\mathcal{D}_{\boxtimes} \cup \mathcal{D}'_{\boxtimes}$ is isomorphic to the octahedral graph by taking $x' = 3$ and $x = -3$ (Fig. 2.9). We have that $d_t = -d_{t'}$ which implies that b_t and $b_{t'}$ are externally tangent. Thus, $\text{int}(\mathcal{X}) \cap \text{int}(\mathcal{X}') = \emptyset$.

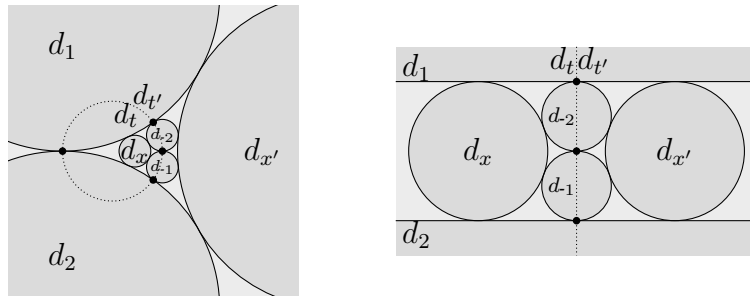


Figure 2.9: (Left) $\mathcal{D}_{\boxtimes} \cup \mathcal{D}'_{\boxtimes}$ for $n = 4$ and the tangency disks (right) $[\mathcal{D}_{\boxtimes} \cup \mathcal{D}'_{\boxtimes}]_2^1$.

Finally, since by Lemma 2.4.1 the bridge spheres are contained in the crossing regions we have that $\mathcal{B}_{\wedge(\mathcal{L})}$, and by consequence $\mathcal{B}_{\mathcal{L}}$, are packings. \square

Remark 3. The method in the previous proof requires two spheres for each bridge in order to connect the closest pair. Unfortunately, this cannot be done with a single sphere since it would be too large to be contained in the crossing region, a central request in the proof.

2.6 An algorithm for knotted necklaces

Here we present an algorithm arising from the constructive proof of Theorem 2.1.1. We believe that this algorithm can be useful to investigate 3D invariants of links, such as the *rope length* or the *stick number*.

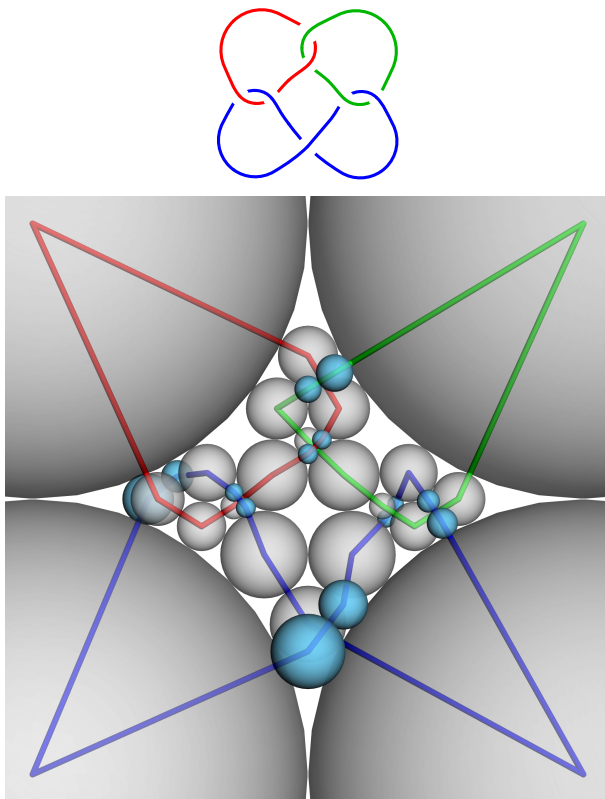
The spheres are given in inversive coordinates. To compute the bridge spheres we use the inversive products $\lambda_{-c,3} := \langle b_{-c}, b_{\varepsilon 3} \rangle = \langle b_c, b'_{\varepsilon 3} \rangle$ and $\lambda_{z,3} := \langle b_{\varepsilon z}, b_{\varepsilon 3} \rangle = \langle b_{\varepsilon z}, b'_{\varepsilon 3} \rangle$. These values are given in the proof of Lemma 2.4.1 in terms of the smaller standard curvature by $\lambda_{-c,3} = -1 - 2\sqrt{\kappa}$ and $\lambda_{z,3} = \sqrt{3 + 2\sqrt{\kappa} - \kappa}$. The smaller standard curvature can be computed by using Lemma 2.3.2 (a) obtaining $\kappa = \frac{1 - \lambda_{c,-c}}{2} = \frac{8}{1 - \lambda_{f,-f}}$ where $\lambda_{c,-c} := \langle b_c, b_{-c} \rangle$ and $\lambda_{f,-f} := \langle b_f, b_{-f} \rangle$. We use the well-known algorithm of Collins and Stephenson [25] for the construction of circle packings from the tangency graph. The radius of the outer disks and the visual precision can be chosen. The necklaces representations of the Figures 2.10 and 2.11 are obtained by this algorithm with outer radii equal to 1 and precision 10^{-4} .

Table 2.1: Algorithm to construct necklace representations.

Input: A link diagram \mathcal{L} with n crossings of a link L .

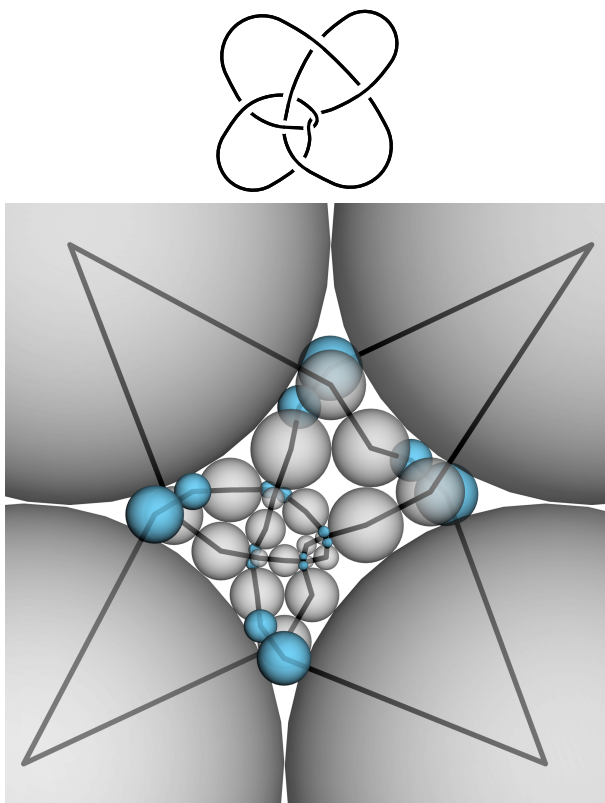
Output: A necklace representation $\mathcal{B}_{\mathcal{L}}$ of the link L with $5n$ spheres.

1. Compute the patchwork graph $P(\mathcal{L})$ of \mathcal{L} .
 2. With a Circle Packing algorithm, construct a circle packing $\mathcal{D}_{P(\mathcal{L})}$ with tangency graph $P(\mathcal{L})$.
 3. Construct a sphere packing $\mathcal{B}_{P(\mathcal{L})}$ obtained by inflating $\mathcal{D}_{P(\mathcal{L})}$.
 4. Set $\mathcal{B}_{\wedge(\mathcal{L})} = \{\}$, $Q = \text{diag}(1, 1, 1, 1, -1)$, $b_z = (0 \ 0 \ 1 \ 0 \ 0)^T$.
 5. For each crossing vertex x of $P(\mathcal{L})$ do:
 - (a) Give to $\mathcal{B}_{\boxtimes}(x)$ a square-pyramidal labeling $\mathcal{B}_{\boxtimes}(x) = \{b_x, b_1, b_2, b_{-1}, b_{-2}\}$.
 - (b) Compute the inversive product $\lambda = b_1^T Q b_{-1}$.
 - (c) If $\lambda \geq -3$, then $B = (b_x | b_1 | b_2 | b_{-1} | b_{-2})$ and $\kappa = \frac{1 - \lambda}{2}$. Else, $B = (b_x | b_2 | b_1 | b_{-2} | b_{-1})$ and $\kappa = \frac{8}{1 - \lambda}$.
 - (d) Define $\lambda_{-c,3} = -1 - 2\sqrt{\kappa}$ and $\lambda_{z,3} = \sqrt{3 + 2\sqrt{\kappa} - \kappa}$.
 - (e) Set $b_3(x) = (-1 \ -1 \ -1 \ \lambda_{-c,3} \ \lambda_{z,3}) B^{-1} Q)^T$
and $b'_3(x) = (-1 \ \lambda_{-c,3} - 1 \ -1 \ \lambda_{z,3}) B^{-1} Q)^T$.
 - (f) If the thread made by the bridge sphere is under-crossing in \mathcal{L} ,
then change the sign of the third coordinate of $b_3(x)$ and $b'_3(x)$.
 - (g) $\mathcal{B}_{\wedge(\mathcal{L})} \leftarrow \mathcal{B}_{\wedge(\mathcal{L})} \cup \{b_3(x), b'_3(x)\}$.
 6. $\mathcal{B}_{\mathcal{L}} := \mathcal{B}_{P(\mathcal{L})} \cup \mathcal{B}_{\wedge(\mathcal{L})}$.
-



	Center			Radius
1	0.	0.	0.	1.
2	0.4068	1.	-0.1882	0.0958
3	0.519	1.083	-0.1184	0.0603
4	0.6344	1.0947	0.	0.1054
5	0.7338	1.0234	0.0655	0.0334
6	0.7762	0.9686	0.071	0.0362
7	0.8407	0.7983	0.	0.1593
8	1.	0.5458	0.	0.1392
9	2.	0.	0.	1.
10	1.4814	0.9131	0.1095	0.0558
11	1.4327	0.9925	0.0815	0.0415
12	1.3656	1.0947	0.	0.1054
13	1.3204	0.9813	-0.0604	0.0307
14	1.2858	0.9279	-0.065	0.0331
15	1.1593	0.7983	0.	0.1593
16	1.1253	0.6243	0.1733	0.0886
17	1.	0.4638	0.2589	0.1323
18	2.	2.	0.	1.
19	1.0949	1.4501	0.1314	0.0671
20	1.	1.3938	0.0956	0.0489
21	0.8873	1.3285	0.	0.1127
22	1.	1.211	0.	0.0501
23	1.1302	1.0863	0.	0.1302
24	1.2695	0.9745	0.	0.0485
25	1.3864	0.9006	0.	0.0898
26	1.546	1.	0.	0.0982
27	0.	2.	0.	1.
28	1.	1.5198	0.	0.1093
29	1.1127	1.3285	0.	0.1127
30	1.0501	1.2136	0.0693	0.0354
31	1.	1.162	0.0714	0.0365
32	0.8698	1.0863	0.	0.1302
33	0.7305	0.9745	0.	0.0485
34	0.6136	0.9006	0.	0.0898
35	0.454	1.	0.	0.0982

Figure 2.10: Necklace representation of the link 7_1^3 with 35 spheres.



	Center			Radius
1	0.	0.	0.	1.
2	0.5168	0.958	0.2146	0.1094
3	0.6549	1.0442	0.1381	0.0704
4	0.7919	1.0508	0.	0.1243
5	0.9356	1.0528	-0.0671	0.0343
6	0.9982	1.0317	-0.0625	0.0319
7	1.081	0.9676	0.	0.09
8	1.1502	0.8904	0.0455	0.0232
9	1.164	0.8497	0.0395	0.0202
10	1.1595	0.7925	0.	0.0494
11	1.0879	0.7759	0.	0.0241
12	1.0007	0.7799	0.	0.0633
13	0.902	0.7895	0.	0.0358
14	0.7559	0.8166	0.	0.1127
15	0.5757	0.9527	0.	0.1132
16	0.1772	1.9921	0.	1.
17	1.1772	1.4541	0.	0.1356
18	1.3308	1.212	0.	0.1511
19	1.4928	1.1678	-0.1645	0.084
20	1.6347	1.0364	-0.2477	0.1265
21	2.	0.	0.	1.
22	1.	0.4186	0.2005	0.1025
23	0.9104	0.5354	0.1241	0.0634
24	0.895	0.6486	0.	0.1053
25	0.876	0.7684	-0.0535	0.0273
26	0.8848	0.8205	-0.0502	0.0256
27	0.9271	0.9005	0.	0.0779
28	0.9571	1.0187	0.	0.044
29	1.0243	1.2064	0.	0.1554
30	1.0559	1.3765	-0.1686	0.0861
31	1.1772	1.533	-0.2525	0.1289
32	2.1772	1.9921	0.	1.
33	1.5588	1.0432	0.	0.1327
34	1.3111	0.9157	0.	0.1459
35	1.1441	0.8682	0.	0.0278
36	1.0843	0.8388	0.	0.0389
37	1.0718	0.7954	0.0305	0.0156
38	1.0717	0.7615	0.0372	0.019
39	1.1051	0.6481	0.	0.1049
40	1.	0.4677	0.	0.1039

Figure 2.11: Necklace representation of the knot 8_{17} with 40 spheres.

Polytopal ball packings

Contents

3.1	Introduction	43
3.2	The projective model of the space of oriented hyperspheres.	45
3.3	Polytopes	46
3.4	The ball-arrangement projection.	49
3.4.1	Centered Ball Packing projections of regular polytopes	50
3.5	Duality of polytopal d-ball packings	51
3.6	Möbius uniqueness of edge-scribable polytopes	52
3.6.1	The Möbius spectra	57
3.6.2	Non edge-scribable 4-polytopes.	58
3.7	Apollonian groups and packings	60
3.7.1	The Platonic Apollonian Groups	62

3.1 Introduction

In this chapter, we study a class of packings which we call *polytopal d -ball packings*. These are packings arising from edge-scribed $(d+1)$ -polytopes and are a central object of this thesis. One of the main differences is that the combinatorial structure of a polytopal d -ball packing is encoded by a polytope, instead of a graph, which is the case for general packings. Consequently, polytopal d -ball packings behave well under duality, and offer a good frame to generalize further constructions such as the

Apollonian group and packings in higher dimensions.

As we will see, polytopal Apollonian packings encompass other known generalizations. For instance, the classic Apollonian Circle Packing, the generalization of Guettler and Mallows [49] and the Apollonian ring packing with $n = 5$ [10] are, respectively, a tetrahedral, octahedral and icosahedral Apollonian packing (Fig. 3.1).

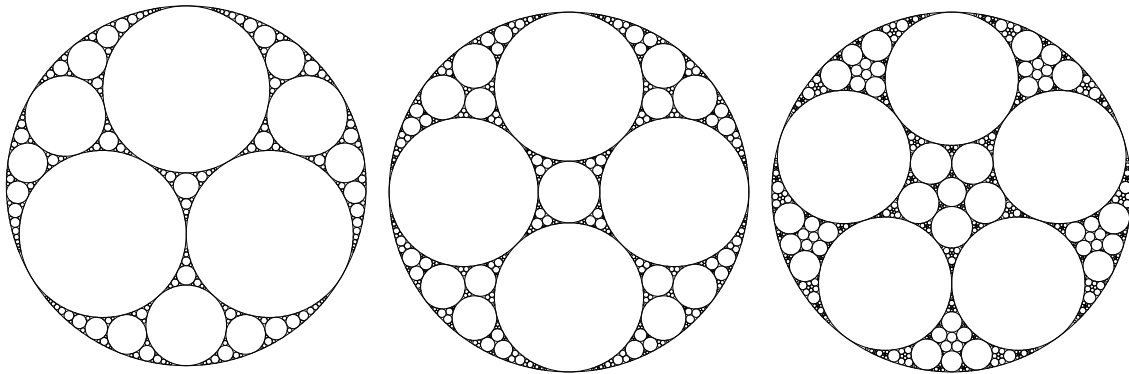


Figure 3.1: From left to right: the classic Apollonian circle packing, the Guettler-Mallows' generalization and the Apollonian ring packing with $n = 5$.

Even if the connection between polytopes and packings has drawn increasing attention in the last decades, this idea is much older. Coxeter, following Beecroft's idea [7], already noticed that the initial setting in the classic Apollonian packing with its dual can be obtained from a circumscribed octahedron [28]. One of the fundamental results which relates edge-scribed polyhedra with circle packings is the Midsphere Theorem, proved by Brightwell and Schneirman [16]. The Midsphere Theorem implies important theorems, such as the KAT and the Steinitz's theorem, and has also numerous applications in polytopes and graph drawing [93, 76, 36]. Kontorovich and Nakamura explored the integrality of the Apollonian packings based on circle packings produced by the Midsphere Theorem, which they call *polyhedral packings* [63]. In higher dimensions, Eppstein, Kuperberg and Ziegler [35] followed a similar approach to construct sphere packings from edge-scribed 4-polytopes which improve the upper bound of the average kissing number. Similarly, Chen studied in [21] the relation between Apollonian d -ball packings and stacked $(d + 1)$ -polytopes, and explored some generalizations of the Midsphere Theorem in higher dimensions.

3.2 The projective model of the space of oriented hyperspheres.

The one-sheet hyperboloid of normalized space-like vectors $S(\mathbb{L}^{d+1,1})$ can be regarded in the *oriented projective space* of $\mathbb{L}^{d+1,1}$

$$\mathbb{P}_+\mathbb{L}^{d+1,1} = \{\mathbf{x} \in \mathbb{L}^{d+1,1} \setminus 0\} / \sim \quad (3.1)$$

where $\mathbf{x} \sim \mathbf{y}$ if there is a real $\lambda > 0$ such that $\mathbf{x} = \lambda\mathbf{y}$. $\mathbb{P}_+\mathbb{L}^{d+1,1}$ is equivalent to the Euclidean unit sphere $\mathbb{S}^{d+1} \subset \mathbb{L}^{d+1,1}$ which, under the gnomonic projection, becomes the union of two affine hyperplanes $\Pi^\uparrow = \{x_{d+2} = 1\}$ and $\Pi^\downarrow = \{x_{d+2} = -1\}$ together with $\Pi^0 = \{(\mathbf{x}, 0) \mid \mathbf{x} \in \mathbb{S}^{d+1}\}$. The composition of the isomorphism $\text{Balls}(\widehat{\mathbb{R}}^d) \rightarrow S(\mathbb{L}^{d+1,1})$ with the projection

$$S(\mathbb{L}^{d+1,1}) \rightarrow \Pi^\uparrow \cup \Pi^0 \cup \Pi^\downarrow$$

$$\mathbf{x} \mapsto \begin{cases} \mathbf{x} & \text{if } x_{d+2} = 0 \\ \frac{1}{|x_{d+2}|}\mathbf{x} & \text{otherwise} \end{cases}$$

gives an isomorphism between $\text{Balls}(\widehat{\mathbb{R}}^d)$ and $\Pi^\uparrow \cup \Pi^0 \cup \Pi^\downarrow$. We call the latter the *projective model* of $\text{Balls}(\widehat{\mathbb{R}}^d)$. We shall identify Π^\uparrow with the $(d+1)$ -dimensional Euclidean space which we shall denote by \mathbb{E}^{d+1} , in order to make the difference with the compactified Euclidean space $\widehat{\mathbb{R}}^d$ where the d -balls are defined. This identification induces a bijection between d -balls whose Lorentzian vector is future-directed and points of \mathbb{E}^{d+1} whose Euclidean norm is strictly greater than 1. Such a point of \mathbb{E}^{d+1} will be called an *outer-sphere point*. The reciprocal bijection between an outer-sphere point $u \in \mathbb{E}^{d+1}$ and a d -ball $b(u) \in \text{Balls}(\widehat{\mathbb{R}}^d)$ can be obtained geometrically by taking a *light source* which illuminates \mathbb{S}^d from u . The spherical illuminated region is a spherical cap which becomes, under the stereographic projection from the North Pole, the d -ball $b(u)$. We say that u is the *light source* of $b(u)$ and, reciprocally, we say that $b(u)$ is the *illuminated region* of u .

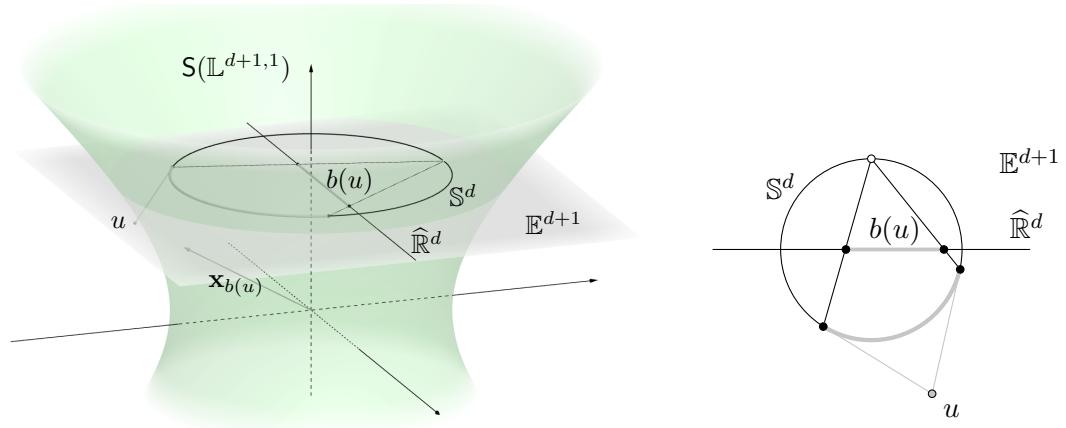


Figure 3.2: A light-source and its illuminated region in the projective model.

For any d -ball whose Lorentzian vector is future-directed, the inversive coordinates can be computed from the coordinates of its light source by

$$\mathbf{i}(b(u)) = \frac{1}{\sqrt{\|u\|^2 - 1}} \begin{pmatrix} u \\ 1 \end{pmatrix} \quad (3.2)$$

This equality implies that for any two d -balls whose Lorentzian vectors are future-directed, their inversive product is related to the Euclidean inner product of their corresponding light sources by the following equation

$$\langle b(u), b(v) \rangle = \frac{1}{\sqrt{(\|u\|^2 - 1)(\|v\|^2 - 1)}} (u \cdot v - 1) \quad (3.3)$$

where \cdot denotes the Euclidean inner product. In the projective model of space of d -balls, the Möbius group acts as the group of projective transformations preserving the unit sphere of \mathbb{E}^{d+1} [106].

3.3 Polytopes

Let us quickly recall some basic polytope notions and definitions needed for the rest of the paper. We refer the reader to [89, 48] for further details. We consider here a d -polytope as the convex hull of a finite collection of points in \mathbb{E}^d . A 2-polytope and a 3-polytope are usually called *polygon* and *polyhedron* respectively.

Let $d \geq 1$ and \mathcal{P} be a $(d + 1)$ -polytope. For every $0 \leq k \leq d + 1$ we denote by $\mathcal{F}_k(\mathcal{P})$ the set of k -faces of \mathcal{P} and by $\mathcal{F}(\mathcal{P}) = \{\emptyset\} \cup \bigcup_{k=0}^{d+1} \mathcal{F}_k(\mathcal{P})$. A *flag* of \mathcal{P} is a chain of faces $(f_0, f_1, \dots, f_d, \mathcal{P})$ where for each $k = 0, \dots, d$, $f_k \subset f_{k+1}$. The elements of $V(\mathcal{P}) := \mathcal{F}_0(\mathcal{P})$, $E(\mathcal{P}) := \mathcal{F}_1(\mathcal{P})$, $R(\mathcal{P}) := \mathcal{F}_{d-1}(\mathcal{P})$ and $F(\mathcal{P}) := \mathcal{F}_d(\mathcal{P})$ are called *vertices*, *edges*, *ridges* and *facets* of \mathcal{P} , respectively. The *graph* of \mathcal{P} (also called *skeleton* or *1-skeleton*) is the graph induced by the vertices and the edges of \mathcal{P} . The face lattice $(\mathcal{F}(\mathcal{P}), \subset)$ encodes all the combinatorial information about \mathcal{P} . Two polytopes \mathcal{P} and \mathcal{P}' are combinatorially equivalent if there exists an isomorphism between their face lattices. If they are combinatorially equivalent, we say they have the same *combinatorial type* and \mathcal{P}' is said to be a *realization* of \mathcal{P} .

The *polar* of a set $X \subset \mathbb{E}^{d+1}$ is defined as

$$X^* := \{u \in \mathbb{E}^{d+1} \mid u \cdot v \leq 1 \text{ for all } v \in X\}. \quad (3.4)$$

If \mathcal{P} is a $(d + 1)$ -polytope containing the origin in its interior then \mathcal{P}^* is also a $(d + 1)$ -polytope containing the origin in its interior and holding the dual relation $(\mathcal{P}^*)^* = \mathcal{P}$. There is a bijection between $\mathcal{F}(\mathcal{P})$ and $\mathcal{F}(\mathcal{P}^*)$ which reverses incidences. Indeed, every facet $f \in \mathcal{F}_d(\mathcal{P})$ corresponds to a unique vertex $v_f \in \mathcal{F}_0(\mathcal{P}^*)$ and they are related by

$$f = \{u \in \mathcal{P} \mid u \cdot v_f = 1\}. \quad (3.5)$$

The *symmetric group* of \mathcal{P} is defined as the group of Euclidean isometries of \mathbb{E}^{d+1} preserving \mathcal{P} . \mathcal{P} is said to be *regular* if its symmetric group acts transitively on the set of flags \mathcal{P} . In this case, the symmetric group of \mathcal{P} can be generated from a flag $(f_0, \dots, f_d, \mathcal{P})$ by considering the maximal simplex C (*chamber*) in the barycentric subdivision of \mathcal{P} whose vertices are the barycenters of the faces in $(f_0, \dots, f_d, \mathcal{P})$. Then C is the fundamental region of the symmetric group of \mathcal{P} which is generated by the reflections r_0, \dots, r_d , where r_k is the reflection in the wall of C containing the barycenter of \mathcal{P} and opposite to the vertex corresponding to the k -face in (f_0, \dots, f_d) . We call the set $\{r_0, \dots, r_d\}$ the *fundamental generators* of the symmetric group of \mathcal{P} with respect to the flag $(f_0, \dots, f_d, \mathcal{P})$. A presentation of the symmetric group of \mathcal{P} in terms of the fundamental generators is given by

$$\begin{cases} r_i^2 = (r_j r_k)^2 = 1 & (0 \leq i, j, k \leq d, |j - k| \geq 2) \\ (r_{i-1} r_i)^{p_i} = 1 & (0 \leq i \leq d) \end{cases}$$

where $\{p_1, p_2, \dots, p_d\}$ is the *Schläfli symbol* of \mathcal{P} . The symmetric group of \mathcal{P} is then the spherical Coxeter group with Coxeter graph $\bullet \text{---} \bullet \cdots \bullet \text{---} \bullet$
 $p_1 \qquad \qquad \qquad p_d$.

All polygons admit a regular realization. The *Platonic solids*, namely, the tetrahedron \mathcal{T}^3 , the octahedron \mathcal{O}^3 , the cube \mathcal{C}^3 , the icosahedron \mathcal{I}^3 and the dodecahedron \mathcal{D}^3 are the five regular 3-polytopes (polyhedra). The 4-simplex \mathcal{T}^4 , the orthoplex \mathcal{O}^4 , the hypercube \mathcal{C}^4 , the 600-cell \mathcal{I}^4 and the 120-cell \mathcal{D}^4 are the five regular 4-polytopes which can be thought as a 4-dimensional analogue of the Platonic solids. The remaining regular 4-polytope, the 24-cell \mathcal{R}^4 (the notation is not standard), completes the list of regular 4-polytopes. For every $d \geq 2$, we shall denote by \mathcal{T}^{d+1} , \mathcal{O}^{d+1} and \mathcal{C}^{d+1} the $(d+1)$ -dimensional analogues of the tetrahedron, octahedron and cube. These are usually called $(d+1)$ -simplex, $(d+1)$ -cross-polytope and $(d+1)$ -cube, respectively. It is well-known that in dimension 5 or above, these three families are the only regular polytopes [29].

For every $0 \leq k \leq d$, a $(d+1)$ -polytope \mathcal{P} is said to be k -scribed if all its k -faces are tangent to the unit sphere of \mathbb{E}^{d+1} . A k -scribed polytope is called *inscribed*, *edge-scribed*, *ridge-scribed* and *circumscribed* if $k = 0, 1, d-1, d$ respectively. A polytope is said to be k -scribable if it admits a realization which is k -scribed. Any regular $(d+1)$ -polytope is k -scribable for every $0 \leq k \leq d$ (by properly centering and rescaling by a suitable value). If \mathcal{P} is a $(d+1)$ -polytope containing the origin in its interior then \mathcal{P} is k -scribed if and only if \mathcal{P}^* is $(d-k)$ -scribed (see [24] for more general results).

For any regular $(d+1)$ -polytope \mathcal{P} , we denote by $\ell_{\mathcal{P}}$ the *midsphere ratio* of \mathcal{P} , obtained by the ratio between the half edge-length of \mathcal{P} and the radius of the *midsphere* (the sphere tangent to every edge). The midsphere ratios of every regular polytope are presented in the Appendix (Table A.1) and were adapted from [29]. For $d = 1, 2$, the midsphere ratios can be computed from the Schläfli symbols by

$$\ell_{\{p\}} = \tan\left(\frac{\pi}{p}\right) \qquad \ell_{\{p,q\}} = \sqrt{\frac{\sin^2\left(\frac{\pi}{q}\right) - \cos^2\left(\frac{\pi}{p}\right)}{\cos^2\left(\frac{\pi}{p}\right)}} \qquad (3.6)$$

3.4 The ball-arrangement projection.

Let \mathcal{P} be an *outer-sphere* $(d + 1)$ -polytope, i.e. with all its vertices outer-sphere. We define the *ball-arrangement projection* of \mathcal{P} , denoted by $\beta(\mathcal{P})$, the arrangement of d -balls whose light sources are the vertices of \mathcal{P} . Reciprocally, we say that \mathcal{P} is the *light-source polytope* of the ball arrangement $\beta(\mathcal{P})$. Chen proved in [21, Th. 5.2] that if $\beta(\mathcal{P})$ is a packing, then the tangency graph of $\beta(\mathcal{P})$ is a spanning subgraph of the graph of \mathcal{P} .

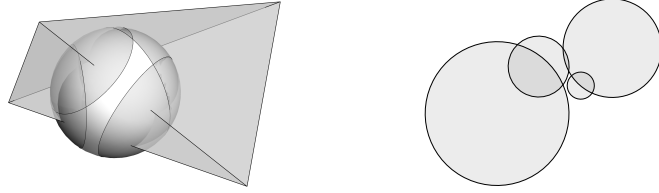


Figure 3.3: (Left) An outer-sphere polyhedron \mathcal{P} with the spherical illuminated regions of its vertices; (right) the ball-arrangement projection $\beta(\mathcal{P})$.

For any two vertices u and v joined by an edge e of \mathcal{P} , the d -balls $b(u)$ and $b(v)$ are disjoint, externally tangent or they have intersecting interiors if and only if e cuts transversely, is tangent or avoids strictly \mathbb{S}^d , respectively. Therefore, \mathcal{P} is an edge-scribed $(d + 1)$ -polytope if and only if $\beta(\mathcal{P})$ is a d -ball packing.

Definition 3.4.1. A d -ball packing \mathcal{B} is *polytopal* if there exist an edge-scribed $(d + 1)$ -polytope \mathcal{P} and $\mu \in \text{Möb}(\widehat{\mathbb{R}}^d)$ such that $\mu(\mathcal{B}) = \beta(\mathcal{P})$.

Analogously to the tangency graph of d -ball packing, we say that \mathcal{P} is the *tangency polytope* of any polytopal d -ball packing $\mathcal{B}_{\mathcal{P}}$ satisfying the previous definition. As Chen noticed in [21, Section 5.2], the graph of \mathcal{P} and the graph of $\mathcal{B}_{\mathcal{P}}$ are isomorphic. We observe that not all the d -ball packings are polytopal. We show an example of a circle packing which is not polytopal in Figure 3.4.

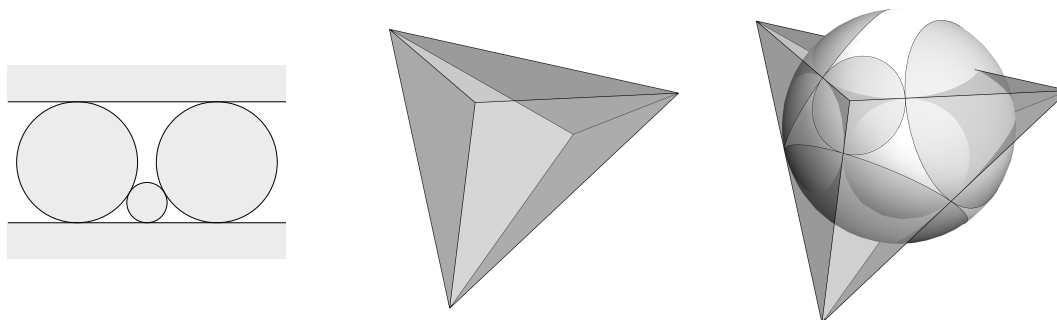


Figure 3.4: (Left) A circle packing which is not polytopal; (center) its light-source polyhedron; (right) same polyhedron with the unit sphere. The edge cutting the sphere does not correspond to any edge of the tangency graph.

3.4.1 Centered Ball Packing projections of regular polytopes

For every $d \geq 1$ and $0 \leq i \leq d$, we define a *Centered Ball Packing (i -CBP) projection* of a regular $(d + 1)$ -polytope \mathcal{P} , as the ball-arrangement projection of an edge-scribed regular realization of \mathcal{P} containing an i -face whose barycenter is in the ray going from the origin to the North Pole of \mathbb{S}^d (∞ in $\widehat{\mathbb{R}}^d$). We show in the Appendices (Tables A.2 and A.3) the CBP projections of the Platonic solids and the regular 4-polytopes.

The d -balls in an i -CBP projection can be grouped by *layers* of d -balls with the same curvature. These curvatures may be expressed as a linear combination of two numbers: $\kappa_{\mathcal{P}}$ and h_i , where $\kappa_{\mathcal{P}}$ is the mean of all the curvatures, and h_i is the minimum of the positive *heights*, in the direction of the North Pole, among all the vertices of \mathcal{P} . By Lemma 4.2.3, we have that $\kappa_{\mathcal{P}}$ is equal to the inverse of the midsphere ratio of \mathcal{P} . CBP projections are similar to the projections of regular polytopes defined by Coxeter in [29], obtained by applying parallel cross-sections. Indeed, the number of d -balls in each layer of an i -CBP projection corresponds to the number of vertices in a layer of a Coxeter's projection where the dimension of the *first* face in the cross-section is i .

3.5 Duality of polytopal d -ball packings

For $d \geq 2$, let \mathcal{P} be an edge-scribed $(d + 1)$ -polytope. We can always send \mathcal{P} by a projective transformation preserving the sphere into an edge-scribed $(d + 1)$ -polytope \mathcal{P}_0 containing the origin in its interior. Therefore, for any polytopal d -ball packing $\mathcal{B}_{\mathcal{P}}$ there is a Möbius transformation μ such that $\mu(\mathcal{B}_{\mathcal{P}}) = \beta(\mathcal{P}_0)$. We define the *dual* of $\mathcal{B}_{\mathcal{P}}$ as the ball arrangement $\mathcal{B}_{\mathcal{P}}^* := \mu^{-1}(\beta(\mathcal{P}_0^*))$. The dual $\mathcal{B}_{\mathcal{P}}^*$ does not depend on the choice of \mathcal{P}_0 . For any vertex v of \mathcal{P}_0 , and for any vertex of \mathcal{P}_0^* corresponding to a facet f of \mathcal{P}_0 containing v , the corresponding d -balls $b_v \in \mathcal{B}_{\mathcal{P}}$ and $b_f \in \mathcal{B}_{\mathcal{P}}^*$ are orthogonal (this can be easily obtained by combining Equations (1.5), (3.3) and (3.5)). Since \mathcal{P} is edge-scribed, \mathcal{P}_0 is edge-scribed and \mathcal{P}_0^* is ridge-scribed. In the case $d = 2$, \mathcal{P}_0^* is also edge-scribed and therefore $\mathcal{B}_{\mathcal{P}}$ and $\mathcal{B}_{\mathcal{P}}^*$ are both circle packings. The union $\mathcal{B}_{\mathcal{P}} \cup \mathcal{B}_{\mathcal{P}}^*$ has been called a *primal-dual circle representation* of \mathcal{P} [36]. We show in Figure 3.5 a primal-dual circle representation of the icosahedron. The Midsphere Theorem of Brightwell and Scheinerman [16] gives the existence and the uniqueness up to Möbius transformations of primal-dual circle representations for every polyhedron. It can be thought of as a stronger version of the Koebe-Andreev-Thurston Circle packing theorem [9].

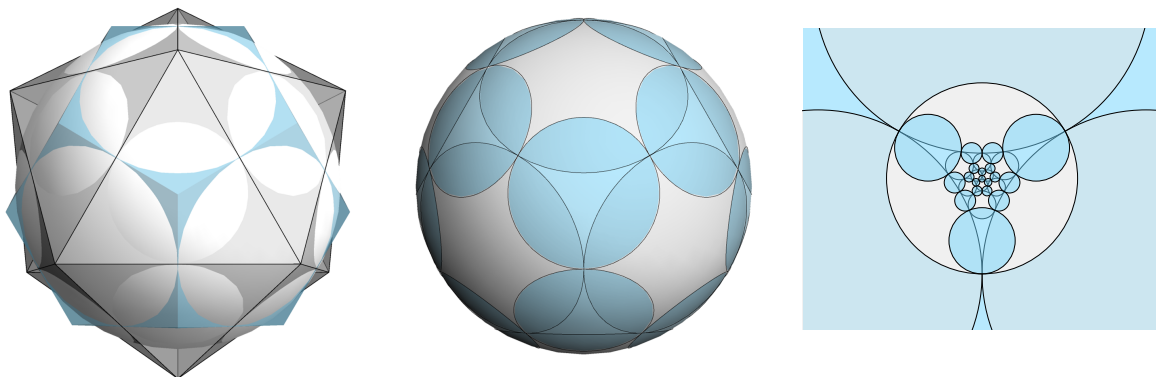


Figure 3.5: (Left) An edge-scribed icosahedron \mathcal{I} and its polar \mathcal{I}^* ; (center) the spherical illuminated regions of \mathcal{I} and \mathcal{I}^* ; (right) a primal-dual circle representation of \mathcal{I} .

3.6 Möbius uniqueness of edge-scribable polytopes

In Section 1.1.7, we define the notion of Möbius uniqueness for d -ball packable graphs. Here, we introduce an analogous uniqueness for edge-scribable $(d + 1)$ -polytopes. We say that an edge-scribable $(d + 1)$ -polytope \mathcal{P} is *Möbius unique* if any two polytopal d -ball packings, whose tangency polytope is an edge-scribed realization of \mathcal{P} , are Möbius equivalent. Equivalently, \mathcal{P} is Möbius unique if all its edge-scribed realizations are connected by a projective transformation preserving the sphere. The following algebraic approach will be useful to detect Möbius uniqueness of edge-scribable polytopes. We say that an arrangement of d -balls has *maximal rank* if the rank of its Gramian is equal to $d + 2$ (it cannot be larger). In particular, polytopal d -ball packings have maximal rank.

Proposition 3.6.1. *Let \mathcal{B} and \mathcal{B}' be two d -ball packings with maximal rank. Then \mathcal{B} is Möbius equivalent to \mathcal{B}' if and only if $\text{Gram}(\mathcal{B}) = \text{Gram}(\mathcal{B}')$.*

Proof. The necessity is trivial since Möbius transformations preserve the inversive product. Now let us suppose that $\text{Gram}(\mathcal{B}) = \text{Gram}(\mathcal{B}')$ is a matrix of rank $d + 2$. Let $V = (\mathbf{x}_1, \dots, \mathbf{x}_n)$ and $V' = (\mathbf{x}'_1, \dots, \mathbf{x}'_n)$ be the Lorentzian vectors of the d -balls of \mathcal{B} and \mathcal{B}' respectively. Without loss of generality we can consider that the vectors of V and V' are future-directed. By the rank condition, V contains a basis $\Delta = \{\mathbf{x}_{i_1}, \dots, \mathbf{x}_{i_{d+2}}\}$ of $\mathbb{L}^{d+1,1}$. Since $\text{Gram}(\mathcal{B}) = \text{Gram}(\mathcal{B}')$ the corresponding collection $\Delta' = \{\mathbf{x}'_{i_1}, \dots, \mathbf{x}'_{i_{d+2}}\} \subset \mathcal{B}'$ is also a basis. Let \mathcal{P} and \mathcal{P}' be the light-source polytopes of the d -balls corresponding to Δ and Δ' , respectively. Since these are basis, then the polytopes \mathcal{P} and \mathcal{P}' are outer-sphere $(d + 1)$ -simplices intersecting the unit sphere $\mathbb{S}^d \subset \mathbb{E}^{d+1}$. If \mathcal{P} does not contain the origin, then we can find a Möbius transformation $\tilde{\mu}_0$ such that the corresponding projective transformation maps \mathcal{P} into another $(d+1)$ -simplex \mathcal{P}_0 containing the origin of \mathbb{E}^{d+1} . Such a Möbius transformation can be easily found by combining translations and rescalings of $\widehat{\mathbb{R}}^d$ which are also Möbius transformations. Let μ_0 be the element in the Orthochronous Lorentz group corresponding to $\tilde{\mu}_0$ and let $V_0 := \mu_0(V)$, $\Delta_0 := \mu_0(\Delta)$. Let M_0 and M_1 be the $(d + 2)$ -square matrices formed by the column-matrices of the Cartesian coordinates of the vectors of Δ_0 and Δ' respectively with respect to the canonical basis of $\mathbb{L}^{d+1,1}$.

The matrices \mathbf{M}_0 and \mathbf{M}_1 are non-singular and therefore we have

$$\begin{aligned} \text{Gram}(\Delta_0) = \text{Gram}(\Delta') &\Leftrightarrow \mathbf{M}_0^T \mathbf{Q}_{d+2} \mathbf{M}_0 = \mathbf{M}_1^T \mathbf{Q}_{d+2} \mathbf{M}_1 \\ &\Leftrightarrow \mathbf{Q}_{d+2} (\mathbf{M}_1^T)^{-1} \mathbf{M}_0^T \mathbf{Q}_{d+2} \mathbf{M}_0 = \mathbf{M}_1 \end{aligned}$$

The matrix $\mathbf{A} := \mathbf{Q}_{d+2} (\mathbf{M}_1^T)^{-1} \mathbf{M}_0^T \mathbf{Q}_{d+2}$ defines a linear map of $\mathbb{L}^{d+1,1}$ to itself which maps Δ_0 to Δ' . Moreover, one can check that

$$\mathbf{A}^T \mathbf{Q}_{d+2} \mathbf{A} = \mathbf{Q}_{d+2}$$

Since the origin belongs to \mathcal{P}_0 we have that $\mathbf{A}e_{d+2} \subset \mathcal{P}' \subset \Pi^\uparrow$. Thus,

$$e_{d+2}^T \mathbf{A} e_{d+2} = \mathbf{A}_{d+2,d+2} > 0$$

and therefore, by Equation (1.13), $\mathbf{A} \in O_{d+1,1}^\uparrow(\mathbb{R})$. The coordinates for the remaining vectors of V_0 and V' with respect to the basis Δ_0 and Δ' respectively can be obtained with the polyspherical coordinates and the entries of $\text{Gram}(\mathcal{B})$. The equality of the Gramians and linearity implies that the Lorentz transformation μ given by \mathbf{A} maps V_0 to V' . Therefore, $\mu\mu_0$ induces a Möbius transformation mapping \mathcal{B} to \mathcal{B}' . \square

Remark 4. *Proposition 3.6.1 does not hold for arrangements of d -balls in general. To see this, one may consider any ball packing $\mathcal{B} = \{b_1, \dots, b_n\}$ whose Gramian is maximal. The arrangement $-\mathcal{B} := \{-b_1, \dots, -b_n\}$ is not a packing, and therefore \mathcal{B} and $-\mathcal{B}$ are not Möbius equivalent. However, $\text{Gram}(\mathcal{B}) = \text{Gram}(-\mathcal{B})$.*

In practice, we shall use Lemma 1.1.1 and Proposition 3.6.1 to study Möbius uniqueness. As an example, the result of Wilker [104, Lemma 6] stating that any two d -ball packings made by $d + 2$ pairwise tangent d -balls are Möbius equivalent, follows directly from Proposition 3.6.1. In terms of the tangency polytope, this result can be restated as follows.

Corollary 3.6.1. *For every $d \geq 1$, the $(d + 1)$ -simplex is Möbius unique.*

It is clear that all polygons are edge-scribable but not all are Möbius unique.

Corollary 3.6.2. *The only polygon which is Möbius unique is the triangle.*

Proof. Let \mathcal{P} be an edge-scribed n -gon with $n > 3$ and let $[\mathcal{B}_{\mathcal{P}}]_1^n = (b_1, b_2, \dots, b_n)$ be the standard 1-ball packing obtained by applying a standard transformation to the ball-arrangement projection of \mathcal{P} . Let $-1 < x < 1$ be the contact point of the two closed intervals b_2 and b_3 . By replacing b_2 and b_3 by two closed intervals b'_2 and b'_3 obtained by moving x a suitable distance we can construct another 1-ball packing $[\mathcal{B}'_{\mathcal{P}}]_1^n$ which is not Euclidean congruent to $[\mathcal{B}_{\mathcal{P}}]_1^n$. By Lemma 1.1.1, $[\mathcal{B}_{\mathcal{P}}]_1^n$ and $[\mathcal{B}'_{\mathcal{P}}]_1^n$ are not Möbius equivalent and therefore \mathcal{P} is not Möbius unique. \square

Möbius uniqueness in dimension 3 is much less restricted. Indeed, the Midsphere theorem of Brightwell and Scheinerman' [16] stating the existence and uniqueness of primal-dual circle representations implies the following.

Corollary 3.6.3 (Corollary of the Midsphere Theorem). *Every polyhedron is edge-scribable and Möbius unique.*

In dimension 4, there are polytopes which are not edge-scribable (see Section 3.6.2). However, we do not know if there are edge-scribable 4-polytopes which are not Möbius unique. Appart of the simplex family, we can also prove that the family of $(d + 1)$ -cross polytopes and $(d + 1)$ -cubes are Möbius unique for every $d \geq 2$. Before proving this, we need the following result.

Theorem 3.6.1. *Let $d \geq 2$ and let $\mathcal{B}_{\mathcal{P}}$ be a polytopal d -ball packing where \mathcal{P} is an edge-scribed realization of the $(d + 1)$ -cross polytope or $(d + 1)$ -cube. Then, for every two vertices u, v of \mathcal{P} , we have*

$$\langle b_u, b_v \rangle = 1 - 2\mathbf{d}_{\mathbf{G}}(u, v) \quad (3.7)$$

where $\mathbf{d}_{\mathbf{G}}(u, v)$ is the distance between u and v in the graph of \mathcal{P} .

Proof. We proceed by induction on $d \geq 2$. The initial case $d = 2$ can be easily checked in a single octahedral or cubical circle packing. Since, by Cor. 3.6.3, polyhedra are Möbius unique, then Eq. (3.7) holds for every edge-scribed realization of the octahedron or cube.

Let us now suppose that (3.7) holds for any edge-scribed realization of the $(d+1)$ -cross polytope or $(d + 1)$ -cube for some $d \geq 2$.

($\mathcal{P} = \mathcal{O}^{d+2}$) Let $\mathcal{B}_{\mathcal{O}^{d+2}}$ be a polytopal $(d+1)$ -ball packing where $\mathcal{O}^{d+2} \subset \mathbb{E}^{d+2}$ is an edge-scribed realization of the $(d+2)$ -octahedron. We give to the vertices of \mathcal{O}^{d+2} an *antipodal labelling*

$$V(\mathcal{O}^{d+2}) = \{v_1, \dots, v_{d+2}, v_{-1}, \dots, v_{-(d+2)}\}$$

where v_i and v_j are connected by an edge of \mathcal{O}^{d+1} if and only if $j \neq -i$. For every $1 \leq i < j \leq d+1$, we consider the following collection of $(d+1)$ -balls

$$\mathcal{B}_{i,j} := \{b_1, \dots, b_{d+1}, b_{-i}, b_{-j}\} \subset \mathcal{B}_{\mathcal{O}^{d+2}}$$

where $b_k := b_{v_k}$. Since $\mathcal{B}_{\mathcal{O}^{d+2}}$ is polytopal, the tangency graph of $\mathcal{B}_{\mathcal{O}^{d+2}}$ is the 1-skeleton of \mathcal{O}^{d+2} . Therefore, b_{d+2} and $b_{-(d+2)}$ are tangent to every $b_k \in \mathcal{B}_{i,j}$. By (1.5), we have that b_{d+2} and $b_{-(d+2)}$ satisfy

$$\langle b_k, b \rangle = -1 \quad \text{for every } b_k \in \mathcal{B}_{i,j} \quad (3.8)$$

and $b \in \{b_{d+2}, b_{-(d+2)}\}$. In inversive coordinates, (3.8) becomes the following linear system

$$\mathbf{B}_{i,j} \mathbf{Q}_{d+3} \mathbf{X} = -\mathbf{1}_{d+3} \quad (3.9)$$

where $\mathbf{B}_{i,j}$ is the matrix of the inversive coordinates of $\mathcal{B}_{i,j}$, \mathbf{Q}_{d+3} is the matrix of the inversive product, \mathbf{X} is a $(d+3)$ -column vector, and $\mathbf{1}_{d+3}$ is the $(d+3)$ -column vector of only 1's. Since b_{d+2} and $b_{-(d+2)}$ are distinct, (3.9) has more than one solution. Therefore, $\mathbf{B}_{i,j}$ is singular, which implies that there is a hyperplane $H_{i,j}$ of \mathbb{E}^{d+2} such that

$$V_{i,j} := \{v_1, \dots, v_{d+1}, v_{-i}, v_{-j}\} \subset H_{i,j}.$$

Moreover, since for every $1 \leq j' \leq d+1$, the hyperplanes $H_{i,j}$ and $H_{i,j'}$ share $d+2$ points of \mathbb{E}^{d+2} , then they must be the same hyperplane. Therefore, there is one hyperplane H containing all the vertices $V(\mathcal{O}^{d+2}) \setminus \{v_{d+2}, v_{-(d+2)}\}$. We thus can find a Möbius transformation $\mu \in \text{Möb}(\mathbb{S}^{d+1})$ such that the corresponding projective transformation sends H to the hyperplane $\{x_{d+2} = 0\} \subset \mathbb{E}^{d+2}$. After identifying $\mu(H)$ with \mathbb{E}^{d+1} we obtain that $\mu(H \cap \mathcal{O}^{d+2})$ becomes an edge-scribed realization of the $(d+1)$ -octahedron \mathcal{O}^{d+1} . The identification $\mu(H) \simeq \mathbb{E}^{d+1}$ preserves the inversive product of the $(d+1)$ -balls corresponding to the points lying in H . Moreover, the

distance between u and v in the graph of \mathcal{O}^{d+2} is equal to the distance in the graph of \mathcal{O}^{d+1} . By the invariance of the inversive product under Möbius transformations and the induction hypothesis, we have that Equation (3.7) holds for any two $(d+1)$ -balls of $\mathcal{B}_{\mathcal{O}^{d+2}} \setminus \{b_{d+2}, b_{-(d+2)}\}$.

The same arguments work if we exchange b_1 and b_{d+2} in $\mathcal{B}_{i,j}$, so (3.7) holds in the remaining cases of $\mathcal{B}_{\mathcal{O}^{d+2}}$.

($\mathcal{P} = \mathcal{C}^{d+2}$) Let $\mathcal{B}_{\mathcal{C}^{d+2}}$ be a polytopal $(d+1)$ -ball packing where $\mathcal{C}^{d+2} \subset \mathbb{E}^{d+2}$ is an edge-scribed realization of the $(d+2)$ -cube. Let u, v be two vertices of \mathcal{C}^{d+2} . We notice that $0 \leq \mathbf{d}_{\mathbf{G}}(u, v) \leq d+2$. Let \bar{u} the unique vertex in \mathcal{C}^{d+1} such that $\mathbf{d}_{\mathbf{G}}(u, \bar{u}) = d+2$. If $v \neq u$ then there is a facet f of \mathcal{C}^{d+2} containing u and v . Let H be the hyperplane obtained by the affine hull of f . As above, there is $\mu \in \text{Möb}(\mathbb{S}^{d+1})$ such that the corresponding projective transformation sends H to the hyperplane $\{x_{d+2} = 0\} \subset \mathbb{E}^{d+2}$, and therefore $\mu(H \cap \mathcal{C}^{d+2})$ induces an edge-scribed realization of the $(d+1)$ -cube. By applying the induction hypothesis we obtain that Equation (3.7) holds for any $b_u, b_v \in \mathcal{B}_{\mathcal{C}^{d+2}}$ corresponding to two vertices of \mathcal{C}^{d+2} at distance strictly less than $d+2$. It remains thus to show that (3.7) holds for b_u and $b_{\bar{u}}$. Let v_1, \dots, v_{d+2} be the neighbours of u in the graph of \mathcal{C}^{d+2} . We consider the $(d+1)$ -ball arrangement $\Delta = (b_u, b_{v_1}, \dots, b_{v_{d+2}}, b_{\bar{u}}) \subset \mathcal{B}_{\mathcal{C}^{d+2}}$. By the induction hypothesis, we have

$$\text{Gram}(\Delta) = \left(\begin{array}{c|ccc|c} 1 & -1 & \cdots & -1 & \lambda \\ \hline -1 & & & & 1-2d \\ \vdots & & \mathbf{A}_{d+2} & & \vdots \\ -1 & & & & 1-2d \\ \hline \lambda & 1-2d & \cdots & 1-2d & 1 \end{array} \right)$$

where \mathbf{A}_n denotes the n -square matrix with 1's in the diagonal entries and -3 everywhere else and $\lambda := \langle b_u, b_{\bar{u}} \rangle$. It can be computed that

$$\det(\text{Gram}(\Delta)) = -4^{d+1}(d(2d-3\lambda+3) - 2\lambda+2)(2d+\lambda+3).$$

Since Δ corresponds to a collection of $d+4$ vectors of $\mathbb{L}^{d+2,1}$ the Gramian of Δ must be singular. Therefore, by the above equality, we obtain

$$\det(\text{Gram}(\Delta)) = 0 \Leftrightarrow \lambda = -3 - 2d \text{ or } \lambda = \frac{2d^2}{3d+2} + 1 > 0 \text{ for every } d \geq 2.$$

Since b_u and $b_{\bar{u}}$ are disjoint then, by Equation (1.5), $\lambda < -1$ and therefore we have that

$$\langle b_u, b_{\bar{u}} \rangle = -3 - 2d = 1 - 2(d + 2) = 1 - 2\mathbf{d}_G(u, \bar{u}). \quad \square$$

Corollary 3.6.4. *For every $d \geq 2$, the $(d+1)$ -cross polytope and the $(d+1)$ -cube are Möbius unique.*

Proof. Let $\mathcal{B}_{\mathcal{P}}$ and $\mathcal{B}_{\mathcal{P}'}$ be two polytopal d -ball packings where \mathcal{P} and \mathcal{P}' are two edge-scribed realizations of the $(d+1)$ -cross polytope (resp. $(d+1)$ -cube). By Theorem 3.6.1, we can find an ordering such that $\text{Gram}(\mathcal{B}_{\mathcal{P}}) = \text{Gram}(\mathcal{B}_{\mathcal{P}'})$. The Möbius uniqueness then follows from Proposition 3.6.1. \square

Corollary 3.6.5. *The 24-cell is Möbius unique.*

Proof. It is well-known that the 1-skeleton of a 24-cell admits a 3-coloring such that the vertices of each color span an orthoplex. By taking the vertices of two out of the three colors, we span a hypercube. Moreover, the edges of this hypercube are also edges of the initial 24-cell. Therefore, every polytopal sphere packing whose tangency polytope is the 24-cell contains a hypercubical sphere packing. Let $\mathcal{B}_{\mathcal{R}^4}$ be the 0-CBP projection of the 24-cell. The even layers of $\mathcal{B}_{\mathcal{R}^4}$ gives a 3-CBP projection $\mathcal{B}_{\mathcal{C}^4}$ of the hypercube (see Table A.3 in the Appendices). Let $\mathcal{B}_{\mathcal{P}}$ be a polytopal sphere packing where \mathcal{P} is another edge-scribed realization of the 24-cell and let $\mathcal{Q} \subset \mathcal{P}$ be one of the hypercubes contained in \mathcal{P} . Since, by Corollary 3.6.4, the hypercube is Möbius unique, then there is a Möbius transformation μ sending the packing $\mathcal{B}_{\mathcal{Q}}$ to $\mathcal{B}_{\mathcal{C}^4}$. Furthermore, every sphere $b \in \mathcal{B}_{\mathcal{R}^4} \setminus \mathcal{B}_{\mathcal{C}^4}$ must be tangent to 6 spheres of $\mathcal{B}_{\mathcal{C}^4}$ corresponding to the vertices of a facet of \mathcal{C}^4 . This condition forces μ to send the spheres in $\mathcal{B}_{\mathcal{P}} \setminus \mathcal{B}_{\mathcal{Q}}$ to $\mathcal{B}_{\mathcal{R}^4} \setminus \mathcal{B}_{\mathcal{C}^4}$ implying that $\mathcal{B}_{\mathcal{P}}$ and $\mathcal{B}_{\mathcal{R}^4}$ are Möbius equivalent. \square

3.6.1 The Möbius spectra

Spectral techniques, based on the eigenvalues and the eigenvectors of the adjacency or the Laplace matrices of graphs are strong and successful tools to investigate different graph's properties. In this spirit, we define the *Möbius spectra* of an edge-scribable Möbius unique $(d+1)$ -polytope \mathcal{P} as the multiset of the eigenvalues of the Gramian of $\beta(\mathcal{P}')$ where \mathcal{P}' is any edge-scribed realization of \mathcal{P} . We believe that

Möbius spectra may shed light on the properties of edge-scribable polytopes. In the appendices, we show in Table A.1 the Möbius spectra of the regular polytopes which we know are Möbius unique.

3.6.2 Non edge-scribable 4-polytopes.

The first examples of 4-polytopes not admitting an edge-scribed realization were given by Schulte in [88]. In [35, Corollary 9], Eppstein, Kupperberg and Ziegler found another type of non edge-scribable 4-polytope by noticing that every stacked 4-polytope with more than 6 vertices is not edge-scribable. We recall that the connected sum of two polytopes \mathcal{P} and \mathcal{P}' along a facet f , denoted by $\mathcal{P}\#_f\mathcal{P}'$, is the glueing of \mathcal{P} and \mathcal{P}' along f where one of them is projectively deformed in such a way that the faces of $\mathcal{P}\#_f\mathcal{P}'$ are the union of the faces of \mathcal{P} and \mathcal{P}' minus f . A *stacked d -polytope* is a polytope obtained by applying consecutively *connected sums* of d -simplices. The main ingredient in the non edge-scribability property of stacked 4-polytopes is the following.

Lemma 3.6.1. *The consecutive connected sum of three 4-simplices is not edge-scribable.*

Proof. We consider the 4-polytope $(\mathcal{T}\#_{f_1}\mathcal{T}')\#_{f_2}\mathcal{T}''$ where \mathcal{T} , \mathcal{T}' and \mathcal{T}'' are three 4-simplices. The facets f_1 and f_2 must intersect in a common ridge r (a triangle) of \mathcal{T} , \mathcal{T}' and \mathcal{T}'' . We label the vertices by $V(r) = \{1, 2, 3\}$, $V(\mathcal{T}) = \{1, 2, 3, 4, 5\}$, $V(\mathcal{T}') = \{1, 2, 3, 5, 6\}$ and $V(\mathcal{T}'') = \{1, 2, 3, 6, 7\}$. Let us suppose that $(\mathcal{T}\#_{f_1}\mathcal{T}')\#_{f_2}\mathcal{T}''$ admits an edge-scribed realization \mathcal{P} . By applying the ball-arrangement projection to \mathcal{P} and then an inversion on a sphere centered at the tangency point of the spheres b_1 and b_2 we obtain a polytopal sphere packing $\mathcal{B}_{\mathcal{P}}$ Euclidean congruent to the packing depicted in Figure 3.6. The Möbius uniqueness of the simplex and Lemma 1.1.1 ensure that there is no other possibility.

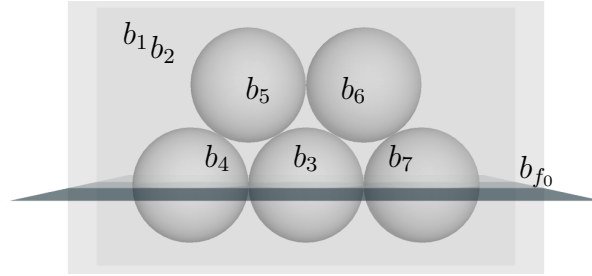


Figure 3.6: The sphere packing obtained by inverting the ball-arrangement projection of a glueing of three 4-simplices.

In this packing, the dual sphere b_{f_0} , corresponding to the facet f_0 of \mathcal{T}_1 with vertices $\{1, 2, 3, 4\}$, cuts orthogonally the sphere b_7 . By combining Equations (3.5), (3.3) and (1.5), we have that the vertex v_7 of \mathcal{T}_3 lies in the affine hull f_0 , so f_0 is not a face of $(\mathcal{T} \#_{f_1} \mathcal{T}') \#_{f_2} \mathcal{T}''$. This contradicts the condition on the set of faces in the definition of connected sum. Therefore, $(\mathcal{T} \#_{f_1} \mathcal{T}') \#_{f_2} \mathcal{T}''$ is not edge-scribable. \square

Chen mentioned in [21, Section 5] similar arguments as above, by considering a 2-CBP projection of the 4-simplex instead of a 1-CBP projection. A natural generalization of stacked polytopes are the *stacked \mathcal{P} -polytopes*, introduced by Chen and Padrol in [24], as polytopes obtained by connected sums of several copies of a given polytope \mathcal{P} . By combining Corollaries 3.6.4 and 3.6.5 with Lemma 1.1.1, we can generalize the construction of Eppstein, Kuperberg and Ziegler by applying the same arguments to the stacked \mathcal{P} -polytopes, where $\mathcal{P} = \mathcal{O}^4, \mathcal{C}^4, \mathcal{R}^4$.

Proposition 3.6.2. *The following 4-polytopes are not edge-scribable:*

- *The connected sum of two orthoplexes.*
- *The connected sum of three hypercubes sharing a ridge.*
- *The connected sum of three 24-cell's sharing a ridge.*

Proof. We may apply the same arguments of the proof of Lemma 3.6.1. By the Möbius uniqueness of the orthoplex, hypercube and 24-cell and Lemma 1.1.1, after applying the corresponding inversion and a proper rescaling, we must obtain a packing which is Euclidean similar to the glueing by reflections of 1-CBP projections

of the corresponding 4-polytope. Then, as above, we would have a dual sphere cutting orthogonally spheres of the different components in the connected sum, and the same contradiction arises. \square

3.7 Apollonian groups and packings

In this section, we introduce a generalization of the Apollonian group introduced by Graham et al. in [45, 46, 47] and Lagarias et al. in [69] for any polytopal d -ball packing.

For $d \geq 2$, let $\mathcal{B}_{\mathcal{P}}$ a polytopal d -ball packing. We consider the following subgroups of $\text{Möb}(\widehat{\mathbb{R}}^d)$:

- The *symmetric group* of $\mathcal{B}_{\mathcal{P}}$ is the group

$$\text{Sym}(\mathcal{B}_{\mathcal{P}}) := \langle \mu \in \text{Möb}(\widehat{\mathbb{R}}^d) \mid \mu(\mathcal{B}_{\mathcal{P}}) = \mathcal{B}_{\mathcal{P}} \rangle.$$

We notice that $\text{Sym}(\mathcal{B}_{\mathcal{P}}) = \text{Sym}(\mathcal{B}_{\mathcal{P}}^*)$.

- The *Apollonian group* of $\mathcal{B}_{\mathcal{P}}$ is the group

$$\text{A}(\mathcal{B}_{\mathcal{P}}) := \langle S(\mathcal{B}_{\mathcal{P}}^*) \rangle$$

where $S(\mathcal{B}_{\mathcal{P}}^*)$ denotes the set of inversions on the d -balls of $\mathcal{B}_{\mathcal{P}}^*$.

- The *symmetrized Apollonian group* of $\mathcal{B}_{\mathcal{P}}$ is the group

$$\text{SA}(\mathcal{B}_{\mathcal{P}}) := \langle \text{Sym}(\mathcal{B}_{\mathcal{P}}) \cup \text{A}(\mathcal{B}_{\mathcal{P}}) \rangle$$

It can be checked that for every $r \in \text{Sym}(\mathcal{B}_{\mathcal{P}})$ and every $b \in \mathcal{B}_{\mathcal{P}}^*$ we have

$$rs_b r = s_{r(b)} \in \text{A}(\mathcal{B}_{\mathcal{P}}) \tag{3.10}$$

where s_b denotes the inversion of b . And consequently, we have that $\text{SA}(\mathcal{B}_{\mathcal{P}}) = \text{A}(\mathcal{B}_{\mathcal{P}}) \rtimes \text{Sym}(\mathcal{B}_{\mathcal{P}})$.

- The *super symmetrized Apollonian group* of $\mathcal{B}_{\mathcal{P}}$ is the group

$$\text{SSA}(\mathcal{B}_{\mathcal{P}}) := \langle \text{A}(\mathcal{B}_{\mathcal{P}}^*) \cup \text{Sym}(\mathcal{B}_{\mathcal{P}}) \cup \text{A}(\mathcal{B}_{\mathcal{P}}) \rangle.$$

By definition, for any polytopal d -ball packing $A(\mathcal{B}_{\mathcal{P}}) < SA(\mathcal{B}_{\mathcal{P}}) < SSA(\mathcal{B}_{\mathcal{P}})$. Therefore, we can find representations of $A(\mathcal{B}_{\mathcal{P}})$ as a subgroup of $SSA(\mathcal{B}_{\mathcal{P}})$. Clearly, $SSA(\mathcal{B}_{\mathcal{P}})$ might have a smaller set of generators than $A(\mathcal{B}_{\mathcal{P}})$. In [45, 46, 47, 63] the authors defined the *dual Apollonian group* and the *super Apollonian group* which, with our notation, correspond to the groups $A(\mathcal{B}_{\mathcal{P}}^*)$ and $\langle A(\mathcal{B}_{\mathcal{P}}) \cup A(\mathcal{B}_{\mathcal{P}}^*) \rangle$, respectively. For the purposes of this manuscript, these groups are not needed. Nevertheless, both groups are subgroups of $SSA(\mathcal{B}_{\mathcal{P}})$.

For any other polytopal d -ball packing $\mathcal{B}'_{\mathcal{P}}$ Möbius equivalent to $\mathcal{B}_{\mathcal{P}}$ the four groups defined above for $\mathcal{B}_{\mathcal{P}}$ are congruent to their analogues in $\mathcal{B}'_{\mathcal{P}}$. Therefore, if \mathcal{P} is Möbius unique, the four groups can be defined for \mathcal{P} independently of the choice of $\mathcal{B}_{\mathcal{P}}$, up to isomorphism.

Since inversions of $\text{Möb}(\widehat{\mathbb{R}}^d)$ can be seen as hyperbolic reflections of the $(d + 1)$ -dimensional hyperbolic space, Apollonian groups are hyperbolic Coxeter groups. This point of view has been well-explored in [22, 23]. The *Apollonian cluster* of $\mathcal{B}_{\mathcal{P}}$, denoted by $\Omega(\mathcal{B}_{\mathcal{P}})$, is the union of the orbits of the action of $A(\mathcal{B}_{\mathcal{P}})$ on $\mathcal{B}_{\mathcal{P}}$. If $\Omega(\mathcal{B}_{\mathcal{P}})$ is a packing we shall call it the *Apollonian packing of $\mathcal{B}_{\mathcal{P}}$* . For $d = 2$, Apollonian clusters are always packings. However, this is not true in higher dimensions. For instance, for $d \geq 4$, the Apollonian cluster $\Omega(\mathcal{B}_{\mathcal{P}})$ where \mathcal{P} is an edge-scribed $(d + 1)$ -simplex, is not a packing [47].

The four groups presented above give different actions on the Apollonian cluster. Indeed, each disk of a polytopal circle packing $\mathcal{B}_{\mathcal{P}}$ has a different orbit under the action of $A(\mathcal{B}_{\mathcal{P}})$. This can be used to present colorings of the disks in the Apollonian packing of $\mathcal{B}_{\mathcal{P}}$. Indeed, if $\mathcal{B}_{\mathcal{P}}$ admits a proper coloring, then is not hard to see that the coloring can be extended to $\Omega(\mathcal{B}_{\mathcal{P}})$ by the action of the $A(\mathcal{B}_{\mathcal{P}})$. We present in Figure 3.7 three Apollonian packings with a minimal coloration. In the first case each orbit has a different color. If \mathcal{P} is regular, then $\text{Sym}(\mathcal{B}_{\mathcal{P}})$ acts transitively on the d -balls of the Apollonian clusters $\Omega(\mathcal{B}_{\mathcal{P}})$ and $\Omega(\mathcal{B}_{\mathcal{P}}^*)$. Moreover, if \mathcal{S} is a set of generators of $\text{Sym}(\mathcal{B}_{\mathcal{P}})$, then Equation (3.10) implies that for any $s_f \in S(\mathcal{B}_{\mathcal{P}})$ and any $s_v \in S(\mathcal{B}_{\mathcal{P}}^*)$ the group $SA(\mathcal{B}_{\mathcal{P}})$ is generated by $\mathcal{S} \cup \{s_f\}$ and $SSA(\mathcal{B}_{\mathcal{P}})$ is generated by $\mathcal{S} \cup \{s_v, s_f\}$.

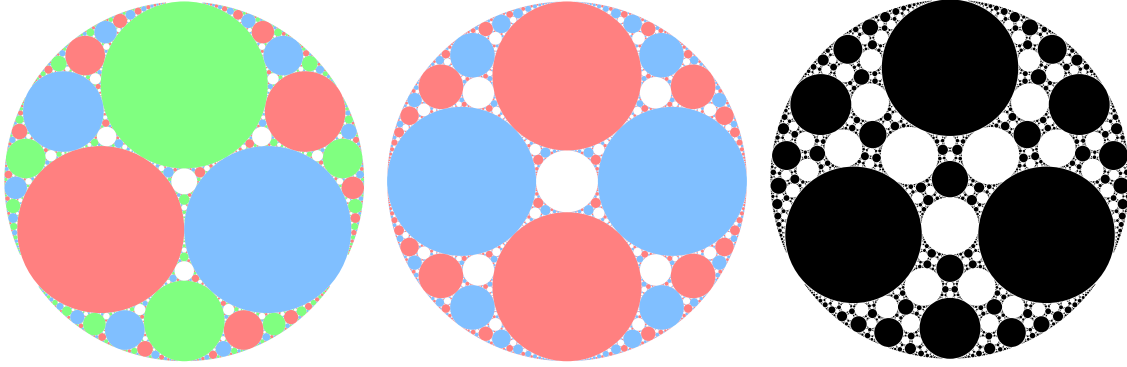


Figure 3.7: A tetrahedral (left), octahedral (center) and cubical (right) Apollonian packing with a minimal coloration.

3.7.1 The Platonic Apollonian Groups

In this section, we compute the Apollonian groups of the Platonic solids, which we shall call the *Platonic Apollonian groups*.

Theorem 3.7.1. *Let $\mathcal{B}_{\mathcal{P}}$ be a polytopal circle packing where \mathcal{P} is a Platonic solid with Schläfli symbol $\{p, q\}$. The group $\text{SSA}(\mathcal{B}_{\mathcal{P}})$ is the hyperbolic Coxeter group with Coxeter graph*

$\bullet \text{---} \bullet \text{---} \bullet \text{---} \bullet$ with labels ∞ , p , q , ∞ above the edges. Moreover, $\text{SSA}(\mathcal{B}_{\mathcal{P}})$ is generated by the following five matrices:

$$\mathbf{S} = \begin{pmatrix} -1 & & & \\ & 1 & & \\ & & 1 & \\ & & & 1 \end{pmatrix}, \quad \mathbf{V} = \begin{pmatrix} 1 & & & \\ & -1 & & \\ & & 1 & \\ & & & 1 \end{pmatrix}, \quad \mathbf{E} = \begin{pmatrix} 1 & 0 & 0 & 0 \\ 0 & 1/2 & 1 & -1/2 \\ 0 & 1 & -1 & 1 \\ 0 & 1/2 & -1 & 3/2 \end{pmatrix}$$

$$\mathbf{F}_q = \begin{pmatrix} -1 & 0 & 4 \cos(\frac{\pi}{q}) & -4 \cos(\frac{\pi}{q}) \\ 0 & 1 & 0 & 0 \\ 4 \cos(\frac{\pi}{q}) & 0 & 1 - 8 \cos^2(\frac{\pi}{q}) & 8 \cos^2(\frac{\pi}{q}) \\ 4 \cos(\frac{\pi}{q}) & 0 & -8 \cos^2(\frac{\pi}{q}) & 1 + 8 \cos^2(\frac{\pi}{q}) \end{pmatrix}, \quad \mathbf{S}^* = \begin{pmatrix} 1 & 0 & 0 & 0 \\ 0 & -1 & -2 & 2 \\ 0 & -2 & -1 & 2 \\ 0 & -2 & -2 & 3 \end{pmatrix}$$

Proof. We follow a similar strategy as in the proof of Theorem 3.7.2. For every $q = 3, 4, 5$, let $[\mathcal{B}_{\mathcal{P}}]_2^1$ be the standard polytopal circle packing where \mathcal{P} is the regular polyhedron of Schläfli symbol $\{3, q\}$. We choose the flag (v, e, f) satisfying the

same conditions as in the proof of Theorem 3.7.2. Let us now apply a translation and a reflection if needed so b_f becomes the half-space $\{x \geq 0\}$. Let $\mathcal{B}_{3,q}$ be the circle packing obtained after the transformations. Since \mathcal{P} is regular, $SSA(\mathcal{B}_{3,q})$ is generated by $\{s_v, r_v, r_e, r_f, s_f\}$ where $\{r_v, r_e, r_f\}$ are the elements in $\text{Sym}(\mathcal{B}_{3,q})$ corresponding to the fundamental generators of the symmetric group of \mathcal{P} with respect to the flag (v, e, f) , s_f is the inversion on the disk in $\mathcal{B}_{3,q}^*$ corresponding to f and s_v is the inversion on the disk in $\mathcal{B}_{3,q}$ corresponding to v . For each $q = 3, 4, 5$ we have that

- s_v is the reflection on the line $\{y = 1\}$,
- r_v is the reflection on the line $\{y = 0\}$,
- r_e is the inversion on the circle centered at $(1, 1)$ and radius 2,
- r_f is the reflection on the line $\{x = -2 \cos(\frac{\pi}{q})\}$,
- s_f is the reflection on the line $\{x = 0\}$.

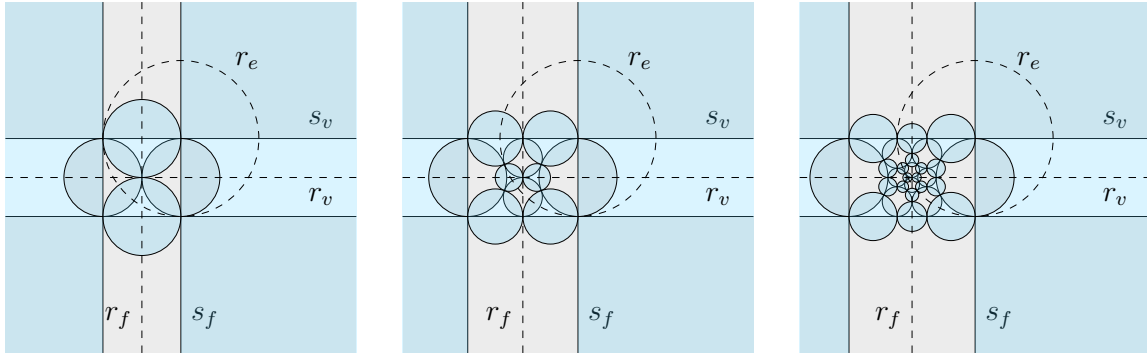


Figure 3.8: The circle packings $\mathcal{B}_{3,q}$ with their dual (in blue) for $q = 3$ (left), $q = 4$ (center) and $q = 5$ (right). In dashed line the generators of the symmetric group of $\mathcal{B}_{3,q}$. The central disk is a unit disk centered at the origin.

By using the inversive coordinates and Eq. (1.14) we obtain a faithful linear representation of $SSA(\mathcal{B}_{3,q})$ as a discrete subgroup of $O_{3,1}^\uparrow(\mathbb{R})$ where the generators are mapped to:

$$s_v \mapsto \mathbf{S}^* \quad r_v \mapsto \mathbf{V} \quad r_e \mapsto \mathbf{E} \quad r_f \mapsto \mathbf{F}_q \quad s_f \mapsto \mathbf{S}$$

The relations of finite order in the Coxeter graph can be checked by straightforward computations on the matrices. For every $n \in \mathbb{N}$ the last entry in the diagonal of $(\mathbf{S}^*\mathbf{V})^n$ and $(\mathbf{F}_q\mathbf{S})^n$ is, respectively, $1 + 2n^2$ and $1 + 8 \cos^2(\frac{\pi}{q})n^2$ and therefore every product has infinite order for every $q = 3, 4, 5$. Since $\text{SSA}(\mathcal{B}_{3,q}) = \text{SSA}(\mathcal{B}_{3,q}^*)$ then the results also hold for the cube and the dodecahedron. Indeed, the generators of $\text{SSA}(\mathcal{B}_{3,q}^*)$ are given by swapping r_v with r_f and s_v with s_f . \square

The previous theorem allows to exhibit a matrix representation of the Platonic Apollonian groups in $O_{3,1}^\uparrow(\mathbb{K})$ where \mathbb{K} is one of these 3 number fields: \mathbb{Z} , $\mathbb{Z}[\sqrt{2}]$ and $\mathbb{Z}[\varphi]$. We illustrates this for the tetrahedron, octahedron and cube.

Corollary 3.7.1. *The tetrahedral Apollonian group is isomorphic to*

$$\langle \mathbf{T}_1, \mathbf{T}_2, \mathbf{T}_3, \mathbf{T}_4 \rangle < O_{3,1}^\uparrow(\mathbb{Z})$$

where

$$\begin{aligned} \mathbf{T}_4 &= \begin{pmatrix} -1 & 0 & 0 & 0 \\ 0 & 1 & 0 & 0 \\ 0 & 0 & 1 & 0 \\ 0 & 0 & 0 & 1 \end{pmatrix} = \mathbf{S} & \mathbf{T}_3 &= \begin{pmatrix} -1 & 0 & 4 & -4 \\ 0 & 1 & 0 & 0 \\ 4 & 0 & -7 & 8 \\ 4 & 0 & -8 & 9 \end{pmatrix} = \mathbf{F}_3 \mathbf{T}_4 \mathbf{F}_3 \\ \mathbf{T}_2 &= \begin{pmatrix} -1 & 2 & 0 & -2 \\ 2 & -1 & 0 & 2 \\ 0 & 0 & 1 & 0 \\ 2 & -2 & 0 & 3 \end{pmatrix} = \mathbf{E} \mathbf{T}_3 \mathbf{E} & \mathbf{T}_1 &= \begin{pmatrix} -1 & -2 & 0 & -2 \\ -2 & -1 & 0 & -2 \\ 0 & 0 & 1 & 0 \\ 2 & 2 & 0 & 3 \end{pmatrix} = \mathbf{V} \mathbf{T}_2 \mathbf{V} \end{aligned}$$

Corollary 3.7.2. *The octahedral Apollonian group is isomorphic to*

$$\langle \mathbf{C}_{123}, \mathbf{C}_{12\bar{3}}, \mathbf{C}_{\bar{1}23}, \mathbf{C}_{\bar{1}2\bar{3}}, \mathbf{C}_{1\bar{2}3}, \mathbf{C}_{1\bar{2}\bar{3}}, \mathbf{C}_{\bar{1}\bar{2}3}, \mathbf{C}_{\bar{1}\bar{2}\bar{3}} \rangle < O_{3,1}^\uparrow(\mathbb{Z}[\sqrt{2}])$$

where

$$\begin{aligned}
\mathbf{C}_{123} &= \begin{pmatrix} -1 & & & \\ & 1 & & \\ & & 1 & \\ & & & 1 \end{pmatrix} = \mathbf{S} & \mathbf{C}_{1\bar{2}\bar{3}} &= \begin{pmatrix} -1 & 0 & 4\sqrt{2} & -4\sqrt{2} \\ 0 & 1 & 0 & 0 \\ 4\sqrt{2} & 0 & -15 & 16 \\ 4\sqrt{2} & 0 & -16 & 17 \end{pmatrix} = \mathbf{F}_4 \mathbf{C}_{123} \mathbf{F}_4 \\
\mathbf{C}_{1\bar{2}3} &= \begin{pmatrix} -1 & 2\sqrt{2} & 0 & -2\sqrt{2} \\ 2\sqrt{2} & -3 & 0 & 4 \\ 0 & 0 & 1 & 0 \\ 2\sqrt{2} & -4 & 0 & 5 \end{pmatrix} = \mathbf{E} \mathbf{C}_{1\bar{2}\bar{3}} \mathbf{E} & \mathbf{C}_{\bar{1}2\bar{3}} &= \begin{pmatrix} -1 & -2\sqrt{2} & 0 & -2\sqrt{2} \\ -2\sqrt{2} & -3 & 0 & -4 \\ 0 & 0 & 1 & 0 \\ 2\sqrt{2} & 4 & 0 & 5 \end{pmatrix} = \mathbf{V} \mathbf{C}_{1\bar{2}\bar{3}} \mathbf{V} \\
\mathbf{C}_{1\bar{2}\bar{3}} &= \begin{pmatrix} -17 & 6\sqrt{2} & 12\sqrt{2} & -18\sqrt{2} \\ 6\sqrt{2} & -3 & -8 & 12 \\ 12\sqrt{2} & -8 & -15 & 24 \\ 18\sqrt{2} & -12 & -24 & 37 \end{pmatrix} = \mathbf{F}_4 \mathbf{C}_{1\bar{2}\bar{3}} \mathbf{F}_4 & \mathbf{C}_{\bar{1}23} &= \begin{pmatrix} -17 & -6\sqrt{2} & 12\sqrt{2} & -18\sqrt{2} \\ -6\sqrt{2} & -3 & 8 & -12 \\ 12\sqrt{2} & 8 & -15 & 24 \\ 18\sqrt{2} & 12 & -24 & 37 \end{pmatrix} = \mathbf{V} \mathbf{C}_{1\bar{2}\bar{3}} \mathbf{V} \\
\mathbf{C}_{\bar{1}\bar{2}3} &= \begin{pmatrix} -17 & 0 & 0 & -12\sqrt{2} \\ 0 & 1 & 0 & 0 \\ 0 & 0 & 1 & 0 \\ 12\sqrt{2} & 0 & 0 & 17 \end{pmatrix} = \mathbf{E} \mathbf{C}_{\bar{1}\bar{2}\bar{3}} \mathbf{E} & \mathbf{C}_{\bar{1}\bar{2}\bar{3}} &= \begin{pmatrix} -49 & 0 & 20\sqrt{2} & -40\sqrt{2} \\ 0 & 1 & 0 & 0 \\ 20\sqrt{2} & 0 & -15 & 32 \\ 40\sqrt{2} & 0 & -32 & 65 \end{pmatrix} = \mathbf{F}_4 \mathbf{C}_{\bar{1}\bar{2}\bar{3}} \mathbf{F}_4
\end{aligned}$$

Corollary 3.7.3. *The cubical Apollonian group is isomorphic to*

$$\langle \mathbf{O}_1, \mathbf{O}_2, \mathbf{O}_3, \mathbf{O}_{\bar{3}}, \mathbf{O}_{\bar{2}}, \mathbf{O}_{\bar{1}} \rangle < O_{3,1}^\dagger(\mathbb{Z}[\sqrt{2}])$$

where

$$\begin{aligned}
\mathbf{O}_1 &= \begin{pmatrix} 1 & 0 & 0 & 0 \\ 0 & -1 & -2 & 2 \\ 0 & -2 & -1 & 2 \\ 0 & -2 & -2 & 3 \end{pmatrix} = \mathbf{S}^* & \mathbf{O}_2 &= \begin{pmatrix} 1 & 0 & 0 & 0 \\ 0 & -1 & 2 & -2 \\ 0 & 2 & -1 & 2 \\ 0 & 2 & -2 & 3 \end{pmatrix} = \mathbf{V} \mathbf{O}_1 \mathbf{V} \\
\mathbf{O}_3 &= \begin{pmatrix} 1 & & & \\ & 1 & & \\ & & -1 & \\ & & & 1 \end{pmatrix} = \mathbf{E} \mathbf{O}_2 \mathbf{E} & \mathbf{O}_{\bar{3}} &= \begin{pmatrix} -15 & 0 & 12\sqrt{2} & -16\sqrt{2} \\ 0 & 1 & 0 & 0 \\ 12\sqrt{2} & 0 & -17 & 24 \\ 16\sqrt{2} & 0 & -24 & 33 \end{pmatrix} = \mathbf{F}_4 \mathbf{O}_3 \mathbf{F}_4 \\
\mathbf{O}_{\bar{2}} &= \begin{pmatrix} -15 & 4\sqrt{2} & 4\sqrt{2} & -12\sqrt{2} \\ 4\sqrt{2} & -1 & -2 & 6 \\ 4\sqrt{2} & -2 & -1 & 6 \\ 12\sqrt{2} & -6 & -6 & 19 \end{pmatrix} = \mathbf{E} \mathbf{O}_{\bar{3}} \mathbf{E} & \mathbf{O}_{\bar{1}} &= \begin{pmatrix} -15 & -4\sqrt{2} & 4\sqrt{2} & -12\sqrt{2} \\ -4\sqrt{2} & -1 & 2 & -6 \\ 4\sqrt{2} & 2 & -1 & 6 \\ 12\sqrt{2} & 6 & -6 & 19 \end{pmatrix} = \mathbf{V} \mathbf{O}_{\bar{2}} \mathbf{V}
\end{aligned}$$

We end this chapter with the following result.

Theorem 3.7.2. *There is a tetrahedral, cubical and dodecahedral Apollonian packing where the set of curvatures of the disks contains all the perfect squares.*

Proof. For every $p = 3, 4, 5$, let $[\mathcal{B}_{\mathcal{P}}]_2^1$ be the standard polytopal circle packing, where \mathcal{P} is the regular polyhedron of Schläfli symbol $\{p, 3\}$. Let (v, e, f) be the flag of \mathcal{P} where v is the vertex corresponding to the half-space $b_v = \{y \leq -1\}$, e is the edge of \mathcal{P} with ends v and v' where $b_{v'} = \{y \leq 1\}$, and f is a face of \mathcal{P} containing e . Let us apply a translation and a reflection if needed, so b_f becomes the half-space $\{x \geq 0\}$. We then rescale by a factor of $\lambda = 4 \cos^2(\frac{\pi}{p})$. Let $\mathcal{B}_{\{p,3\}}$, for $p = 3, 4, 5$, be the transformed circle packing obtained from $[\mathcal{B}_{\mathcal{P}}]_2^1$ (Fig. 3.9). The rescaling factor has been chosen to obtain that the disks with minimal non-zero curvature of $\mathcal{B}_{\{p,3\}}$ have curvature equal to one.

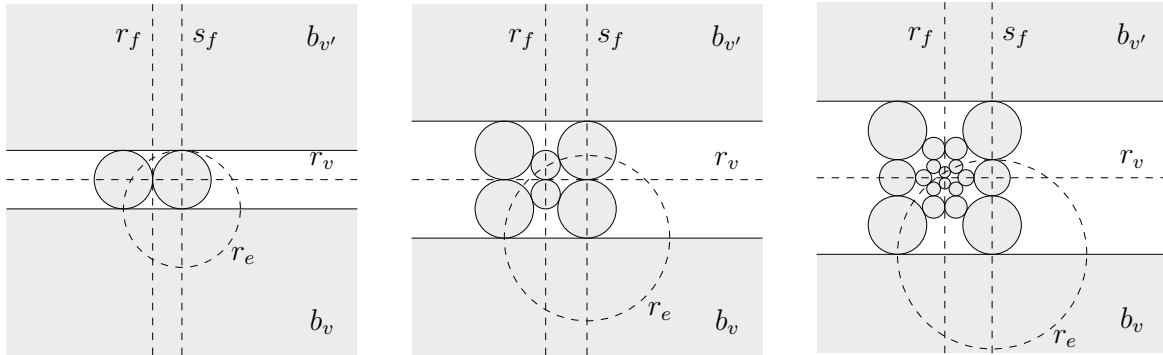


Figure 3.9: The circle packings $\mathcal{B}_{\{p,3\}}$ for $p = 3$ (left), $p = 4$ (center) and $p = 5$ (right). In dashed line the generators of $\text{Sym}(\mathcal{B}_{\{p,3\}})$.

Since \mathcal{P} is regular then $\text{SA}(\mathcal{B}_{\{p,3\}})$ is generated by $\{r_v, r_e, r_f, s_f\}$ where $\{r_v, r_e, r_f\}$ are the elements in $\text{Sym}(\mathcal{B}_{\{p,3\}})$ corresponding to the fundamental generators of the symmetric group of \mathcal{P} with respect to the flag (v, e, f) and s_f is the inversion on the b_f . Therefore, for $p = 3, 4, 5$, we have the following:

- b_v is the half-space $\{y \leq -\lambda\}$ and $b_{v'}$ is the half-space $\{y \geq \lambda\}$,
- r_v is the reflection on the line $\{y = 0\}$,

- r_e is the inversion on the circle centered at $(0, -\lambda)$ and radius $2\sqrt{\lambda}$,
- r_f is the reflection on the line $\{x = -\sqrt{\lambda}\}$,
- s_f is the reflection on the line $\{x = 0\}$.

For every $p = 3, 4, 5$ and for every integer $n \geq 0$ we define the element

$$\mu_{p,n} := r_e(r_f s_f)^n r_e \in \text{SA}(\mathcal{B}_{\{p,3\}}) \text{ and the disk } b_n := \mu_{p,n}(b_{v'}) \in \Omega(\mathcal{B}_{\{p,3\}}).$$

Let us compute the curvature of b_n . The inversive coordinates of $b_{v'}$ and the matrices representing r_e, r_f and s_f obtained by Eq. (1.14), are given by

$$\mathbf{i}(b_{v'}) = \begin{pmatrix} 0 \\ 1 \\ \lambda \\ \lambda \end{pmatrix}, \quad r_e \mapsto \mathbf{E}_\lambda = \begin{pmatrix} 1 & 0 & 0 & 0 \\ 0 & 1 - \frac{\lambda}{2} & \frac{1}{4}(\lambda^2 - 4\lambda - 1) & -\frac{1}{4}(\lambda^2 - 4\lambda + 1) \\ 0 & \frac{1}{4}(\lambda^2 - 4\lambda - 1) & 1 - \frac{(\lambda^2 - 4\lambda - 1)^2}{8\lambda} & -\frac{1 - (\lambda - 4)^2 \lambda^2}{8\lambda} \\ 0 & \frac{1}{4}(\lambda^2 - 4\lambda + 1) & \frac{1 - (\lambda - 4)^2 \lambda^2}{8\lambda} & 1 + \frac{(\lambda^2 - 4\lambda + 1)^2}{8\lambda} \end{pmatrix},$$

$$r_f \mapsto \mathbf{F}_\lambda = \begin{pmatrix} -1 & 0 & 2\sqrt{\lambda} & -2\sqrt{\lambda} \\ 0 & 1 & 0 & 0 \\ 2\sqrt{\lambda} & 0 & 1 - 2\lambda & 2\lambda \\ 2\sqrt{\lambda} & 0 & -2\lambda & 2\lambda + 1 \end{pmatrix}, \quad s_f \mapsto \mathbf{S} = \begin{pmatrix} -1 & & & \\ & 1 & & \\ & & 1 & \\ & & & 1 \end{pmatrix},$$

By induction on n we obtain

$$(\mathbf{F}_\lambda \mathbf{S})^n = \begin{pmatrix} 1 & 0 & 2\sqrt{\lambda}n & -2\sqrt{\lambda}n \\ 0 & 1 & 0 & 0 \\ -2\sqrt{\lambda}n & 0 & 1 - 2\lambda n^2 & 2\lambda n^2 \\ -2\sqrt{\lambda}n & 0 & -2\lambda n^2 & 1 + 2\lambda n^2 \end{pmatrix}$$

and therefore, by Eq. (1.9), we have

$$\begin{aligned} \kappa(b_n) &= \kappa(\mu_{p,n}(b_{v'})) \\ &= \mathbf{k}_4 \mathbf{E}_\lambda (\mathbf{F}_\lambda \mathbf{S})^n \mathbf{E}_\lambda \mathbf{i}(b_{v'}) \\ &= n^2 \end{aligned}$$

where $\mathbf{k}_4 = \begin{pmatrix} 0 & 0 & -1 & 1 \end{pmatrix}$. □

We show in Fig. 3.10 the tetrahedral, cubical and dodecahedral Apollonian packings containing the sequence of perfect squares.

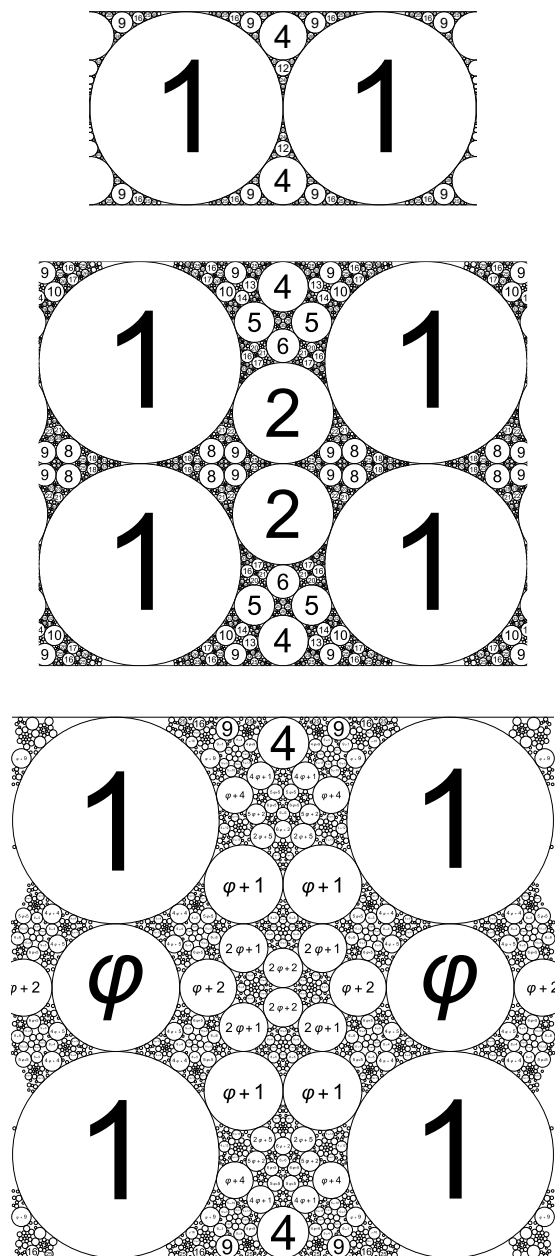


Figure 3.10: The tetrahedral, cubical and dodecahedral Apollonian packings containing the sequence of perfect squares.

The Polytopal Descartes' Theorem

Contents

4.1	Introduction	69
4.2	The Polytopal Descartes' Theorem	71
4.3	Integrality of the Platonic Apollonian packings	80
4.3.1	Octahedral Apollonian packings	82
4.3.2	Cubical Apollonian packings	84
4.3.3	Icosahedral Apollonian packings	85
4.3.4	Dodecahedral Apollonian packings	86

4.1 Introduction

The classical Apollonian circle packing is constructed from an initial configuration of four pairwise tangent disks in \mathbb{R}^2 , also known as a *Descartes configuration* [21]. The name comes from René Descartes who stated, in his correspondence with the Princess Elizabeth of Bohemia in 1643, an algebraic relation equivalent to the following theorem [11].

Theorem 4.1.1 (Descartes). *The curvatures of four pairwise tangent disks in the plane satisfy*

$$(\kappa_1 + \kappa_2 + \kappa_3 + \kappa_4)^2 = 2(\kappa_1^2 + \kappa_2^2 + \kappa_3^2 + \kappa_4^2) \quad (4.1)$$

In 1936, Sir Frederick Soddy¹ published in *Nature* a paper extending the Descartes' Theorem in dimension three. One year later, Thorold Gosset presented in [43] a proof for a generalization of the Descartes' Theorem in arbitrary dimensions.

Theorem 4.1.2 (Soddy-Gosset). *The curvatures of $d + 2$ pairwise tangent d -balls in \mathbb{R}^d satisfy*

$$(\kappa_1 + \cdots + \kappa_{d+2})^2 = d(\kappa_1^2 + \cdots + \kappa_{d+2}^2) \quad (4.2)$$

Soddy-Gosset's theorem was discovered and rediscovered many times [69, 68, 7]. A different type of generalization of the Descartes' Theorem was given by Guettler and Mallows in [49] for octahedral circle packings.

Theorem 4.1.3 (Guettler-Mallows). *Let $\kappa_1, \kappa_2, \kappa_3, \kappa_{-1}, \kappa_{-2}, \kappa_{-3}$ be the curvatures of the disks in an octahedral circle packing where the labelling satisfies that κ_i and κ_{-i} are the curvatures of disjoint disks. Then, the curvatures satisfy the following relations*

$$\kappa_1 + \kappa_{-1} = \kappa_2 + \kappa_{-2} = \kappa_3 + \kappa_{-3} =: 2\kappa_\mu \quad (4.3)$$

$$\kappa_\mu^2 - 2(\kappa_1 + \kappa_2 + \kappa_3)\kappa_\mu + (\kappa_1^2 + \kappa_2^2 + \kappa_3^2) = 0 \quad (4.4)$$

In two independent works, Dias and Nakamura push forward the Guettler and Mallows' generalization to *orthoplicial* sphere packings, the analogue of octahedral circle packings in dimension 3. We shall study in detail these packings in Chapter 5.

Theorem 4.1.4 (Dias-Nakamura). *Let $\kappa_1, \kappa_2, \kappa_3, \kappa_4, \kappa_{-1}, \kappa_{-2}, \kappa_{-3}, \kappa_{-4}$ be the curvatures of the spheres in an orthoplicial sphere packing where the labelling satisfies that κ_i and κ_{-i} are the curvatures of disjoint spheres. Then, the curvatures satisfy the following relations*

$$\kappa_1 + \kappa_{-1} = \kappa_2 + \kappa_{-2} = \kappa_3 + \kappa_{-3} = \kappa_4 + \kappa_{-4} =: 2\kappa_\mu \quad (4.5)$$

$$\kappa_\mu^2 - 2(\kappa_1 + \kappa_2 + \kappa_3 + \kappa_4)\kappa_\mu + (\kappa_1^2 + \kappa_2^2 + \kappa_3^2 + \kappa_4^2) = 0 \quad (4.6)$$

The Descartes' Theorem and its generalizations are a key ingredient for the construction of integral Apollonian packings. In this chapter, we present a generalization of the Descartes' Theorem for all the polytopal d -ball packings whose tangency polytope is regular. We call this new generalization the *Polytopal Descartes' Theorem*. We will see that the Descartes' Theorem can be obtained as a particular case of

¹Chemistry Nobel Prize laureate in 1921 for discovering isotopes.

the Polytopal Descartes' Theorem, as can the generalizations of Soddy and Gosset, Guettler and Mallows, and Dias and Nakamura. Then, we shall use the Polytopal Descartes' Theorem to construct integral Apollonian packings based on the Platonic solids.

4.2 The Polytopal Descartes' Theorem

In the background given in Chapter 1, we explained that the curvature of a d -ball b can be obtained from the Lorentzian product of the corresponding space-like normalized vector $\mathbf{x}_b \in S(\mathbb{L}^{d+1,1})$ with a specific vector $\mathbf{x}_N = e_{d+1} + e_{d+2}$ where e_i denotes the i -th vector of the canonical basis \mathcal{B}_0 of $\mathbb{L}^{d+1,1}$ (Eq. (1.9)). Let us extend this notion of *curvature* to any vector $\mathbf{x} \in \mathbb{L}^{d+1,1}$ by

$$\kappa(\mathbf{x}) = -\langle \mathbf{x}_N, \mathbf{x} \rangle \quad (4.7)$$

Let $\mathcal{P} \subset \mathbb{E}^{d+1}$ be an outer-sphere polytope. For every face f of \mathcal{P} , we define the *Lorentzian barycenter* of f as the vector $\mathbf{x}_f \in \mathbb{L}^{d+1,1}$ given by

$$\mathbf{x}_f := \frac{1}{|V(f)|} \sum_{v \in V(f)} \mathbf{x}_{b(v)} \quad (4.8)$$

where $V(f)$ is the set of vertices of f and $b(v)$ is the illuminated region of v . We also define the *Lorentzian curvature* of f as $\kappa_f := \kappa(\mathbf{x}_f)$. By linearity, we have that

$$\kappa_f = \frac{1}{|V(f)|} \sum_{v \in V(f)} \kappa(b(v)) \quad (4.9)$$

Let us now suppose that \mathcal{P} is edge-scribed and $\mathcal{B}_{\mathcal{P}}$ is a polytopal d -ball packing. For every f of \mathcal{P} , we shall say that κ_f is a *polytopal curvature* of $\mathcal{B}_{\mathcal{P}}$. The polytopal curvature of a vertex v is exactly the curvature of the corresponding d -ball b_v of $\mathcal{B}_{\mathcal{P}}$. A first relation between the polytopal curvatures of polytopal d -ball packing is the following.

Lemma 4.2.1 (Antipodal relation). *Let $\mathcal{B}_{\mathcal{P}}$ be a polytopal d -ball packing where \mathcal{P} is a regular edge-scribed $(d+1)$ -polytope which is centrally symmetric. Then, for any two vertices v, \bar{v} at maximal distance in the 1-skeleton of \mathcal{P} , we have*

$$\kappa_{\mathcal{P}} = \frac{\kappa_v + \kappa_{\bar{v}}}{2}$$

Proof. Since \mathcal{P} is centrally symmetric, then $\frac{1}{2}(\mathbf{x}_{b_v} + \mathbf{x}_{b_{\bar{v}}})$ is the Lorentzian barycenter of \mathcal{P} . The Lemma follows from Eq. (4.7) and linearity. \square

The above lemma applies to every centrally symmetric regular $(d+1)$ -polytope. These are the p -gons with p even when $d = 1$ and all the regular polytopes not belonging to the simplex family when $d \geq 2$.

We define the *flag quadratic form* of a regular $(d+1)$ -polytope \mathcal{P} as

$$\Phi_{\mathcal{P}}(x_0, x_1, \dots, x_{d+1}) := \sum_{i=0}^d \frac{(x_{i+1} - x_i)^2}{L_{\mathcal{P}}(i+1) - L_{\mathcal{P}}(i)} - \frac{x_{d+1}^2}{L_{\mathcal{P}}(d+1)} \quad (4.10)$$

where

$$L_{\mathcal{P}}(i) := \begin{cases} -1 & i = 0 \\ 0 & i = 1 \\ \ell_{f_i}^{-2} & \text{if } 2 \leq i \leq d+1 \end{cases}$$

and ℓ_{f_i} denotes the midsphere ratio of f_i . From the values of the midsphere ratio given in Table A.1, one can compute that, for every $d \geq 1$, the flag quadratic form of the $(d+1)$ -simplex, $(d+1)$ -cross polytope and $(d+1)$ -cube is

$$\Phi_{\mathcal{T}^{d+1}}(x_0, \dots, x_{d+1}) = \sum_{i=0}^d \binom{i+2}{2} (x_i - x_{i+1})^2 - \frac{d+2}{d} x_{d+1}^2 \quad (4.11)$$

$$\Phi_{\mathcal{O}^{d+1}}(x_0, \dots, x_{d+1}) = \sum_{i=0}^{d-1} \binom{i+2}{2} (x_i - x_{i+1})^2 + \frac{d+1}{2} (x_d - x_{d+1})^2 - x_{d+1}^2 \quad (4.12)$$

$$\Phi_{\mathcal{C}^{d+1}}(x_0, \dots, x_{d+1}) = \sum_{i=0}^d (x_i - x_{i+1})^2 - \frac{1}{d} x_{d+1}^2. \quad (4.13)$$

We now can state the main theorem.

Theorem 4.2.1 (Polytopal Descartes' Theorem). *Let $\mathcal{B}_{\mathcal{P}}$ be a polytopal d -ball packing where \mathcal{P} is a regular edge-scribed $(d+1)$ -polytope with $d \geq 1$. Then, for any flag $(v, e, \dots, f, \mathcal{P})$, the polytopal curvatures $\kappa_v, \kappa_e, \dots, \kappa_f, \kappa_{\mathcal{P}}$ of $\mathcal{B}_{\mathcal{P}}$ satisfy*

$$\Phi_{\mathcal{P}}(\kappa_v, \kappa_e, \dots, \kappa_f, \kappa_{\mathcal{P}}) = 0 \quad (4.14)$$

The following lemmas are needed for the proof of Theorem 4.2.1.

Lemma 4.2.2. *Let $\Delta = (\mathbf{x}_1, \dots, \mathbf{x}_{d+2})$ be a collection of $d + 2$ vectors in $\mathbb{L}^{d+1,1}$. Then Δ is a basis if and only if $\text{Gram}(\Delta)$ is non-singular. Moreover, the vector $(\kappa_1, \dots, \kappa_{d+2})$ where $\kappa_i := \kappa(\mathbf{x}_i)$ satisfies*

$$(\kappa_1, \dots, \kappa_{d+2}) \text{Gram}(\Delta)^{-1} \begin{pmatrix} \kappa_1 \\ \vdots \\ \kappa_{d+2} \end{pmatrix} = 0 \quad (4.15)$$

Proof. Let \mathbf{M} be the matrix whose columns are the coordinates of the vectors of Δ with respect to the canonical basis of $\mathbb{L}^{d+1,1}$, $\mathbf{N} = (0, \dots, 0, 1, 1)^T$ and $\mathbf{Q}_{d+2} = \text{Diag}(1, \dots, 1, -1)$. We have that $(\kappa_1, \dots, \kappa_{d+2}) = (\kappa(\mathbf{x}_1), \dots, \kappa(\mathbf{x}_{d+2})) = -\mathbf{M}^T \mathbf{Q}_{d+2} \mathbf{N}$. Therefore,

$$\begin{aligned} (\kappa_1, \dots, \kappa_{d+2}) \text{Gram}(\Delta)^{-1} \begin{pmatrix} \kappa_1 \\ \vdots \\ \kappa_{d+2} \end{pmatrix} &= (-\mathbf{N}^T \mathbf{Q}_{d+2} \mathbf{M}) (\mathbf{M}^{-1} \mathbf{Q}_{d+2} (\mathbf{M}^T)^{-1}) (-\mathbf{M}^T \mathbf{Q}_{d+2} \mathbf{N}) \\ &= \mathbf{N}^T \mathbf{Q}_{d+2} \mathbf{N} = 0 \end{aligned}$$

□

As Boyd noticed in [14], the Soddy-Gosset's generalization (Th. 4.1.2) follows directly by applying the above lemma to the Lorentzian vectors of a packing of $d + 2$ pairwise tangent d -balls.

Lemma 4.2.3. *Let \mathcal{P} be a regular edge-scribed $(d + 1)$ -polytope with $d \geq 1$. The Lorentzian vectors of the vertices of \mathcal{P} are contained in the hyperplane $\{x_{d+2} = \frac{1}{\ell_{\mathcal{P}}}\}$ where $\ell_{\mathcal{P}}$ is the midsphere ratio of \mathcal{P} . Furthermore, for every $f \in \mathcal{F}(\mathcal{P})$ we have $\langle \mathbf{x}_f - \mathbf{x}_{\mathcal{P}}, \mathbf{x}_{\mathcal{P}} \rangle = 0$.*

Proof. Since \mathcal{P} is regular and edge-scribed the barycenter of \mathcal{P} is at the origin of \mathbb{E}^{d+1} and any vertex v of \mathcal{P} has the same Euclidean norm $\|v\|$. Therefore, the length of each half edge of \mathcal{P} is equal to $\ell_{\mathcal{P}} = \sqrt{\|v\|^2 - 1}$. By Eq. (3.2), the Lorentzian vectors of the vertices of \mathcal{P} are contained in the hyperplane

$$H = \{x_{d+2} = \frac{1}{\sqrt{\|v\|^2 - 1}} = \frac{1}{\ell_{\mathcal{P}}}\} \subset \mathbb{L}^{d+1,1}$$

implying that for every face f of \mathcal{P} the Lorentzian vector \mathbf{x}_f is also in H . Since the barycenter of \mathcal{P} is the origin of \mathbb{E}^{d+1} then $\mathbf{x}_{\mathcal{P}} = \frac{1}{\ell_{\mathcal{P}}} e_{d+2}$ implying the second part of the Lemma. □

Let a_1, \dots, a_n be a sequence of real numbers. We define the *corner matrix* $\mathbf{C}(a_1, \dots, a_n)$ as the matrix with the following shape

$$\mathbf{C}(a_1, \dots, a_n) := \begin{pmatrix} a_1 & a_2 & a_3 & \cdots & a_{n-1} & a_n \\ a_2 & a_2 & a_3 & \cdots & a_{n-1} & a_n \\ a_3 & a_3 & a_3 & \cdots & a_{n-1} & a_n \\ \vdots & \vdots & \vdots & \ddots & \vdots & \vdots \\ a_{n-1} & a_{n-1} & a_{n-1} & \cdots & a_{n-1} & a_n \\ a_n & a_n & a_n & \cdots & a_n & a_n \end{pmatrix} \quad (4.16)$$

If $a_i \neq a_{i+1}$ for each $i = 1, \dots, n-1$ then $\mathbf{C}(a_1, \dots, a_n)$ is non-singular. It can be easily checked that its inverse is equal to

$$\begin{pmatrix} \frac{1}{a_1 - a_2} & \frac{-1}{a_1 - a_2} & 0 & \cdots & 0 & 0 & 0 \\ \frac{-1}{a_1 - a_2} & \frac{1}{a_1 - a_2} + \frac{1}{a_2 - a_3} & \frac{-1}{a_2 - a_3} & \ddots & 0 & 0 & 0 \\ 0 & \frac{-1}{a_2 - a_3} & \frac{1}{a_2 - a_3} + \frac{1}{a_3 - a_4} & \ddots & \ddots & 0 & 0 \\ \vdots & \ddots & \ddots & \ddots & \ddots & \ddots & \vdots \\ 0 & 0 & \ddots & \ddots & \frac{1}{a_{n-3} - a_{n-2}} + \frac{1}{a_{n-2} - a_{n-1}} & \frac{-1}{a_{n-2} - a_{n-1}} & 0 \\ 0 & 0 & 0 & \ddots & \frac{-1}{a_{n-2} - a_{n-1}} & \frac{1}{a_{n-2} - a_{n-1}} + \frac{1}{a_{n-1} - a_n} & \frac{-1}{a_{n-1} - a_n} \\ 0 & 0 & 0 & \cdots & 0 & \frac{-1}{a_{n-1} - a_n} & \frac{1}{a_{n-1} - a_n} + \frac{1}{a_n} \end{pmatrix}$$

Moreover, if $\mathbf{X}_n = (x_1, \dots, x_n)$ then it can also be checked that

$$\mathbf{X}_n \mathbf{C}(a_1, \dots, a_n)^{-1} \mathbf{X}_n^T = \sum_{i=1}^{n-1} \left(\frac{(x_i - x_{i+1})^2}{a_i - a_{i+1}} \right) + \frac{x_n^2}{a_n} \quad (4.17)$$

Proof of Theorem 4.2.1. Let $(f_0 = v, f_1 = e, \dots, f_d = f, f_{d+1} = \mathcal{P})$ be a flag of \mathcal{P} and let $\Delta = (\mathbf{x}_{f_0}, \dots, \mathbf{x}_{f_d}, \mathbf{x}_{\mathcal{P}}) \subset \mathbb{L}^{d+1,1}$. We shall show that

$$\text{for any } d \geq 1, \quad \text{Gram}(\Delta) = \mathbf{C}(-L_{\mathcal{P}}(0), -L_{\mathcal{P}}(1), \dots, -L_{\mathcal{P}}(d+1)) \quad (4.18)$$

The desired equality will then follow from this as explained below. Since Gramians and corner matrices are symmetric, then Eq. (4.18) is equivalent to

$$\text{for any } d \geq 1, \quad \text{Gram}(\Delta)_{i,j} = -L_{\mathcal{P}}(j-1) \text{ for every } 1 \leq i \leq j \leq d+2 \quad (4.19)$$

where $\text{Gram}(\Delta)_{i,j}$ denotes the (i, j) -entry of $\text{Gram}(\Delta)$. We shall consider three cases according to the value of j in (4.19):

(i) $j = 1, 2$. Let v' be the other vertex of e . Then,

- $\text{Gram}(\Delta)_{1,1} = \langle \mathbf{x}_v, \mathbf{x}_v \rangle = \langle \mathbf{x}_{b(v)}, \mathbf{x}_{b(v)} \rangle = 1 = -L_{\mathcal{P}}(0)$.
- $\text{Gram}(\Delta)_{1,2} = \langle \mathbf{x}_v, \mathbf{x}_e \rangle = \langle \mathbf{x}_v, \frac{1}{2}(\mathbf{x}_v + \mathbf{x}_{v'}) \rangle = \frac{1}{2}(1 - 1) = 0 = -L_{\mathcal{P}}(1)$.
- $\text{Gram}(\Delta)_{2,2} = \langle \mathbf{x}_e, \mathbf{x}_e \rangle = \langle \frac{1}{2}(\mathbf{x}_v + \mathbf{x}_{v'}), \frac{1}{2}(\mathbf{x}_v + \mathbf{x}_{v'}) \rangle = \frac{1}{4}(1 - 2 + 1) = 0 = -L_{\mathcal{P}}(1)$.

(ii) $j = d + 2$. Since \mathcal{P} is a regular edge-scribed realization, the first part of the Lemma 4.2.3 implies that $\mathbf{x}_{\mathcal{P}} = \frac{1}{\ell_{\mathcal{P}}} e_{d+2}$ where e_{d+2} is the $(d + 2)$ -th vector of the canonical basis of $\mathbb{L}^{d+1,1}$. Therefore,

- $\text{Gram}(\Delta)_{d+2,d+2} = \langle \mathbf{x}_{\mathcal{P}}, \mathbf{x}_{\mathcal{P}} \rangle = -\ell_{\mathcal{P}}^{-2} = -L_{\mathcal{P}}(d + 1)$.

The second part of Lemma 4.2.3 implies that for each $i = 1, \dots, d + 2$ we have

- $\text{Gram}(\Delta)_{i,d+2} = \langle \mathbf{x}_{f_{i-1}}, \mathbf{x}_{\mathcal{P}} \rangle = \langle \mathbf{x}_{\mathcal{P}}, \mathbf{x}_{\mathcal{P}} \rangle = -L_{\mathcal{P}}(d + 1)$.

(iii) $3 \leq j \leq d + 2$. If $d = 1$, then (i) and (ii) cover all the possible values for j . Let $d > 1$. First, we shall prove that (4.19) holds for $j = d + 1$. Since \mathcal{P} is edge-scribed, the facet f_d intersects the unit sphere $\mathbb{S}^d \subset \mathbb{E}^{d+1}$ in a $(d - 1)$ -sphere \mathcal{S} . Let $\mu \in \text{Möb}(\widehat{\mathbb{R}}^d)$ given by the composition of the following two Möbius transformations:

- A rotation of \mathbb{S}^d which sends the barycenter of f_d to the line spanned by the North pole of \mathbb{S}^d .
- The Möbius transformation corresponding to a rescaling of $\widehat{\mathbb{R}}^d$, which sends the rotated \mathcal{S} to the equator of \mathbb{S}^d .

By identifying the hyperplane $\{x_{d+1} = 0\} \subset \mathbb{E}^{d+1}$ with \mathbb{E}^d we have that $\mu(f_d)$ becomes a regular edge-scribed realization \widetilde{f}_d of the regular d -polytope f_d . We can then apply again Lemma 4.2.3 to obtain

$$\langle \mathbf{x}_{\widetilde{f}_{i-1}}, \mathbf{x}_{\widetilde{f}_d} \rangle = -\ell_{\widetilde{f}_d}^{-2} \text{ for every } 1 \leq i \leq d + 1$$

where \widetilde{f}_i is the i -polytope obtained from $\mu(f_i)$ after the identification $\{x_{d+1} = 0\} \simeq \mathbb{E}^d$. This identification preserves the inversive product of the illuminated regions of the outer-sphere points lying in $\{x_{d+1} = 0\}$. Since the inversive product is also invariant under Möbius transformations then, for each $i = 1, \dots, d + 1$, we have:

- $\text{Gram}(\Delta)_{i,d+1} = \langle \mathbf{x}_{f_{i-1}}, \mathbf{x}_{f_d} \rangle = \langle \mathbf{x}_{\tilde{f}_{i-1}}, \mathbf{x}_{\tilde{f}_d} \rangle = -L_{\mathcal{P}}(d)$.

Then, to prove (4.19) for $j = d$ we apply the same arguments as above by considering this time \tilde{f}_{d-1} as a facet of the regular edge-scribed d -polytope \tilde{f}_d . By carrying on these arguments for the rest of the values $3 \leq j \leq d + 2$ we obtain (4.19) which gives (4.18).

Finally, since the sequence

$$(-L_{\mathcal{P}}(0), -L_{\mathcal{P}}(1), \dots, -L_{\mathcal{P}}(d + 1)) = (1, 0, -\ell_{f_2}^{-2}, \dots, -\ell_{\mathcal{P}}^{-2})$$

is strictly decreasing then $\text{Gram}(\Delta)$ is non-singular. Therefore, by applying the Lemma 4.2.2 to Δ we obtain

$$\begin{aligned} 0 &= (\kappa_{f_0}, \dots, \kappa_{f_{d+1}}) \text{Gram}(\Delta)^{-1} (\kappa_{f_0}, \dots, \kappa_{f_{d+1}})^T \\ &= (\kappa_{f_0}, \dots, \kappa_{f_{d+1}}) \mathbf{C}(-L_{\mathcal{P}}(0), \dots, -L_{\mathcal{P}}(d + 1))^{-1} (\kappa_{f_0}, \dots, \kappa_{f_{d+1}})^T \\ &= \sum_{i=0}^d \left(\frac{(\kappa_{f_{i+1}} - \kappa_{f_i})^2}{L_{\mathcal{P}}(i + 1) - L_{\mathcal{P}}(i)} \right) - \frac{\kappa_{\mathcal{P}}^2}{L_{\mathcal{P}}(d + 1)} \\ &= \Phi_{\mathcal{P}}(\kappa_v, \kappa_e, \dots, \kappa_f, \kappa_{\mathcal{P}}) \end{aligned}$$

We finally notice that Eq. (4.15) in Lemma 4.2.2 is invariant under Lorentz transformations. Therefore, Eq. (4.14) holds for any polytopal d -ball packing whose tangency polytope is \mathcal{P} . \square

Corollary 4.2.1. *Let $\mathcal{B}_{\mathcal{P}^+}$ and $\mathcal{B}_{\mathcal{P}^-}$ be two regular polytopal d -ball packings where one is obtained from the other by the inversion on a dual d -ball b_f . Then,*

$$\kappa_{\mathcal{P}^{\pm}} = \left(\frac{\ell_f}{\ell_{\mathcal{P}}} \right)^2 \kappa_f \pm \ell_{\mathcal{P}}^{-2} \sqrt{(\ell_f^2 - \ell_{\mathcal{P}}^2) \Phi_f(\kappa_v, \dots, \kappa_f)} \quad (4.20)$$

Proof. It follows from the definition (4.10) that

$$\Phi_{\mathcal{P}}(x_0, x_1, \dots, x_{d+1}) = \Phi_f(x_0, x_1, \dots, x_d) - \frac{(\ell_f^2 x_d - \ell_{\mathcal{P}}^2 x_{d+1})^2}{\ell_f^2 - \ell_{\mathcal{P}}^2} \quad (4.21)$$

By combining this with (4.14) and then resolving for $\kappa_{\mathcal{P}}$ we obtain (4.20). \square

Let us explain in detail why Theorem 4.2.1 generalizes the Descartes' Theorem. We define the *simplicial*, *hyperoctahedral* and *hypercubical quadratic form* as

$$\begin{aligned}\mathfrak{T}_{d+1}(u_1, \dots, u_{d+2}) &:= \Phi_{\mathcal{T}^{d+1}} \left(u_1, \frac{1}{2}(u_1 + u_2), \dots, \frac{1}{d+2}(u_1 + \dots + u_{d+2}) \right) \\ &= \frac{1}{2} \left(\frac{1}{d} \left(\sum_{i=1}^{d+2} u_i \right)^2 - \sum_{i=1}^{d+2} u_i^2 \right)\end{aligned}\quad (4.22)$$

$$\begin{aligned}\mathfrak{D}_{d+1}(u_1, \dots, u_{d+2}) &:= \Phi_{\mathcal{O}^{d+1}} \left(u_1, \frac{1}{2}(u_1 + u_2), \dots, \frac{1}{d+1}(u_1 + \dots + u_{d+1}), u_{d+2} \right) \\ &= u_{d+2}^2 - \frac{1}{2} \sum_{i=1}^{d+1} (u_i - u_{d+2})^2\end{aligned}\quad (4.23)$$

$$\begin{aligned}\mathfrak{C}_{d+1}(u_1, \dots, u_{d+2}) &:= \Phi_{\mathcal{C}^{d+1}} \left(u_1, \frac{1}{2}(u_1 + u_2), \dots, \frac{1}{2}(u_1 + u_{d+2}) \right) \\ &= \frac{1}{4} \left(\frac{1}{d} (u_1 + u_{d+2})^2 - \sum_{i=1}^{d+1} (u_i - u_{i+1})^2 \right)\end{aligned}\quad (4.24)$$

Corollary 4.2.2 (Soddy-Gosset). *Let $\kappa_1, \dots, \kappa_{d+2}$ be the curvatures of a polytopal d -ball packing $\mathcal{B}_{\mathcal{T}^{d+1}}$. Then,*

$$d \sum_{i=1}^{d+2} \kappa_i^2 = \left(\sum_{i=1}^{d+2} \kappa_i \right)^2 \quad (4.25)$$

Proof. Since \mathcal{T}^{d+1} is Möbius unique, the Polytopal Descartes' Theorem holds for any polytopal d -ball packing $\mathcal{B}_{\mathcal{T}^{d+1}}$. For every $i = 0, \dots, d+1$, let v_i be the vertex of \mathcal{T}^{d+1} corresponding to the d -ball of curvature κ_i . Since \mathcal{T}^{d+1} is a $(d+1)$ -neighborly polytope, every set of vertices span a face. Thus, we can find a flag $(f_0, \dots, f_d, f_{d+1} = \mathcal{T}^{d+1})$ where the vertices of f_i are v_0, \dots, v_i . Therefore, we have

$$\kappa_{f_i} = \frac{1}{i} (\kappa_1 + \dots + \kappa_i). \quad (4.26)$$

Then, by the Polytopal Descartes' Theorem,

$$\mathfrak{T}_{d+1}(\kappa_1, \dots, \kappa_{d+2}) = \Phi_{\mathcal{T}^{d+1}}(\kappa_{f_0}, \dots, \kappa_{f_{d+1}}) = 0$$

which is equivalent to (4.25). \square

In the above corollary, “polytopal d -ball packing $\mathcal{B}_{\mathcal{T}^{d+1}}$ ” can be replaced by a “ d -ball packing made by $d+2$ pairwise tangent d -balls”, as in the original statement of Th. 4.1.2. By Prop. 3.6.1, both definitions are equivalent.

Corollary 4.2.3. *Let $\kappa_1, \dots, \kappa_{d+1}$ be the curvatures of $d+1$ pairwise tangent d -balls of a polytopal d -ball packing $\mathcal{B}_{\mathcal{O}^{d+1}}$. Then,*

$$\sum_{i=1}^{d+1} (\kappa_i - \kappa_{\mathcal{O}^{d+1}})^2 = 2\kappa_{\mathcal{O}^{d+1}}^2 \quad (4.27)$$

Proof. We can apply the same arguments as in the proof of Corollary 4.2.2. The vertices corresponding to the curvatures are the vertices of a facet of \mathcal{O}^{d+1} , which is a d -simplex. Therefore, we can find a flag $(f_0, \dots, f_d, \mathcal{O}^{d+1})$ where Eq. (4.26) is satisfied for every $i = 0, \dots, d$. The Polytopal Descartes' Theorem combined with the hyperoctahedral quadratic form gives the result. \square

For $d = 2, 3$, Eq. (4.27) is equivalent to the second equation given in the Guettler-Mallows and Dias-Nakamura generalizations (Theorems 4.1.3 and 4.1.4), respectively, where $\kappa_\mu = \kappa_{\mathcal{O}^{d+1}}$. The first equation in both theorems corresponds to the Antipodal relation of Lemma 4.2.1.

Corollary 4.2.4. *For every $d \geq 1$, let $\kappa_1, \dots, \kappa_{d+2}$ be the curvatures of $d+2$ consecutive tangent d -balls of a polytopal d -ball packing $\mathcal{B}_{\mathcal{C}^{d+1}}$ where κ_1 and κ_{d+2} are the curvatures of two d -balls at distance $d+1$ in the tangency graph of $\mathcal{B}_{\mathcal{C}^{d+1}}$. Then we have*

$$d \sum_{i=1}^{d+1} (\kappa_i - \kappa_{i+1})^2 = (\kappa_1 + \kappa_{d+2})^2. \quad (4.28)$$

Proof. By Möbius uniqueness, we can consider that \mathcal{C}^{d+1} is regular. Let (v_1, \dots, v_{d+2}) be a path passing through the vertices of \mathcal{C}^{d+1} corresponding to the curvatures. There is a flag (f_0, \dots, f_{d+1}) where f_i is the unique i -face containing the vertices v_1, \dots, v_i . For every $i = 2, \dots, d+1$, the intersection $f_i \cap \mathbb{S}^d$ gives a polytopal i -ball packing $\mathcal{B}_{\mathcal{C}^i}$. By applying the Antipodal relation to $\mathcal{B}_{\mathcal{C}^{i+1}}$ we obtain that, for every $i = 1, \dots, d+2$,

$$\kappa_{f_i} = \frac{1}{2}(\kappa_1 + \kappa_i). \quad (4.29)$$

and therefore,

$$\mathfrak{C}_{d+1}(\kappa_1, \dots, \kappa_{d+2}) = \Phi_{\mathcal{C}^{d+1}}(\kappa_{f_0}, \dots, \kappa_{f_d}, \kappa_{f_{d+1}}) = 0$$

which is equivalent to (4.28). □

In the case when all the curvatures in the d -ball packing in Corollaries 4.2.2, 4.2.3 and 4.2.4 are integers, we obtain a geometric method to find solutions to three Diophantine equations.

Corollary 4.2.5. *Let $d \geq 1$. If there is an integral polytopal d -ball packing $\mathcal{B}_{\mathcal{T}^{d+1}}$, $\mathcal{B}_{\mathcal{O}^{d+1}}$ or $\mathcal{B}_{\mathcal{C}^{d+1}}$ then the following Diophantine equations, respectively, have integer solutions.*

$$d(m_1^2 + \dots + m_{d+2}^2) = n^2 \tag{4.30}$$

$$m_1^2 + \dots + m_{d+1}^2 = 2n^2 \tag{4.31}$$

$$d(m_1^2 + \dots + m_{d+1}^2) = n^2 \tag{4.32}$$

Proof. The three equations are obtained by adding the numbers inside the parenthesis in (4.25), (4.27) and (4.28), respectively. □

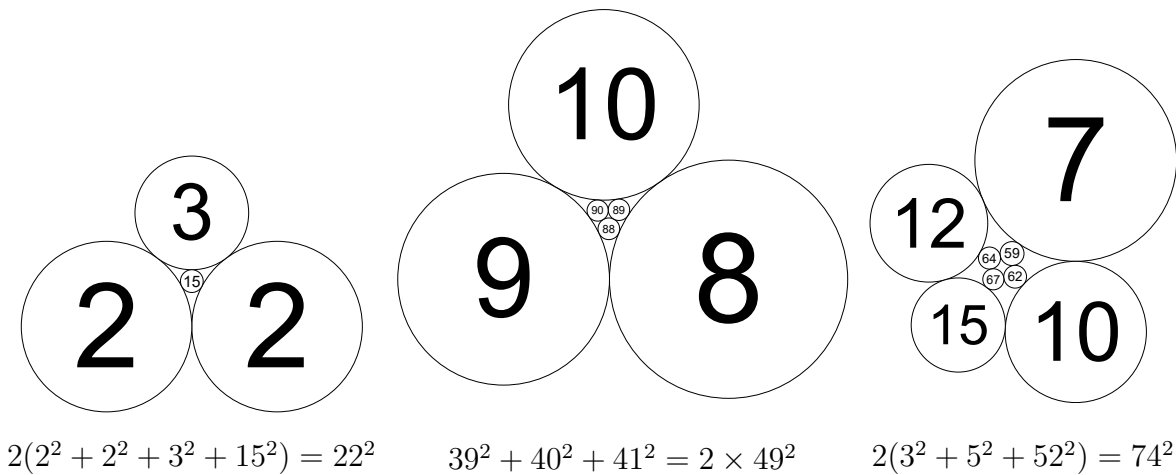


Figure 4.1: Three primitive solutions to Eq. (4.30), (4.31), (4.32) for $d = 2$, obtained by the relations between the polytopal curvatures given in Corollaries 4.2.2, 4.2.3 and 4.2.4, respectively.

4.3 Integrality of the Platonic Apollonian packings

In the same paper where Soddy found the generalization of Descartes' Theorem in three dimensions [92], he noticed, by resolving the quadratic equation (4.25) appearing in the Descartes' Theorem for κ_4 , that if $\kappa_1, \kappa_2, \kappa_3$ are the curvatures of three disks in a Descartes configuration, such that

$$\kappa_1, \kappa_2, \kappa_3 \text{ and } \sqrt{\kappa_1\kappa_2 + \kappa_1\kappa_3 + \kappa_2\kappa_3} \text{ are integers} \quad (4.33)$$

then *all* the curvatures in the Apollonian packing containing the Descartes configuration are integers. An Apollonian packing satisfying this property is said to be *integral* (Fig. 4.2). This simple but deep observation of Soddy opened several lines of research in number theory (see [38, 40] for two excellent surveys). In this section, we apply the Polytopal Descartes' Theorem to obtain integrality conditions analogous to (4.33) for the Platonic Apollonian packings.

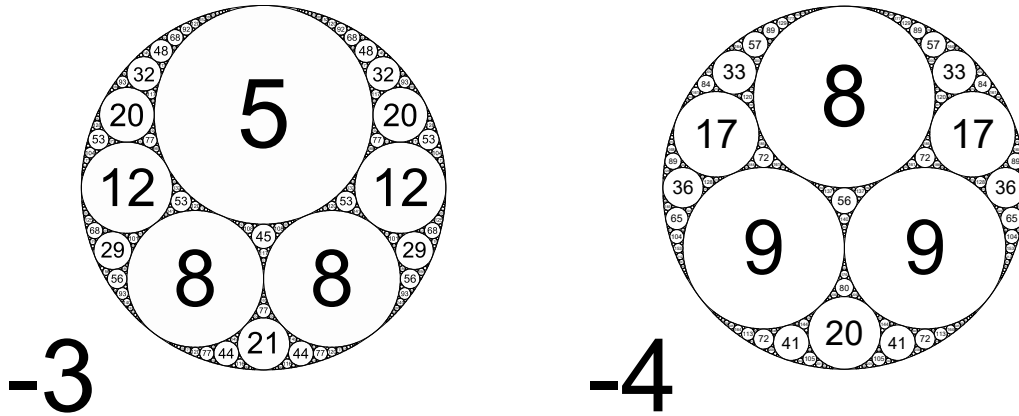


Figure 4.2: Two integral tetrahedral Apollonian packings.

First, we present two corollaries of the Polytopal Descartes' Theorem for $d = 2$.

Corollary 4.3.1. *Let $\mathcal{B}_{\mathcal{P}}$ be a polytopal circle packing where \mathcal{P} is an edge-scribed realization of the Platonic solid with Schläfli symbol $\{p, q\}$. Then, for any flag (v, e, f, \mathcal{P}) , the following relations on the polytopal curvatures of $\mathcal{B}_{\mathcal{P}}$ hold:*

- Relation between two consecutive vertices:

$$\frac{\kappa_v + \kappa_{v'}}{2} = \kappa_e \quad (4.34)$$

where v' is the vertex in $V(\mathcal{P}) \setminus \{v\}$ satisfying $v' \subset e$.

- Relation between two consecutive edges:

$$\frac{\kappa_e + \kappa_{e'}}{2} = \cos\left(\frac{\pi}{p}\right)^2 \kappa_v + \sin\left(\frac{\pi}{p}\right)^2 \kappa_f \quad (4.35)$$

where e' is the edge in $E(\mathcal{P}) \setminus \{e\}$ satisfying $v \subset e' \subset f$.

- Relation between two consecutive faces:

$$\frac{\kappa_f + \kappa_{f'}}{2} = \frac{\cos^2\left(\frac{\pi}{q}\right)}{\sin^2\left(\frac{\pi}{p}\right)} \kappa_e + \frac{\sin^2\left(\frac{\pi}{q}\right) - \cos^2\left(\frac{\pi}{p}\right)}{\sin^2\left(\frac{\pi}{p}\right)} \kappa_{\mathcal{P}} \quad (4.36)$$

where f' is the face in $F(\mathcal{P}) \setminus \{f\}$ satisfying $e \subset f' \subset \mathcal{P}$.

- Relation between two consecutive polyhedra:

$$\frac{\kappa_{\mathcal{P}} + \kappa_{\mathcal{P}'}}{2} = \frac{\sin^2\left(\frac{\pi}{p}\right)}{\sin^2\left(\frac{\pi}{p}\right) - \cos^2\left(\frac{\pi}{q}\right)} \kappa_f \quad (4.37)$$

where $\kappa_{\mathcal{P}'}$ is the polytopal curvature of $\mathcal{B}_{\mathcal{P}'}$:= $s_f(\mathcal{B}_{\mathcal{P}})$ and s_f is the inversion on the disk $b_f \in \mathcal{B}_{\mathcal{P}}^*$.

Proof. Each relation follows by first combining Eq. (3.6) with the Polytopal Descartes' Theorem, then resolving explicitly the quadratic equation for κ_v , κ_e , κ_f and $\kappa_{\mathcal{P}}$, respectively, and finally taking the arithmetic mean of both solutions. \square

Corollary 4.3.2. *The set of curvatures of a Platonic Apollonian packing $\Omega(\mathcal{B}_{\mathcal{P}})$ can be obtained from the curvatures of three consecutive tangent disks of $\mathcal{B}_{\mathcal{P}}$ corresponding to three vertices of \mathcal{P} lying in the same face.*

Proof. Let κ_{i-1} , κ_i and κ_{i+1} be the curvatures of three consecutive tangent disks $d_{i-1}, d_i, d_{i+1} \in \mathcal{B}_{\mathcal{P}}$ corresponding to three vertices of \mathcal{P} lying in the same face f . Let e and e' be the edges of \mathcal{P} with vertices v_{i-1}, v_i and v_i, v_{i+1} , respectively. By replacing $\kappa_e = \frac{1}{2}(\kappa_i + \kappa_{i+1})$ and $\kappa_{e'} = \frac{1}{2}(\kappa_i + \kappa_{i-1})$ in Eq. (4.35), we obtain

$$\kappa_f = \frac{1}{4 \sin^2\left(\frac{\pi}{p}\right)} (\kappa_{i+1} + \kappa_{i-1}) + \left(1 - \frac{1}{2 \sin^2\left(\frac{\pi}{p}\right)}\right) \kappa_i \quad (4.38)$$

By replacing κ_v by κ_i , κ_e by $\frac{1}{2}(\kappa_i + \kappa_{i+1})$ and κ_f by the right-hand side of (4.38) in Eq. (4.20), and then combining with Eq. (3.6), we obtain

$$\kappa_{\mathcal{P}\pm} = \frac{-\cos\left(\frac{2\pi}{p}\right)\kappa_i + \frac{1}{2}(\kappa_{i+1} + \kappa_{i-1}) \pm \cos\left(\frac{\pi}{q}\right)\sqrt{(1 - 4\cos^2\left(\frac{\pi}{p}\right))\kappa_i^2 + \kappa_i\kappa_{i+1} + \kappa_i\kappa_{i-1} + \kappa_{i+1}\kappa_{i-1}}}{2(\sin^2\left(\frac{\pi}{q}\right) - \cos^2\left(\frac{\pi}{p}\right))} \quad (4.39)$$

where the two values correspond to the polytopal curvature $\kappa_{\mathcal{P}}$ and $\kappa_{\mathcal{P}'}$ of $\mathcal{B}_{\mathcal{P}}$ and $s_f(\mathcal{B}_{\mathcal{P}})$, respectively. If we fix $\kappa_{\mathcal{P}}$, we can obtain the curvatures of the disks corresponding to the vertices of \mathcal{P} by iterating Eq. (4.39). If, instead, we fix $\kappa(\mathcal{P}')$, we obtain the curvatures of the disks corresponding to the vertices of \mathcal{P}' . By changing faces and polyhedra we can obtain the curvatures for all the disks in $\Omega(\mathcal{B}_{\mathcal{P}})$ in terms of κ_i , κ_{i+1} and κ_{i-1} . \square

4.3.1 Octahedral Apollonian packings

In the same paper where Guettler and Mallows presented the octahedral Descartes' Theorem, they were able to construct integral octahedral Apollonian packings by giving an integrality condition. Here, we review their result and we prove the reciprocal, which will be useful in the next chapter.

Corollary 4.3.3 (Integrality condition for octahedral Apollonian packings). *Let $\kappa_1, \kappa_2, \kappa_3$ be the curvatures of the three pairwise tangent disks of an octahedral circle packing $\mathcal{B}_{\mathcal{O}^3}$. Then $\Omega(\mathcal{B}_{\mathcal{O}^3})$ is integral if and only if $\kappa_1, \kappa_2, \kappa_3$ and $\sqrt{2\mathfrak{I}_2(\kappa_1, \kappa_2, \kappa_3)}$ are integers.*

Proof. We mimic the same method used by Nakamura for orthoplicial Apollonian packings (see [79]). Let us first suppose that $\kappa_1, \kappa_2, \kappa_3$ and $\sqrt{2\mathfrak{I}_2(\kappa_1, \kappa_2, \kappa_3)}$ are integers. Then, by Cor. 4.2.1, we have that $\kappa_{\mathcal{O}^3}$ is equal to one of the following two expressions

$$\kappa_1 + \kappa_2 + \kappa_3 \pm \sqrt{2\mathfrak{I}_2(\kappa_1, \kappa_2, \kappa_3)} \quad (4.40)$$

Hence, $\kappa_{\mathcal{O}^3}$ is also an integer and therefore, by the Antipodal relation, we have that the remaining curvatures $\kappa_{-1} = 2\kappa_{\mathcal{O}^3} - \kappa_1$, $\kappa_{-2} = 2\kappa_{\mathcal{O}^3} - \kappa_2$ and $\kappa_{-3} = 2\kappa_{\mathcal{O}^3} - \kappa_3$ are also integers. The other value in Eq. (4.40) is the polytopal curvature $\kappa'_{\mathcal{O}^3}$ of

$s_f(\mathcal{B}_{\mathcal{O}^3}) \subset \Omega(\mathcal{B}_{\mathcal{O}^3})$, which again must be an integer. We can then apply the same arguments to obtain that all the curvatures in $s_f(\mathcal{B}_{\mathcal{O}^3})$ are integers. By iterating the same process with other triples, we obtain that $\Omega(\mathcal{B}_{\mathcal{O}^3})$ is integral.

Now let us suppose that $\Omega(\mathcal{B}_{\mathcal{O}^3})$ is integral. Then

$$\mathfrak{I}_2(\kappa_1, \kappa_2, \kappa_3) = \kappa_1\kappa_2 + \kappa_2\kappa_3 + \kappa_1\kappa_3 \in \mathbb{Z} \tag{4.41}$$

By combining the Antipodal relation with Corollary 4.2.1, we have that

$$2(\kappa_1 + \kappa_2 + \kappa_3) \pm 2\sqrt{2\mathfrak{I}_2(\kappa_1, \kappa_2, \kappa_3)} = 2\kappa_{\mathcal{O}^3} = \kappa_1 + \kappa_{-1} \in \mathbb{Z}$$

Therefore, $2\sqrt{2\mathfrak{I}_2(\kappa_1, \kappa_2, \kappa_3)}$ is an integer. Let us show it is an even integer. If there is $m \in \mathbb{Z}$ such that $2\sqrt{2\mathfrak{I}_2(\kappa_1, \kappa_2, \kappa_3)} = 2m + 1$, then we would have

$$\sqrt{2\mathfrak{I}_2(\kappa_1, \kappa_2, \kappa_3)} = m + \frac{1}{2} \Leftrightarrow 2\mathfrak{I}_2(\kappa_1, \kappa_2, \kappa_3) = m^2 + m + \frac{1}{4} \notin \mathbb{Z}$$

contradicting Eq. (4.41). Hence, $2\sqrt{2\mathfrak{I}_2(\kappa_1, \kappa_2, \kappa_3)}$ is an even integer, so $\sqrt{2\mathfrak{I}_2(\kappa_1, \kappa_2, \kappa_3)}$ is also an integer. □

We show in Figure 4.3, two integral octahedral Apollonian packings obtained from three initial disks whose curvatures satisfy the integrality condition of the previous proposition.

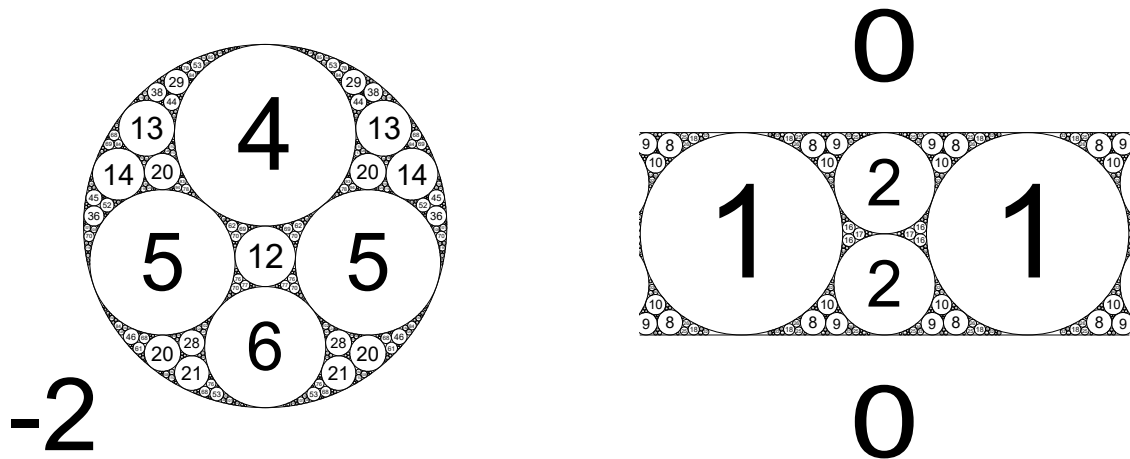


Figure 4.3: Two integral octahedral Apollonian packings with initial curvatures $(-2, 4, 5)$ and $(0, 0, 1)$.

4.3.2 Cubical Apollonian packings

Cubical Apollonian packings have been studied by Stange in [95] as a particular case of the Schmidt arrangement $\mathbb{Q}[\sqrt{-2}]$. They are also mentioned at the end of the paper of Apollonian ring packings of Bolt et al. [10]. Before giving the corresponding integrality condition, let us discuss some useful relations between the curvatures of a cubical circle packing. Since the cube is centrally symmetric, the Antipodal relation of Lemma 4.2.1 holds. Moreover, by applying the Antipodal relation to any square-face we obtain the following relation (which was already noticed by Stange in [95]).

Corollary 4.3.4. *For any cyclic chain of tangent disks d_1, d_2, d_3, d_4 of a cubical circle packing, the curvatures of the disks satisfy*

$$\kappa_1 + \kappa_3 = \kappa_2 + \kappa_4 \quad (4.42)$$

By combining the corollary above with the Antipodal relation, the curvatures of all the disks in a cubical circle packing can be easily deduced from the curvatures of four disks which are not in a cyclic chain. Now we give the corresponding integrality condition, which can be proved similarly to the proof of Cor. 4.3.3.

Corollary 4.3.5 (Integrality condition for cubical Apollonian packings). *Let $\kappa_1, \kappa_2, \kappa_3$ be the curvatures of three consecutive tangent disks in a cubical circle packing \mathcal{B}_{C^3} . Then $\Omega(\mathcal{B}_{C^3})$ is integral if and only if $\kappa_1, \kappa_2, \kappa_3$ and $\sqrt{2\mathfrak{C}_2(\kappa_1, \kappa_2, \kappa_3)}$ are integers.*

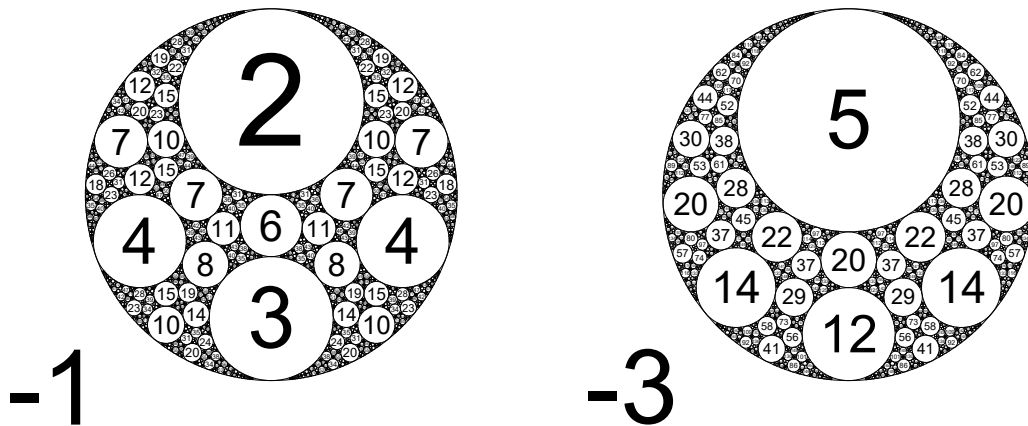


Figure 4.4: Two cubical Apollonian packings with initial curvatures $(-1, 2, 3)$ and $(-3, 5, 12)$.

4.3.3 Icosahedral Apollonian packings

The curvatures of an icosahedral Apollonian packing cannot be in \mathbb{Z} but in $\mathbb{Z}[\varphi]$. We say that such a packing is φ -integral. The corresponding integrality condition for icosahedral Apollonian packings, which can be proved similarly to Cor. 4.3.3, is the following.

Corollary 4.3.6 (Integrality condition of icosahedral Apollonian packings). *Let $\kappa_1, \kappa_2, \kappa_3$ be the curvatures of three mutually tangent disks of an icosahedral circle packing $\mathcal{B}_{\mathcal{I}^3}$. Then, $\Omega(\mathcal{B}_{\mathcal{I}^3})$ is φ -integral if and only if $\kappa_1, \kappa_2, \kappa_3$ and $\sqrt{\mathfrak{I}_2(\kappa_1, \kappa_2, \kappa_3)}$ are in $\mathbb{Z}[\varphi]$.*

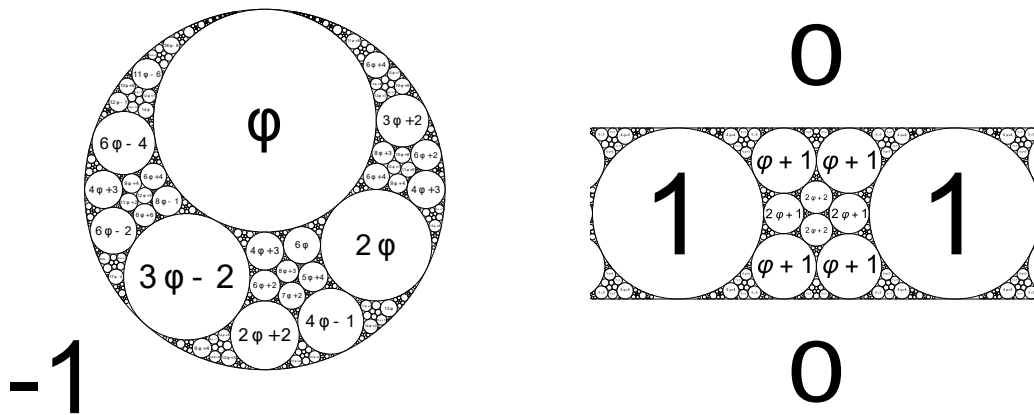


Figure 4.5: Two icosahedral Apollonian packings with initial curvatures $(-1, \varphi, 2\varphi)$ (left) and $(0, 0, 1)$ (right).

4.3.4 Dodecahedral Apollonian packings

Like the cube, the dodecahedron is not simplicial. However, we can obtain from Eq. (4.38) a relation between the curvatures of the disks corresponding to the vertices lying in the same pentagonal face.

Corollary 4.3.7. *For any cyclic chain of tangent disks d_1, d_2, d_3, d_4, d_5 of a dodecahedral circle packing, their curvatures satisfy*

$$\varphi(\kappa_{i+1} - \kappa_i) = \kappa_{i+2} - \kappa_{i-1} \tag{4.43}$$

where i runs cyclically from 1 to 5.

Corollary 4.3.8. *Let $\kappa_{i-1}, \kappa_i, \kappa_{i+1}$ be the curvatures of three consecutive tangent disks in a dodecahedral circle packing $\mathcal{B}_{\mathcal{D}^3}$. Then $\Omega(\mathcal{B}_{\mathcal{D}^3})$ is φ -integral if and only if $\kappa_{i-1}, \kappa_i, \kappa_{i+1}$ and $\sqrt{-\varphi^2\kappa_i^2 + \kappa_i\kappa_{i+1} + \kappa_i\kappa_{i-1} + \kappa_{i-1}\kappa_{i+1}}$ are in $\mathbb{Z}[\varphi]$.*

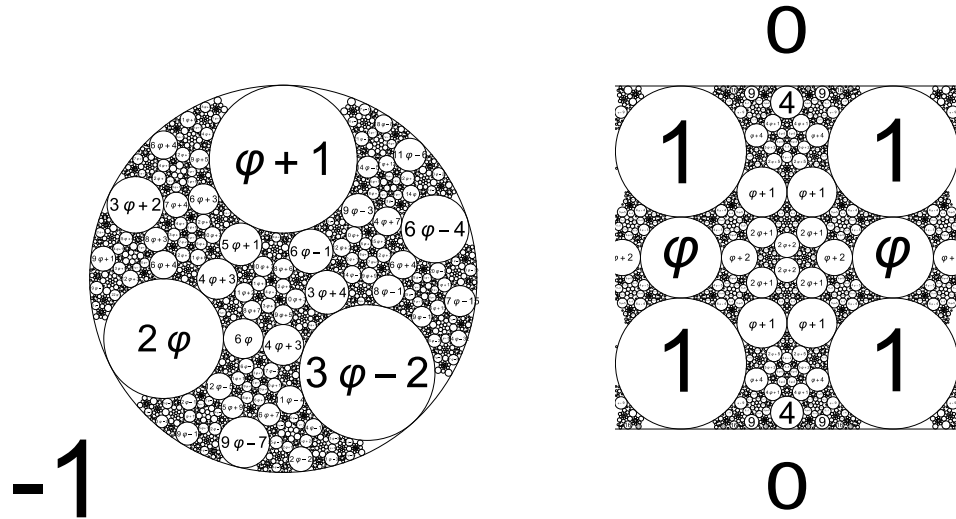


Figure 4.6: Two φ -integral dodecahedral Apollonian packings with initial curvatures $(-1, \varphi + 1, 2\varphi)$ (left) and $(0, 0, 1)$ (right).

Apollonian sections of the orthoplicial Apollonian packing

Contents

5.1 Introduction	87
5.2 The orthoplicial sphere packing	88
5.2.1 Orthoplicial trinities	90
5.2.2 Apollonian groups of the orthoplicial sphere packing	91
5.3 Apollonian sections	94
5.3.1 Construction of orthoplicial Apollonian packings containing a given integral section	99

5.1 Introduction

In this chapter, we revisit the orthoplicial Apollonian packings introduced by Dias [33] and Nakamura [79] as a three-dimensional generalization of the construction of Guettler and Mallows. An orthoplicial Apollonian packing can be obtained as follows. Consider a packing of 8 spheres whose tangency graph is the 1-skeleton of an orthoplex. For each subset of four pairwise tangent spheres, there is a unique dual sphere orthogonal to the four. Invert the whole configuration through every dual sphere, and then repeat this process indefinitely (Fig. 5.1).

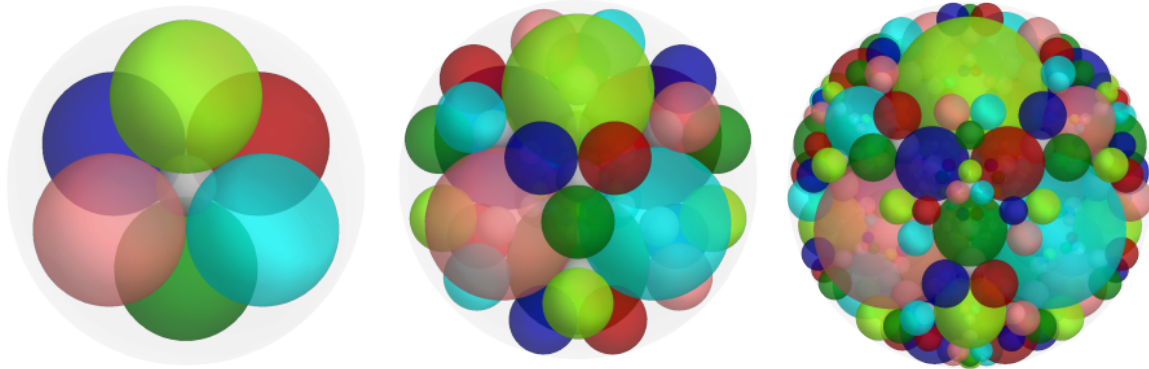


Figure 5.1: The orthoplicial Apollonian sphere packing at 0, 1 and 2 iterations. Each color represents an orbit.

Cross sections are a natural way to study Apollonian configurations in higher dimensions. In [6], Baragar showed several cross sections of d -simplicial Apollonian clusters for $d = 4$ to 8. In order to recognize planar structures in sphere packings, not only geometrically but also arithmetically, we shall present an algebraic generalization of cross sections of Apollonian clusters that we call *Apollonian sections*. We shall use the notion of Apollonian section to prove that the curvatures in every integral tetrahedral, octahedral or cubical Apollonian packing are contained in an integral orthoplicial Apollonian packing.

The structures introduced in this chapter will be used in Chapter 6.

5.2 The orthoplicial sphere packing

Nakamura defined a sphere packing to be *orthoplicial* if its tangency graph is the graph of an orthoplex [79]. These packings were also studied by Sheydvasser as a packing arising from rational quaternion algebras [91]. They can also be obtained as a particular case of Boyd-Maxwell packing [23] or a crystallographic sphere packing [63]. In this section, we shall study orthoplicial sphere packings as *polytopal* sphere packings, i.e. as packings Möbius equivalent to the ball-arrangement projection of an edge-scribed orthoplex. As we show below, orthoplicial sphere packings, in the sense of Nakamura, are polytopal.

Lemma 5.2.1. *All the sphere packings whose tangency graph is the graph of the orthoplex are polytopal.*

Proof. Let \mathcal{B} such a packing. The tangency relations give all the entries of $\text{Gram}(\mathcal{B})$ except for the entries corresponding to the inversive product of disjoint spheres. We shall prove that these inversive products must be all equal to -3 . This would imply, by Th. 3.6.1, that we can reorder the spheres of \mathcal{B} such that $\text{Gram}(\mathcal{B}) = \text{Gram}(\mathcal{B}_{\mathcal{O}^4})$, where $\mathcal{B}_{\mathcal{O}^4}$ is the ball-arrangement projection of an edge-scribed orthoplex. Then, by Prop. 3.6.1, we would have that \mathcal{B} and $\mathcal{B}_{\mathcal{O}^4}$ are Möbius equivalent, and therefore \mathcal{B} would be polytopal.

Let us give an antipodal labelling to $\mathcal{B} = \{b_1, b_2, b_3, b_4, b_{-1}, b_{-2}, b_{-3}, b_{-4}\}$ so b_i is always disjoint to b_{-i} . For every $1 \leq i < j \leq 4$, let $\mathcal{B}_{i,j} \subset \mathcal{B}$ the collection $\{b_i, b_j, b_k, b_l, b_{-i}, b_{-j}\}$ where $\{i, j, k, l\} = \{1, 2, 3, 4\}$. Then, we have

$$\text{Gram}(\mathcal{B}_{i,j}) = \begin{pmatrix} 1 & -1 & -1 & -1 & \lambda_i & -1 \\ -1 & 1 & -1 & -1 & -1 & \lambda_j \\ -1 & -1 & 1 & -1 & -1 & -1 \\ -1 & -1 & -1 & 1 & -1 & -1 \\ \lambda_i & -1 & -1 & -1 & 1 & -1 \\ -1 & \lambda_j & -1 & -1 & -1 & 1 \end{pmatrix}$$

where $\lambda_i := \langle b_i, b_{-i} \rangle$. Since $\mathcal{B}_{i,j}$ corresponds to a collection of 6 vectors of $\mathbb{L}^{4,1}$, then $\text{Gram}(\mathcal{B}_{i,j})$ must be singular. Therefore, the entries $\lambda_1, \lambda_2, \lambda_3, \lambda_4$ must verify the following conditions

$$\lambda_i < -1 \quad \text{and} \quad (\lambda_i - 1)(\lambda_j - 1)(\lambda_i + \lambda_j + 6) = 0 \quad \text{for every } 1 \leq i < j \leq 4 \quad (5.1)$$

There is an only solution to the previous equations which is

$$\lambda_1 = \lambda_2 = \lambda_3 = \lambda_4 = -3$$

□

The first example of orthoplacial sphere packing considered by Nakamura and Dias is the *standard orthoplacial sphere packing* $[\mathcal{B}_{\mathcal{O}^4}]_2^1$ depicted in Fig. 5.2.

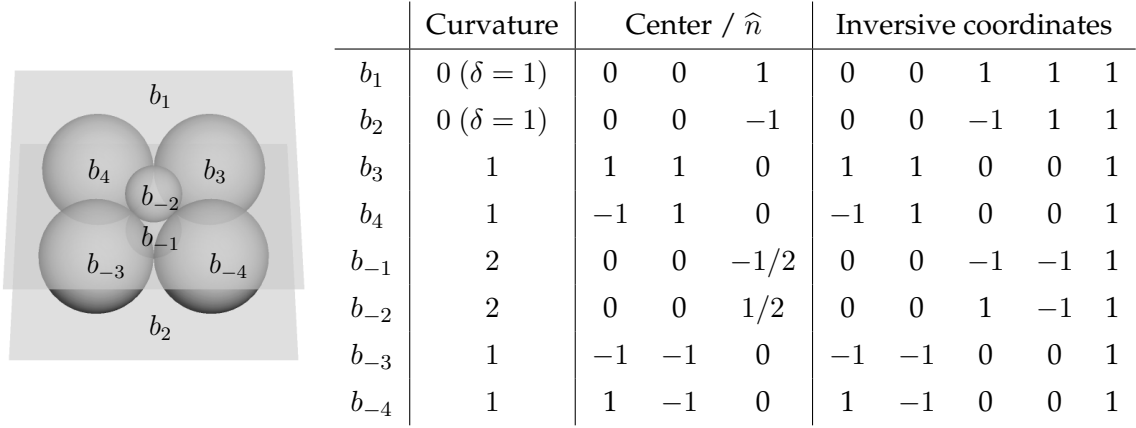


Figure 5.2: The standard orthoplacial sphere packing $[\mathcal{B}_{O^4}]_2^1$.

Remark 5. Nakamura defined in [79] the Platonic orthoplacial sphere packings as orthoplacial sphere packings which are Möbius equivalent to the standard $[\mathcal{B}_{O^4}]_2^1$. By the Möbius uniqueness of the orthoplex given in Cor. 3.6.4 and Lemma 5.2.1, all orthoplacial sphere packings are Platonic in the sense of Nakamura.

5.2.1 Orthoplacial trinities

By polarity, the dual $\mathcal{B}_{O^4}^*$ of an orthoplacial sphere packing is Möbius equivalent to the ball-arrangement projection of a ridge-scribed hypercube. Therefore, $\mathcal{B}_{O^4}^*$ is not a packing. However, by alternating the vertices of the hypercube, we can split the dual in two orthoplacial sphere packings $\mathcal{B}_{O^4}^* = \mathcal{B}'_{O^4} \cup \mathcal{B}''_{O^4}$. Such arrangement of three orthoplacial sphere packings $\{\mathcal{B}_{O^4}, \mathcal{B}'_{O^4}, \mathcal{B}''_{O^4}\}$ will be called an *orthoplacial trinity*.

Lemma 5.2.2. Let $\{\mathcal{B}_{O^4}, \mathcal{B}'_{O^4}, \mathcal{B}''_{O^4}\}$ be an orthoplacial trinity. Then, for any $\mathcal{B} \in \{\mathcal{B}_{O^4}, \mathcal{B}'_{O^4}, \mathcal{B}''_{O^4}\}$, we have that $\mathcal{B}^* = \{\mathcal{B}_{O^4}, \mathcal{B}'_{O^4}, \mathcal{B}''_{O^4}\} \setminus \mathcal{B}$.

Proof. By Cor. 3.6.4, it is enough to prove the result in a particular case. Let us consider the standard orthoplacial sphere packing $[\mathcal{B}_{O^4}]_2^1$ given in Fig. 5.2. The dual of $[\mathcal{B}_{O^4}]_2^1$ can be split into two orthoplacial sphere packings, both obtained from $[\mathcal{B}_{O^4}]_2^1$ by a rotation of $\frac{\pi}{2}$ degree, one around the x -axis and the other around the y -axis, as shown in Fig. 5.3. \square

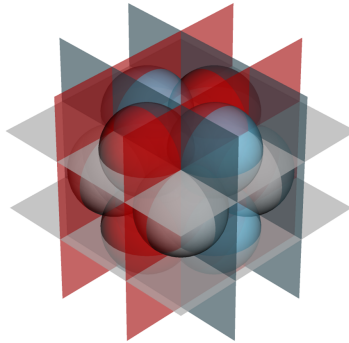


Figure 5.3: An orthoplicial trinity containing the standard $[\mathcal{B}_{O^4}]_2^1$.

The three packings in the previous trinity are 1-CBP projections of the orthoplex. A similar case arises when an orthoplicial trinity contains a 0-CBP projection of the orthoplex. In this case the other two packings must be 3-CBP projections as it is shown in Figure 5.4.

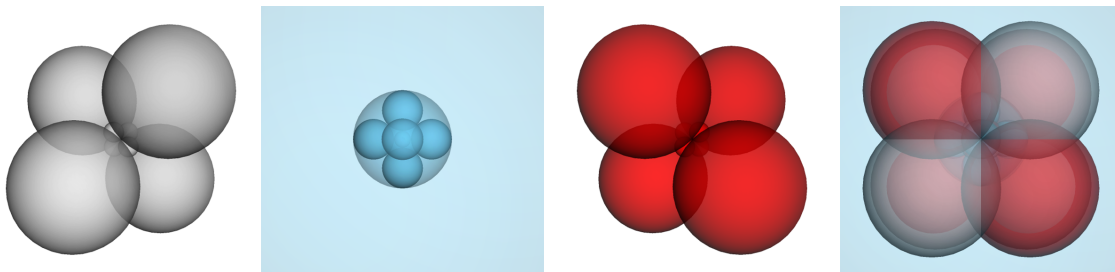


Figure 5.4: From left to right: a 3-CBP projection, a 0-CBP projection and another 3-CBP projection of the orthoplex, and the orthoplicial trinity formed by the three.

5.2.2 Apollonian groups of the orthoplicial sphere packing

In this context, the *orthoplicial Apollonian group* $A(\mathcal{B}_{O^4})$, introduced by Nakamura in [79] and also by Dias in [33], corresponds to the Apollonian group of the standard orthoplicial sphere packing $[\mathcal{B}_{O^4}]_2^1$.

Lemma 5.2.3. *The symmetrized orthoplicial Apollonian group is the hyperbolic Coxeter group with Coxeter graph $\bullet \text{---} \bullet \text{---} \bullet \text{---} \bullet$ and it is isomorphic to the group generated by the*

following five matrices:

$$\mathbf{V} = \begin{pmatrix} -1 & & & & \\ & 1 & & & \\ & & 1 & & \\ & & & 1 & \\ & & & & 1 \end{pmatrix}, \mathbf{E} = \frac{1}{2} \begin{pmatrix} 1 & 1 & -1 & -1 & 0 \\ 1 & 1 & 1 & 1 & 0 \\ -1 & 1 & 1 & -1 & 0 \\ -1 & 1 & -1 & 1 & 0 \\ 0 & 0 & 0 & 0 & 2 \end{pmatrix}, \mathbf{R} = \begin{pmatrix} 1 & & & & \\ & 1 & & & \\ & & -1 & & \\ & & & 1 & \\ & & & & 1 \end{pmatrix},$$

$$\mathbf{F} = \begin{pmatrix} 1 & & & & \\ & 1 & & & \\ & & 0 & 1 & \\ & & 1 & 0 & \\ & & & & 1 \end{pmatrix}, \mathbf{S} = \begin{pmatrix} 1 & 0 & 0 & 0 & 0 \\ 0 & -1 & 0 & -2 & 2 \\ 0 & 0 & 1 & 0 & 0 \\ 0 & -2 & 0 & -1 & 2 \\ 0 & -2 & 0 & -2 & 3 \end{pmatrix}.$$

Proof. Let $[\mathcal{B}_{\mathcal{O}^4}]_2^1$ be the standard orthoplacial sphere packing given in Figure 5.2. Let $\{r_v, r_e, r_r, r_f\}$ be the fundamental generators of the symmetric group of $[\mathcal{B}_{\mathcal{O}^4}]_2^1$, with respect to the flag $(v, e, r, f, \mathcal{O}^4)$, where $v = 1, e = 12, r = 123$ and $f = 1234$. Then, $\{r_v, r_e, r_r, r_f\}$ are represented by the following Möbius transformations:

- r_v is the reflection on the plane $\{x = 0\}$.
- r_e is the inversion on the sphere with center $(-1, 1, -1)$ and radius 2.
- r_r is the reflection on the plane $\{z = 0\}$.
- r_f is the inversion on the sphere with center $(0, 0, 1)$ and radius $\sqrt{2}$.

Since the orthoplex is regular, then $\text{SA}([\mathcal{B}_{\mathcal{O}^4}]_2^1)$ is generated by $\{r_v, r_e, r_r, r_f, s_f\}$, where s_f is the inversion on the sphere orthogonal to b_1, b_2, b_3 and b_4 . By using the inversive coordinates, we obtain a linear faithful representation of $\text{SA}([\mathcal{B}_{\mathcal{O}^4}]_2^1)$ as the discrete subgroup of $O_{4,1}^\uparrow(\mathbb{Q})$, where the generators $\{r_v, r_e, r_r, r_f, s_f\}$ are represented by the matrices $\{\mathbf{V}, \mathbf{E}, \mathbf{R}, \mathbf{F}, \mathbf{S}\}$, respectively. The relations in the Coxeter graph can be checked by straightforward computations on the matrices. By the Möbius uniqueness of the orthoplex, the symmetrized Apollonian group of any other orthoplacial ball packing is isomorphic to $\text{SA}([\mathcal{B}_{\mathcal{O}^4}]_2^1)$. \square

Corollary 5.2.1. *The orthoplacial Apollonian group is isomorphic to the subgroup of $O_{4,1}^\uparrow(\mathbb{Z})$ generated by the following 16 matrices:*

$$\begin{aligned}
\mathbf{S}_{1234} &= \begin{pmatrix} 1 & 0 & 0 & 0 & 0 \\ 0 & -1 & 0 & -2 & 2 \\ 0 & 0 & 1 & 0 & 0 \\ 0 & -2 & 0 & -1 & 2 \\ 0 & -2 & 0 & -2 & 3 \end{pmatrix} = \mathbf{S}, & \mathbf{S}_{123\bar{4}} &= \begin{pmatrix} 1 & 0 & 0 & 0 & 0 \\ 0 & -1 & -2 & 0 & 2 \\ 0 & -2 & -1 & 0 & 2 \\ 0 & 0 & 0 & 1 & 0 \\ 0 & -2 & -2 & 0 & 3 \end{pmatrix} = \mathbf{F}\mathbf{S}_{1234}\mathbf{F}, \\
\mathbf{S}_{12\bar{3}4} &= \begin{pmatrix} 1 & 0 & 0 & 0 & 0 \\ 0 & -1 & 2 & 0 & 2 \\ 0 & 2 & -1 & 0 & -2 \\ 0 & 0 & 0 & 1 & 0 \\ 0 & -2 & 2 & 0 & 3 \end{pmatrix} = \mathbf{R}\mathbf{S}_{1234}\mathbf{R}, & \mathbf{S}_{12\bar{3}\bar{4}} &= \begin{pmatrix} 1 & 0 & 0 & 0 & 0 \\ 0 & -1 & 0 & 2 & 2 \\ 0 & 0 & 1 & 0 & 0 \\ 0 & 2 & 0 & -1 & -2 \\ 0 & -2 & 0 & 2 & 3 \end{pmatrix} = \mathbf{F}\mathbf{S}_{12\bar{3}4}\mathbf{F}, \\
\mathbf{S}_{\bar{1}234} &= \begin{pmatrix} -1 & 0 & 0 & -2 & 2 \\ 0 & 1 & 0 & 0 & 0 \\ 0 & 0 & 1 & 0 & 0 \\ -2 & 0 & 0 & -1 & 2 \\ -2 & 0 & 0 & -2 & 3 \end{pmatrix} = \mathbf{E}\mathbf{S}_{1234}\mathbf{E}, & \mathbf{S}_{\bar{1}23\bar{4}} &= \begin{pmatrix} -1 & 0 & -2 & 0 & 2 \\ 0 & 1 & 0 & 0 & 0 \\ -2 & 0 & -1 & 0 & 2 \\ 0 & 0 & 0 & 1 & 0 \\ -2 & 0 & -2 & 0 & 3 \end{pmatrix} = \mathbf{F}\mathbf{S}_{\bar{1}234}\mathbf{F}, \\
\mathbf{S}_{\bar{1}2\bar{3}4} &= \begin{pmatrix} -1 & 0 & 2 & 0 & 2 \\ 0 & 1 & 0 & 0 & 0 \\ 2 & 0 & -1 & 0 & -2 \\ 0 & 0 & 0 & 1 & 0 \\ -2 & 0 & 2 & 0 & 3 \end{pmatrix} = \mathbf{R}\mathbf{S}_{\bar{1}234}\mathbf{R}, & \mathbf{S}_{\bar{1}2\bar{3}\bar{4}} &= \begin{pmatrix} -1 & 0 & 0 & 2 & 2 \\ 0 & 1 & 0 & 0 & 0 \\ 0 & 0 & 1 & 0 & 0 \\ 2 & 0 & 0 & -1 & -2 \\ -2 & 0 & 0 & 2 & 3 \end{pmatrix} = \mathbf{F}\mathbf{S}_{\bar{1}2\bar{3}4}\mathbf{F}, \\
\mathbf{S}_{\bar{1}\bar{2}34} &= \begin{pmatrix} -1 & 0 & 0 & 2 & -2 \\ 0 & 1 & 0 & 0 & 0 \\ 0 & 0 & 1 & 0 & 0 \\ 2 & 0 & 0 & -1 & 2 \\ 2 & 0 & 0 & -2 & 3 \end{pmatrix} = \mathbf{V}\mathbf{S}_{\bar{1}234}\mathbf{V}, & \mathbf{S}_{\bar{1}\bar{2}3\bar{4}} &= \begin{pmatrix} -1 & 0 & 2 & 0 & -2 \\ 0 & 1 & 0 & 0 & 0 \\ 2 & 0 & -1 & 0 & 2 \\ 0 & 0 & 0 & 1 & 0 \\ 2 & 0 & -2 & 0 & 3 \end{pmatrix} = \mathbf{F}\mathbf{S}_{\bar{1}\bar{2}34}\mathbf{F}, \\
\mathbf{S}_{\bar{1}\bar{2}\bar{3}4} &= \begin{pmatrix} -1 & 0 & -2 & 0 & -2 \\ 0 & 1 & 0 & 0 & 0 \\ -2 & 0 & -1 & 0 & -2 \\ 0 & 0 & 0 & 1 & 0 \\ 2 & 0 & 2 & 0 & 3 \end{pmatrix} = \mathbf{R}\mathbf{S}_{\bar{1}\bar{2}34}\mathbf{R}, & \mathbf{S}_{\bar{1}\bar{2}\bar{3}\bar{4}} &= \begin{pmatrix} -1 & 0 & 0 & -2 & -2 \\ 0 & 1 & 0 & 0 & 0 \\ 0 & 0 & 1 & 0 & 0 \\ -2 & 0 & 0 & -1 & -2 \\ 2 & 0 & 0 & 2 & 3 \end{pmatrix} = \mathbf{F}\mathbf{S}_{\bar{1}\bar{2}\bar{3}4}\mathbf{F}, \\
\mathbf{S}_{\bar{1}\bar{2}3\bar{4}} &= \begin{pmatrix} 1 & 0 & 0 & 0 & 0 \\ 0 & -1 & 0 & 2 & -2 \\ 0 & 0 & 1 & 0 & 0 \\ 0 & 2 & 0 & -1 & 2 \\ 0 & 2 & 0 & -2 & 3 \end{pmatrix} = \mathbf{E}\mathbf{S}_{\bar{1}\bar{2}34}\mathbf{E}, & \mathbf{S}_{\bar{1}\bar{2}\bar{3}\bar{4}} &= \begin{pmatrix} 1 & 0 & 0 & 0 & 0 \\ 0 & -1 & 2 & 0 & -2 \\ 0 & 2 & -1 & 0 & 2 \\ 0 & 0 & 0 & 1 & 0 \\ 0 & 2 & -2 & 0 & 3 \end{pmatrix} = \mathbf{F}\mathbf{S}_{\bar{1}\bar{2}3\bar{4}}\mathbf{F}, \\
\mathbf{S}_{\bar{1}\bar{2}\bar{3}4} &= \begin{pmatrix} 1 & 0 & 0 & 0 & 0 \\ 0 & -1 & -2 & 0 & -2 \\ 0 & 0 & 0 & 1 & 0 \\ 0 & 0 & 0 & 1 & 0 \\ 0 & 2 & 2 & 0 & 3 \end{pmatrix} = \mathbf{R}\mathbf{S}_{\bar{1}\bar{2}\bar{3}4}\mathbf{R}, & \mathbf{S}_{\bar{1}\bar{2}\bar{3}\bar{4}} &= \begin{pmatrix} 1 & 0 & 0 & 0 & 0 \\ 0 & -1 & 0 & -2 & -2 \\ 0 & 0 & 1 & 0 & 0 \\ 0 & -2 & 0 & -1 & -2 \\ 0 & 2 & 0 & 2 & 3 \end{pmatrix} = \mathbf{F}\mathbf{S}_{\bar{1}\bar{2}\bar{3}\bar{4}}\mathbf{F}.
\end{aligned}$$

The previous representation of the orthoplial Apollonian group in $O_{4,1}^\uparrow(\mathbb{Z})$ can be obtained by conjugating the matrix representation $O_W^\uparrow(\mathbb{Z})$ given by Nakamura in [79], where W is the matrix of the inversive product in augmented curvature-center coordinates (see [69]). Both representations satisfy the following relations:

(R1) $S_{ijkl}^2 = 1$ for every $(i, j, k, l) = (\pm 1, \pm 2, \pm 3, \pm 4)$.

(R2) $(S_{ijkl}S_{i'j'k'l'})^2 = 1$ if the labels $ijkl$ and $i'j'k'l'$ differ by only one letter.

5.3 Apollonian sections

Let $\mathcal{B}_{\mathcal{P}}$ be a polytopal d -ball packing and let $A(\mathcal{B}_{\mathcal{P}})$ and $\Omega(\mathcal{B}_{\mathcal{P}})$ be the *Apollonian group* and the Apollonian cluster of $\mathcal{B}_{\mathcal{P}}$. We say that a subset $\Sigma \subset \Omega(\mathcal{B}_{\mathcal{P}})$ is an *Apollonian section* of $\Omega(\mathcal{B}_{\mathcal{P}})$ if there is subgroup $\Gamma < A(\mathcal{B}_{\mathcal{P}})$ and a subset $X \subseteq \mathcal{B}_{\mathcal{P}}$ such that $\Sigma = \Gamma \cdot X$. Two Apollonian sections $\Sigma = \Gamma \cdot X$ and $\Sigma' = \Gamma' \cdot X'$ of two different polytopal Apollonian clusters $\Omega(\mathcal{B}_{\mathcal{P}})$ and $\Omega(\mathcal{B}_{\mathcal{P}'})$, respectively, are said to be *algebraically equivalent* if Γ and Γ' are isomorphic and there is an equivariant bijection between $\Gamma \cdot X$ and $\Gamma' \cdot X'$ with respect to the actions. More specifically, Σ and Σ' are algebraically equivalent if there exist two bijections $\phi : \Gamma \rightarrow \Gamma'$ and $\psi : \Sigma \rightarrow \Sigma'$ such that

(i) $\phi : \Gamma \rightarrow \Gamma'$ is a group isomorphism

(ii) For all $g \in \Gamma$ and all $b \in X$, $\psi(g \cdot b) = \phi(g) \cdot \psi(b)$

If in addition ψ preserves curvatures, we say that Σ and Σ' are *arithmetically equivalent*. We shall say that an Apollonian cluster has a tetrahedral, octahedral, cubical, icosahedral or dodecahedral Apollonian section if it contains an Apollonian section algebraically equivalent to an Apollonian packing of the corresponding Platonic solid.

Proposition 5.3.1. *Every orthoplicial Apollonian packing contains a tetrahedral, octahedral and cubical Apollonian section.*

Proof. Since the orthoplex is Möbius unique, it is enough to find the desired Apollonian sections in a particular orthoplicial Apollonian packing. First, we shall construct a tetrahedral and octahedral Apollonian section in $\Omega([\mathcal{B}_{\mathcal{O}^4}]_2^1)$ (Fig. 5.5).

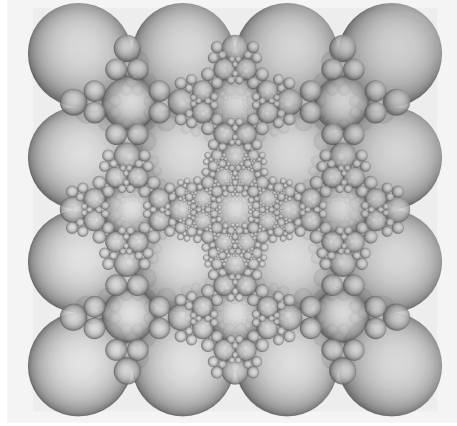


Figure 5.5: The orthoplicial Apollonian packing $\Omega([\mathcal{B}_{\mathcal{O}^4}]_2^1)$ at depth ≤ 3 , view from above.

(Tetrahedral section) Let $\Sigma_{\mathcal{T}} = \Gamma_{\mathcal{T}} \cdot X_{\mathcal{T}}$ where $X_{\mathcal{T}} = \{b_1, b_2, b_3, b_4\} \subset [\mathcal{B}_{\mathcal{O}^4}]_2^1$, $\Gamma_{\mathcal{T}} = \langle s_{\bar{1}234}, s_{1\bar{2}34}, s_{12\bar{3}4}, s_{123\bar{4}} \rangle < A([\mathcal{B}_{\mathcal{O}^4}]_2^1)$ and let $b_{1234} \in ([\mathcal{B}_{\mathcal{O}^4}]_2^1)^*$. One can check that $\Gamma_{\mathcal{T}}$ leaves invariant b_{1234} . Let $H_{\mathcal{T}}$ be the boundary of b_{1234} . In $[\mathcal{B}_{\mathcal{O}^4}]_2^1$, $H_{\mathcal{T}}$ is the plane $\{y = 1\}$. After identifying $H_{\mathcal{T}}$ with $\widehat{\mathbb{R}^2}$, we obtain that

$$X_{\mathcal{T}} \cap H_{\mathcal{T}} := \{b_1 \cap H_{\mathcal{T}}, b_2 \cap H_{\mathcal{T}}, b_3 \cap H_{\mathcal{T}}, b_4 \cap H_{\mathcal{T}}\}$$

becomes a tetrahedral circle packing $\mathcal{B}_{\mathcal{T}^3}$. Moreover, the restriction of $\Gamma_{\mathcal{T}}$ on $H_{\mathcal{T}}$ induces an isomorphism between $\Gamma_{\mathcal{T}}$ and $A(\mathcal{B}_{\mathcal{T}^3})$ given by

$$\begin{aligned} \phi_{\mathcal{T}} : \Gamma_{\mathcal{T}} &\longrightarrow A(\mathcal{B}_{\mathcal{T}^3}) \\ s_b &\longmapsto s_{b \cap H_{\mathcal{T}}} \end{aligned}$$

where s_b denotes the inversion on b . On the other hand, we can construct a bijection

$$\begin{aligned} \psi_{\mathcal{T}} : \Sigma_{\mathcal{T}} &\longrightarrow \Omega(\mathcal{B}_{\mathcal{T}^3}) \\ g \cdot b &\longmapsto (g \cdot b) \cap H_{\mathcal{T}} \end{aligned}$$

By inspection, one can check that for every $ijkl \in \{\bar{1}234, 1\bar{2}34, 12\bar{3}4, 123\bar{4}\}$ and for every $m = 1, 2, 3, 4$, we have

$$\begin{aligned} \psi_{\mathcal{T}}(s_{ijkl} \cdot b_m) &= (s_{ijkl} \cdot b_m) \cap H_{\mathcal{T}} \\ &= \phi_{\mathcal{T}}(s_{ijkl}) \cdot (b_m \cap H_{\mathcal{T}}) \\ &= \phi_{\mathcal{T}}(s_{ijkl}) \cdot \psi_{\mathcal{T}}(b_m) \end{aligned}$$

which gives the equivariance of $\psi_{\mathcal{T}}$. Therefore, $\Sigma_{\mathcal{T}}$ is algebraically equivalent to the tetrahedral Apollonian packing $\Omega(\mathcal{B}_{\mathcal{T}^3})$.

(Octahedral section) We may apply a similar strategy to construct an octahedral section in $\Omega([\mathcal{B}_{\mathcal{O}^4}]_2^1)$ by intersecting with the plane $H_{\mathcal{O}} := \{x - y = 1\}$, orthogonal to every $b \in X_{\mathcal{O}} := [\mathcal{B}_{\mathcal{O}^4}]_2^1 \setminus \{b_4, b_{-4}\}$. The intersection $H_{\mathcal{O}} \cap X_{\mathcal{O}}$ gives an octahedral circle packing $\mathcal{B}_{\mathcal{O}^3}$. We define then $\Sigma_{\mathcal{O}} := \Gamma_{\mathcal{O}} \cdot X_{\mathcal{O}} \subset \Omega([\mathcal{B}_{\mathcal{O}^4}]_2^1)$ where

$$\Gamma_{\mathcal{O}} = \langle t_{123}, t_{\bar{1}23}, t_{1\bar{2}3}, t_{12\bar{3}}, t_{\bar{1}\bar{2}3}, t_{1\bar{2}\bar{3}}, t_{\bar{1}2\bar{3}} \mid t_{ijk} := s_{ijk4}s_{ijk\bar{4}} \rangle$$

In this case, the group isomorphism $\phi_{\mathcal{O}} : \Gamma_{\mathcal{O}} \mapsto A(\mathcal{B}_{\mathcal{O}^3})$ is given by $t_{ijk} \mapsto s_{ijk}$, where s_{ijk} denotes the inversion on the disk orthogonal to the three disks $\{b_i \cap H_{\mathcal{O}}, b_j \cap H_{\mathcal{O}}, b_k \cap H_{\mathcal{O}}\}$. The equivariant bijection $\psi_{\mathcal{O}} : \Sigma_{\mathcal{O}} \rightarrow \Omega(\mathcal{B}_{\mathcal{O}^3})$ is then given by $g(b) \mapsto g(b) \cap H_{\mathcal{O}}$. We illustrate in Figure 5.6 the tetrahedral and octahedral sections $\Sigma_{\mathcal{T}}$ and $\Sigma_{\mathcal{O}}$.

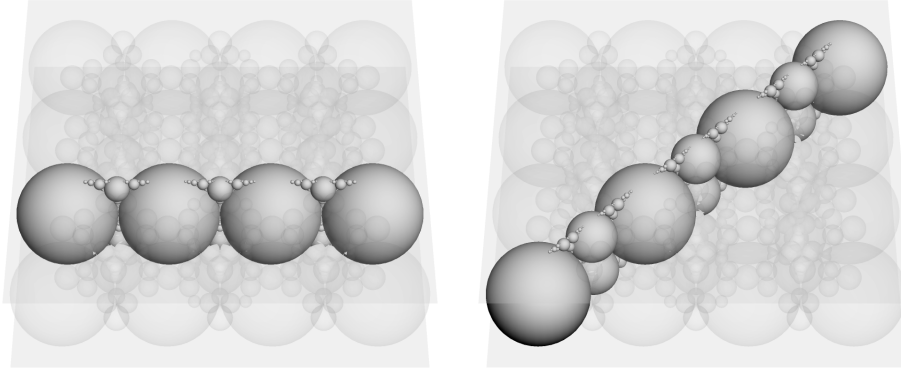
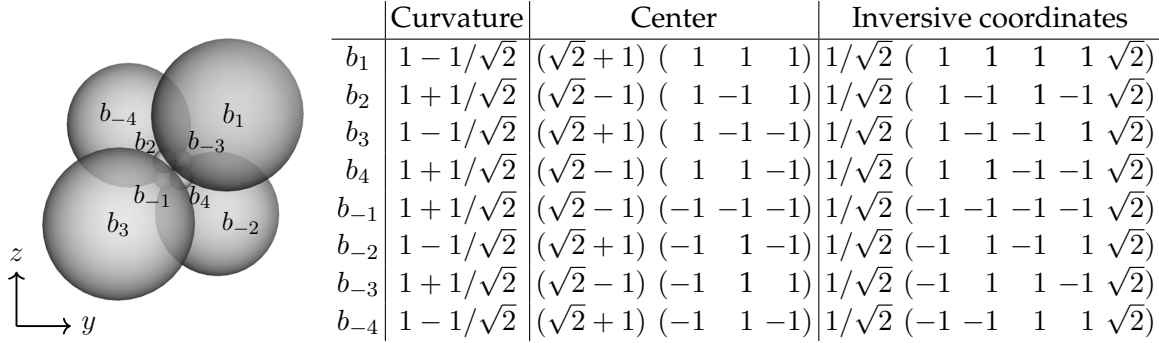


Figure 5.6: A tetrahedral (left) and octahedral (right) Apollonian section of $\Omega([\mathcal{B}_{\mathcal{O}^4}]_2^1)$.

(Cubical section) This case is a bit more tricky. We consider the orthoplacial sphere packing $\mathcal{B}_{\mathcal{O}^4}^{\uparrow x}$ obtained by a 3-CBP projection of the orthoplex, with the labelling and coordinates given in Figure 5.7. We call the labelling given in Figure 5.7 the *x-labelling*. We notice that in the *x-labelling*, i is positive if and only if the first coordinate of the center of b_i is positive.

Figure 5.7: The orthoplacial sphere packing $\mathcal{B}_{\mathcal{O}^4}^{\uparrow x}$.

The orthoplacial Apollonian packing $\Omega(\mathcal{B}_{\mathcal{O}^4}^{\uparrow x})$ and a cubical Apollonian section of $\Omega(\mathcal{B}_{\mathcal{O}^4}^{\uparrow x})$ are shown in Figure 5.9. Let us describe the construction. First, we consider the ridge-scribed cube and hypercube

$$\mathcal{C}^3 := \text{conv}\left\{\frac{1}{\sqrt{2}}(\pm 1, \pm 1, \pm 1)\right\} \quad \mathcal{C}^4 := \text{conv}\left\{\frac{1}{\sqrt{2}}(\pm 1, \pm 1, \pm 1, \pm 1)\right\}$$

We split \mathcal{C}^4 into two edge-scribed orthoplexes induced by the classes of a 2-coloring of its vertices. Let \mathcal{O}^4 be the orthoplex in the class of the vertex $\frac{1}{\sqrt{2}}(1, 1, 1, 1)$. Then we have that $\mathcal{B}_{\mathcal{O}^4}^{\uparrow x} = \beta(\mathcal{O}^4)$. Let $\pi : \mathbb{E}^4 \rightarrow \mathbb{E}^3$ be the orthographic projection onto the hyperplane $\{x_1 = 0\} \subset \mathbb{E}^4$ made by deleting the first coordinate. We have that $\pi(\mathcal{O}^4) = \mathcal{C}^3$. Now let $\mathcal{B}_{\mathcal{C}^3} = \beta(\mathcal{C}^3)$. By mapping b_v to $b_{\pi(v)}$, for every $v \in \mathcal{O}^4$, we construct a bijection $\tilde{\pi} : \mathcal{B}_{\mathcal{O}^4}^{\uparrow x} \rightarrow \mathcal{B}_{\mathcal{C}^3}$. Now we consider the packing $\mathcal{B}_{H_C}^{\perp} \subset (\mathcal{B}_{\mathcal{O}^4}^{\uparrow x})^*$ made by the six spheres of $(\mathcal{B}_{\mathcal{O}^4}^{\uparrow x})^*$ which are orthogonal to $H_C := \{x = 0\} \subset \widehat{\mathbb{R}}^3$ (see the blue packing in Figure 5.4), and let $\Gamma_C < A(\mathcal{B}_{\mathcal{O}^4}^{\uparrow x})$ be the group generated by the inversions on the spheres of $\mathcal{B}_{H_C}^{\perp}$. According to the x -labelling, we have that Γ_C corresponds to the parabolic subgroup of $A(\mathcal{B}_{\mathcal{O}^4}^{\uparrow x})$ given by

$$\langle s_{12\bar{3}4}, s_{1\bar{2}34}, s_{\bar{1}234}, s_{1\bar{2}3\bar{4}}, s_{\bar{1}2\bar{3}4}, s_{1\bar{2}\bar{3}\bar{4}} \rangle$$

The intersection of $\mathcal{B}_{H_C}^{\perp}$ with H_C induces a map of $\mathcal{B}_{H_C}^{\perp}$ to $\mathcal{B}_{\mathcal{C}^3}^*$ (see Figure 5.8). Therefore, we can define a group isomorphism $\phi_C : \Gamma_C \rightarrow A(\mathcal{B}_{\mathcal{C}^3})$ by mapping the inversion on every sphere $b \in \mathcal{B}_{H_C}^{\perp}$ to the inversion on the circle $(b \cap H_C) \in \mathcal{B}_{\mathcal{C}^3}^*$. Let $\Sigma_C := \Gamma_C \cdot \mathcal{B}_{\mathcal{O}^4}^{\uparrow x}$. It can be checked that for every $g \in \Gamma_C$ and every $b \in \mathcal{B}_{\mathcal{O}^4}^{\uparrow x}$, the

mapping

$$\begin{aligned}\psi_C : \Sigma_C &\rightarrow \Omega(\mathcal{B}_{C^3}) \\ g \cdot b &\mapsto \phi(g) \cdot \tilde{\pi}(b)\end{aligned}$$

defines an equivariant bijection with respect to the action of Γ_C on $\mathcal{B}_{\mathcal{O}^4}^{\uparrow x}$. Therefore, Σ_C is a cubical Apollonian section of $\Omega(\mathcal{B}_{\mathcal{O}^4}^{\uparrow x})$. \square

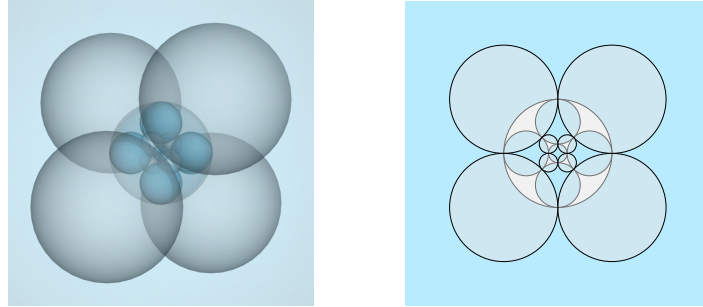


Figure 5.8: (Left) $\mathcal{B}_{\mathcal{O}^4}^{\uparrow x}$ in gray with $\mathcal{B}_{H_C}^{\perp}$ in blue; (right) \mathcal{B}_{C^3} in gray with $\mathcal{B}_{C^3}^*$ in blue.

The bijections $\psi_{\mathcal{T}}$ and $\psi_{\mathcal{O}}$ described above, both preserve the inversive product, which is not the case for ψ_C . Indeed, spheres which are tangent in the cubical Apollonian section may correspond to disjoint disks in the cubical Apollonian packing. To see this, we might consider the cubical Apollonian packing $\Omega(\mathcal{B}_{C^3})$ given above with a 2-coloring. Then, two disks $\psi_C(b)$ and $\psi_C(b')$ have the same color if and only if the centers of b and b' both lie on the same side of the plane H_C . When two disks with the same color (and therefore disjoint), correspond to two vertices lying in the same square-face, then the corresponding spheres are tangent (see Fig. 5.9).

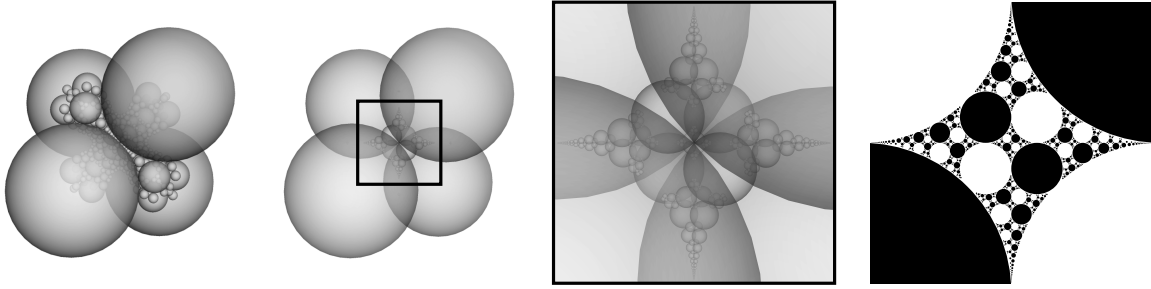


Figure 5.9: (From left to right) The orthoplicial Apollonian sphere packing $\Omega(\mathcal{B}_{\mathcal{O}^4}^{\uparrow x})$; a cubical Apollonian section Σ_C of $\Omega(\mathcal{B}_{\mathcal{O}^4}^{\uparrow x})$; Σ_C zoomed; the corresponding cubical Apollonian circle packing with a minimal coloration.

On the arithmetic side, the bijections $\psi_{\mathcal{T}}$ and $\psi_{\mathcal{O}}$ preserve the curvatures, contrarily to ψ_C . However, by composing ψ_C with a rescaling of $\widehat{\mathbb{R}}^2$ of factor $\sqrt{2}$ we obtain a bijection that does preserve the curvatures. These properties will be important in the next section in order to construct integral orthoplicial Apollonian packings containing an Apollonian section with prescribed curvatures.

5.3.1 Construction of orthoplicial Apollonian packings containing a given integral section

In this section, we prove the main result of this chapter.

Theorem 5.3.1. *Let $\Omega(\mathcal{B}_{\mathcal{P}})$ be either a tetrahedral, an octahedral or a cubical Apollonian packing. There is an orthoplicial Apollonian packing $\Omega(\mathcal{B}_{\mathcal{O}^4})$ containing an Apollonian section arithmetically equivalent to $\Omega(\mathcal{B}_{\mathcal{P}})$. Moreover, $\Omega(\mathcal{B}_{\mathcal{P}})$ is integral if and only if $\Omega(\mathcal{B}_{\mathcal{O}^4})$ is integral.*

For the integrality part, we need the integrality condition for orthoplicial Apollonian sphere packings.

Lemma 5.3.1 (Integrality condition for orthoplicial Apollonian packings). *Let $\kappa_1, \kappa_2, \kappa_3$ and κ_4 be the curvatures of four pairwise tangent spheres of an orthoplicial sphere packing $\mathcal{B}_{\mathcal{O}^4}$. Then, $\Omega(\mathcal{B}_{\mathcal{O}^4})$ is integral if and only if $\kappa_1, \kappa_2, \kappa_3, \kappa_4$ and $\sqrt{\mathfrak{T}_3(\kappa_1, \kappa_2, \kappa_3, \kappa_4)}$ are integers.*

Proof. Nakamura gave a proof in [79] for all orthoplacial sphere packings Möbius equivalent to the standard $[\mathcal{B}_{\mathcal{O}^4}]_2^1$. Since the orthoplex is Möbius unique, Nakamura's lemma applies to every orthoplacial sphere packing. \square

Proof of Theorem 5.3.1. Let $\mathcal{B}_{\mathcal{O}^4}$ be the orthoplacial sphere packing obtained from $[\mathcal{B}_{\mathcal{O}^4}]_2^1$ by applying a translation of \mathbb{R}^3 of vector $(-1, 0, 0)$, so $H_{\mathcal{T}}$ becomes the plane given by $\{x = 0\}$. Let $\Sigma_{\mathcal{T}} = \Gamma_{\mathcal{T}} \cdot X_{\mathcal{T}}$ be the corresponding tetrahedral section of $\Omega(\mathcal{B}_{\mathcal{O}^4})$ and let $\mathcal{B}_{\mathcal{T}^3}$ be the tetrahedral circle packing given by $\psi_{\mathcal{T}}(X_{\mathcal{T}})$. In inversive coordinates, the bijection $\psi_{\mathcal{T}}^{-1} : \Omega(\mathcal{B}_{\mathcal{T}^3}) \rightarrow \Sigma_{\mathcal{T}} \subset \Omega(\mathcal{B}_{\mathcal{O}^4})$ is given by

$$\begin{aligned} \psi_{\mathcal{T}}^{-1} : \Omega(\mathcal{B}_{\mathcal{T}^3}) &\longrightarrow \Sigma_{\mathcal{T}} \\ \mathbf{i}(b) &\longmapsto \begin{pmatrix} 0 \\ \mathbf{i}(b) \end{pmatrix} \end{aligned}$$

Let $\mathcal{B}'_{\mathcal{T}^3}$ be any tetrahedral circle packing. Since the tetrahedron is Möbius unique, there exists $\mu \in \text{Möb}(\widehat{\mathbb{R}^2})$ such that $\mu \cdot \mathcal{B}_{\mathcal{T}^3} = \mathcal{B}'_{\mathcal{T}^3}$. Therefore, $\mu \cdot \Omega(\mathcal{B}_{\mathcal{T}^3}) = \Omega(\mathcal{B}'_{\mathcal{T}^3})$. Let $\mathbf{M} \in O_{3,1}^{\uparrow}(\mathbb{R})$ be the matrix corresponding to μ and let $\tilde{\mu} \in \text{Möb}(\widehat{\mathbb{R}^3})$ be the Möbius transformation corresponding to the matrix

$$\left(\begin{array}{c|c} 1 & \mathbf{0}_4^T \\ \hline \mathbf{0}_4 & \mathbf{M} \end{array} \right) \in O_{4,1}^{\uparrow}(\mathbb{R})$$

where $\mathbf{0}_4$ is the null column-matrix of size 4. We have that $\Sigma'_{\mathcal{T}} := \tilde{\mu} \cdot \Sigma_{\mathcal{T}}$ is a tetrahedral section of the orthoplacial Apollonian packing $\Omega(\mathcal{B}'_{\mathcal{O}^4}) = \tilde{\mu} \cdot \Omega(\mathcal{B}_{\mathcal{O}^4})$. We define the bijection

$$\tilde{\psi}_{\mathcal{T}} := \mu \circ \psi_{\mathcal{T}} \circ \tilde{\mu}^{-1}$$

mapping $\Sigma'_{\mathcal{T}}$ to $\Omega(\mathcal{B}'_{\mathcal{T}^3})$. Let us show that $\Sigma'_{\mathcal{T}}$ preserves curvatures. For every disk $b \in \Omega(\mathcal{B}'_{\mathcal{O}^3})$, we have

$$\begin{aligned} \kappa(\tilde{\psi}_{\mathcal{T}}^{-1}(b)) &= \kappa(\tilde{\mu} \circ \psi_{\mathcal{T}}^{-1} \circ \mu^{-1}(b)) \\ &= \mathbf{k}_5 \left(\begin{array}{c|c} 1 & \mathbf{0}_4^T \\ \hline \mathbf{0}_4 & \mathbf{M} \end{array} \right) \begin{pmatrix} \mathbf{0}_4^T \\ \mathbf{I}_4 \end{pmatrix} \mathbf{M}^{-1} \mathbf{i}(b) \quad \text{where } \mathbf{I}_4 \text{ is the identity matrix of size 4} \\ &= \mathbf{k}_5 \begin{pmatrix} 0 \\ \mathbf{i}(b) \end{pmatrix} \\ &= \mathbf{k}_4 \mathbf{i}(b) = \kappa(b) \end{aligned}$$

and therefore, $\Omega(\mathcal{B}'_{\mathcal{T}^3})$ and $\Sigma'_{\mathcal{T}} \subset \Omega(\mathcal{B}'_{\mathcal{O}^4})$ are arithmetically equivalent.

We may use the beginning of the proof to show the octahedral case in a similar way as above. In this case, we may consider the orthoplacial sphere packing obtained from $[\mathcal{B}_{\mathcal{O}^4}]_2^1$ after a rotation around the z -axis of angle $\frac{\pi}{4}$, so the plane $H_{\mathcal{O}}$ becomes the plane $\{x = 0\}$. Then, the bijection $\psi_{\mathcal{O}}^{-1} : \Omega(\mathcal{B}_{\mathcal{O}^3}) \rightarrow \Sigma_{\mathcal{O}}$ has the same expression in inversive coordinates as $\psi_{\mathcal{T}}^{-1}$ and the rest of computations are identical as in the tetrahedral case.

As before, the cubical case is more delicate. Let $\mathcal{B}_{\mathcal{O}^4}^{\uparrow x}$ be the orthoplacial sphere packing of Figure 5.7 and let $\Sigma_{\mathcal{C}} = \Gamma_{\mathcal{C}} \cdot \mathcal{B}_{\mathcal{O}^4}^{\uparrow x}$ be the cubical Apollonian section described in the proof of Prop. 5.3.1. Let $\mathcal{B}_{\mathcal{C}^3}$ be the cubical circle packing given by $\psi_{\mathcal{C}}(\mathcal{B}_{\mathcal{O}^4}^{\uparrow x})$. We define the mapping

$$\begin{aligned} \varepsilon : \mathcal{B}_{\mathcal{C}^3} &\longrightarrow \{1, -1\} \\ b &\longmapsto \text{sign}(x_1(b)) \end{aligned} \quad (5.2)$$

where $x_1(b)$ is the first coordinate of the center of $\psi_{\mathcal{C}}^{-1}(b)$. Then, in inversive coordinates, the bijection $\psi_{\mathcal{C}}^{-1} : \mathcal{B}_{\mathcal{C}^3} \rightarrow \mathcal{B}_{\mathcal{O}^4}^{\uparrow x}$ and the group isomorphism $\phi_{\mathcal{C}}^{-1} : A(\mathcal{B}_{\mathcal{C}^3}) \rightarrow \Gamma_{\mathcal{C}}$ are given by

$$\begin{aligned} \psi_{\mathcal{C}}^{-1} : \mathcal{B}_{\mathcal{C}^3} &\longrightarrow \mathcal{B}_{\mathcal{O}^4}^{\uparrow x} & \phi_{\mathcal{C}}^{-1} : A(\mathcal{B}_{\mathcal{C}^3}) &\rightarrow \Gamma_{\mathcal{C}} \\ \mathbf{i}(b) &\longmapsto \frac{1}{\sqrt{2}} \begin{pmatrix} \varepsilon(b) \\ \mathbf{i}(b) \end{pmatrix} & \mathbf{A} &\mapsto \left(\begin{array}{c|c} 1 & \mathbf{0}_4^T \\ \hline \mathbf{0}_4 & \mathbf{A} \end{array} \right) \end{aligned} \quad (5.3)$$

The equivariance of $\psi_{\mathcal{C}}$ allows us to extend $\psi_{\mathcal{C}}^{-1} : \Omega(\mathcal{B}_{\mathcal{C}^3}) \rightarrow \Sigma_{\mathcal{C}}$ by

$$\psi_{\mathcal{C}}^{-1}(g \cdot b) = \phi_{\mathcal{C}}^{-1}(g) \cdot \psi_{\mathcal{C}}^{-1}(b) \quad (5.4)$$

for every $g \in A(\mathcal{B}_{\mathcal{C}^3})$ and every $b \in \mathcal{B}_{\mathcal{C}^3}$. Let $\mathcal{B}'_{\mathcal{C}^3}$ be any cubical circle packing. As before, the Möbius uniqueness of the cube implies that there is $\mu \in \text{Möb}(\widehat{\mathbb{R}^2})$ such that $\mu \cdot \Omega(\mathcal{B}_{\mathcal{C}^3}) = \Omega(\mathcal{B}'_{\mathcal{C}^3})$. We define $\tilde{\mu} \in \text{Möb}(\widehat{\mathbb{R}^3})$ as above in the tetrahedral case. Let $\hat{\mu} = \lambda_{\frac{1}{\sqrt{2}}} \circ \tilde{\mu} \in \text{Möb}(\widehat{\mathbb{R}^3})$ where $\lambda_{\frac{1}{\sqrt{2}}}$ is the rescaling of $\widehat{\mathbb{R}^3}$ with factor $\frac{1}{\sqrt{2}}$. We have that $\Sigma'_{\mathcal{C}} := \hat{\mu} \cdot \Sigma_{\mathcal{C}}$ is a cubical Apollonian section of the orthoplacial Apollonian packing $\Omega(\mathcal{B}'_{\mathcal{O}^4}) := \hat{\mu} \cdot \Omega(\mathcal{B}_{\mathcal{O}^4}^{\uparrow x})$. We define the bijection $\hat{\psi}_{\mathcal{C}} = \mu \circ \psi_{\mathcal{C}} \circ \hat{\mu}^{-1}$ which maps $\Sigma'_{\mathcal{C}} \rightarrow \Omega(\mathcal{B}'_{\mathcal{C}^3})$. Again, we shall prove that $\hat{\psi}_{\mathcal{C}}$ preserves curvatures. First, we notice that for any disk $b \in \Omega(\mathcal{B}'_{\mathcal{C}^3})$, there is $g' \in A(\mathcal{B}'_{\mathcal{C}^3})$ and $b' \in \mathcal{B}'_{\mathcal{C}^3}$ such that $b = g' \cdot b'$, by

definition. Then, for any $b \in \Omega(\mathcal{B}'_{\mathcal{O}3})$ we have

$$\begin{aligned}
\kappa(\widehat{\psi}_{\mathcal{C}}^{-1}(b)) &= \kappa(\widehat{\psi}_{\mathcal{C}}^{-1}(g' \cdot b')) \\
&= \kappa(\widehat{\mu} \circ \psi_{\mathcal{C}}^{-1} \circ \mu^{-1}(g' \cdot b')) \\
&= \kappa\left(\lambda_{\frac{1}{\sqrt{2}}} \circ \widetilde{\mu} \circ \psi_{\mathcal{C}}^{-1} \circ \mu^{-1}(g' \cdot b')\right) \\
&= \sqrt{2}\kappa(\widetilde{\mu} \circ \psi_{\mathcal{C}}^{-1} \circ \mu^{-1}(\mu g \mu^{-1}) \cdot (b')) \quad \text{where } g = \mu^{-1}g'\mu \in \mathbf{A}(\mathcal{B}_{\mathcal{C}3}) \\
&= \sqrt{2}\kappa(\widetilde{\mu} \circ \phi_{\mathcal{C}}^{-1}(g) \cdot \psi_{\mathcal{C}}^{-1} \circ \mu^{-1}(b')) \quad \text{by (5.4)} \\
&= \sqrt{2}\mathbf{k}_5 \left(\begin{array}{c|c} 1 & \mathbf{0}_4^T \\ \hline \mathbf{0}_4 & \mathbf{M} \end{array} \right) \left(\begin{array}{c|c} 1 & \mathbf{0}_4^T \\ \hline \mathbf{0}_4 & \mathbf{A} \end{array} \right) \frac{1}{\sqrt{2}} \begin{pmatrix} \varepsilon(\mu^{-1}(b')) \\ \mathbf{i}(\mu^{-1}(b')) \end{pmatrix} \quad \text{where } \mathbf{A} \text{ is the matrix of } g \\
&= \mathbf{k}_5 \begin{pmatrix} \varepsilon(\mu^{-1}(b')) \\ \mathbf{MAi}(\mu^{-1}(b')) \end{pmatrix} \\
&= \mathbf{k}_4 \mathbf{MAi}(\mu^{-1}(b')) \\
&= \mathbf{k}_4 \mathbf{MAM}^{-1}\mathbf{i}(b') \\
&= \kappa(\mu g \mu^{-1} \cdot b') \\
&= \kappa(g' \cdot b') = \kappa(b)
\end{aligned}$$

Now we suppose that $\Omega(\mathcal{B}'_{\mathcal{T}3})$, $\Omega(\mathcal{B}'_{\mathcal{O}3})$ and $\Omega(\mathcal{B}'_{\mathcal{C}3})$ are integral. We shall show that in the three cases we can find four pairwise tangent spheres of $\mathcal{B}'_{\mathcal{O}4}$ with curvatures κ_1 , κ_2 , κ_3 and κ_4 satisfying that $\sqrt{\mathfrak{I}_3(\kappa_1, \kappa_2, \kappa_3, \kappa_4)} \in \mathbb{Z}$. The integrality of $\Omega(\mathcal{B}'_{\mathcal{O}4})$ then follows from Prop 5.3.1.

(Tetrahedral section) Let $\kappa_1, \kappa_2, \kappa_3, \kappa_4$ be the curvatures of the four disks of $\mathcal{B}'_{\mathcal{T}3}$. By the Descartes' Theorem, we have that

$$\mathfrak{I}_3(\kappa_1, \kappa_2, \kappa_3, \kappa_4) = 0$$

Since $\widetilde{\psi}_{\mathcal{T}}^{-1}$ preserves curvatures, then $\kappa_1, \kappa_2, \kappa_3, \kappa_4$ are the curvatures of four pairwise tangent spheres of $\mathcal{B}'_{\mathcal{O}4}$ satisfying that $\sqrt{\mathfrak{I}_3(\kappa_1, \kappa_2, \kappa_3, \kappa_4)} \in \mathbb{Z}$.

(Octahedral section) Let $\kappa_1, \kappa_2, \kappa_3, \kappa_{-1}, \kappa_{-2}, \kappa_{-3}$ be the curvatures of the six disks of $\mathcal{B}'_{\mathcal{O}3}$ under an antipodal labelling, so κ_i and κ_{-i} are the curvatures of non-tangent disks. By (4.27), we have

$$(\kappa_1 - \kappa_{\mathcal{O}3})^2 + (\kappa_2 - \kappa_{\mathcal{O}3})^2 + (\kappa_3 - \kappa_{\mathcal{O}3})^2 = 2\kappa_{\mathcal{O}3}^2 \quad (5.5)$$

where $\kappa_{\mathcal{O}^3} = \frac{1}{2}(\kappa_i + \kappa_{-i})$ for every $i = 1, 2, 3$. Since $\tilde{\psi}_{\mathcal{O}}^{-1}$ preserves curvatures, then $\kappa_1, \kappa_2, \kappa_3, \kappa_{-1}, \kappa_{-2}, \kappa_{-3}$ are also the curvatures of six spheres of $\mathcal{B}'_{\mathcal{O}^4}$. Let κ_4 and κ_{-4} be the curvatures of the remaining spheres of $\mathcal{B}'_{\mathcal{O}^4}$. By the antipodal relation, which holds for $\mathcal{B}'_{\mathcal{O}^3}$ and $\mathcal{B}'_{\mathcal{O}^4}$, we have

$$\kappa_{\mathcal{O}^3} = \frac{\kappa_1 + \kappa_{-1}}{2} = \kappa_{\mathcal{O}^4} \quad (5.6)$$

We also have that $\kappa_1, \kappa_2, \kappa_3, \kappa_4$ are the curvatures of four pairwise tangent spheres of $\mathcal{B}'_{\mathcal{O}^4}$. By combining (5.6) with Cor. 4.2.3 we obtain

$$\begin{aligned} (\kappa_1 - \kappa_{\mathcal{O}^4})^2 + (\kappa_2 - \kappa_{\mathcal{O}^4})^2 + (\kappa_3 - \kappa_{\mathcal{O}^4})^2 + (\kappa_4 - \kappa_{\mathcal{O}^4})^2 &= 2\kappa_{\mathcal{O}^4}^2 \\ \Leftrightarrow (\kappa_1 - \kappa_{\mathcal{O}^3})^2 + (\kappa_2 - \kappa_{\mathcal{O}^3})^2 + (\kappa_3 - \kappa_{\mathcal{O}^3})^2 + (\kappa_4 - \kappa_{\mathcal{O}^3})^2 &= 2\kappa_{\mathcal{O}^3}^2 \\ &\Leftrightarrow \kappa_4 = \kappa_{\mathcal{O}^3} \end{aligned}$$

Therefore,

$$\begin{aligned} \sqrt{\mathfrak{I}_3(\kappa_1, \kappa_2, \kappa_3, \kappa_4)} &= \sqrt{\mathfrak{I}_3(\kappa_1, \kappa_2, \kappa_3, \kappa_{\mathcal{O}^3})} \\ &= \frac{1}{2} \sqrt{(\kappa_1 + \kappa_2 + \kappa_3 + \kappa_{\mathcal{O}^3})^2 - 2(\kappa_1^2 + \kappa_2^2 + \kappa_3^2 + \kappa_{\mathcal{O}^3}^2)} \\ &= \frac{1}{2} \sqrt{2(\kappa_1\kappa_2 + \kappa_2\kappa_3 + \kappa_1\kappa_3) + 2\kappa_{\mathcal{O}^3}^2 - (\kappa_1 - \kappa_{\mathcal{O}^3})^2 - (\kappa_2 - \kappa_{\mathcal{O}^3})^2 - (\kappa_3 - \kappa_{\mathcal{O}^3})^2} \\ &= \frac{1}{2} \sqrt{2(\kappa_1\kappa_2 + \kappa_2\kappa_3 + \kappa_1\kappa_3)} \quad \text{by (5.5)} \\ &= \frac{1}{2} \sqrt{2\mathfrak{I}_2(\kappa_1, \kappa_2, \kappa_3)} \end{aligned}$$

Since $\Omega(\mathcal{B}'_{\mathcal{O}^3})$ is integral, then, $2\mathfrak{I}_2(\kappa_1, \kappa_2, \kappa_3)$ is an even integer. Moreover, by Cor. 4.3.3, $\sqrt{2\mathfrak{I}_2(\kappa_1, \kappa_2, \kappa_3)}$ is also an even integer. Consequently, $\sqrt{\mathfrak{I}_3(\kappa_1, \kappa_2, \kappa_3, \kappa_4)} \in \mathbb{Z}$. (Cubical section) Let $\kappa_1, \kappa_2, \kappa_3, \kappa_4$ be the curvatures of four consecutive tangent disks b_1, b_2, b_3, b_4 of $\mathcal{B}'_{\mathcal{O}^3}$ with b_4 tangent to b_1 . By Cor. 4.3.4, we have

$$\kappa_1 + \kappa_3 = \kappa_2 + \kappa_4$$

Since $\widehat{\psi}_{\mathcal{C}}^{-1}$ preserves curvatures, then $\kappa_1, \kappa_2, \kappa_3, \kappa_4$ are the curvatures of four pairwise tangent spheres of $\mathcal{B}_{\mathcal{O}^4}$. Then, we have

$$\begin{aligned} \sqrt{\mathfrak{I}_3(\kappa_1, \kappa_2, \kappa_3, \kappa_4)} &= \sqrt{\mathfrak{I}_3(\kappa_1, \kappa_2, \kappa_3, \kappa_1 + \kappa_3 - \kappa_2)} \\ &= \sqrt{\kappa_1\kappa_2 + \kappa_2\kappa_3 + \kappa_1\kappa_3 - \kappa_2^2} \\ &= \sqrt{2\mathfrak{C}_3(\kappa_1, \kappa_2, \kappa_3)} \end{aligned}$$

The integrality of $\Omega(\mathcal{B}'_{\mathcal{O}^3})$ and Cor. 4.3.5 give that $\sqrt{\mathfrak{I}_3(\kappa_1, \kappa_2, \kappa_3, \kappa_4)} \in \mathbb{Z}$. \square

The previous proof is constructive and gives a method to obtain integral orthoplacial Apollonian packings containing a given tetrahedral, octahedral or cubical section. The three orthoplacial Apollonian packings shown in Table 5.1 were obtained by this method.

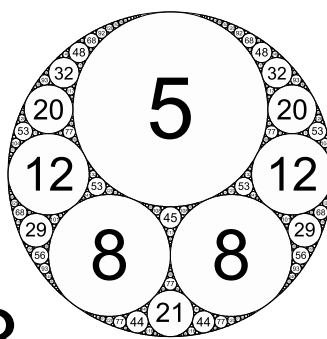
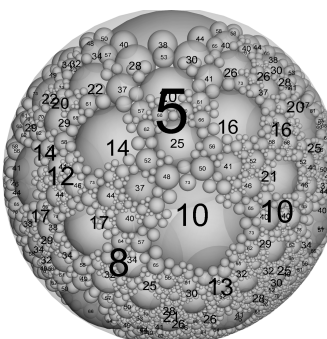
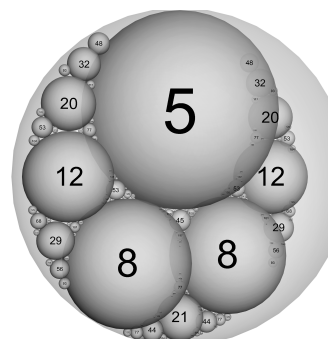
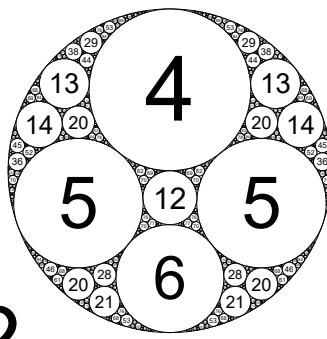
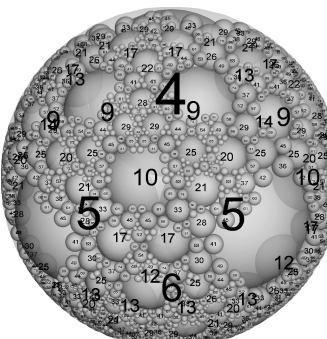
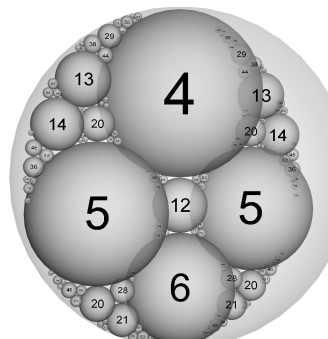
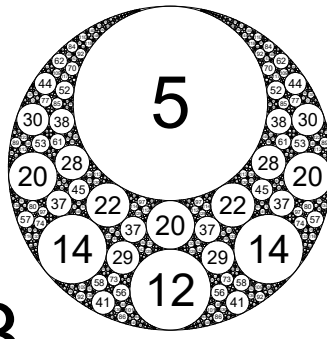
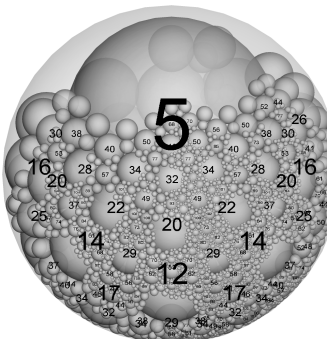
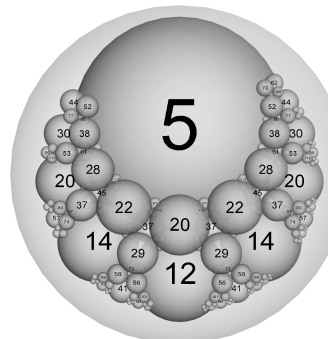
	Platonic AP	Orthoplacial AP	Apollonian section
-3			
-2			
-3			

Table 5.1: An integral tetrahedral, octahedral and cubical Apollonian circle packing and an orthoplacial Apollonian sphere packing containing an Apollonian section arithmetically equivalent to the packing on the left.

Orthoplicial Apollonian packings and rational links

Contents

6.1	Introduction	105
6.2	Orthoplicial necklace representations	106
6.3	Algebraic links in the cubical Apollonian section	108
6.3.1	Orthocubical shifts	110
6.3.2	An upper bound on the ball number of rational links	113
6.4	A geometric interpretation of continued fractions	117

6.1 Introduction

In [74], Maehara and Oshiro studied two necklace representations of the simplest link: the Hopf link (Fig. 6.1). Chen used the same two constructions to obtain graphs which can not be realized as the tangency graph of a sphere packing [21]. The first known necklace is the *Soddy's Hexlet*, a nice construction discovered by Soddy in the same paper where he introduced the integral Apollonian packings and the three-dimensional generalization of Descartes' theorem [92]. Soddy's Hexlet appears naturally as a subset of the classic Apollonian sphere packing [62]. The second construction considered by Maehara and Oshiro is a standard orthoplicial sphere packing, and they used it to compute the ball number of the Hopf link, which is 8 [72]. As far as we are aware, the Hopf link is the only link whose ball number is known.

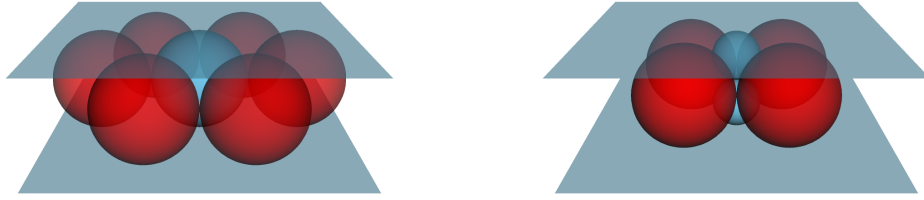


Figure 6.1: Two necklace representations of the Hopf link: the Soddy's Hexlet (left) and the orthoplicial sphere packing (right).

In this last chapter before the conclusion, we shall take advantage of the fractal structure of the orthoplicial Apollonian sphere packing to construct necklace representations of links with few spheres. After showing that any link admits an orthoplicial necklace representation, we shall improve the upper bound on the ball number given in Theorem 2.1.1 for rational links. We conclude with an unexpected relation between the arithmetical properties of rational links and the inversive coordinates of a tangency point of two spheres in an orthoplicial necklace representation. The latter puts forward a connection between continued fractions, a cubic Apollonian packing and a Diophantine equation.

6.2 Orthoplicial necklace representations

We say that a necklace representation of a link is *orthoplicial* if it is contained in an orthoplicial Apollonian packing. In the following result, we show that *any* link admits an orthoplicial necklace representation.

Theorem 6.2.1. *Any link admits a necklace representation in any orthoplicial Apollonian sphere packing.*

Proof. Let L be a link. By Th. 1.2.3, there is an n -braid γ such that its closure is isotopically equivalent to L . We shall show that the closure of γ can be constructed geometrically in the carrier of the orthoplicial Apollonian sphere packing $[\mathcal{B}_{\mathcal{O}^4}]_2^1$ shown in the Figure 5.2.

First, we construct the Apollonian section $\Sigma_{12} := \Gamma_{12} \cdot [\mathcal{B}_{\mathcal{O}^4}]_2^1 \subset \Omega([\mathcal{B}_{\mathcal{O}^4}]_2^1)$ where

$$\Gamma_{12} := \langle s_{1234}, s_{12\bar{3}4}, s_{123\bar{4}}, s_{12\bar{3}\bar{4}} \rangle \tag{6.1}$$

We have that Σ_{12} is an infinite sphere packing whose carrier is a square-grid with two vertices, one above the other, at the center of each square. Therefore, via square-grid diagrams, we can construct a polygonal path in the carrier of Σ_{12} equivalent to the closure of γ by using the vertices at the center of the squares for the crossings (see Fig. 6.2). Since Möbius transformations preserving the orientation of \mathbb{R}^3 are ambient isotopies, the Möbius uniqueness of the orthoplex implies that any orthoplacial Apollonian sphere packing contains a necklace representation of L . \square

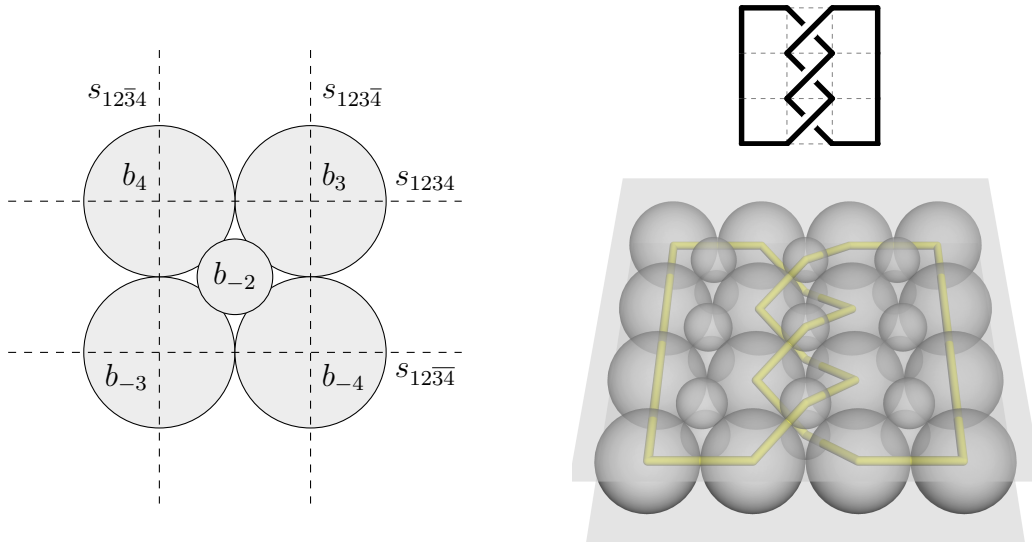


Figure 6.2: (Left) $[\mathcal{B}_{\mathcal{O}^4}]_2^1$ with the generators of Σ_{12} , view from above; (top right) a square-grid braid diagram of the trefoil knot and the corresponding embedding of the trefoil in the carrier of Σ_{12} (bottom right).

The method used in the previous proof can be used to give an upper bound of the ball number of a link in terms of its braid length. However, this method only improves the upper bound of Theorem 2.1.1 for links whose braid index is 2.

Corollary 6.2.1. *Let L be a link with braid index equal to 2. Then,*

$$\text{ball}(L) \leq 4cr(L)$$

Proof. Let L be a link equivalent to a closed 2-braid with n crossings. The corresponding square-grid diagram is a reduced alternating diagram of L . Therefore, by Th. 1.2.1, $cr(L) = n$. On the other hand, by using the half-spaces b_1 and b_2 in Σ_{12} for closing the 2-braid, we can obtain a necklace representation of L with $4n$ spheres. \square

The closure of a 2-braid with n crossings is equivalent to the rational link $C(n)$. In the next section, we shall extend the improved upper bound of Corollary 6.2.1 to every rational link with the help of a cubical Apollonian section of an orthoplacial Apollonian packing.

6.3 Algebraic links in the cubical Apollonian section

In order to simplify the latter computations, instead of working with the orthoplacial sphere packing $\mathcal{B}_{\mathcal{O}^4}^{\uparrow x}$ where the cubical Apollonian section was defined in the proof of Prop. 5.3.1, we consider the orthoplacial sphere packing $\mathcal{B}_{\mathcal{O}^4}^{\uparrow z}$ obtained by relabelling of $\mathcal{B}_{\mathcal{O}^4}^{\uparrow x}$ according to the Figure 6.3. We call the given labelling the z -labelling. Analogously to the x -labelling, a label i is positive in the z -labelling if and only if the third coordinate of the center of b_i is positive.

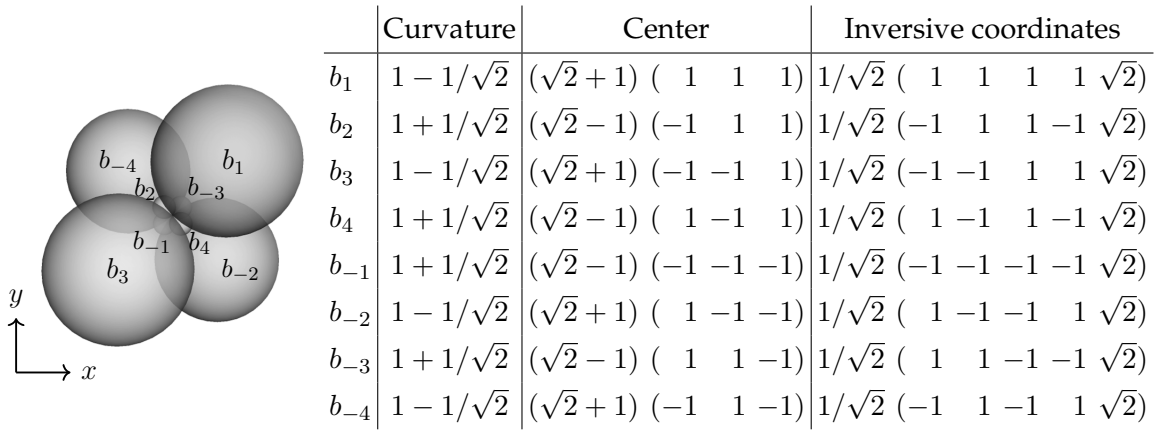


Figure 6.3: The orthoplacial sphere packing $\mathcal{B}_{\mathcal{O}^4}^{\uparrow z}$.

We define the *orthocubical sphere packing* as the cubical Apollonian section of $\Omega(\mathcal{B}_{\mathcal{O}^4}^{\uparrow z})$ given by $\Sigma_{\mathcal{C}} := \Gamma_{\mathcal{C}} \cdot \mathcal{B}_{\mathcal{O}^4}^{\uparrow z}$ where

$$\Gamma_{\mathcal{C}} := \langle s_{12\bar{3}\bar{4}}, s_{1\bar{2}\bar{3}4}, s_{\bar{1}23\bar{4}}, s_{\bar{1}\bar{2}34}, s_{1\bar{2}3\bar{4}}, s_{1\bar{2}\bar{3}4} \rangle$$

Here, the plane $H_{\mathcal{C}}$ intersecting all the spheres of $\Sigma_{\mathcal{C}}$ is the plane $\{z = 0\}$ (c.f. proof of Prop. 5.3.1 (cubical section)). Let $\mathcal{B}_{\mathcal{C}^3}$ be the cubical circle packing corresponding to $\Sigma_{\mathcal{C}}$. As it was done in Figure 5.9, the disks of $\Omega(\mathcal{B}_{\mathcal{C}^3})$ whose center is above (resp. below) the plane $\{z = 0\}$ are represented in black (resp. white). We call this coloring the *z-coloring*. By extending the *z-coloring* to the vertices of the tangency graph of $\Omega(\mathcal{B}_{\mathcal{C}^3})$, we obtain a proper 2-coloring of the tangency graph $\Omega(\mathcal{B}_{\mathcal{C}^3})$. This graph is a spanning subgraph of the tangency graph of $\Sigma_{\mathcal{C}}$. The missing edges are exactly those which join the vertices of the same color belonging to the same square-face. We call these edges the *diagonal edges*.

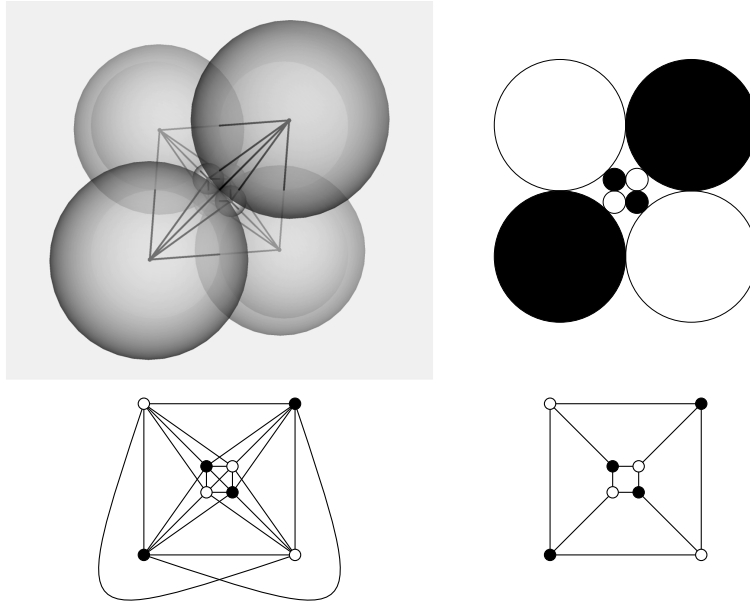


Figure 6.4: (Top left) $\mathcal{B}_{\mathcal{O}^4}^{\uparrow z}$ with its carrier and the plane $\{z = 0\}$, view from above; (top right) the corresponding cubical circle packing $\mathcal{B}_{\mathcal{C}^3}$ with the *z-coloring*; (bottom left) the tangency graph of $\mathcal{B}_{\mathcal{O}^4}^{\uparrow z}$ with the *z-coloring*; (bottom right) the tangency graph of $\mathcal{B}_{\mathcal{C}^3}$ with the *z-coloring*.

We point out that any two tangent spheres of Σ_c joined by a non-diagonal edge meet at the plane $\{z = 0\}$. A diagonal edge shall be called *black* or *white* according to the color of the joined vertices. Diagonal edges will play an important role in the construction of necklace representations in order to represent the crossings. With the information given by the z -coloring, the over/under crossing information can be deduced from the color of the vertices of the diagonal edges (Fig. 6.5).

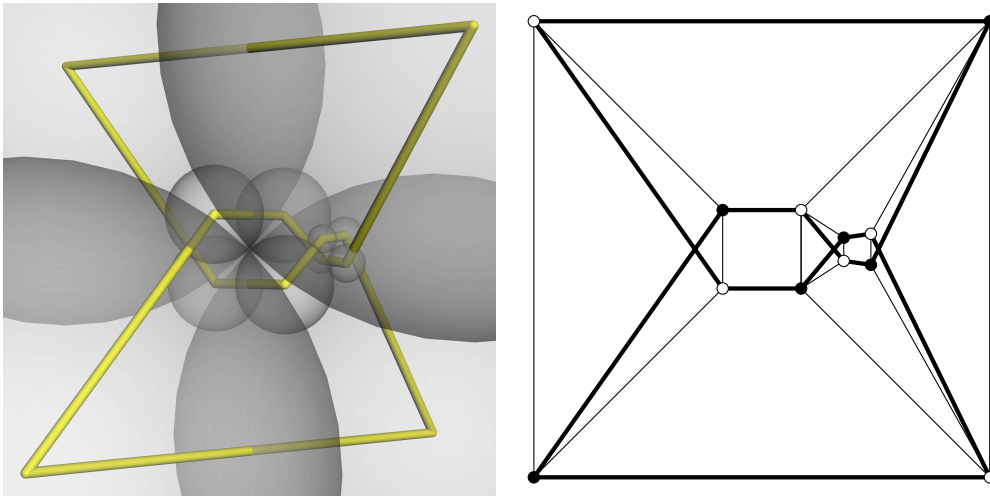


Figure 6.5: An orthocubical necklace representation of the trefoil knot (left) and the corresponding cubical diagram (right).

6.3.1 Orthocubical shifts

We consider the dual $\mathcal{B}_{C^3}^* = \{d_1, d_2, d_3, d_{-1}, d_{-2}, d_{-3}\}$ with the antipodal labelling depicted in Figure 6.6 and the elements $\{r_{12}, r_{13}, r_{23}, r_{-13}, r_{-23}, r_{-33}\} \subset \text{Sym}(\mathcal{B}_{C^3}^*)$ where r_{ij} denotes the inversion which exchanges the disks d_i with d_j , d_{-i} with d_{-j} , and fixes the rest. In $\mathcal{B}_{C^3}^*$ we have that r_{12} corresponds to the reflection on the line $\{x = y\}$, $r_{\pm i3}$ is the inversion on the circle centered at $\pm e_i$ and radius $\sqrt{2}$, for $i = 1, 2$, and r_{-33} is the inversion on the unit circle centered at the origin (see Fig. 6.6).

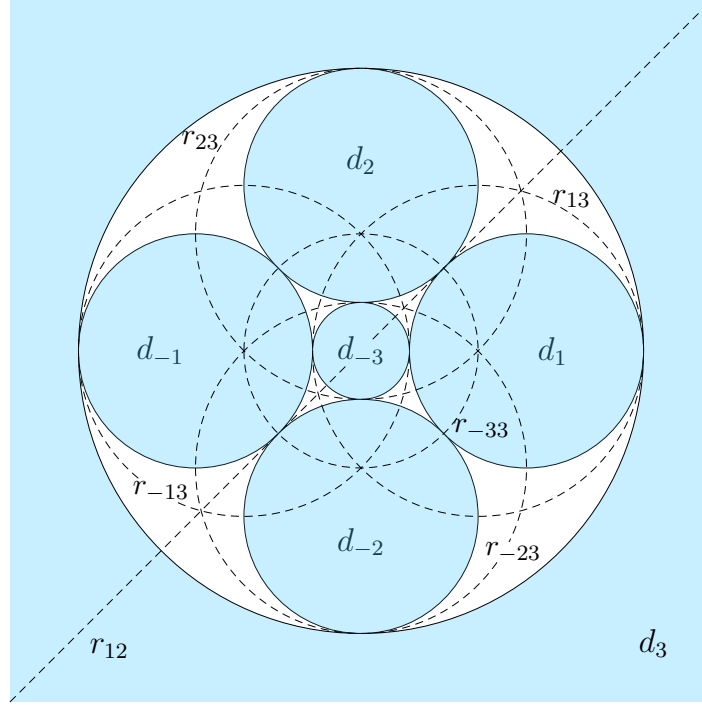


Figure 6.6: The disks of the dual $\mathcal{B}_{\mathcal{C}^3}^*$ in blue and the walls of the symmetries $\{r_{12}, r_{13}, r_{23}, r_{-13}, r_{-23}, r_{-33}\}$ in dashed lines.

Since $\text{Sym}(\mathcal{B}_{\mathcal{C}^3}) = \text{Sym}(\mathcal{B}_{\mathcal{C}^3}^*)$, the elements $\{r_{12}, r_{13}, r_{23}, r_{-13}, r_{-23}, r_{-33}\}$ belong also to the symmetrized Apollonian group $\text{SA}(\mathcal{B}_{\mathcal{C}^3})$. We define the *cubical shifts* as the elements $\{\mu_x, \mu_y, \mu_z, \mu_{-x}, \mu_{-y}, \mu_{-z}\} \subset \text{SA}(\mathcal{B}_{\mathcal{C}^3})$ given by

$$\mu_{\pm x} := s_{\pm 1} r_{\pm 13} \quad \mu_{\pm y} := s_{\pm 2} r_{\pm 23} \quad \mu_{\pm z} := s_{\pm 3} r_{-33} \quad (6.2)$$

where s_i denotes the inversion on the disk $d_i \in \mathcal{B}_{\mathcal{C}^3}^*$. In the Figure 6.7, we show the action of the cubical shifts on the carrier of $\mathcal{B}_{\mathcal{C}^3}$. We notice that $\mu_{\pm x}$ and $\mu_{\pm y}$ preserve and $\mu_{\pm z}$ reverses the z -coloring, and the subgroup generated by $\{\mu_x, \mu_y, \mu_{-x}, \mu_{-y}, \mu_{-z}\}$ is free.

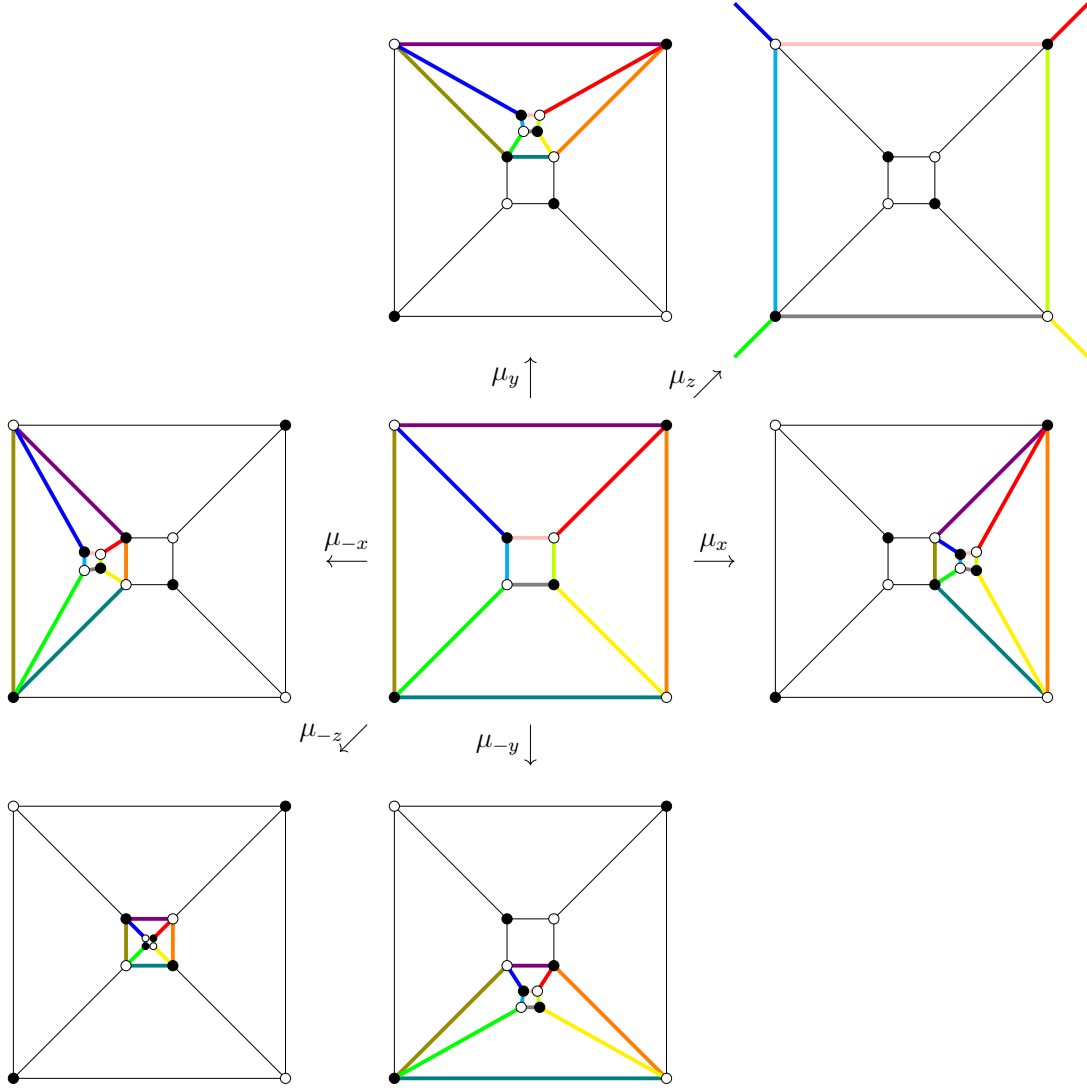


Figure 6.7: The action of the cubical shifts on the cubical carrier.

We define the *orthocubical shifts* as the elements $\{\widehat{\mu}_x, \widehat{\mu}_y, \widehat{\mu}_z, \widehat{\mu}_{-x}, \widehat{\mu}_{-y}, \widehat{\mu}_{-z}\} \subset \text{SA}(\mathcal{B}_{O_4}^{\uparrow z})$ corresponding to the cubical shifts after conjugation with ψ_C^{-1} , where ψ_C is the bijection mapping Σ_C to $\Omega(\mathcal{B}_{C^3})$ described in the proof of Prop. 5.3.1. According to the z -labelling, we have that

$$\begin{aligned} \widehat{\mu}_x &= s_{1\overline{234}} \widehat{r}_{34} & \widehat{\mu}_y &= s_{12\overline{34}} \widehat{r}_{23} & \widehat{\mu}_z &= s_{12\overline{34}} \widehat{r}_{-13} \widehat{r}_{-24} \\ \widehat{\mu}_{-x} &= s_{\overline{1234}} \widehat{r}_{12} & \widehat{\mu}_{-y} &= s_{\overline{1234}} \widehat{r}_{23} & \widehat{\mu}_{-z} &= s_{\overline{1234}} \widehat{r}_{-13} \widehat{r}_{-24} \end{aligned}$$

where, $\widehat{r}_{ij} \in \text{Sym}(\mathcal{B}_{O_4}^{\uparrow z})$ denotes the inversion which exchanges the spheres b_i with b_j , b_{-i} with b_{-j} , and fixes the rest of spheres of $\mathcal{B}_{O_4}^{\uparrow z}$.

6.3.2 An upper bound on the ball number of rational links

We shall present here a discrete analogue of algebraic links by using the algebraic structure given by the Apollonian groups of the orthocubical sphere packing.

First, we define an *orthocubical path* γ as a polygonal curve in the carrier of Σ_C connecting the centers of two spheres of Σ_C . Orthocubical paths shall be represented by *cubical diagrams* (see Figure 6.5) which are obtained by adding the diagonal edges to the carrier of the corresponding cubical Apollonian packing. We recall that the over/under information for the crossings in the cubical diagrams is given by the color of the vertices in the diagonal edges (black=over/white=under). We shall also encode an orthocubical path by a vector $(c_{i_1}, \dots, c_{i_n})$ which denotes the centers of the spheres in the linear order induced by γ . The *endpoints* of γ are the centers c_{i_1} and c_{i_n} and the *length* of γ , denoted by $|\gamma|$, is the number n counting the centers in γ . Since we shall consider unoriented paths, and the concatenation of two paths gives another path, vectors encoding orthocubical paths must be considered modulo the following relations:

$$(i) \text{ (Symmetry) } (c_{i_1}, \dots, c_{i_n}) = (c_{i_n}, \dots, c_{i_1})$$

$$(ii) \text{ (Concatenation) } \{(c_i, \dots, c_j), (c_j, \dots, c_k)\} = \{(c_i, \dots, c_j, \dots, c_k)\}$$

Let \mathcal{T} be the tetrahedron $\mathcal{T} := \text{conv}(\{c_1, c_{-2}, c_3, c_{-4}\})$ where c_i is the center of the sphere $b_i \in \mathcal{B}_{\mathcal{O}^4}^z$. We define an *orthocubical tangle* as a 2-tangle (\mathcal{T}, \boxed{t}) where \boxed{t} is a collection $\{\gamma_1, \gamma_2, \dots, \gamma_m\}$ of $m \geq 2$ disjoint orthocubical paths contained in \mathcal{T} satisfying that the endpoints of γ_1 and γ_2 are $\{c_1, c_{-2}, c_3, c_{-4}\}$ and the rest of the orthocubical paths are closed. The length of \boxed{t} , denoted by $|\boxed{t}|$, is the sum of the lengths of the orthocubical paths in \boxed{t} . We denote by $\boxed{t_0}$, $\boxed{t_1}$ and $\boxed{t_\infty}$ the *elementary* orthocubical tangles depicted in Fig. 6.8.

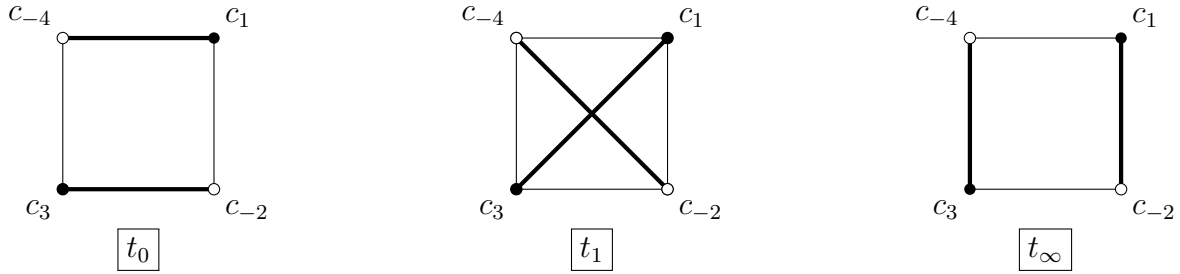
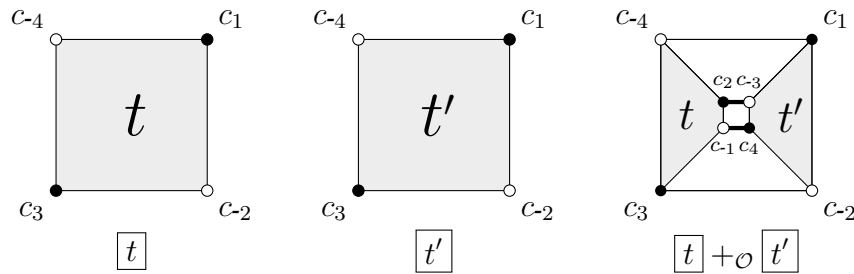


Figure 6.8: The elementary orthocubical tangles.

Now we introduce the *orthoapollonian* tangle operations. We define

- (i) the *orthoapollonian sum* $\boxed{t} +_{\mathcal{O}} \boxed{t'} := \widehat{\mu}_x \boxed{t} \cup \{(c_{-1}, c_4), (c_{-3}, c_2)\} \cup \widehat{\mu}_x \boxed{t'}$.



and the unary operations

- (ii) the *orthoapollonian flip* $F_{\mathcal{O}} \boxed{t} := \widehat{r}_{24} \boxed{t}$,
- (iii) the *orthoapollonian positive half-twist* $H_{\mathcal{O}}^+ \boxed{t} := \boxed{t_1} +_{\mathcal{O}} \boxed{t}$,
- (iv) the *orthoapollonian negative half-twist* $H_{\mathcal{O}}^- \boxed{t} := \widehat{\mu}_x \boxed{t} \cup \{(c_3, c_{-1}, c_{-3}), (c_{-4}, c_2, c_4)\}$.

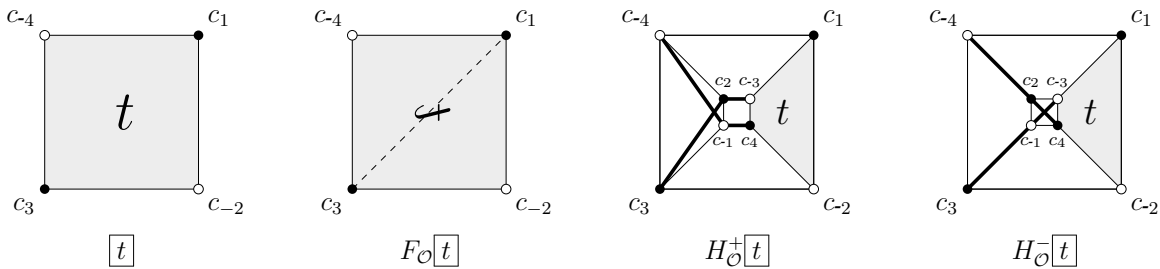


Figure 6.9: Orthoapollonian unary operations of tangles.

The *orthoapollonian tangle closures* are given by:

- The orthocubical numerator

$$N_{\mathcal{O}}\boxed{t} := \boxed{t} \cup \{(c_1, \widehat{\mu}_z(c_1), \widehat{\mu}_z(c_{-4}), c_{-4}), (c_3, \widehat{\mu}_z(c_3), \widehat{\mu}_z(c_{-2}), c_{-2})\}.$$

- The orthocubical denominator

$$D_{\mathcal{O}}\boxed{t} := \boxed{t} \cup \{(c_1, \widehat{\mu}_z(c_1), \widehat{\mu}_z(c_{-2}), c_{-2}), (c_3, \widehat{\mu}_z(c_3), \widehat{\mu}_z(c_{-4}), c_{-4})\}.$$

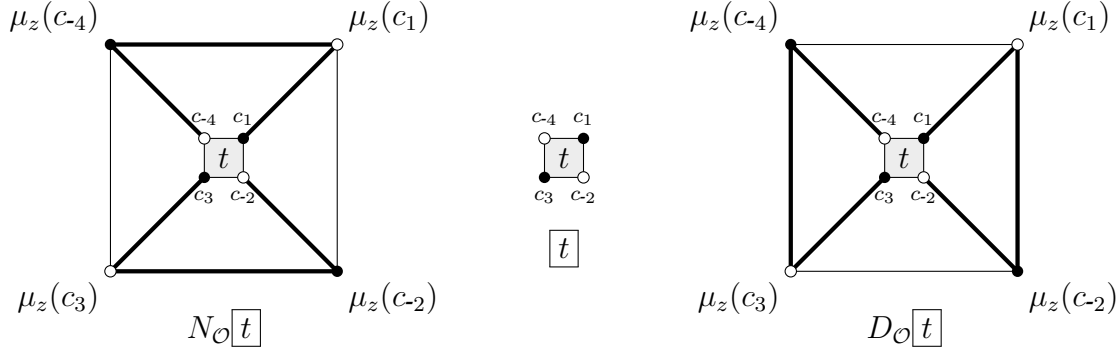


Figure 6.10: The orthocubical tangle closures.

The orthocubical elementary tangles, orthocubical tangle operations and the orthocubical closures are isotopically equivalent to their homonym in the 2-tangle definitions. Thus, we can mimic Conway’s algorithm to construct an *orthocubical* rational tangle $\boxed{t}(a_1, \dots, a_n)$ equivalent to the rational tangle $t(a_1, \dots, a_n)$ by

$$\boxed{t}(a_1, \dots, a_n) := M_{\mathcal{O}}(a_1) \cdots M_{\mathcal{O}}(a_n) \boxed{t_{\infty}} \quad \text{where } M_{\mathcal{O}}(a_i) := \begin{cases} (H_{\mathcal{O}}^+)^{a_i} F_{\mathcal{O}} & \text{if } a_i \geq 0 \\ (H_{\mathcal{O}}^-)^{a_i} F_{\mathcal{O}} & \text{if } a_i < 0 \end{cases} \quad (6.3)$$

By combining the orthocubical rational tangles with the orthocubical operations $(+_{\mathcal{O}}, F_{\mathcal{O}}, N_{\mathcal{O}}, D_{\mathcal{O}})$ we have the following.

Proposition 6.3.1. *Any algebraic link admits a necklace representation in the orthocubical sphere packing.*

The orthocubical version of Conway’s algorithm also allows us to improve the upper bound on the ball number of rational links.

Theorem 6.3.1. *Let L be a rational link. Then*

$$\text{ball}(L) \leq 4cr(L)$$

Proof. Let L be a link equivalent to the closure of rational tangle $t_{p/q}$, where $p/q \in \mathbb{Q} \cup \{\infty\}$. Let $a_1 + \frac{1}{\dots + \frac{1}{n}}$ be a continued fraction expansion of p/q where all the coefficients have the same sign (a_1 might be zero). Then, L is equivalent to the rational link $C(a_1, \dots, a_n)$. If $n = 1$, then the upper bound was given in the Corollary 6.2.1. Let us suppose that $n \geq 2$. Since the ball number of a link and its mirror is the same, we can suppose that $a_1 \geq 0$ and $a_i \geq 1$ for $2 \leq i \leq n$. By the equivalence between orthocubical rational tangles and rational tangles, we have that L is equivalent to the orthocubical tangle closure $N_{\mathcal{O}}\boxed{t}$ where

$$\begin{aligned} \boxed{t} &= (H_{\mathcal{O}}^+)^{a_1} F_{\mathcal{O}} \cdots (H_{\mathcal{O}}^+)^{a_n} F_{\mathcal{O}} \boxed{t_{\infty}} \\ &= (H_{\mathcal{O}}^+)^{a_1} F_{\mathcal{O}} \cdots (H_{\mathcal{O}}^+)^{a_n} \boxed{t_0} \\ &= (H_{\mathcal{O}}^+)^{a_1} F_{\mathcal{O}} \cdots (H_{\mathcal{O}}^+)^{a_n-1} (\boxed{t_1} + \boxed{t_0}) \\ &\simeq (H_{\mathcal{O}}^+)^{a_1} F_{\mathcal{O}} \cdots (H_{\mathcal{O}}^+)^{a_n-1} \boxed{t_1} && \text{since } \boxed{t_1} + \boxed{t_0} \simeq \boxed{t_1} \\ &=: \boxed{t'} \end{aligned}$$

It follows from the definition of the orthocubical tangle operations that

$$\begin{aligned} |\boxed{t'}| &= 4(a_1 + \dots + a_n - 1) + |\boxed{t_1}| \\ &= 4(a_1 + \dots + a_n) \\ &= 4\text{cr}(L) && \text{by Eq. (1.20).} \end{aligned}$$

Finally, since $a_i \geq 1$, the orthocubical paths (c_1, c_{-4}) and (c_3, c_{-2}) are not in $\boxed{t'}$. Therefore, we can use these paths to close $\boxed{t'}$, and in this way obtain a necklace representation of L with $4\text{cr}(L)$ spheres. \square

The improved upper bound can be extended to algebraic links admitting an alternating algebraic presentation of sums and flips of rational tangles. In the non-alternating case, the number of spheres in the orthocubical necklace representation may be reduced to less than 4 times the crossing number. The first non-trivial example that we have found satisfying this property, is precisely the Pretzel knot $P(3, -2, 3)$ (Fig. 1.12). This knot is not alternating [30], it admits an orthocubical necklace representation with 28 spheres (Fig. 6.11), and its crossing number is 8 [30]. However, it becomes more difficult to establish a relation with the crossing number in the non-alternating case since, in general, the crossing number does not correspond to the sum of the crossings of its rational factors.

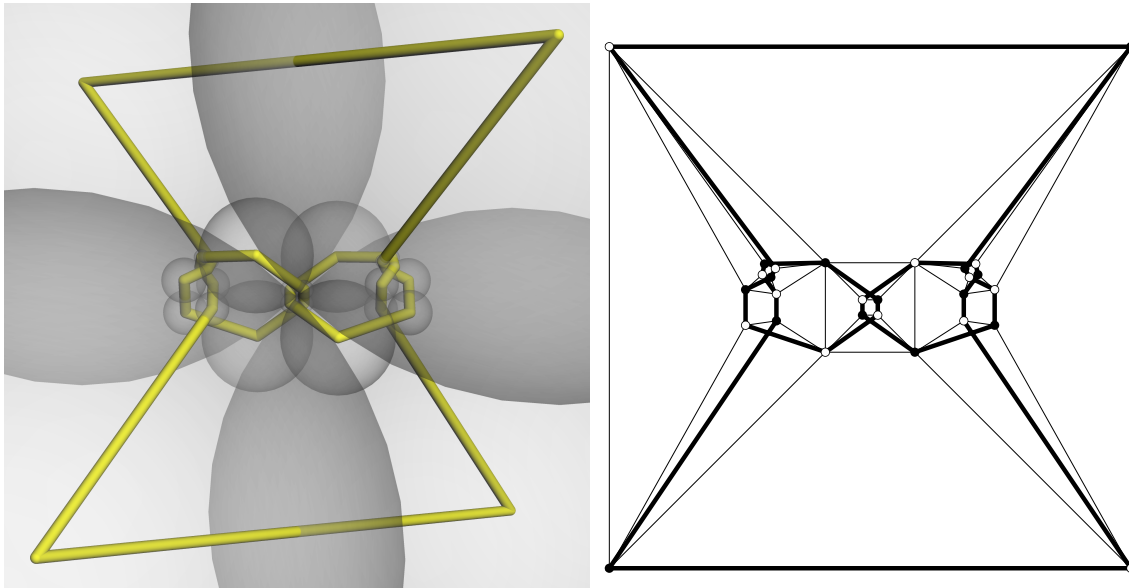


Figure 6.11: An orthocubical representation of the Pretzel knot $P(3, -2, 3)$ with 28 spheres.

6.4 A geometric interpretation of continued fractions

In the words of Karpenkov, the ubiquity of continued fractions is due to the simple operations that compose a continued fraction: *sum* $a + b$ and *inversion* $1/a$ [58]. When a mathematical object admits an analogue of these two operations, there is probably a way to connect it with a rational number via continued fractions.

In [19], Chaubey, Fuchs, Hines and Stange related continued fractions with the tetrahedral Apollonian packings and Pythagorean triples by using the generators of the Super Apollonian group introduced in [45] which is provided by the Lorentzian model of the space of disks. In this last section, we shall show that the continued fraction involved in the construction of a rational tangle can be read from the inversive coordinates of a tangency point in the orthocubical version of Conway's algorithm. This result might be related with another work of Stange [96], where the author computed the complex coordinates of the tangency points of certain disks in the standard tetrahedral Apollonian packing by relating Apollonian packings with another work of Conway and Fung on quadratic forms [27].

Definition 6.4.1. Let $t_{p/q}$ be a rational tangle with positive continued fraction expansion $a_1 + \frac{1}{\dots + \frac{1}{a_n}} = \frac{p}{q}$. We define:

- The **first edge** of $t_{p/q}$ as the segment $\widehat{e}_{p/q}$ of $\square(a_1, \dots, a_n)$ containing the center c_1 .
- The **first tangency point** of $t_{p/q}$ is the tangency point $\widehat{\eta}_{p/q}$ of the two spheres corresponding to the vertices of $\widehat{e}_{p/q}$ in the orthocubical sphere packing.

We shall represent both $\widehat{e}_{p/q}$ and $\widehat{\eta}_{p/q}$ by their respective projections $e_{p/q}$ and $\eta_{p/q}$ in the cubical diagrams as is shown in Fig. 6.12.

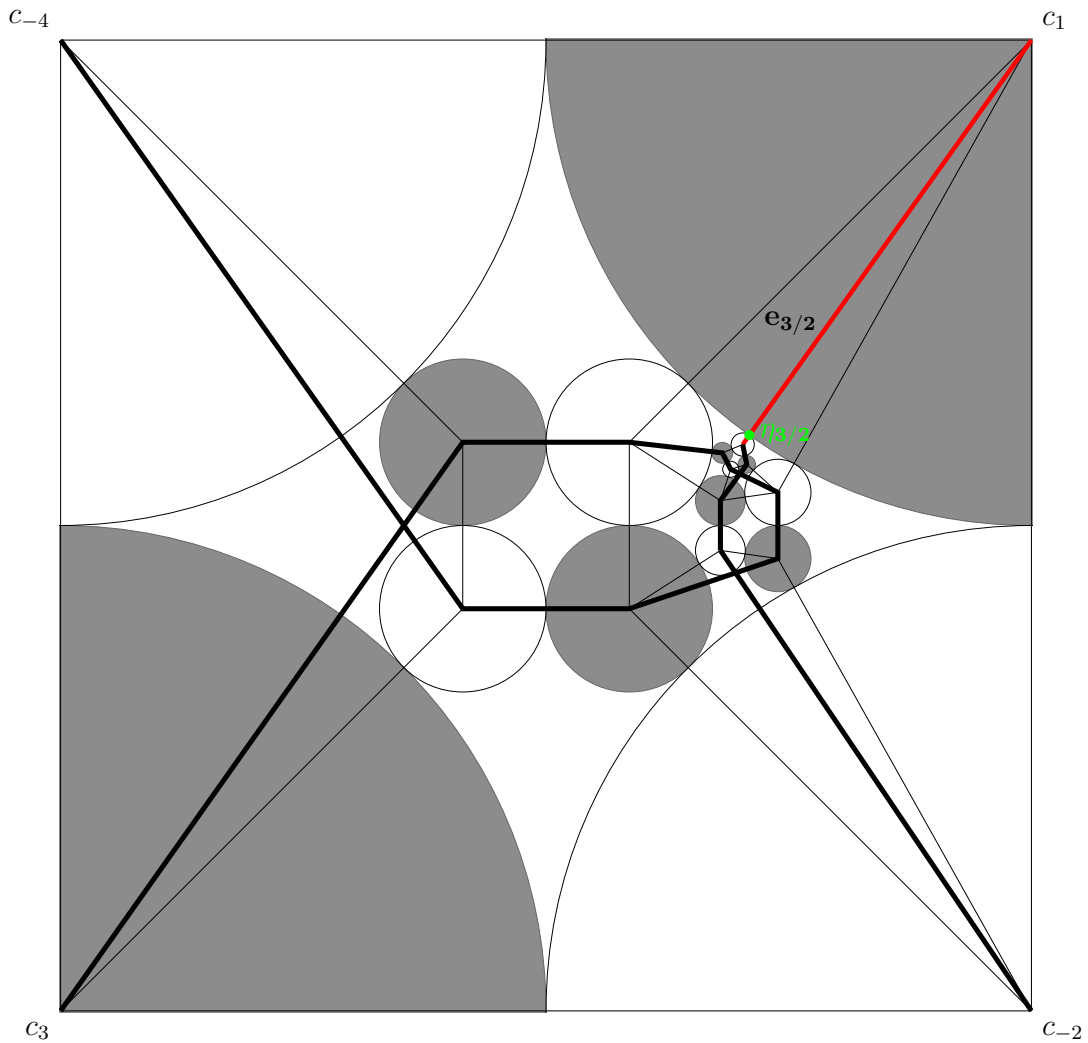


Figure 6.12: The projection of the first edge (red) and first tangency point (green) of the rational tangle $t_{3/2}$ in a cubical diagram.

Since the vertices of $e_{p/q}$ have different colors under the z -coloring, we have that $\widehat{\eta}_{p/q}$ lies in the plane $\{z = 0\}$. This implies that the Cartesian coordinates of $\widehat{\eta}_{p/q}$ can be computed from the Cartesian coordinates of $\eta_{p/q}$ by adding 0 in the third coordinate. The inversive coordinates of the latter will allow us to find the fraction p/q from the geometric construction of the corresponding orthocubical tangle when the fraction is positive.

Theorem 6.4.1. *For every coprime integers p, q with $q \geq 0$ and $p \leq 1$, we have*

$$\mathbf{i}(\eta_{p/q}) = \begin{pmatrix} p^2 \\ q^2 \\ (p-q)^2 \\ \sqrt{2}(p^2 - pq + q^2) \end{pmatrix} \quad (6.4)$$

Proof. The positiveness of p and q implies that we can find a positive continued fraction expansion $a_1 + \frac{1}{\dots + \frac{1}{a_n}} = p/q$ with $a_1 \geq 0$ and $a_i \geq 1$ for every $i > 1$. Let $\eta_{p/q}$ and η_∞ be the first tangency points of $t_{p/q}$ and t_∞ respectively. By the definition of the orthocubical Conway's algorithm (c.f. 6.3), we have that

$$\widehat{e}_{p/q} = (c_1, \widehat{m}_{a_1} \cdots \widehat{m}_{a_n}(c_{-2}))$$

where $\widehat{m}_{a_i} := \widehat{\mu}_x^{a_i} \widehat{r}_{24}$. Recall that $\widehat{\mu}_x$ is an orthocubical shift and $\widehat{r}_{24} \in \text{Sym}(\mathcal{B}_{\mathcal{O}_4}^{\uparrow z})$. Therefore,

$$\widehat{\eta}_{p/q} = \widehat{m}_{a_1} \cdots \widehat{m}_{a_n}(\eta_\infty) \Rightarrow \eta_{p/q} = m_{a_1} \cdots m_{a_n}(\eta_\infty)$$

where $m_{a_i} = \mu_x^{a_i} r_{12} = (s_1 r_{13})^{a_i} r_{12}$. The elements s_1, r_{13} and r_{12} are the elements of $\text{Sym}(\mathcal{B}_{\mathcal{C}_3}^*)$ described at the beginning of Section 6.3.1. The inversive coordinates of η_∞ and the matrices representing s_1, r_{13} and r_{12} can be computed with Equations (1.11) (we chose $\lambda = \frac{1}{\sqrt{2}}$) and (1.14), which give

$$\mathbf{i}(\eta_\infty) = \begin{pmatrix} 1 \\ 0 \\ 1 \\ \sqrt{2} \end{pmatrix} \quad s_1 \mapsto \mathbf{S}_1 = \begin{pmatrix} -3 & 0 & 0 & 2\sqrt{2} \\ 0 & 1 & 0 & 0 \\ 0 & 0 & 1 & 0 \\ -2\sqrt{2} & 0 & 0 & 3 \end{pmatrix}$$

$$r_{13} \mapsto \mathbf{R}_{13} = \begin{pmatrix} 0 & 0 & 1 & 0 \\ 0 & 1 & 0 & 0 \\ 1 & 0 & 0 & 0 \\ 0 & 0 & 0 & 1 \end{pmatrix} \quad r_{12} \mapsto \mathbf{R}_{12} = \begin{pmatrix} 0 & 1 & 0 & 0 \\ 1 & 0 & 0 & 0 \\ 0 & 0 & 1 & 0 \\ 0 & 0 & 0 & 1 \end{pmatrix}$$

Consequently, m_k is represented by the matrix $\mathbf{M}(k) := (\mathbf{S}_1 \mathbf{R}_{13})^k \mathbf{R}_{12}$. By induction on k , we find that

$$\mathbf{M}(k) = \begin{pmatrix} 0 & 1 - k^2 & -k(k+2) & \sqrt{2}k(k+1) \\ 1 & 0 & 0 & 0 \\ 0 & -k(k-2) & 1 - k^2 & \sqrt{2}k(k-1) \\ 0 & -\sqrt{2}k(k-1) & -\sqrt{2}k(k+1) & 2k^2 + 1 \end{pmatrix}$$

We prove the statement of the theorem by induction on the number of coefficients n in the fraction expansion of p/q . For $n = 1$ (so $p = a_1$ and $q = 1$) we have

$$\mathbf{M}(a_1) \begin{pmatrix} 1 \\ 0 \\ 1 \\ \sqrt{2} \end{pmatrix} = \begin{pmatrix} a_1^2 \\ 1 \\ (a_1 - 1)^2 \\ \sqrt{2}(a_1^2 - a_1 + 1) \end{pmatrix}$$

which satisfies the theorem.

Now let us suppose the theorem to be true for $n - 1$. Let $r/s = a_2 + \frac{1}{\dots + \frac{1}{a_n}}$. Then,

$$\begin{aligned} \mathbf{M}(a_1) \mathbf{M}(a_2) \cdots \mathbf{M}(a_n) \begin{pmatrix} 1 \\ 0 \\ 1 \\ \sqrt{2} \end{pmatrix} &= \mathbf{M}(a_1) \begin{pmatrix} r^2 \\ s^2 \\ (r-s)^2 \\ \sqrt{2}(r^2 - rs + s) \end{pmatrix} \\ &= \begin{pmatrix} (ra_1 + s)^2 \\ r^2 \\ (ra_1 + s - r)^2 \\ \sqrt{2}((ra_1 + s)^2 - r(ra_1 + s) + r^2) \end{pmatrix} \end{aligned}$$

We finally notice that

$$\frac{ra_1 + s}{r} = a_1 + \frac{s}{r} = a_1 + \frac{1}{r/s} = a_1 + \frac{1}{a_2 + \frac{1}{\dots + \frac{1}{a_n}}} = \frac{p}{q}$$

so the theorem holds for n . □

The following two corollaries follow from the previous theorem and the formula giving the inversive coordinates of a point.

Corollary 6.4.1. *For every $p/q > 0$, $\eta_{p/q}$ is the first point in the intersection of the circle centered at $(1 + \sqrt{2}, 1 + \sqrt{2})$ and radius $1 + \sqrt{2}$ with the line $\{p^2y = q^2x\}$.*

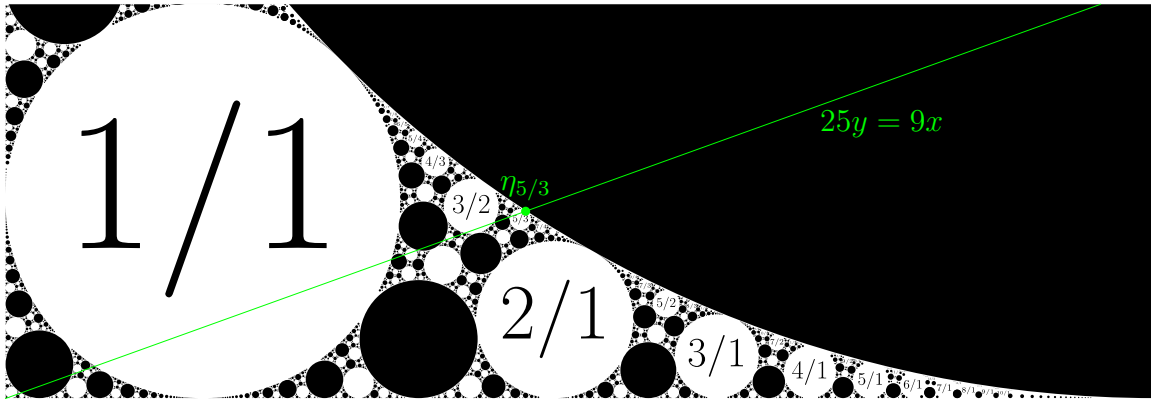


Figure 6.13: The cubical Apollonian packing $\Omega(\mathcal{B}_{\mathbb{C}^3})$ under the z -coloring with plot range $[0, 1 + \sqrt{2}] \times [0, 2(\sqrt{2} - 1)]$, together with the first tangency point $\eta_{5/3}$ obtained as the intersection described in Corollary 6.4.1. For every $p \geq q > 1$, the fraction p/q is printed at the center of the white disk corresponding to the vertex $e_{p/q}$ distinct from c_1 .

Corollary 6.4.2. *The Diophantine equation $x^4 + y^4 + z^4 = 2t^2$ has an infinite number of primitive solutions.*

Proof. Let p and q be two coprime positive integers. Since points of $\widehat{\mathbb{R}}^2$ correspond to light-like vectors of $\mathbb{L}^{3,1}$, we have

$$\langle \eta_{p/q}, \eta_{p/q} \rangle = \mathbf{i}(\eta_{p/q})^T \mathbf{Q}_4 \mathbf{i}(\eta_{p/q}) = 0 \tag{6.5}$$

where $\mathbf{Q}_4 = \text{diag}(1, 1, 1, -1)$. By combining Equations (6.4) and (6.5), we obtain a primitive solution of the Diophantine equation by setting

$$x = p, \quad y = q, \quad z = p - q \quad \text{and} \quad t = p^2 - pq + q^2$$

□

Conclusions: current and future work

We summarize here the main results of this thesis and we discuss the current work and future perspectives.

7.1 Möbius uniqueness

In Chapter 1, we have discuss the notion of Möbius uniqueness for planar graphs, which arises from the uniqueness of planar embeddings of graphs under Möbius transformations involved in the KAT theorem. We then extend this notion to edge-scribable polytopes in Chapter 3. We studied the Möbius uniqueness for most of regular polytopes, and used the derived results in the Chapters 4, 5 and 6. In particular, we have shown that the family of d -simplices, $(d + 1)$ -cross polytopes, $(d + 1)$ -cube for every $d \geq 2$, and also the 24-cell, are Möbius unique (Corollaries 3.6.1, 3.6.4, 3.6.5). For the non-regular case, we have shown that the non-regular 2-polytopes are not Möbius unique (Corollary 3.6.2), contrarily to the 3-polytopes, which, as a consequence of the Midsphere Theorem, are all Möbius unique. Unfortunately, for $d \geq 4$, there is no analogue of the Midsphere Theorem, but we believe that all edge-scribable 4-polytopes are Möbius unique. In light of all this, we propose the following conjecture, see [82].

Conjecture 1. *For every $d \geq 3$, all edge-scribable d -polytopes are Möbius unique.*

In view of the family of polytopes that we found to be Möbius unique, a natural next step would be to show the validity of the Conjecture 1 for regular polytopes.

Question 1. *Are the 600-cell and the 120-cell Möbius unique?*

After discussing Möbius uniqueness, we introduced a related spectral invariant for edge-scribable polytopes that are Möbius unique that we have called *Möbius spectra*. On the other hand, the well-known Steinitz's Theorem [97] states that the graph of a polyhedron is a 3-connected simple planar graph. Such graphs are usually called *polyhedral graphs*. Since all the polyhedra are edge-scribable and Möbius

unique, the Möbius spectra can be defined for any polyhedral graph. Möbius uniqueness implies that the Möbius spectra does not depend on the edge-scribed realization. It would be interesting to verify if the Möbius spectra is a complete invariant for edge-scribable Möbius unique polytopes and, in particular, for polyhedral graphs.

Question 2. *Are there two combinatorially different edge-scribable and Möbius unique $(d+1)$ -polytopes with the same Möbius spectra? In particular, are there two non-isomorphic polyhedral graphs with the same Möbius spectra?*

7.2 Integral packings

Among the many corollaries of the Polytopal Descartes' theorem proved in Chapter 4, we obtained the integrality conditions needed to construct integral Apollonian packings based on the Platonic solids. Queries studied in the literature about the behavior of the integers (multiplicity, density, primes...) appearing in the integral tetrahedral Apollonian packings [38, 40, 12, 64], can be also considered for the Platonic Apollonian packings. For instance, by comparing the integrality conditions of tetrahedral (Eq. 4.33) and icosahedral Apollonian packings (Prop. 4.3.6), we find that every triple of integers which produces an integral tetrahedral Apollonian packing also produces a φ -integral icosahedral Apollonian packing (see Fig. 7.14).

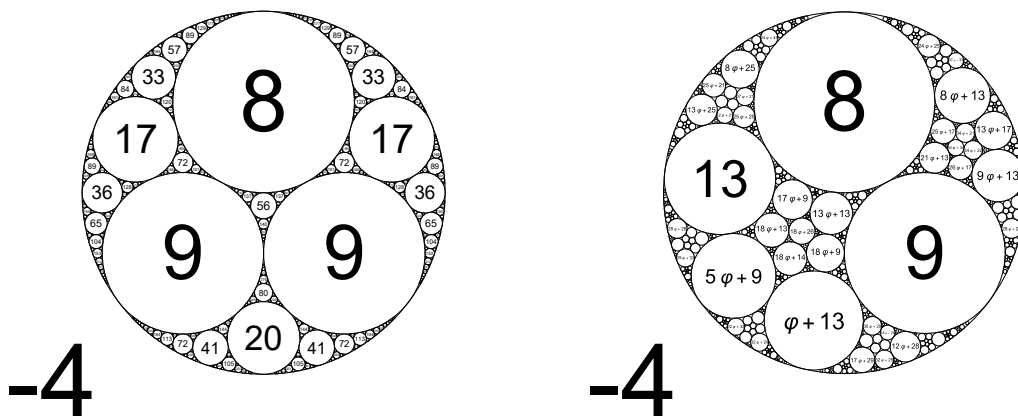


Figure 7.14: An integral tetrahedral (left) and a φ -integral icosahedral (right) Apollonian packings both with initial curvatures $(-4, 8, 9)$.

Question 3. *What is the maximum number of distinct integers that one can find in an icosahedral Apollonian packing?*

In Chapter 5, we applied the techniques used in the previous chapters on the orthoplicial Apollonian packings studied by Dias [33] and Nakamura [79]. Moreover, we have introduced the notion of Apollonian section as an algebraic generalization of geometric cross-sections. We found that the tetrahedral, octahedral and cubical Apollonian packings studied in Chapter 4 can be found as slices of the orthoplicial Apollonian packing. The main point of this result is that the inclusion between the different Apollonian packings, is not only geometrically obtained (or algebraically regarding Apollonian groups) but also *arithmetically*, that is, *every* integral tetrahedral, octahedral and cubical Apollonian packing can be obtained by intersecting an integral orthoplicial Apollonian packing with a plane (Th. 5.3.1).

An interesting open problem in number theory on Apollonian circle packings is the Local-to-Global conjecture of Graham et al. [44], and improved by Fuchs and Sanden [39]. This conjecture says that in any integral tetrahedral Apollonian circle packing $\Omega(\mathcal{B}_{\mathcal{T}^3})$, every integer avoiding certain restrictions modulo 24 must appear as the curvature of $\Omega(\mathcal{B}_{\mathcal{T}^3})$. Zhang [105], Kontorovich [62], Dias [33] and Nakamura [79] proved the analogue of the Local-to-Global conjecture for octahedral, simplicial and orthoplicial Apollonian packings, respectively. We believe that Th. 5.3.1 may be helpful to better understand the original Local-to-Global conjecture in the tetrahedral case.

The choice of studying orthoplicial Apollonian packings in Chapter 5, among the Apollonian packings based on regular 4-polytopes like the simplex or the hypercube, was not arbitrary. We decided to explore this case from the results on the ball number that are developed in the last chapter of this thesis. Nevertheless, we believe that it would be interesting to study the Apollonian groups, packings and sections of the other regular 4-polytopes. On the integrality side, numerical experiments on the Apollonian packing of the 24-cell suggested the following two conjectures, see [84].

Conjecture 2. *Let $\mathcal{B}_{\mathcal{R}^4}$ be a standard polytopal sphere packing, obtained by rescaling a 1-CBP projection of the 24-cell by a factor of $\frac{1}{\sqrt{3}}$. Then, the set of curvatures of its Apollonian packing $\Omega(\mathcal{B}_{\mathcal{R}^4})$ is \mathbb{N} .*

Conjecture 3. *There is a chain of tangent spheres $(b_0, b_1, \dots) \subset \Omega(\mathcal{B}_{\mathcal{R}^4})$ such that, for every $n \in \mathbb{N}$, the curvature of b_n is n .*

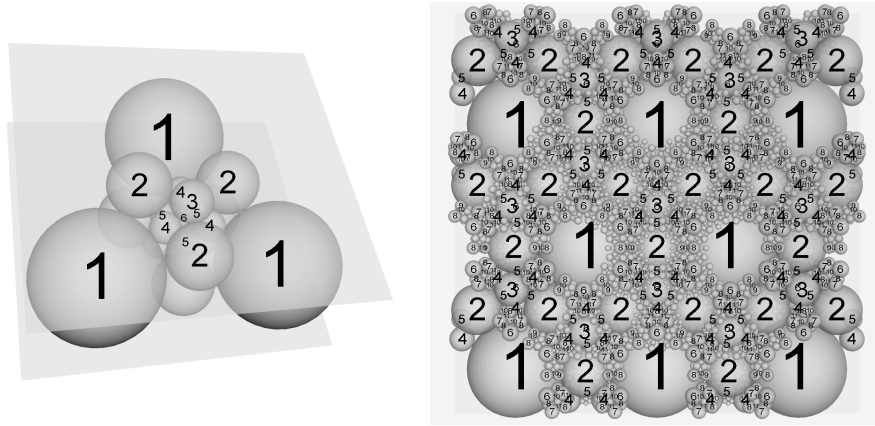


Figure 7.15: The sphere packing $\mathcal{B}_{\mathcal{R}^4}$ (left) and its Apollonian packing $\Omega(\mathcal{B}_{\mathcal{R}^4})$ (right) with the curvatures.

7.3 Diophantine equations

Besides the quadratic equations obtained by the Descartes' theorem and its generalizations, the curvatures of an integral Apollonian packing have been used to find integers solutions to other Diophantine equations [60, 37]. In Corollaries 4.2.5 and 6.4.2, we have presented two geometric methods based on integral polytopal d -ball packings to obtain solutions of several Diophantine equations. The first method follows from the Polytopal Descartes' theorem, and is obtained from the curvatures in the corresponding integral packing, as usual. The second method is slightly different, since the solutions do not come from the curvatures, but from the inversive coordinates of tangency points in a polytopal Apollonian packing. We believe that the parametrization given in Eq. (??) gives all the positive primitive solutions of the Diophantine equation in Cor. 6.4.2, which is equivalent to the following conjecture.

Conjecture 4. *The positive primitive integer solutions of $x^4 + y^4 + z^4 = 2t^2$ are in bijection with the set of first tangency points $\eta_{p/q}$ with p and q positive coprime integers.*

7.4 Necklace representations and the ball number

In Chapters 2 and 6, we presented two methods of construction of necklace representations of knots and links with relatively few spheres. The first method is based on the KAT theorem and yields the first upper bound on the ball number of nonsplittable and nontrivial links, which is 5 times the crossing number. The second method uses the fractal structure of the orthoplicial Apollonian packing and improves the previous upper bound for rational links to 4 times the crossing number. In addition, all the necklace representations that we found with less than 4 times the crossing number, such as the Pretzel knot $P(3, -2, 3)$ (Fig. 6.11), were for non-alternating knots or links. The reason is that non-alternating crossings can be done with fewer spheres. Hence, we believe that the second upper bound is actually tight for alternating links. This leads to the following conjecture, see [81].

Conjecture 5. *The ball number of an alternating link L is $4cr(L)$.*

Regarding lower bounds on the ball number, we were not able to find any non-trivial lower bound other than the one provided by the stick number. On this line, Maehara compared in [71] the stick number against the *pearl number* (defined similarly as the ball number but with equal size spheres) and gave non-trivial lower bounds on the pearl number of knots.

We have chosen the orthoplex for the construction of necklace representations for two main reasons. Firstly, it is the only regular 4-polytope whose standard Apollonian packing contains clearly a square-grid in the carrier (Fig. 6.2). This is due to the fact that the *edge-link* of the orthoplex is a square, unlike the other regular 4-polytopes, whose edge-link is a triangle (4-simplex, hypercube, 24-cell and 120-cell) or a pentagon (600-cell). The latter was used to prove that the orthoplicial Apollonian packing has a structure complex enough to contain any link in its carrier (Th. 6.2.1). Secondly, such structure is manageable, since it can be seen as the action of a reflection group with relatively few generators. This was helpful in order to find the good elements in the corresponding symmetrized Apollonian group to produce the desired constructions. We believe that analogous methods, for the other regular 4-polytopes, should be considered. For instance, we have started to explore necklace representations of three interesting links, that can be found in a CBP projection

of the orthoplex \mathcal{O}^4 , 24-cell \mathcal{R}^4 and 600-cell \mathcal{I}^4 , respectively. For the construction, we use a well-known fact, that the vertices of three 4-polytopes \mathcal{O}^4 , \mathcal{R}^4 and \mathcal{I}^4 , can be equally partitioned into 2, 4 and 12 subsets of 4, 6 and 10 vertices, respectively, where each subset is contained in a fiber of the Hopf fibration (see [29, 5, 87]). On the other hand, it is also known that the link obtained from selecting n fibers in the Hopf fibration is a link of n components satisfying that any two form a Hopf link [54]. Let us denote this link by $Hf(n)$. Therefore, the latter partitions produce necklace representations of the links $Hf(2)$, $Hf(4)$ and $Hf(12)$, respectively. It seems that the number of spheres obtained from this construction, with respect to the crossing number, is much smaller than the constructions presented here. We show in Figures 7.16, 7.17 and 7.23 the three constructions.

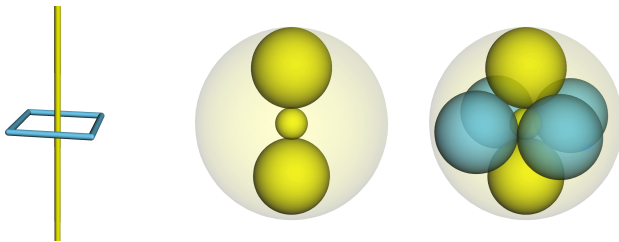


Figure 7.16: The Hopf link $Hf(2)$ (left), and the construction of a necklace representation of $Hf(2)$ with 8 spheres contained in a 0-CBP projection of the orthoplex.

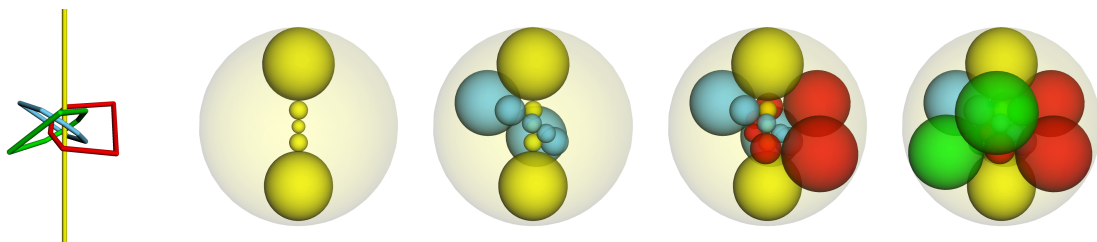


Figure 7.17: The link $Hf(4)$ (left) and the construction of a necklace representation of $Hf(4)$ in a 0-CBP projection of the 24-cell.

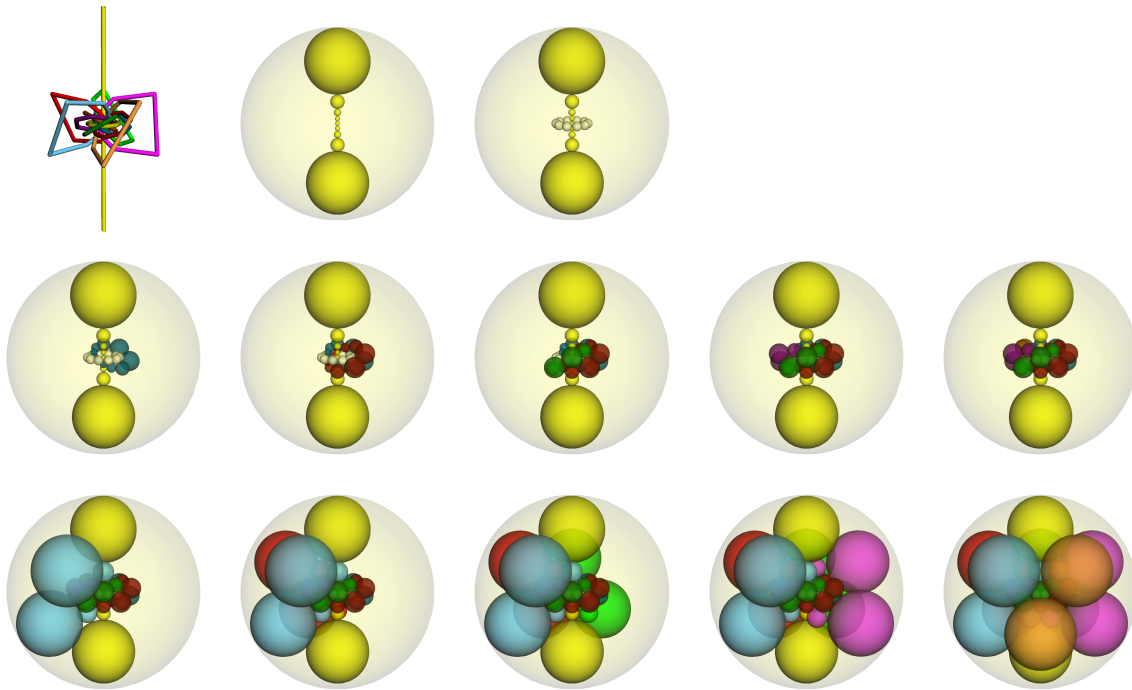


Figure 7.18: The link $Hf(12)$ (top left) and the construction of a necklace representation of $Hf(12)$ in a 0-CBP projection of the 600-cell.

Finally, we would like to point out an important difference between the different methods of construction of necklaces. Since the algorithms of circle packings, induced by the KAT theorem, are an infinite limit process, the inversive coordinates obtained by the method given in Chapter 2 have approximate values. On the contrary, the orthoplicial necklace representations obtained by either closing orthoplicial braids or the orthocubical Conway's algorithm, give *algebraic* values for the inversive coordinates of the spheres. We believe that this can be interesting for the study of the hyperbolic volume of hyperbolic 3-manifolds [41].

7.5 Further knotted constructions

Beyond knots and links, we are also applying the techniques developed in this thesis in the realization of other spatial constructions. We recall that a *Seifert surface* of a link is an oriented surface containing the link as a boundary. By applying the

Seifert's algorithm [90] to orthocubical diagrams of rational links, we are able to construct polyhedral Seifert surfaces of links with a small number of planar triangles. In Fig. 7.19, we show a polyhedral Seifert surface of the knot $4_1 = C(2, 2)$ with 18 triangles, obtained from an orthocubical diagram.

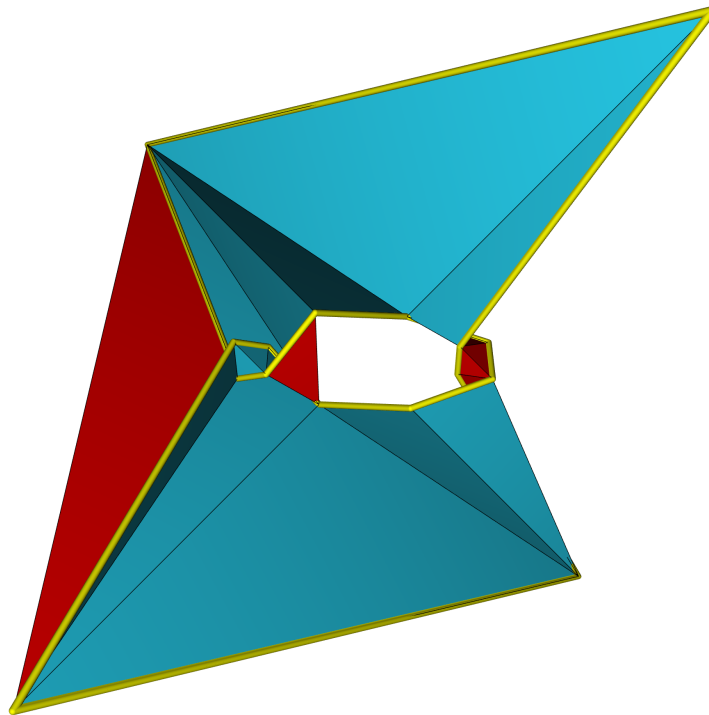


Figure 7.19: A polyhedral Seifert surface of the knot 4_1 with 18 triangles.

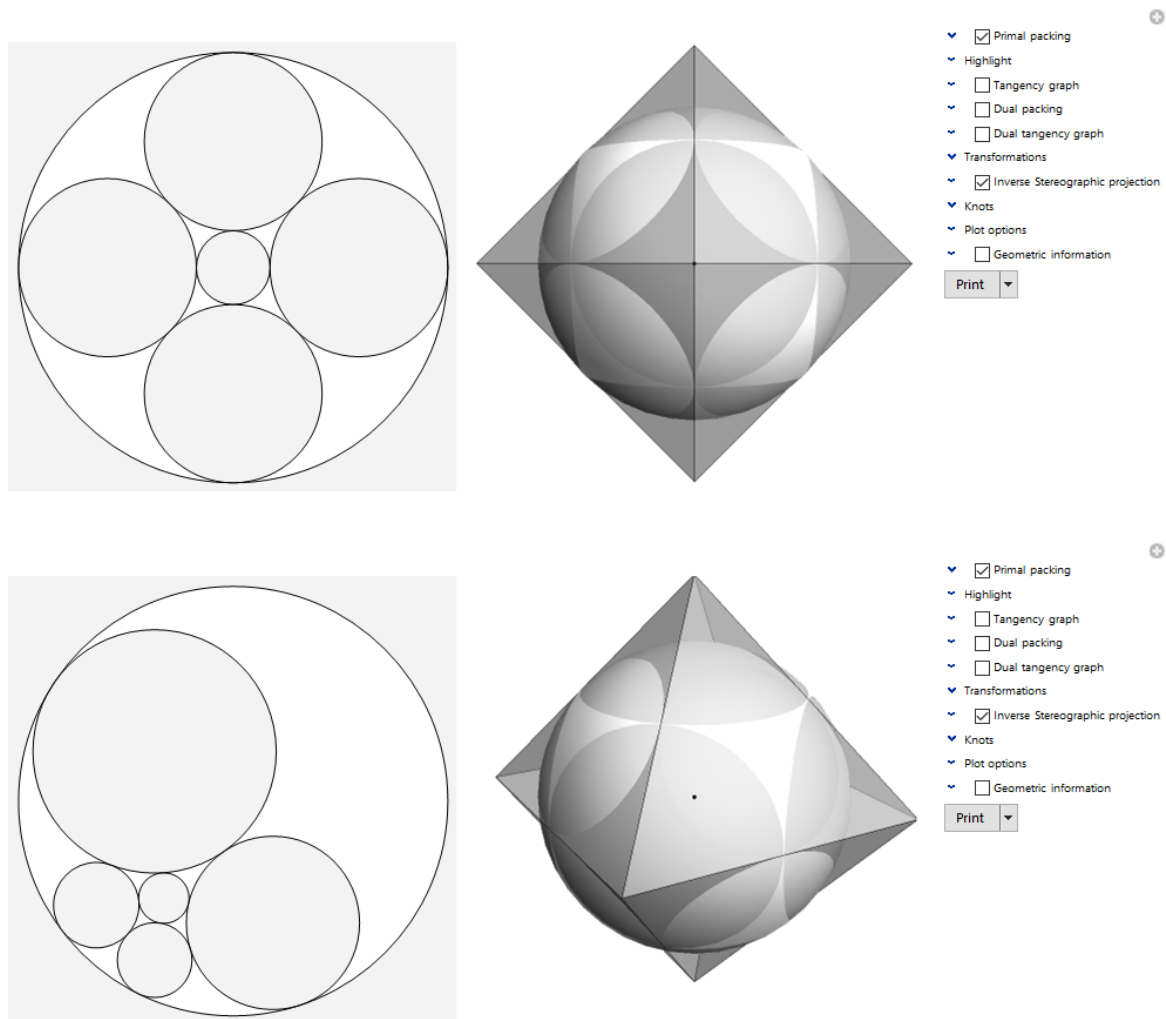
7.6 Software Polytopack

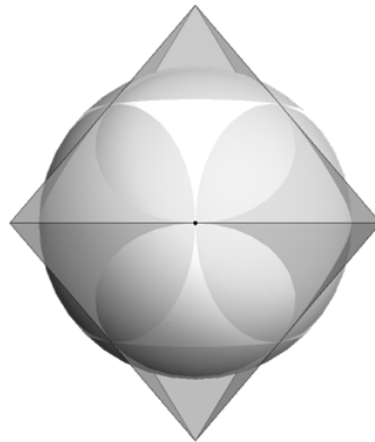
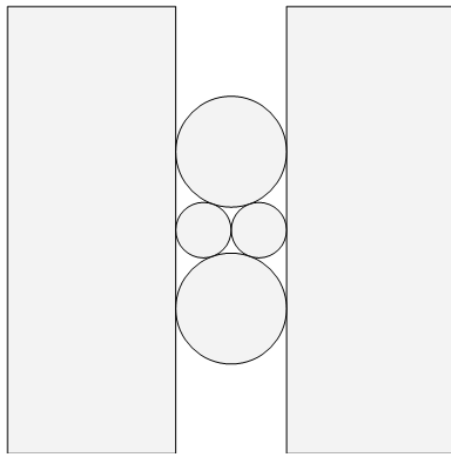
Besides the theoretical topics investigated in this thesis, we developed a software on Mathematica [57] that we called `Polytopack` [85] and used to plot all the 2D and 3D figures of this thesis. This helped us to better understand some objects, testing geometric properties on necklace representations, as well as the arithmetical behaviors of the curvatures of Apollonian packings. This software has been continuously improved through the last years, and it counts now with multiple options dealing

with polytopes, Apollonian packings and knots. Polytopack will eventually be made available for researchers and other users interested in these topics.

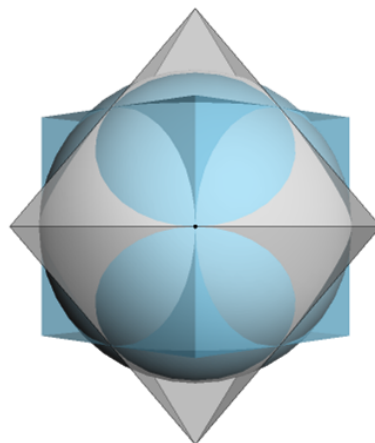
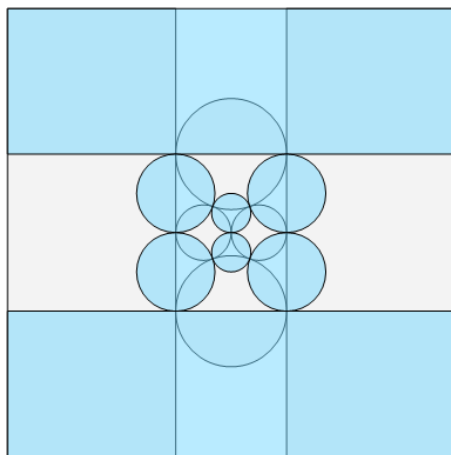
Below, we give a few examples of the tools that have been implemented in Polytopack.

Figure 7.20: Manipulation of a polytopal circle packing with Polytopack.

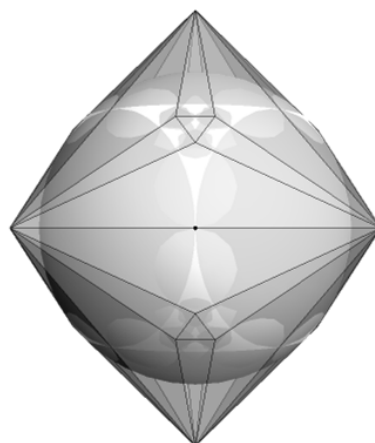
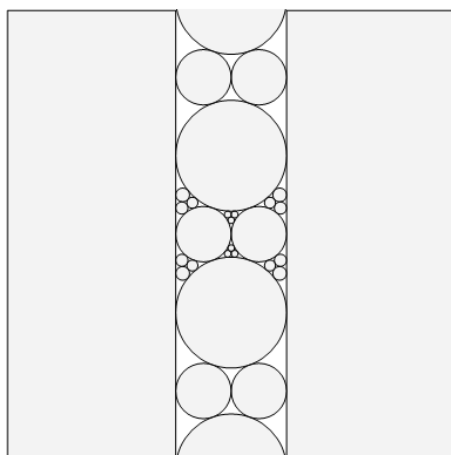




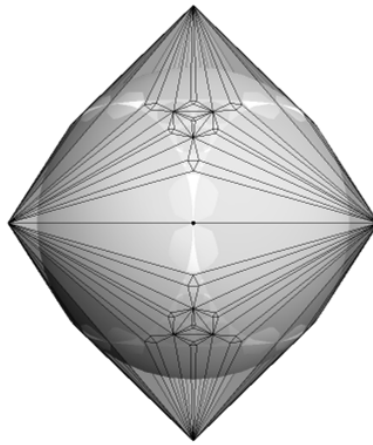
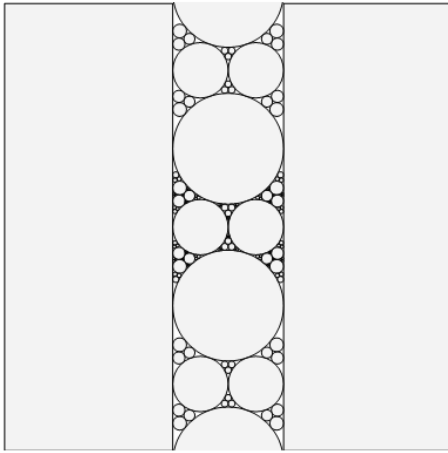
- Primal packing
 - Highlight
 - Tangency graph
 - Dual packing
 - Dual tangency graph
 - Transformations
 - Inverse Stereographic projection
 - Knots
 - Plot options
 - Geometric information
- Print ▾



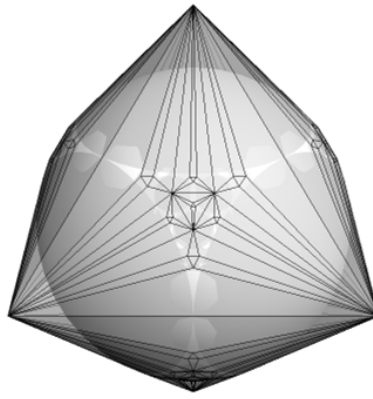
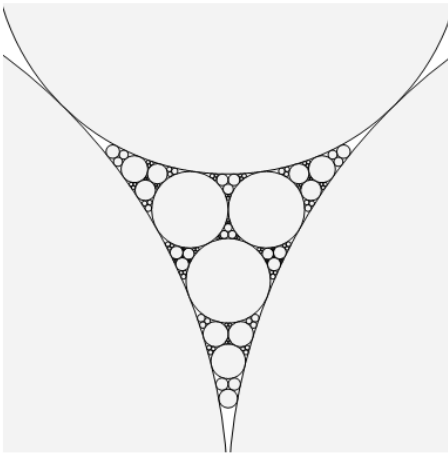
- Primal packing
 - Highlight
 - Tangency graph
 - Dual packing
 - Dual tangency graph
 - Transformations
 - Inverse Stereographic projection
 - Knots
 - Plot options
 - Geometric information
- Print ▾



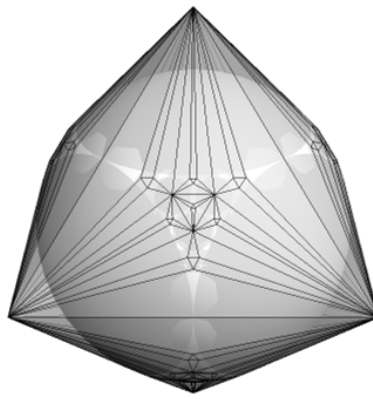
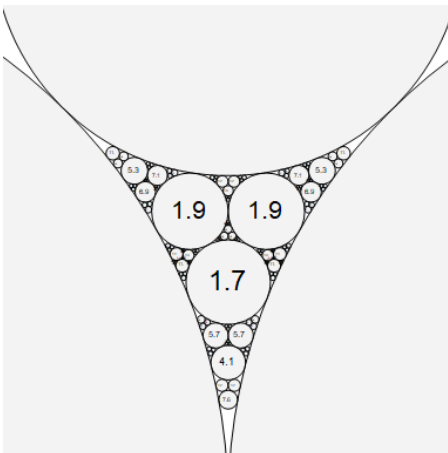
- Primal packing
 - Highlight
 - Tangency graph
 - Dual packing
 - Dual tangency graph
 - Transformations
 - Inverse Stereographic projection
 - Knots
 - Plot options
 - Geometric information
- Print ▾



- Primal packing
 - Highlight
 - Tangency graph
 - Dual packing
 - Dual tangency graph
 - Transformations
 - Inverse Stereographic projection
 - Knots
 - Plot options
 - Geometric information
- Print ▾

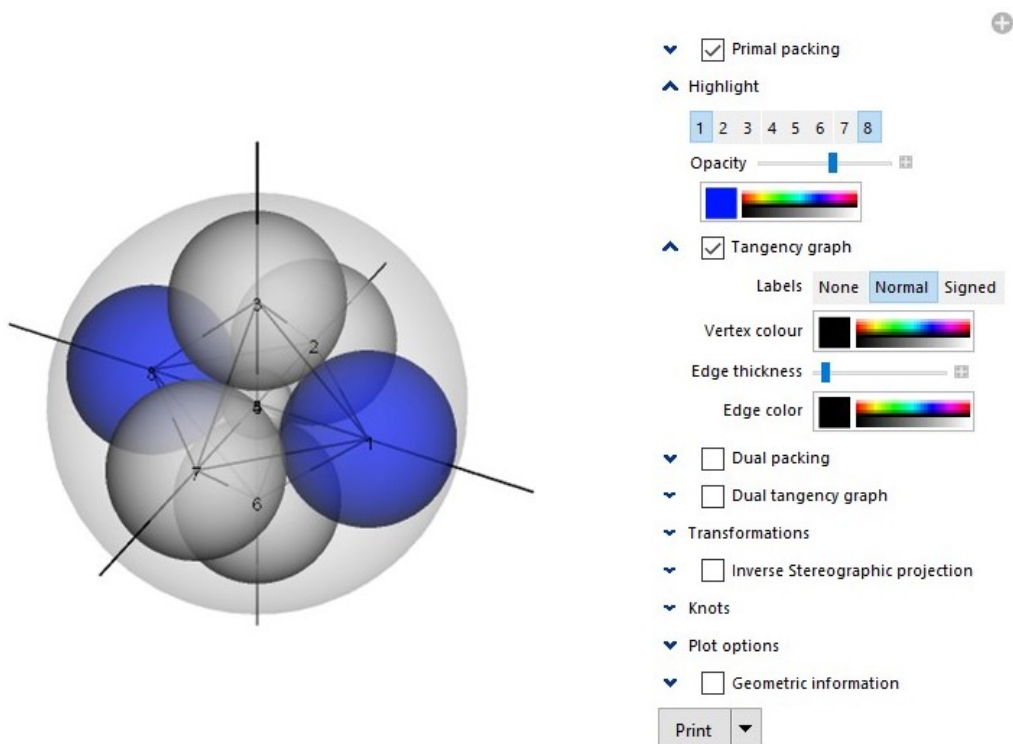
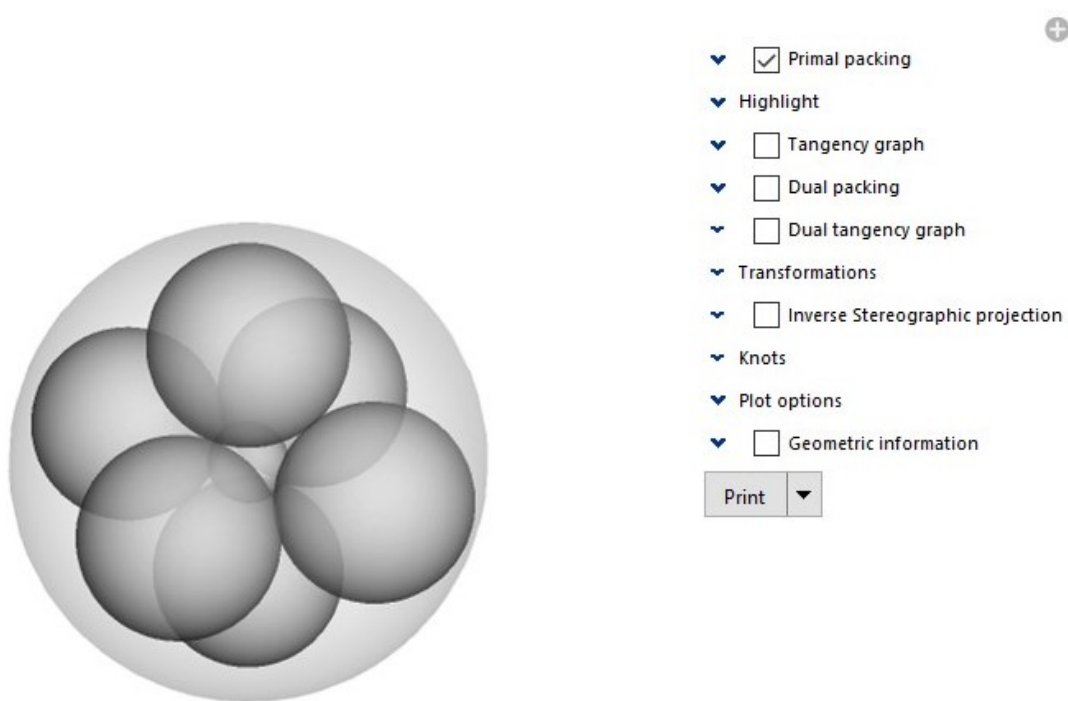


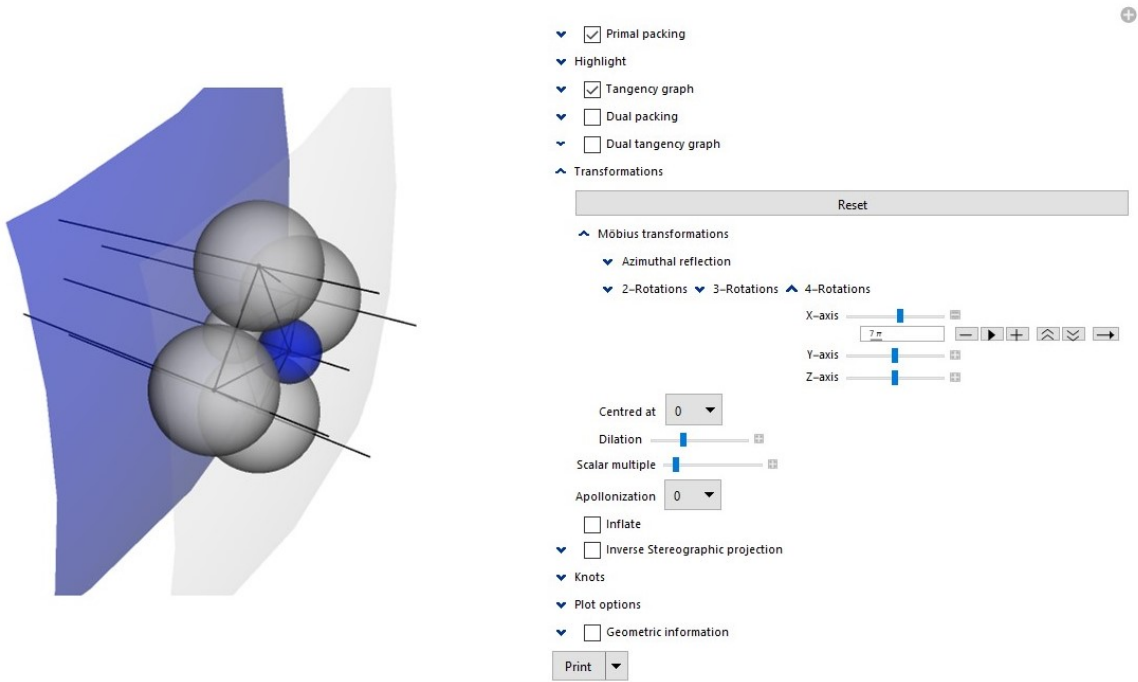
- Primal packing
 - Highlight
 - Tangency graph
 - Dual packing
 - Dual tangency graph
 - Transformations
 - Inverse Stereographic projection
 - Knots
 - Plot options
 - Geometric information
- Print ▾



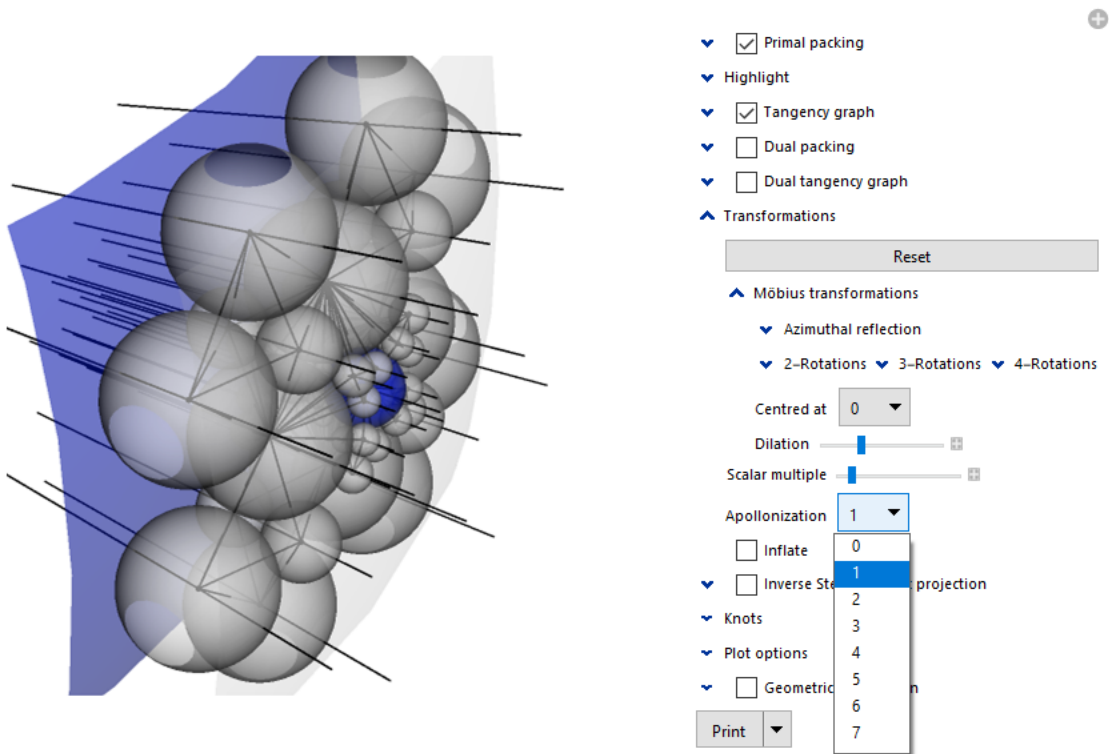
- Primal packing
 - Highlight
 - Tangency graph
 - Dual packing
 - Dual tangency graph
 - Transformations
 - Inverse Stereographic projection
 - Knots
 - Plot options
 - Geometric information
- Print ▾

Figure 7.21: Manipulation of a polytopal sphere packing with Polytopack.





Primal packing
 Highlight
 Tangency graph
 Dual packing
 Dual tangency graph
 Transformations
 Reset
 Möbius transformations
 Azimuthal reflection
 2-Rotations 3-Rotations **4-Rotations**
 X-axis
 Y-axis
 Z-axis
 Centred at
 Dilation
 Scalar multiple
 Apollonization
 Inflate
 Inverse Stereographic projection
 Knots
 Plot options
 Geometric information
 Print



Primal packing
 Highlight
 Tangency graph
 Dual packing
 Dual tangency graph
 Transformations
 Reset
 Möbius transformations
 Azimuthal reflection
 2-Rotations 3-Rotations 4-Rotations
 Centred at
 Dilation
 Scalar multiple
 Apollonization
 Inflate
 Inverse Stereographic projection
 Knots
 Plot options
 Geometric information
 Print

We end by illustrating some mathematical applications of `Polytopack` that have not been treated in this dissertation.

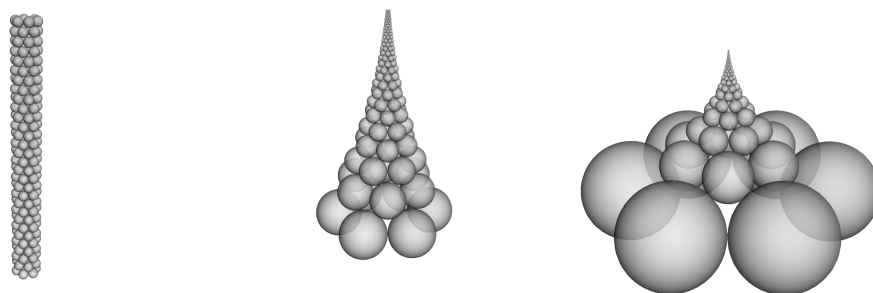


Figure 7.22: Deformations of 3D-meshes with sphere packings preserving the tangency graph.

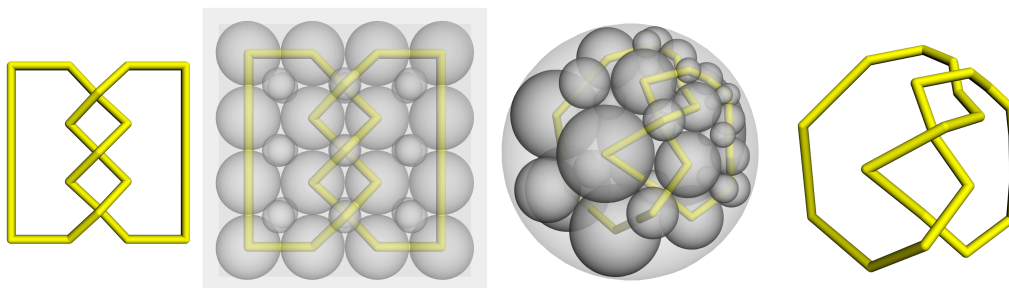


Figure 7.23: Deformations of knots and links preserving the knot-type.

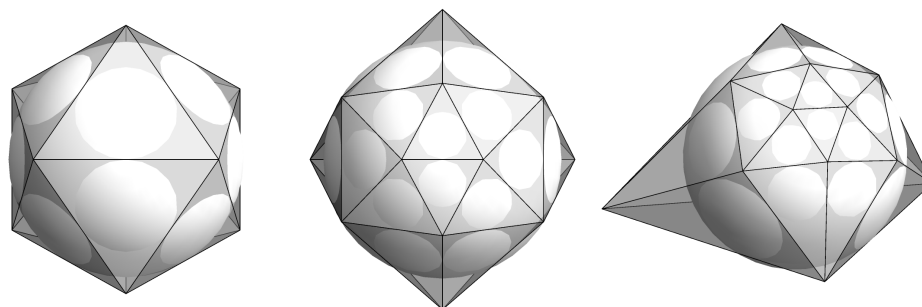


Figure 7.24: Projective transformations of edge-scribed polyhedra preserving edge-scribedness.



Figure 7.25: Projective transformations of inscribed polyhedra preserving inscribedness.

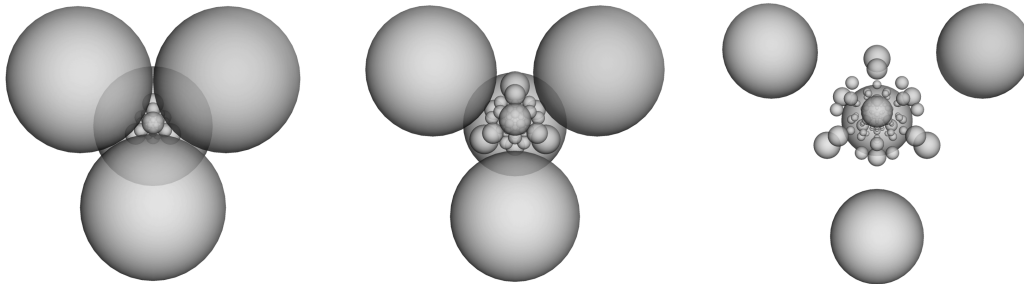


Figure 7.26: Study of internal structures of the ball-arrangement projections of 4-polytopes.

APPENDIX A

Appendices

d	Name	Notation	Schläfli symbol	Eigenvalues	Multiplicities	Midsphere ratio
$d = 1$	p -gone ($p \geq 3$)	-	$\{p\}$	Not Möbius unique for $p > 3$		$\tan(\pi/p)$
$d \geq 1$	$(d + 1)$ -Simplex	\mathcal{T}^{d+1}	$\underbrace{\{3, \dots, 3, 3\}}_{d-1}$	$-d$ 2	1 $d + 1$	$\sqrt{\frac{d+2}{d}}$
$d \geq 2$	$(d + 1)$ -Cross polytope	\mathcal{O}^{d+1}	$\underbrace{\{3, \dots, 3, 4\}}_{d-1}$	$-2(d + 1)$ 4 0	1 $d + 1$ d	1
$d \geq 2$	$(d + 1)$ -Cube	\mathcal{C}^{d+1}	$\{4, \underbrace{3, \dots, 3}_{d-1}\}$	$-2^{d+1}d$ 2^{d+1} 0	1 $d + 1$ $2^{d+1} - d - 2$	$d^{-1/2}$
$d = 2$	Icosahedron	\mathcal{I}^3	$\{3, 5\}$	$-12\varphi^2$ $4(\varphi^2 + 1)$ 0	1 3 8	φ^{-1}
$d = 2$	Dodecahedron	\mathcal{D}^3	$\{5, 3\}$	$-20\varphi^4$ $20\varphi^2$ 0	1 3 16	φ^{-2}
$d = 3$	24-cell	\mathcal{R}^4	$\{3, 4, 3\}$	-72 24 0	1 4 19	$3^{-1/2}$
$d = 3$	600-cell	\mathcal{I}^4	$\{3, 3, 5\}$	Möbius unique?		$5^{-1/4}\varphi^{-3/2}$
$d = 3$	120-cell	\mathcal{D}^4	$\{5, 3, 3\}$	Möbius unique?		$3^{-1/2}\varphi^{-3}$

Table A.1: Notations, Möbius spectra and midsphere ratio of regular $(d + 1)$ -polytopes for $d \geq 1$.

Table A.2: CBP projections of the Platonic solids.

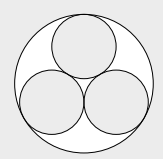
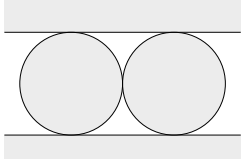
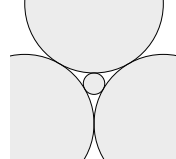
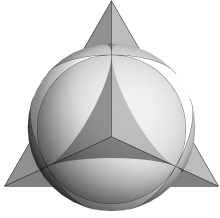
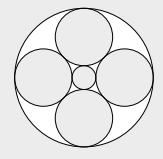
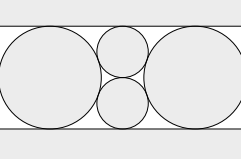
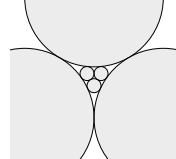
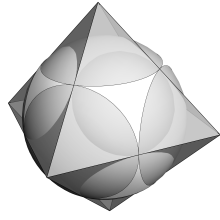
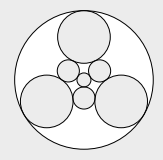
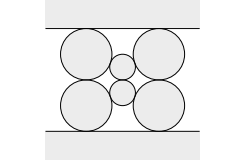
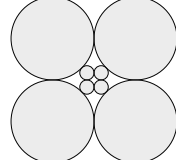
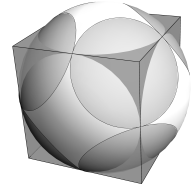
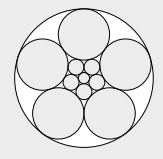
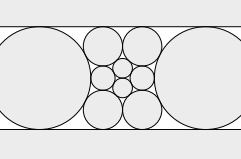
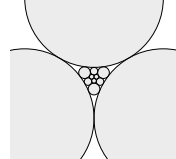
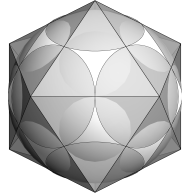
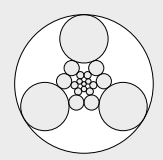
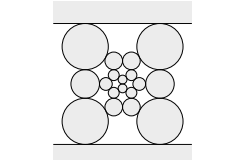
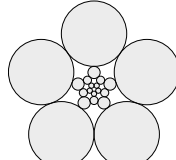
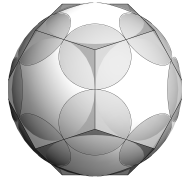
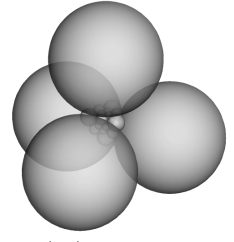
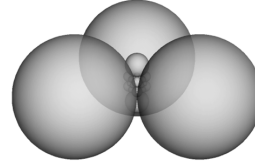
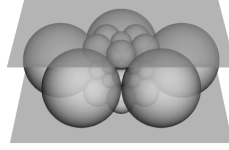
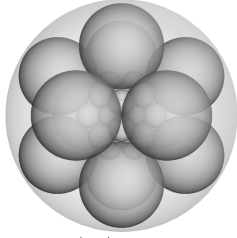
	Vertex centered at ∞	Edge centered at ∞	Face centered at ∞	Edge-scribed realization																																																												
\mathcal{T}^3 Tetrahedron $\{3, 3\}$ $\kappa_{\mathcal{P}} = \sqrt{1/2}$ $h_0 = \sqrt{1/6}$ $h_1 = \sqrt{1/2}$ $h_2 = \sqrt{1/6}$	 <table border="1"> <thead> <tr> <th>Layer</th> <th>n</th> <th>Curvatures</th> </tr> </thead> <tbody> <tr> <td>1</td> <td>1</td> <td>$\kappa_{\mathcal{P}} - 3h_0$</td> </tr> <tr> <td>2</td> <td>3</td> <td>$\kappa_{\mathcal{P}} + h_0$</td> </tr> </tbody> </table>	Layer	n	Curvatures	1	1	$\kappa_{\mathcal{P}} - 3h_0$	2	3	$\kappa_{\mathcal{P}} + h_0$	 <table border="1"> <thead> <tr> <th>Layer</th> <th>n</th> <th>Curvatures</th> </tr> </thead> <tbody> <tr> <td>1</td> <td>2</td> <td>$\kappa_{\mathcal{P}} - h_1$</td> </tr> <tr> <td>2</td> <td>2</td> <td>$\kappa_{\mathcal{P}} + h_1$</td> </tr> </tbody> </table>	Layer	n	Curvatures	1	2	$\kappa_{\mathcal{P}} - h_1$	2	2	$\kappa_{\mathcal{P}} + h_1$	 <table border="1"> <thead> <tr> <th>Layer</th> <th>n</th> <th>Curvatures</th> </tr> </thead> <tbody> <tr> <td>1</td> <td>3</td> <td>$\kappa_{\mathcal{P}} - h_2$</td> </tr> <tr> <td>2</td> <td>1</td> <td>$\kappa_{\mathcal{P}} + 3h_2$</td> </tr> </tbody> </table>	Layer	n	Curvatures	1	3	$\kappa_{\mathcal{P}} - h_2$	2	1	$\kappa_{\mathcal{P}} + 3h_2$																																		
Layer	n	Curvatures																																																														
1	1	$\kappa_{\mathcal{P}} - 3h_0$																																																														
2	3	$\kappa_{\mathcal{P}} + h_0$																																																														
Layer	n	Curvatures																																																														
1	2	$\kappa_{\mathcal{P}} - h_1$																																																														
2	2	$\kappa_{\mathcal{P}} + h_1$																																																														
Layer	n	Curvatures																																																														
1	3	$\kappa_{\mathcal{P}} - h_2$																																																														
2	1	$\kappa_{\mathcal{P}} + 3h_2$																																																														
\mathcal{O}^3 Octahedron $\{3, 4\}$ $\kappa_{\mathcal{P}} = 1$ $h_0 = \sqrt{2}$ $h_1 = 1$ $h_2 = \sqrt{2/3}$	 <table border="1"> <thead> <tr> <th>Layer</th> <th>n</th> <th>Curvatures</th> </tr> </thead> <tbody> <tr> <td>1</td> <td>1</td> <td>$\kappa_{\mathcal{P}} - h_0$</td> </tr> <tr> <td>2</td> <td>4</td> <td>$\kappa_{\mathcal{P}}$</td> </tr> <tr> <td>3</td> <td>1</td> <td>$\kappa_{\mathcal{P}} + h_0$</td> </tr> </tbody> </table>	Layer	n	Curvatures	1	1	$\kappa_{\mathcal{P}} - h_0$	2	4	$\kappa_{\mathcal{P}}$	3	1	$\kappa_{\mathcal{P}} + h_0$	 <table border="1"> <thead> <tr> <th>Layer</th> <th>n</th> <th>Curvatures</th> </tr> </thead> <tbody> <tr> <td>1</td> <td>2</td> <td>$\kappa_{\mathcal{P}} - h_1$</td> </tr> <tr> <td>2</td> <td>2</td> <td>$\kappa_{\mathcal{P}}$</td> </tr> <tr> <td>3</td> <td>2</td> <td>$\kappa_{\mathcal{P}} + h_1$</td> </tr> </tbody> </table>	Layer	n	Curvatures	1	2	$\kappa_{\mathcal{P}} - h_1$	2	2	$\kappa_{\mathcal{P}}$	3	2	$\kappa_{\mathcal{P}} + h_1$	 <table border="1"> <thead> <tr> <th>Layer</th> <th>n</th> <th>Curvatures</th> </tr> </thead> <tbody> <tr> <td>1</td> <td>3</td> <td>$\kappa_{\mathcal{P}} - h_2$</td> </tr> <tr> <td>2</td> <td>3</td> <td>$\kappa_{\mathcal{P}} + h_2$</td> </tr> </tbody> </table>	Layer	n	Curvatures	1	3	$\kappa_{\mathcal{P}} - h_2$	2	3	$\kappa_{\mathcal{P}} + h_2$																												
Layer	n	Curvatures																																																														
1	1	$\kappa_{\mathcal{P}} - h_0$																																																														
2	4	$\kappa_{\mathcal{P}}$																																																														
3	1	$\kappa_{\mathcal{P}} + h_0$																																																														
Layer	n	Curvatures																																																														
1	2	$\kappa_{\mathcal{P}} - h_1$																																																														
2	2	$\kappa_{\mathcal{P}}$																																																														
3	2	$\kappa_{\mathcal{P}} + h_1$																																																														
Layer	n	Curvatures																																																														
1	3	$\kappa_{\mathcal{P}} - h_2$																																																														
2	3	$\kappa_{\mathcal{P}} + h_2$																																																														
\mathcal{C}^3 Cube $\{4, 3\}$ $\kappa_{\mathcal{P}} = \sqrt{2}$ $h_0 = \sqrt{1/3}$ $h_1 = \sqrt{2}$ $h_2 = 1$	 <table border="1"> <thead> <tr> <th>Layer</th> <th>n</th> <th>Curvatures</th> </tr> </thead> <tbody> <tr> <td>1</td> <td>1</td> <td>$\kappa_{\mathcal{P}} - 3h_0$</td> </tr> <tr> <td>2</td> <td>3</td> <td>$\kappa_{\mathcal{P}} - h_0$</td> </tr> <tr> <td>3</td> <td>3</td> <td>$\kappa_{\mathcal{P}} + h_0$</td> </tr> <tr> <td>4</td> <td>1</td> <td>$\kappa_{\mathcal{P}} + 3h_0$</td> </tr> </tbody> </table>	Layer	n	Curvatures	1	1	$\kappa_{\mathcal{P}} - 3h_0$	2	3	$\kappa_{\mathcal{P}} - h_0$	3	3	$\kappa_{\mathcal{P}} + h_0$	4	1	$\kappa_{\mathcal{P}} + 3h_0$	 <table border="1"> <thead> <tr> <th>Layer</th> <th>n</th> <th>Curvatures</th> </tr> </thead> <tbody> <tr> <td>1</td> <td>2</td> <td>$\kappa_{\mathcal{P}} - h_1$</td> </tr> <tr> <td>2</td> <td>4</td> <td>$\kappa_{\mathcal{P}}$</td> </tr> <tr> <td>3</td> <td>2</td> <td>$\kappa_{\mathcal{P}} + h_1$</td> </tr> </tbody> </table>	Layer	n	Curvatures	1	2	$\kappa_{\mathcal{P}} - h_1$	2	4	$\kappa_{\mathcal{P}}$	3	2	$\kappa_{\mathcal{P}} + h_1$	 <table border="1"> <thead> <tr> <th>Layer</th> <th>n</th> <th>Curvatures</th> </tr> </thead> <tbody> <tr> <td>1</td> <td>4</td> <td>$\kappa_{\mathcal{P}} - h_2$</td> </tr> <tr> <td>2</td> <td>4</td> <td>$\kappa_{\mathcal{P}} + h_2$</td> </tr> </tbody> </table>	Layer	n	Curvatures	1	4	$\kappa_{\mathcal{P}} - h_2$	2	4	$\kappa_{\mathcal{P}} + h_2$																									
Layer	n	Curvatures																																																														
1	1	$\kappa_{\mathcal{P}} - 3h_0$																																																														
2	3	$\kappa_{\mathcal{P}} - h_0$																																																														
3	3	$\kappa_{\mathcal{P}} + h_0$																																																														
4	1	$\kappa_{\mathcal{P}} + 3h_0$																																																														
Layer	n	Curvatures																																																														
1	2	$\kappa_{\mathcal{P}} - h_1$																																																														
2	4	$\kappa_{\mathcal{P}}$																																																														
3	2	$\kappa_{\mathcal{P}} + h_1$																																																														
Layer	n	Curvatures																																																														
1	4	$\kappa_{\mathcal{P}} - h_2$																																																														
2	4	$\kappa_{\mathcal{P}} + h_2$																																																														
\mathcal{I}^3 Icosahedron $\{3, 5\}$ $\kappa_{\mathcal{P}} = \varphi$ $h_0 = \sqrt{(\varphi^2 + 1)/5}$ $h_1 = 1$ $h_2 = \varphi^{-1} \sqrt{1/3}$	 <table border="1"> <thead> <tr> <th>Layer</th> <th>n</th> <th>Curvatures</th> </tr> </thead> <tbody> <tr> <td>1</td> <td>1</td> <td>$\kappa_{\mathcal{P}} - \sqrt{5}h_0$</td> </tr> <tr> <td>2</td> <td>5</td> <td>$\kappa_{\mathcal{P}} - h_0$</td> </tr> <tr> <td>3</td> <td>5</td> <td>$\kappa_{\mathcal{P}} + h_0$</td> </tr> <tr> <td>4</td> <td>1</td> <td>$\kappa_{\mathcal{P}} + \sqrt{5}h_0$</td> </tr> </tbody> </table>	Layer	n	Curvatures	1	1	$\kappa_{\mathcal{P}} - \sqrt{5}h_0$	2	5	$\kappa_{\mathcal{P}} - h_0$	3	5	$\kappa_{\mathcal{P}} + h_0$	4	1	$\kappa_{\mathcal{P}} + \sqrt{5}h_0$	 <table border="1"> <thead> <tr> <th>Layer</th> <th>n</th> <th>Curvatures</th> </tr> </thead> <tbody> <tr> <td>1</td> <td>2</td> <td>$\kappa_{\mathcal{P}} - \varphi h_1$</td> </tr> <tr> <td>2</td> <td>2</td> <td>$\kappa_{\mathcal{P}} - h_1$</td> </tr> <tr> <td>3</td> <td>4</td> <td>$\kappa_{\mathcal{P}}$</td> </tr> <tr> <td>4</td> <td>2</td> <td>$\kappa_{\mathcal{P}} + h_1$</td> </tr> <tr> <td>5</td> <td>2</td> <td>$\kappa_{\mathcal{P}} + \varphi h_1$</td> </tr> </tbody> </table>	Layer	n	Curvatures	1	2	$\kappa_{\mathcal{P}} - \varphi h_1$	2	2	$\kappa_{\mathcal{P}} - h_1$	3	4	$\kappa_{\mathcal{P}}$	4	2	$\kappa_{\mathcal{P}} + h_1$	5	2	$\kappa_{\mathcal{P}} + \varphi h_1$	 <table border="1"> <thead> <tr> <th>Layer</th> <th>n</th> <th>Curvatures</th> </tr> </thead> <tbody> <tr> <td>1</td> <td>3</td> <td>$\kappa_{\mathcal{P}} - \varphi^3 h_2$</td> </tr> <tr> <td>2</td> <td>3</td> <td>$\kappa_{\mathcal{P}} - h_2$</td> </tr> <tr> <td>3</td> <td>3</td> <td>$\kappa_{\mathcal{P}} + h_2$</td> </tr> <tr> <td>4</td> <td>3</td> <td>$\kappa_{\mathcal{P}} + \varphi^3 h_2$</td> </tr> </tbody> </table>	Layer	n	Curvatures	1	3	$\kappa_{\mathcal{P}} - \varphi^3 h_2$	2	3	$\kappa_{\mathcal{P}} - h_2$	3	3	$\kappa_{\mathcal{P}} + h_2$	4	3	$\kappa_{\mathcal{P}} + \varphi^3 h_2$													
Layer	n	Curvatures																																																														
1	1	$\kappa_{\mathcal{P}} - \sqrt{5}h_0$																																																														
2	5	$\kappa_{\mathcal{P}} - h_0$																																																														
3	5	$\kappa_{\mathcal{P}} + h_0$																																																														
4	1	$\kappa_{\mathcal{P}} + \sqrt{5}h_0$																																																														
Layer	n	Curvatures																																																														
1	2	$\kappa_{\mathcal{P}} - \varphi h_1$																																																														
2	2	$\kappa_{\mathcal{P}} - h_1$																																																														
3	4	$\kappa_{\mathcal{P}}$																																																														
4	2	$\kappa_{\mathcal{P}} + h_1$																																																														
5	2	$\kappa_{\mathcal{P}} + \varphi h_1$																																																														
Layer	n	Curvatures																																																														
1	3	$\kappa_{\mathcal{P}} - \varphi^3 h_2$																																																														
2	3	$\kappa_{\mathcal{P}} - h_2$																																																														
3	3	$\kappa_{\mathcal{P}} + h_2$																																																														
4	3	$\kappa_{\mathcal{P}} + \varphi^3 h_2$																																																														
\mathcal{D}^3 Dodecahedron $\{5, 3\}$ $\kappa_{\mathcal{P}} = \varphi^2$ $h_0 = \varphi \sqrt{1/3}$ $h_1 = 1$ $h_2 = \sqrt{(\varphi^{-2} + 1)/5}$	 <table border="1"> <thead> <tr> <th>Layer</th> <th>n</th> <th>Curvatures</th> </tr> </thead> <tbody> <tr> <td>1</td> <td>1</td> <td>$\kappa_{\mathcal{P}} - 3h_0$</td> </tr> <tr> <td>2</td> <td>3</td> <td>$\kappa_{\mathcal{P}} - \sqrt{5}h_0$</td> </tr> <tr> <td>3</td> <td>6</td> <td>$\kappa_{\mathcal{P}} - h_0$</td> </tr> <tr> <td>4</td> <td>6</td> <td>$\kappa_{\mathcal{P}} + h_0$</td> </tr> <tr> <td>5</td> <td>3</td> <td>$\kappa_{\mathcal{P}} + \sqrt{5}h_0$</td> </tr> <tr> <td>6</td> <td>1</td> <td>$\kappa_{\mathcal{P}} + 3h_0$</td> </tr> </tbody> </table>	Layer	n	Curvatures	1	1	$\kappa_{\mathcal{P}} - 3h_0$	2	3	$\kappa_{\mathcal{P}} - \sqrt{5}h_0$	3	6	$\kappa_{\mathcal{P}} - h_0$	4	6	$\kappa_{\mathcal{P}} + h_0$	5	3	$\kappa_{\mathcal{P}} + \sqrt{5}h_0$	6	1	$\kappa_{\mathcal{P}} + 3h_0$	 <table border="1"> <thead> <tr> <th>Layer</th> <th>n</th> <th>Curvatures</th> </tr> </thead> <tbody> <tr> <td>1</td> <td>2</td> <td>$\kappa_{\mathcal{P}} - \varphi^2 h_2$</td> </tr> <tr> <td>2</td> <td>4</td> <td>$\kappa_{\mathcal{P}} - \varphi h_2$</td> </tr> <tr> <td>3</td> <td>2</td> <td>$\kappa_{\mathcal{P}} - h_2$</td> </tr> <tr> <td>4</td> <td>4</td> <td>$\kappa_{\mathcal{P}}$</td> </tr> <tr> <td>5</td> <td>2</td> <td>$\kappa_{\mathcal{P}} + h_2$</td> </tr> <tr> <td>6</td> <td>4</td> <td>$\kappa_{\mathcal{P}} + \varphi h_2$</td> </tr> <tr> <td>7</td> <td>2</td> <td>$\kappa_{\mathcal{P}} - \varphi^2 h_2$</td> </tr> </tbody> </table>	Layer	n	Curvatures	1	2	$\kappa_{\mathcal{P}} - \varphi^2 h_2$	2	4	$\kappa_{\mathcal{P}} - \varphi h_2$	3	2	$\kappa_{\mathcal{P}} - h_2$	4	4	$\kappa_{\mathcal{P}}$	5	2	$\kappa_{\mathcal{P}} + h_2$	6	4	$\kappa_{\mathcal{P}} + \varphi h_2$	7	2	$\kappa_{\mathcal{P}} - \varphi^2 h_2$	 <table border="1"> <thead> <tr> <th>Layer</th> <th>n</th> <th>Curvatures</th> </tr> </thead> <tbody> <tr> <td>1</td> <td>5</td> <td>$\kappa_{\mathcal{P}} - \varphi^3 h_2$</td> </tr> <tr> <td>2</td> <td>5</td> <td>$\kappa_{\mathcal{P}} - h_2$</td> </tr> <tr> <td>3</td> <td>5</td> <td>$\kappa_{\mathcal{P}} + h_2$</td> </tr> <tr> <td>4</td> <td>5</td> <td>$\kappa_{\mathcal{P}} + \varphi^3 h_2$</td> </tr> </tbody> </table>	Layer	n	Curvatures	1	5	$\kappa_{\mathcal{P}} - \varphi^3 h_2$	2	5	$\kappa_{\mathcal{P}} - h_2$	3	5	$\kappa_{\mathcal{P}} + h_2$	4	5	$\kappa_{\mathcal{P}} + \varphi^3 h_2$	
Layer	n	Curvatures																																																														
1	1	$\kappa_{\mathcal{P}} - 3h_0$																																																														
2	3	$\kappa_{\mathcal{P}} - \sqrt{5}h_0$																																																														
3	6	$\kappa_{\mathcal{P}} - h_0$																																																														
4	6	$\kappa_{\mathcal{P}} + h_0$																																																														
5	3	$\kappa_{\mathcal{P}} + \sqrt{5}h_0$																																																														
6	1	$\kappa_{\mathcal{P}} + 3h_0$																																																														
Layer	n	Curvatures																																																														
1	2	$\kappa_{\mathcal{P}} - \varphi^2 h_2$																																																														
2	4	$\kappa_{\mathcal{P}} - \varphi h_2$																																																														
3	2	$\kappa_{\mathcal{P}} - h_2$																																																														
4	4	$\kappa_{\mathcal{P}}$																																																														
5	2	$\kappa_{\mathcal{P}} + h_2$																																																														
6	4	$\kappa_{\mathcal{P}} + \varphi h_2$																																																														
7	2	$\kappa_{\mathcal{P}} - \varphi^2 h_2$																																																														
Layer	n	Curvatures																																																														
1	5	$\kappa_{\mathcal{P}} - \varphi^3 h_2$																																																														
2	5	$\kappa_{\mathcal{P}} - h_2$																																																														
3	5	$\kappa_{\mathcal{P}} + h_2$																																																														
4	5	$\kappa_{\mathcal{P}} + \varphi^3 h_2$																																																														

Table A.3: CBP projections of the regular 4-polytopes.

	Vertex centered at ∞	Edge centered at ∞	Ridge centered at ∞	Facet centered at ∞																																																																								
\mathcal{T}^4 4-Simplex {3, 3, 3}																																																																												
	$\kappa_{\mathcal{P}} = \sqrt{3/5}$ $h_0 = \sqrt{1/10}$ $h_1 = \sqrt{2/15}$ $h_2 = \sqrt{2/15}$ $h_3 = \sqrt{1/10}$	<table border="1"> <thead> <tr> <th>Layer</th> <th>n</th> <th>Curvatures</th> </tr> </thead> <tbody> <tr> <td>1</td> <td>1</td> <td>$\kappa_{\mathcal{P}} - 4h_0$</td> </tr> <tr> <td>2</td> <td>4</td> <td>$\kappa_{\mathcal{P}} + h_0$</td> </tr> </tbody> </table>	Layer	n	Curvatures	1	1	$\kappa_{\mathcal{P}} - 4h_0$	2	4	$\kappa_{\mathcal{P}} + h_0$	<table border="1"> <thead> <tr> <th>Layer</th> <th>n</th> <th>Curvatures</th> </tr> </thead> <tbody> <tr> <td>1</td> <td>2</td> <td>$\kappa_{\mathcal{P}} - \frac{3}{2}h_1$</td> </tr> <tr> <td>2</td> <td>3</td> <td>$\kappa_{\mathcal{P}} + h_1$</td> </tr> </tbody> </table>	Layer	n	Curvatures	1	2	$\kappa_{\mathcal{P}} - \frac{3}{2}h_1$	2	3	$\kappa_{\mathcal{P}} + h_1$	<table border="1"> <thead> <tr> <th>Layer</th> <th>n</th> <th>Curvatures</th> </tr> </thead> <tbody> <tr> <td>1</td> <td>3</td> <td>$\kappa_{\mathcal{P}} - h_2$</td> </tr> <tr> <td>2</td> <td>2</td> <td>$\kappa_{\mathcal{P}} + \frac{3}{2}h_2$</td> </tr> </tbody> </table>	Layer	n	Curvatures	1	3	$\kappa_{\mathcal{P}} - h_2$	2	2	$\kappa_{\mathcal{P}} + \frac{3}{2}h_2$	<table border="1"> <thead> <tr> <th>Layer</th> <th>n</th> <th>Curvatures</th> </tr> </thead> <tbody> <tr> <td>1</td> <td>4</td> <td>$\kappa_{\mathcal{P}} - h_3$</td> </tr> <tr> <td>2</td> <td>1</td> <td>$\kappa_{\mathcal{P}} + 4h_3$</td> </tr> </tbody> </table>	Layer	n	Curvatures	1	4	$\kappa_{\mathcal{P}} - h_3$	2	1	$\kappa_{\mathcal{P}} + 4h_3$																																			
Layer	n	Curvatures																																																																										
1	1	$\kappa_{\mathcal{P}} - 4h_0$																																																																										
2	4	$\kappa_{\mathcal{P}} + h_0$																																																																										
Layer	n	Curvatures																																																																										
1	2	$\kappa_{\mathcal{P}} - \frac{3}{2}h_1$																																																																										
2	3	$\kappa_{\mathcal{P}} + h_1$																																																																										
Layer	n	Curvatures																																																																										
1	3	$\kappa_{\mathcal{P}} - h_2$																																																																										
2	2	$\kappa_{\mathcal{P}} + \frac{3}{2}h_2$																																																																										
Layer	n	Curvatures																																																																										
1	4	$\kappa_{\mathcal{P}} - h_3$																																																																										
2	1	$\kappa_{\mathcal{P}} + 4h_3$																																																																										
\mathcal{O}^4 Orthoplex {3, 3, 4}																																																																												
	$\kappa_{\mathcal{P}} = 1$ $h_0 = \sqrt{2}$ $h_1 = 1$ $h_2 = \sqrt{2/3}$ $h_3 = \sqrt{1/2}$	<table border="1"> <thead> <tr> <th>Layer</th> <th>n</th> <th>Curvatures</th> </tr> </thead> <tbody> <tr> <td>1</td> <td>1</td> <td>$\kappa_{\mathcal{P}} - h_0$</td> </tr> <tr> <td>2</td> <td>4</td> <td>$\kappa_{\mathcal{P}}$</td> </tr> <tr> <td>3</td> <td>1</td> <td>$\kappa_{\mathcal{P}} + h_0$</td> </tr> </tbody> </table>	Layer	n	Curvatures	1	1	$\kappa_{\mathcal{P}} - h_0$	2	4	$\kappa_{\mathcal{P}}$	3	1	$\kappa_{\mathcal{P}} + h_0$	<table border="1"> <thead> <tr> <th>Layer</th> <th>n</th> <th>Curvatures</th> </tr> </thead> <tbody> <tr> <td>1</td> <td>2</td> <td>$\kappa_{\mathcal{P}} - h_1$</td> </tr> <tr> <td>2</td> <td>4</td> <td>$\kappa_{\mathcal{P}}$</td> </tr> <tr> <td>3</td> <td>2</td> <td>$\kappa_{\mathcal{P}} + h_1$</td> </tr> </tbody> </table>	Layer	n	Curvatures	1	2	$\kappa_{\mathcal{P}} - h_1$	2	4	$\kappa_{\mathcal{P}}$	3	2	$\kappa_{\mathcal{P}} + h_1$	<table border="1"> <thead> <tr> <th>Layer</th> <th>n</th> <th>Curvatures</th> </tr> </thead> <tbody> <tr> <td>1</td> <td>3</td> <td>$\kappa_{\mathcal{P}} - h_2$</td> </tr> <tr> <td>2</td> <td>2</td> <td>$\kappa_{\mathcal{P}}$</td> </tr> <tr> <td>3</td> <td>3</td> <td>$\kappa_{\mathcal{P}} + h_2$</td> </tr> </tbody> </table>	Layer	n	Curvatures	1	3	$\kappa_{\mathcal{P}} - h_2$	2	2	$\kappa_{\mathcal{P}}$	3	3	$\kappa_{\mathcal{P}} + h_2$	<table border="1"> <thead> <tr> <th>Layer</th> <th>n</th> <th>Curvatures</th> </tr> </thead> <tbody> <tr> <td>1</td> <td>4</td> <td>$\kappa_{\mathcal{P}} - h_3$</td> </tr> <tr> <td>2</td> <td>4</td> <td>$\kappa_{\mathcal{P}} + h_3$</td> </tr> </tbody> </table>	Layer	n	Curvatures	1	4	$\kappa_{\mathcal{P}} - h_3$	2	4	$\kappa_{\mathcal{P}} + h_3$																										
Layer	n	Curvatures																																																																										
1	1	$\kappa_{\mathcal{P}} - h_0$																																																																										
2	4	$\kappa_{\mathcal{P}}$																																																																										
3	1	$\kappa_{\mathcal{P}} + h_0$																																																																										
Layer	n	Curvatures																																																																										
1	2	$\kappa_{\mathcal{P}} - h_1$																																																																										
2	4	$\kappa_{\mathcal{P}}$																																																																										
3	2	$\kappa_{\mathcal{P}} + h_1$																																																																										
Layer	n	Curvatures																																																																										
1	3	$\kappa_{\mathcal{P}} - h_2$																																																																										
2	2	$\kappa_{\mathcal{P}}$																																																																										
3	3	$\kappa_{\mathcal{P}} + h_2$																																																																										
Layer	n	Curvatures																																																																										
1	4	$\kappa_{\mathcal{P}} - h_3$																																																																										
2	4	$\kappa_{\mathcal{P}} + h_3$																																																																										
\mathcal{C}^4 Hypercube {4, 3, 3}																																																																												
	$\kappa_{\mathcal{P}} = \sqrt{3}$ $h_0 = 1$ $h_1 = \sqrt{1/3}$ $h_2 = \sqrt{2}$ $h_3 = 1$	<table border="1"> <thead> <tr> <th>Layer</th> <th>n</th> <th>Curvatures</th> </tr> </thead> <tbody> <tr> <td>1</td> <td>1</td> <td>$\kappa_{\mathcal{P}} - 2h_0$</td> </tr> <tr> <td>2</td> <td>4</td> <td>$\kappa_{\mathcal{P}} - h_0$</td> </tr> <tr> <td>3</td> <td>6</td> <td>$\kappa_{\mathcal{P}}$</td> </tr> <tr> <td>4</td> <td>4</td> <td>$\kappa_{\mathcal{P}} + h_0$</td> </tr> <tr> <td>5</td> <td>1</td> <td>$\kappa_{\mathcal{P}} + 2h_0$</td> </tr> </tbody> </table>	Layer	n	Curvatures	1	1	$\kappa_{\mathcal{P}} - 2h_0$	2	4	$\kappa_{\mathcal{P}} - h_0$	3	6	$\kappa_{\mathcal{P}}$	4	4	$\kappa_{\mathcal{P}} + h_0$	5	1	$\kappa_{\mathcal{P}} + 2h_0$	<table border="1"> <thead> <tr> <th>Layer</th> <th>n</th> <th>Curvatures</th> </tr> </thead> <tbody> <tr> <td>1</td> <td>2</td> <td>$\kappa_{\mathcal{P}} - 3h_1$</td> </tr> <tr> <td>2</td> <td>6</td> <td>$\kappa_{\mathcal{P}} - h_1$</td> </tr> <tr> <td>3</td> <td>6</td> <td>$\kappa_{\mathcal{P}} + h_1$</td> </tr> <tr> <td>4</td> <td>2</td> <td>$\kappa_{\mathcal{P}} + 3h_1$</td> </tr> </tbody> </table>	Layer	n	Curvatures	1	2	$\kappa_{\mathcal{P}} - 3h_1$	2	6	$\kappa_{\mathcal{P}} - h_1$	3	6	$\kappa_{\mathcal{P}} + h_1$	4	2	$\kappa_{\mathcal{P}} + 3h_1$	<table border="1"> <thead> <tr> <th>Layer</th> <th>n</th> <th>Curvatures</th> </tr> </thead> <tbody> <tr> <td>1</td> <td>4</td> <td>$\kappa_{\mathcal{P}} - h_2$</td> </tr> <tr> <td>2</td> <td>8</td> <td>$\kappa_{\mathcal{P}}$</td> </tr> <tr> <td>3</td> <td>4</td> <td>$\kappa_{\mathcal{P}} + h_2$</td> </tr> </tbody> </table>	Layer	n	Curvatures	1	4	$\kappa_{\mathcal{P}} - h_2$	2	8	$\kappa_{\mathcal{P}}$	3	4	$\kappa_{\mathcal{P}} + h_2$	<table border="1"> <thead> <tr> <th>Layer</th> <th>n</th> <th>Curvatures</th> </tr> </thead> <tbody> <tr> <td>1</td> <td>8</td> <td>$\kappa_{\mathcal{P}} - h_3$</td> </tr> <tr> <td>2</td> <td>8</td> <td>$\kappa_{\mathcal{P}} + h_3$</td> </tr> </tbody> </table>	Layer	n	Curvatures	1	8	$\kappa_{\mathcal{P}} - h_3$	2	8	$\kappa_{\mathcal{P}} + h_3$																	
Layer	n	Curvatures																																																																										
1	1	$\kappa_{\mathcal{P}} - 2h_0$																																																																										
2	4	$\kappa_{\mathcal{P}} - h_0$																																																																										
3	6	$\kappa_{\mathcal{P}}$																																																																										
4	4	$\kappa_{\mathcal{P}} + h_0$																																																																										
5	1	$\kappa_{\mathcal{P}} + 2h_0$																																																																										
Layer	n	Curvatures																																																																										
1	2	$\kappa_{\mathcal{P}} - 3h_1$																																																																										
2	6	$\kappa_{\mathcal{P}} - h_1$																																																																										
3	6	$\kappa_{\mathcal{P}} + h_1$																																																																										
4	2	$\kappa_{\mathcal{P}} + 3h_1$																																																																										
Layer	n	Curvatures																																																																										
1	4	$\kappa_{\mathcal{P}} - h_2$																																																																										
2	8	$\kappa_{\mathcal{P}}$																																																																										
3	4	$\kappa_{\mathcal{P}} + h_2$																																																																										
Layer	n	Curvatures																																																																										
1	8	$\kappa_{\mathcal{P}} - h_3$																																																																										
2	8	$\kappa_{\mathcal{P}} + h_3$																																																																										
\mathcal{R}^4 24-cell {3, 4, 3}																																																																												
	$\kappa_{\mathcal{P}} = \sqrt{3}$ $h_0 = 1$ $h_1 = \sqrt{1/3}$ $h_2 = \sqrt{2/3}$ $h_3 = \sqrt{2}$	<table border="1"> <thead> <tr> <th>Layer</th> <th>n</th> <th>Curvatures</th> </tr> </thead> <tbody> <tr> <td>1</td> <td>1</td> <td>$\kappa_{\mathcal{P}} - 2h_0$</td> </tr> <tr> <td>2</td> <td>8</td> <td>$\kappa_{\mathcal{P}} - h_0$</td> </tr> <tr> <td>3</td> <td>6</td> <td>$\kappa_{\mathcal{P}}$</td> </tr> <tr> <td>4</td> <td>8</td> <td>$\kappa_{\mathcal{P}} + h_0$</td> </tr> <tr> <td>5</td> <td>1</td> <td>$\kappa_{\mathcal{P}} + 2h_0$</td> </tr> </tbody> </table>	Layer	n	Curvatures	1	1	$\kappa_{\mathcal{P}} - 2h_0$	2	8	$\kappa_{\mathcal{P}} - h_0$	3	6	$\kappa_{\mathcal{P}}$	4	8	$\kappa_{\mathcal{P}} + h_0$	5	1	$\kappa_{\mathcal{P}} + 2h_0$	<table border="1"> <thead> <tr> <th>Layer</th> <th>n</th> <th>Curvatures</th> </tr> </thead> <tbody> <tr> <td>1</td> <td>2</td> <td>$\kappa_{\mathcal{P}} - 3h_1$</td> </tr> <tr> <td>2</td> <td>3</td> <td>$\kappa_{\mathcal{P}} - 2h_1$</td> </tr> <tr> <td>3</td> <td>6</td> <td>$\kappa_{\mathcal{P}} - h_1$</td> </tr> <tr> <td>4</td> <td>2</td> <td>$\kappa_{\mathcal{P}}$</td> </tr> <tr> <td>5</td> <td>6</td> <td>$\kappa_{\mathcal{P}} + h_1$</td> </tr> <tr> <td>6</td> <td>3</td> <td>$\kappa_{\mathcal{P}} + 2h_1$</td> </tr> <tr> <td>7</td> <td>2</td> <td>$\kappa_{\mathcal{P}} + 3h_1$</td> </tr> </tbody> </table>	Layer	n	Curvatures	1	2	$\kappa_{\mathcal{P}} - 3h_1$	2	3	$\kappa_{\mathcal{P}} - 2h_1$	3	6	$\kappa_{\mathcal{P}} - h_1$	4	2	$\kappa_{\mathcal{P}}$	5	6	$\kappa_{\mathcal{P}} + h_1$	6	3	$\kappa_{\mathcal{P}} + 2h_1$	7	2	$\kappa_{\mathcal{P}} + 3h_1$	<table border="1"> <thead> <tr> <th>Layer</th> <th>n</th> <th>Curvatures</th> </tr> </thead> <tbody> <tr> <td>1</td> <td>3</td> <td>$\kappa_{\mathcal{P}} - 2h_2$</td> </tr> <tr> <td>2</td> <td>6</td> <td>$\kappa_{\mathcal{P}} - h_2$</td> </tr> <tr> <td>3</td> <td>6</td> <td>$\kappa_{\mathcal{P}}$</td> </tr> <tr> <td>4</td> <td>6</td> <td>$\kappa_{\mathcal{P}} + h_2$</td> </tr> <tr> <td>5</td> <td>3</td> <td>$\kappa_{\mathcal{P}} + 2h_2$</td> </tr> </tbody> </table>	Layer	n	Curvatures	1	3	$\kappa_{\mathcal{P}} - 2h_2$	2	6	$\kappa_{\mathcal{P}} - h_2$	3	6	$\kappa_{\mathcal{P}}$	4	6	$\kappa_{\mathcal{P}} + h_2$	5	3	$\kappa_{\mathcal{P}} + 2h_2$	<table border="1"> <thead> <tr> <th>Layer</th> <th>n</th> <th>Curvatures</th> </tr> </thead> <tbody> <tr> <td>1</td> <td>6</td> <td>$\kappa_{\mathcal{P}} - h_3$</td> </tr> <tr> <td>2</td> <td>12</td> <td>$\kappa_{\mathcal{P}}$</td> </tr> <tr> <td>3</td> <td>6</td> <td>$\kappa_{\mathcal{P}} + h_3$</td> </tr> </tbody> </table>	Layer	n	Curvatures	1	6	$\kappa_{\mathcal{P}} - h_3$	2	12	$\kappa_{\mathcal{P}}$	3	6
Layer	n	Curvatures																																																																										
1	1	$\kappa_{\mathcal{P}} - 2h_0$																																																																										
2	8	$\kappa_{\mathcal{P}} - h_0$																																																																										
3	6	$\kappa_{\mathcal{P}}$																																																																										
4	8	$\kappa_{\mathcal{P}} + h_0$																																																																										
5	1	$\kappa_{\mathcal{P}} + 2h_0$																																																																										
Layer	n	Curvatures																																																																										
1	2	$\kappa_{\mathcal{P}} - 3h_1$																																																																										
2	3	$\kappa_{\mathcal{P}} - 2h_1$																																																																										
3	6	$\kappa_{\mathcal{P}} - h_1$																																																																										
4	2	$\kappa_{\mathcal{P}}$																																																																										
5	6	$\kappa_{\mathcal{P}} + h_1$																																																																										
6	3	$\kappa_{\mathcal{P}} + 2h_1$																																																																										
7	2	$\kappa_{\mathcal{P}} + 3h_1$																																																																										
Layer	n	Curvatures																																																																										
1	3	$\kappa_{\mathcal{P}} - 2h_2$																																																																										
2	6	$\kappa_{\mathcal{P}} - h_2$																																																																										
3	6	$\kappa_{\mathcal{P}}$																																																																										
4	6	$\kappa_{\mathcal{P}} + h_2$																																																																										
5	3	$\kappa_{\mathcal{P}} + 2h_2$																																																																										
Layer	n	Curvatures																																																																										
1	6	$\kappa_{\mathcal{P}} - h_3$																																																																										
2	12	$\kappa_{\mathcal{P}}$																																																																										
3	6	$\kappa_{\mathcal{P}} + h_3$																																																																										

I^4
600-cell
{3, 3, 5}



$$\begin{aligned}\kappa_P &= \sqrt{5}\varphi^{3/2} \\ h_0 &= 1 \\ h_1 &= (\varphi^2 + 1)^{-\frac{1}{2}} \\ h_2 &= (\varphi^4 + 1)^{-\frac{1}{2}} \\ h_3 &= (\varphi^3 + 1)^{-\frac{1}{2}}\end{aligned}$$

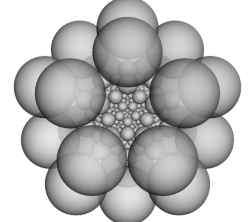
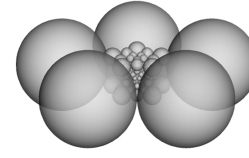
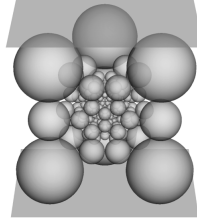
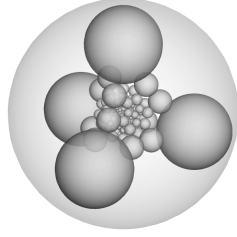
Layer	n	Curvatures
1	1	$\kappa_P - 2\varphi h_0$
2	12	$\kappa_P - \varphi^2 h_0$
3	20	$\kappa_P - \varphi h_0$
4	12	$\kappa_P - h_0$
5	30	κ_P
6	12	$\kappa_P + h_0$
7	20	$\kappa_P + \varphi h_0$
8	12	$\kappa_P + \varphi^2 h_0$
9	1	$\kappa_P + 2\varphi h_0$

Layer	n	Curvatures
1	2	$\kappa_P - (\varphi^3 + \varphi)h_1$
2	5	$\kappa_P - (\varphi^3 + 1)h_1$
3	10	$\kappa_P - \varphi^3 h_1$
4	2	$\kappa_P - (\varphi^2 + 1)h_1$
5	5	$\kappa_P - (\varphi^3 - 1)h_1$
6	10	$\kappa_P - \varphi^2 h_1$
7	10	$\kappa_P - \varphi h_1$
8	10	$\kappa_P - h_1$
9	12	κ_P
10	10	$\kappa_P + h_1$
...
17	2	$\kappa_P + (\varphi^3 + \varphi)h_1$

Layer	n	Curvatures
1	3	$\kappa_P - (\varphi^4 + \varphi)h_2$
2	2	$\kappa_P - (\varphi^4 + 1)h_2$
3	6	$\kappa_P - \varphi^4 h_2$
4	6	$\kappa_P - (\varphi^3 + \varphi)h_2$
5	6	$\kappa_P - (\varphi^3 + 1)\varphi h_2$
6	6	$\kappa_P - \varphi^3 h_2$
7	3	$\kappa_P - (\varphi^3 - 1)h_2$
8	12	$\kappa_P - \varphi^2 h_2$
9	6	$\kappa_P - \varphi h_2$
10	6	$\kappa_P - h_2$
11	8	κ_P
12	6	$\kappa_P + h_2$
...
21	3	$\kappa_P + (\varphi^4 + \varphi)h_2$

Layer	n	Curvatures
1	4	$\kappa_P - \varphi^4 h_3$
2	4	$\kappa_P - (\varphi^3 + \varphi)h_3$
3	6	$\kappa_P - (\varphi^3 + 1)h_3$
4	12	$\kappa_P - \varphi^3 h_3$
5	12	$\kappa_P - \varphi^2 h_3$
6	12	$\kappa_P - \varphi h_3$
7	4	$\kappa_P - h_3$
8	12	κ_P
9	4	$\kappa_P + h_3$
...
15	4	$\kappa_P + \varphi^4 h_3$

D^4
120-cell
{5, 3, 3}



$$\begin{aligned}\kappa_P &= \varphi^3\sqrt{3} \\ h_0 &= \sqrt{1/2} \\ h_1 &= (\varphi^4 + 1)^{-\frac{1}{2}} \\ h_2 &= (\varphi^2 + 1)^{-\frac{1}{2}} \\ h_3 &= 1\end{aligned}$$

Layer	n	Curvatures
1	1	$\kappa_P - (\varphi^5 - \varphi^{-1})h_0$
2	4	$\kappa_P - (\varphi^5 - 1)h_0$
3	12	$\kappa_P - (\varphi^4 + \varphi^2)h_0$
4	24	$\kappa_P - (\varphi^4 + \varphi)h_0$
5	12	$\kappa_P - (\varphi^4 + 1)h_0$
6	4	$\kappa_P - (\varphi^4 + \varphi^{-1})h_0$
7	24	$\kappa_P - \varphi^4 h_0$
8	24	$\kappa_P - (\varphi^3 + \varphi)h_0$
9	32	$\kappa_P - (\varphi^3 + 1)h_0$
10	24	$\kappa_P - \varphi^3 h_0$
11	12	$\kappa_P - (\varphi^2 + 1)h_0$
12	24	$\kappa_P - (\varphi^2 + \varphi^{-1})h_0$
13	28	$\kappa_P - \varphi^2 h_0$
15	24	$\kappa_P - \varphi h_0$
16	24	$\kappa_P - h_0$
17	54	κ_P
18	24	$\kappa_P + h_0$
...
33	1	$\kappa_P + (\varphi^5 - \varphi^{-1})h_0$

Layer	n	Curvatures
1	2	$\kappa_P - (\varphi^6 + \varphi^2)h_1$
2	6	$\kappa_P - (\varphi^6 + \varphi)h_1$
3	3	$\kappa_P - (\varphi^6 + 1)h_1$
4	12	$\kappa_P - \varphi^6 h_1$
5	6	$\kappa_P - (\varphi^6 - 1)h_1$
6	12	$\kappa_P - (\varphi^6 - \varphi)h_1$
7	18	$\kappa_P - (\varphi^5 + \varphi^3)h_1$
8	12	$\kappa_P - (\varphi^5 + \varphi^2)h_1$
9	14	$\kappa_P - (\varphi^5 + \varphi)h_1$
10	12	$\kappa_P - (\varphi^5 + 1)h_1$
11	18	$\kappa_P - \varphi^5 h_1$
12	6	$\kappa_P - (\varphi^5 - 1)h_1$
13	24	$\kappa_P - (\varphi^4 + \varphi^2)h_1$
14	15	$\kappa_P - (\varphi^4 + \varphi)h_1$
15	2	$\kappa_P - (\varphi^4 + 1)h_1$
16	24	$\kappa_P - \varphi^4 h_1$
17	18	$\kappa_P - (\varphi^3 + \varphi)h_1$
18	12	$\kappa_P - (\varphi^3 + 1)h_1$
19	18	$\kappa_P - \varphi^3 h_1$
20	24	$\kappa_P - \varphi^2 h_1$
21	18	$\kappa_P - \varphi h_1$
22	12	$\kappa_P - h_1$
23	24	κ_P
24	12	$\kappa_P + h_1$
...
47	2	$\kappa_P + (\varphi^6 + \varphi^2)h_1$

Layer	n	Curvatures
1	5	$\kappa_P - (\varphi^5 + \varphi^2)h_2$
2	10	$\kappa_P - (\varphi^5 + \varphi)h_2$
3	10	$\kappa_P - (\varphi^5 + 1)h_2$
4	20	$\kappa_P - \varphi^5 h_2$
5	10	$\kappa_P - (\varphi^5 - 1)h_2$
6	20	$\kappa_P - (\varphi^4 + \varphi^2)h_2$
7	20	$\kappa_P - (\varphi^4 + \varphi)h_2$
8	10	$\kappa_P - (\varphi^4 + 1)h_2$
9	30	$\kappa_P - \varphi^4 h_2$
10	20	$\kappa_P - (\varphi^3 + \varphi)h_2$
11	20	$\kappa_P - (\varphi^3 + 1)h_2$
12	30	$\kappa_P - \varphi^3 h_2$
13	5	$\kappa_P - (\varphi^3 - 1)h_2$
14	30	$\kappa_P - \varphi^2 h_2$
15	30	$\kappa_P - \varphi h_2$
16	20	$\kappa_P - h_2$
17	20	κ_P
18	20	$\kappa_P + h_2$
...
35	5	$\kappa_P + (\varphi^5 + \varphi^2)h_2$

Layer	n	Curvatures
1	20	$\kappa_P - \varphi^4 h_3$
2	20	$\kappa_P - (\varphi^3 + \varphi)h_3$
3	30	$\kappa_P - (\varphi^3 + 1)h_3$
4	60	$\kappa_P - \varphi^3 h_3$
5	60	$\kappa_P - \varphi^2 h_3$
6	60	$\kappa_P - \varphi h_3$
7	20	$\kappa_P - h_3$
8	60	κ_P
9	20	$\kappa_P + h_3$
...
17	20	$\kappa_P + \varphi^4 h_3$

Bibliography

- [1] ADAMS, C. C. *The knot book*. American Mathematical Soc., 1994. (Cited on pages [17](#) and [22](#).)
- [2] ADAMS, C. C. Why knot: knots, molecules and stick numbers. (Cited on page [25](#).)
- [3] ALEXANDER, J. W. A lemma on systems of knotted curves. *Proceedings of the National Academy of Sciences of the United States of America* 9, 3 (1923), 93. (Cited on page [23](#).)
- [4] ANISHCHIK, S. V., AND MEDVEDEV, N. N. Three-dimensional Apollonian packing as a model for dense granular systems. *Phys. Rev. Lett.* 75 (1995), 4314–4317. (Cited on page [1](#).)
- [5] BANCHOFF, T. *Torus Decompositions of Regular Polytopes in 4-space*. 11 2013, pp. 257–266. (Cited on page [128](#).)
- [6] BARAGAR, A. Higher dimensional Apollonian packings, revisited. *Geometriae Dedicata* 195, 1 (Aug 2018), 137–161. (Cited on page [88](#).)
- [7] BEECROFT, P. Properties of circles in mutual contact. *Lady's and Gentleman's Diary* 139 (1842), 91–96. (Cited on pages [44](#) and [70](#).)
- [8] BEZDEK, K., AND REID, S. Contact graphs of unit sphere packings revisited. *Journal of Geometry* 104, 1 (2013), 57–83. (Cited on page [15](#).)
- [9] BOBENKO, A., AND SPRINGBORN, B. Variational principles for circle patterns and Koebe's theorem. *Transactions of the American Mathematical Society* 356 (02 2004). (Cited on page [51](#).)
- [10] BOLT, A., BUTLER, S., AND HOVLAND, E. Apollonian Ring Packings. *Connections in Discrete Mathematics: A Celebration of the Work of Ron Graham* (2018), 283. (Cited on pages [44](#) and [84](#).)

- [11] BOS, E. J. Princess Elizabeth of Bohemia and Descartes' letters (1650–1665). *Historia Mathematica* 37, 3 (2010), 485–502. Contexts, emergence and issues of Cartesian geometry: In honour of Henk Bos's 70th birthday. (Cited on page 69.)
- [12] BOURGAIN, J., AND FUCHS, E. A proof of the positive density conjecture for integer Apollonian circle packings. *Journal of the American Mathematical Society* 24, 4 (2011), 945–967. (Cited on page 124.)
- [13] BOWERS, P. L. Combinatorics encoding geometry: the legacy of Bill Thurston in the story of one theorem. In *In the Tradition of Thurston*. Springer, 2020, pp. 173–239. (Cited on page 15.)
- [14] BOYD, D. W. A new class of infinite sphere packings. *Pacific Journal of Mathematics* 50, 2 (1974), 383 – 398. (Cited on pages 13 and 73.)
- [15] BREU, H., AND KIRKPATRICK, D. G. On the complexity of recognizing intersection and touching graphs of disks. In *Graph Drawing* (Berlin, Heidelberg, 1996), F. J. Brandenburg, Ed., Springer Berlin Heidelberg, pp. 88–98. (Cited on page 15.)
- [16] BRIGHTWELL, G. R., AND SCHEINERMAN, E. R. Representations of planar graphs. *SIAM Journal on Discrete Mathematics* 6, 2 (1993), 214–229. (Cited on pages 44, 51 and 54.)
- [17] CALVO, J. A. Geometric knot spaces and polygonal isotopy. *Journal of Knot Theory and Its Ramifications* 10, 02 (2001), 245–267. (Cited on page 26.)
- [18] CECIL, T. E. *Lie sphere geometry*. Springer, 2008. (Cited on pages 5 and 9.)
- [19] CHAUBEY, S., FUCHS, E., HINES, R., AND STANGE, K. The dynamics of super-Apollonian continued fractions. *Transactions of the American Mathematical Society* 372, 4 (2019), 2287–2334. (Cited on page 117.)
- [20] CHEN, H. *Ball Packings and Lorentzian Discrete Geometry*. PhD thesis, 2014. (Cited on page 5.)

- [21] CHEN, H. Apollonian ball packings and stacked polytopes. *Discrete & Computational Geometry* 55, 4 (2016), 801–826. (Cited on pages 1, 14, 44, 49, 59, 69 and 105.)
- [22] CHEN, H. Even more infinite ball packings from Lorentzian root systems. *The Electronic Journal of Combinatorics* 23, 3 (2016). (Cited on page 61.)
- [23] CHEN, H., AND LABBÉ, J. P. Lorentzian Coxeter systems and Boyd–Maxwell ball packings. *Geometriae Dedicata* 174, 1 (Feb 2015), 43–73. (Cited on pages 15, 61 and 88.)
- [24] CHEN, H., AND PADROL, A. Scribability problems for polytopes. *European Journal of Combinatorics* 64 (2017), 1–26. (Cited on pages 48 and 59.)
- [25] COLLINS, C. R., AND STEPHENSON, K. A circle packing algorithm. *Computational Geometry* 25, 3 (2003), 233–256. (Cited on page 40.)
- [26] CONWAY, J. H. An enumeration of knots and links, and some of their algebraic properties. In *Computational problems in abstract algebra* (1970), Elsevier, pp. 329–358. (Cited on pages 21 and 22.)
- [27] CONWAY, J. H., AND FUNG, F. Y. *The sensual (quadratic) form*. No. 26. Cambridge University Press, 1997. (Cited on page 117.)
- [28] COXETER, H. S. M. The problem of Apollonius. *The American Mathematical Monthly* 75, 1 (1968), 5–15. (Cited on page 44.)
- [29] COXETER, H. S. M. *Regular Polytopes*. Dover books on advanced mathematics. Dover Publications, 1973. (Cited on pages 48, 50 and 128.)
- [30] CROMWELL, P. R. *Knots and Links*. Cambridge University Press, 2004. (Cited on pages 17, 19, 22 and 116.)
- [31] D’ALEXANDRIE, P., AND VER EECKE, P. *Pappus d’Alexandrie: la collection mathématique*. Desclée de Brouwer, 1933. (Cited on page 1.)
- [32] DIAO, Y. Minimal knotted polygons on the cubic lattice. *Journal of Knot Theory and its Ramifications* 2, 04 (1993), 413–425. (Cited on page 26.)

- [33] DIAS, D. The Local-Global Principle for integral generalized Apollonian sphere packings. *arXiv: Number Theory* (2014). (Cited on pages 2, 87, 91 and 125.)
- [34] ELRIFAI, E. A. On stick number of knots and links. *Chaos, Solitons & Fractals* 27, 1 (2006), 233–236. (Cited on page 24.)
- [35] EPPSTEIN, D., KUPERBERG, G., AND ZIEGLER, G. M. Fat 4-polytopes and fatter 3-spheres. *arXiv: Combinatorics* (2002). (Cited on pages 44 and 58.)
- [36] FELSNER, S., AND ROTE, G. On primal-dual circle representations. In *SOSA* (2019). (Cited on pages 44 and 51.)
- [37] FRISCH, S., AND VASERSTEIN, L. Polynomial parametrization of Pythagorean quadruples, quintuples and sextuples. *Journal of Pure and applied Algebra* 216, 1 (2012), 184–191. (Cited on page 126.)
- [38] FUCHS, E. Counting problems in Apollonian packings. *Bulletin of the American Mathematical Society* 50 (2013), 229–266. (Cited on pages 80 and 124.)
- [39] FUCHS, E., AND SANDEN, K. Some experiments with integral Apollonian circle packings. *Experimental Mathematics* 20, 4 (2011), 380–399. (Cited on page 125.)
- [40] FUCHS, E., STANGE, K. E., AND ZHANG, X. Local-global principles in circle packings. *Compositio Mathematica* 155, 6 (2019), 1118–1170. (Cited on pages 80 and 124.)
- [41] GABAI, D., HARAWAY, R., MEYERHOFF, R., THURSTON, N., AND YARMOLA, A. Hyperbolic 3-manifolds of low cusp volume, 2021. (Cited on pages 2, 25 and 129.)
- [42] GABAI, D., AND THURSTON, W. P. *Genera of Arborescent Links: 1986*, vol. 339. American Mathematical Soc., 1986. (Cited on page 22.)
- [43] GOSSET, T. The Hexlet. *Nature* 139 (1937), 62. (Cited on page 70.)

- [44] GRAHAM, R., LAGARIAS, J. C., MALLOWS, C. L., WILKS, A. R., AND YAN, C. H. Apollonian circle packings: number theory. *Journal of Number Theory* 100, 1 (2003), 1–45. (Cited on pages [1](#) and [125](#).)
- [45] GRAHAM, R., LAGARIAS, J. C., MALLOWS, C. L., WILKS, A. R., AND YAN, C. H. Apollonian circle packings: Geometry and group theory i. the Apollonian group. *Discrete & Computational Geometry* 34, 4 (2005), 547–585. (Cited on pages [1](#), [14](#), [60](#), [61](#) and [117](#).)
- [46] GRAHAM, R., LAGARIAS, J. C., MALLOWS, C. L., WILKS, A. R., AND YAN, C. H. Apollonian circle packings: Geometry and group theory II. super-Apollonian group and integral packings. *Discrete & Computational Geometry* 35 (09 2006), 1–36. (Cited on pages [1](#), [60](#) and [61](#).)
- [47] GRAHAM, R., LAGARIAS, J. C., MALLOWS, C. L., WILKS, A. R., AND YAN, C. H. Apollonian circle packings: Geometry and group theory III. higher dimensions. *Discrete & Computational Geometry* 35 (2006). (Cited on pages [1](#), [60](#) and [61](#).)
- [48] GRÜNBAUM, B., KAIBEL, V., KLEE, V., AND ZIEGLER, G. M. *Convex polytopes*. Springer, New York, 2003. (Cited on page [46](#).)
- [49] GUETTLER, G., AND MALLOWS, C. L. A generalization of Apollonian packing of circles. *Journal of Combinatorics* 1 (01 2008). (Cited on pages [44](#) and [70](#).)
- [50] HLINENY, P. *Touching graphs of unit balls*, vol. 1353. 04 2006, pp. 350–358. (Cited on page [15](#).)
- [51] HONG, K., KIM, H., OH, S., AND NO, S. Minimum lattice length and ropelength of knots. *Journal of Knot Theory and Its Ramifications* 23, 07 (2014), 1460009. (Cited on page [24](#).)
- [52] HONG, K., NO, S., AND OH, S. Upper bound on lattice stick number of knots. In *Mathematical Proceedings of the Cambridge Philosophical Society* (2013), vol. 155, Cambridge University Press, pp. 173–179. (Cited on page [26](#).)

- [53] HONG, K., NO, S., AND OH, S. Links with small lattice stick numbers. *Journal of Physics A: Mathematical and Theoretical* 47, 15 (2014), 155202. (Cited on page 25.)
- [54] HOPF, H. Über die abbildungen der dreidimensionalen sphäre auf die kugelfläche. In *Selecta Heinz Hopf*. Springer, 1964, pp. 38–63. (Cited on page 128.)
- [55] HUH, Y., AND OH, S. Lattice stick numbers of small knots. *Journal of Knot Theory and Its Ramifications* 14, 07 (2005), 859–867. (Cited on page 25.)
- [56] HUH, Y., AND OH, S. An upper bound on stick number of knots. *Journal of Knot Theory and Its Ramifications* 20, 05 (2011), 741–747. (Cited on page 26.)
- [57] INC., W. R. Mathematica, Version 12.2, 2021. Champaign, IL. (Cited on page 130.)
- [58] KARPENKOV, O. *Geometry of continued fractions*, vol. 26. Springer Science & Business Media, 2013. (Cited on page 117.)
- [59] KAUFFMAN, L. H. State models and the Jones polynomial. *Topology* 26, 3 (1987), 395–407. (Cited on page 18.)
- [60] KOCIK, J. On a Diophantine equation that generates all integral Apollonian gaskets. *ISRN Geometry 2012* (Apr 2012), 348618. (Cited on page 126.)
- [61] KOEBE, P. *Kontaktprobleme der konformen Abbildung*. Hirzel, 1936. (Cited on page 15.)
- [62] KONTOROVICH, A. The local-global principle for integral soddy sphere packings. *Journal of Modern Dynamics* 15, 0 (2019), 209–236. (Cited on pages 105 and 125.)
- [63] KONTOROVICH, A., AND NAKAMURA, K. Geometry and arithmetic of crystallographic sphere packings. *Proceedings of the National Academy of Sciences* 116, 2 (2019), 436–441. (Cited on pages 44, 61 and 88.)

- [64] KONTOROVICH, A., AND OH, H. Apollonian circle packings and closed horospheres on hyperbolic 3-manifolds. *Journal of the American Mathematical Society* 24, 3 (2011), 603–648. (Cited on page [124](#).)
- [65] KRANZ, J., ARAÚJO, N., ANDRADE JR, J., AND HERRMANN, H. J. Complex networks from space-filling bearings. *Physical Review E* 92, 1 (2015), 012802. (Cited on page [1](#).)
- [66] KUPERBERG, G., AND SCHRAMM, O. Average kissing numbers for non-congruent sphere packings. *arXiv preprint math/9405218* (1994). (Cited on page [15](#).)
- [67] KWOK, S., BOTET, R., SHARPNACK, L., AND CABANE, B. Apollonian packing in polydisperse emulsions. *Soft Matter* 16 (2020), 2426–2430. (Cited on page [1](#).)
- [68] LACHLAN, R. Xv. on systems of circles and spheres. *Philosophical Transactions of the Royal Society of London*, 177 (1886), 481–625. (Cited on page [70](#).)
- [69] LAGARIAS, J., MALLOWS, C. L., AND WILKS, A. Beyond the Descartes circle theorem. *The American Mathematical Monthly* 109 (2001). (Cited on pages [60](#), [70](#) and [93](#).)
- [70] LEIBNIZ, G. W., LOOK, B. C., AND RUTHERFORD, D. *Leibniz to Des Bosses: 11 March 1706*. Yale University Press, 2007, pp. 30–38. (Cited on page [1](#).)
- [71] MAEHARA, H. Pearl numbers versus stick numbers for knots. *Revue Roumaine de Mathématiques Pures et Appliquées* 51 (01 2006). (Cited on page [127](#).)
- [72] MAEHARA, H. On configurations of solid balls in 3-space: Chromatic numbers and knotted cycles. *Graphs and Combinatorics* 23, 1 (2007), 307–320. (Cited on pages [25](#) and [105](#).)
- [73] MAEHARA, H., AND NOHA, H. On the graph represented by a family of solid balls on a table. *Ryukyu Math. J* 10 (1997), 51–64. (Cited on page [15](#).)
- [74] MAEHARA, H., AND OSHIRO, A. On soddy’s hexlet and a linked 4-pair. In *Japanese Conference on Discrete and Computational Geometry* (1998), Springer, pp. 188–193. (Cited on page [105](#).)

- [75] MAEHARA, H., AND OSHIRO, A. On knotted necklaces of pearls. *European Journal of Combinatorics* 20, 5 (1999), 411–420. (Cited on pages 15, 25 and 26.)
- [76] MOHAR, B. Circle packings of maps in polynomial time. *European Journal of Combinatorics* 18, 7 (1997), 785–805. (Cited on page 44.)
- [77] MURASUGI, K. Jones polynomials and classical conjectures in knot theory. *Topology* 26, 2 (1987), 187–194. (Cited on page 18.)
- [78] MURASUGI, K. *Knot theory and its applications*. Springer Science & Business Media, 2007. (Cited on page 24.)
- [79] NAKAMURA, K. The local-global principle for integral bends in orthoplicial Apollonian sphere packings, 2014. (Cited on pages 2, 82, 87, 88, 90, 91, 93, 100 and 125.)
- [80] NEGAMI, S. Ramsey theorems for knots, links and spatial graphs. *Transactions of the American Mathematical Society* 324, 2 (1991), 527–541. (Cited on page 26.)
- [81] RAMÍREZ ALFONSÍN, J. L., AND RASSKIN, I. Ball packings for links. *European Journal of Combinatorics* 96 (2021), 103351. (Cited on pages 3 and 127.)
- [82] RAMÍREZ ALFONSÍN, J. L., AND RASSKIN, I. A polytopal generalization of Apollonian packings and Descartes’ theorem. (Cited on pages 3 and 123.)
- [83] RAMÍREZ ALFONSÍN, J. L., AND RASSKIN, I. Rational links and the orthoplicial apollonian packing. *In preparation* (2021). (Cited on page 3.)
- [84] RASSKIN, I. Regular polytopes, sphere packings and Apollonian sections. *arXiv preprint arXiv:2109.00655* (2021). (Cited on pages 3 and 125.)
- [85] RASSKIN, I. Polytopack: a framework for polytopal sphere packings (in preparation), 2021. (Cited on page 130.)
- [86] SAUERBREI, S., HASS, E. C., AND PLATH, P. The Apollonian decay of beer foam bubble size distribution and the lattices of young diagrams and their correlated mixing functions. *Discrete Dynamics in Nature and Society* 2006 (05 2006). (Cited on page 1.)

- [87] SCHLEIMER, S., AND SEGERMAN, H. Puzzling the 120-cell. *Notices of the American Mathematical Society* 62 (10 2013). (Cited on page 128.)
- [88] SCHULTE, E. Analogues of Steinitz's theorem about non-inscribable polytopes. *Colloq. Math. Soc. János Bolyai* 48 (01 1987). (Cited on page 58.)
- [89] SCHULTE, E. Symmetry of polytopes and polyhedra. In *Handbook of Discrete and Computational Geometry, 2nd Ed.* (2004). (Cited on page 46.)
- [90] SEIFERT, H. Über das geschlecht von knoten. *Mathematische Annalen* 110, 1 (1935), 571–592. (Cited on page 130.)
- [91] SHEYDVASSER, A. Quaternion orders and sphere packings. *Journal of Number Theory* 204 (2019), 41–98. (Cited on page 88.)
- [92] SODDY, F. The Kiss Precise. *Nature* 137, 3477 (Jun 1936), 1021–1021. (Cited on pages 80 and 105.)
- [93] SPRINGBORN, B. A. A unique representation of polyhedral types. Centering via Möbius transformations. *Mathematische Zeitschrift* 249, 3 (2005), 513–517. (Cited on page 44.)
- [94] STÄGER, D. V., AND HERRMANN, H. J. Cutting self-similar space-filling sphere packings. *Fractals* 26, 01 (2018), 1850013. (Cited on page 1.)
- [95] STANGE, K. E. The Apollonian structure of Bianchi groups. *Transactions of the American Mathematical Society* 370 (05 2015). (Cited on page 84.)
- [96] STANGE, K. E. The sensual Apollonian circle packing. *Expositiones Mathematicae* 34, 4 (2016), 364–395. (Cited on page 117.)
- [97] STEINITZ, E. Über isoperimetrische probleme bei konvexen polyedern. (Cited on page 123.)
- [98] STEPHENSON, K. *Introduction to circle packing: The theory of discrete analytic functions*. Cambridge University Press, 2005. (Cited on page 14.)
- [99] TAIT, P. G. On knots I, II, III, scientific papers, vol. i. *Cambridge Univ. Press, London 18980* (1898), 273–347. (Cited on page 18.)

- [100] THISTLETHWAITE, M. B. A spanning tree expansion of the Jones polynomial. *Topology* 26, 3 (1987), 297–309. (Cited on page 18.)
- [101] THURSTON, W. P. *Three-Dimensional Geometry and Topology, Volume 1: Volume 1*. Princeton University Press, 2014. (Cited on page 11.)
- [102] VAN COTT, C. Relationships between braid length and the number of braid strands. *Algebraic & Geometric Topology* 7, 1 (2007), 181–196. (Cited on page 23.)
- [103] VARRATO, F., AND FOFFI, G. Apollonian packings as physical fractals. *Molecular Physics* 109, 23-24 (2011), 2923–2928. (Cited on page 1.)
- [104] WILKER, J. B. Inversive geometry. 379–442. (Cited on pages 5, 10, 12, 13 and 53.)
- [105] ZHANG, X. On the local-global principle for integral Apollonian 3-circle packings:. *Journal für die reine und angewandte Mathematik (Crelles Journal)* 2018, 737 (2018), 71–110. (Cited on page 125.)
- [106] ZIEGLER, G. Convex polytopes: Extremal constructions and f-vector shapes. (Cited on page 46.)